UNIVERSIDAD D CÓRDOBA

Facultad de Ciencias

Departamento de Genética

Role of urease in pH modulation and virulence of *Fusarium oxysporum*

A thesis presented for the degree of Doctor of Philosophy in Biology at the University of Córdoba

Katja Schäfer

TITULO: *Role of urease in pH modulation and virulence of Fusarium oxysporum*

AUTOR: *Katja Schäfer*

Campus de Rabanales
Ctra. Nacional IV, Km. 396 A
14071 Córdoba

www.uco.es/publicaciones
publicaciones@uco.es

TÍTULO DE LA TESIS: Role of urease in pH modulation and virulence of *Fusarium oxysporum*

DOCTORANDO/A: Katja Schäfer

INFORME RAZONADO DEL/DE LOS DIRECTOR/ES DE LA TESIS

(se hará mención a la evolución y desarrollo de la tesis, así como a trabajos y publicaciones derivados de la misma).

La Tesis doctoral de Dña. Katja Schäfer se ha llevado a cabo en el Departamento de Genética de la Universidad de Córdoba en el seno del grupo "Genética Molecular de la Patogénesis fúngica (BIO-3138). Su desarrollo ha permitido al doctorando adquirir una sólida formación en Genética y Biología Molecular. Durante la realización de la tesis, Dña. Katja ha demostrado tener una gran capacidad de trabajo y aptitud para la investigación científica. El trabajo realizado ha permitido identificar nuevas proteínas determinantes de la virulencia del hongo patógeno Fusarium y caracterizar su modo de infección en plantas y en mamíferos.

Los resultados obtenidos se ha comunicado en varios congresos nacionales e internacionales, y parte de ellos se han recogido en la siguiente publicación.

Schäfer K, Di Pietro A, Gow NA, Maccallum D (2014) Murine Model for *Fusarium oxysporum* Invasive Fusariosis Reveals Organ-Specific Structures for Dissemination and Long-Term Persistence. PLoS One 9:e89920. doi: 10.1371/journal.pone.0089920.

Por todo ello, se autoriza la presentación de la tesis doctoral.

Córdoba, 19 de marzo de 2014

Firma del/de los director/es

Fdo.: Antonio Di Pietro

This work has been conducted in the Department of Genetics of the University of Córdoba and financially supported by the ARIADNE Marie Curie Research Training Network (FP7-PEOPLE-ITN-237936).

1. General Introduction

1.1. *Fusarium oxysporum*

Fungi of the genus *Fusarium* are important plant pathogens commonly found in soil, water and decaying organic matter (Naggie and Perfect, 2009). In addition, *Fusaria* can cause a broad spectrum of diseases in humans, ranging from superficial or localized infections in healthy hosts to lethal disseminated fusarioses in immunocompromised patients (Dignani and Anaissie, 2004).

The soil-borne ascomycete *Fusarium oxysporum* is the causal agent of vascular wilt, a devastating disease affecting a large variety of economically important crops worldwide (Beckman, 1987b). Different isolates of *F. oxysporum* attack a wide range of economically important crops leading to *Fusarium* crown and root rot, damping-off and, most commonly, vascular wilts (Agrios, 2005a). Vascular wilt disease is a major limiting factor in the production of many agricultural crops, including tomato (*Lycopersicon* spp.), banana (Musa spp.), cabbage (*Brassica* spp.), onion (*Allium* spp.), cotton (*Gossypium* spp), flax (*Linum* spp.), muskmelon (*Cucumis* spp.), pea (*Pisum* spp.), watermelon (*Citrullus* spp.), carnation (*Dianthus* spp.), chrysanthemum (*Chrysanthemum* spp.), gladiolus (*Gladiolus* spp.) and tulip (*Tulipa* spp.) (Armstrong, 1981). The widespread distribution of the genus stems from its ability to grow on a wide range of substrates and on its efficient high persistence in the soil (Burgess, 1981).

1.2. History and Taxonomy

F. oxysporum is an ascomycete, although it lacks a known sexual cycle (Table 1). Based on the structures bearing conidiogenous hyphae, *Fusarium* spp. are classified under the subclass Hyphomycetidae within the Deuteromycetes. Morphological characterization of *F. oxysporum* is based on the shape of macroconidia, the structure of microconidiophores, and the formation and disposition of chlamydospores (Beckman, 1987a). The first description of

Fusarium was made by Link in 1809 (Figure 1). In 1940, Snyder and Hansen grouped all the species of the genus in nine taxa and reclassified the infrageneric group called *elegans* into a single species *F. oxysporum*, designating different *formae speciales* (f. spp.), based on their pathogenicity on different plant species (Snyder and Hansen, 1940; Snyder, 1940). To date, more than 150 f. spp. have been reported (Michielse and Rep, 2009b). Further subdivisions of formae speciales into physiological races are based on their capacity to cause disease on different host cultivars (Correll, 1991). The genetic basis of host specificity (formae speciales) and cultivar specificity (races) in *F. oxysporum* is currently the subject of intense studies (Takken and Rep, 2010).

Table 1. Overview of biological features of *F. oxysporum*.

Taxonomy	Predominant cell-type	Sexual cycle	Mating-type system	Spores	Pathogenicity	Other
Phylum: Ascomycota Class: Sordariomyctes Order: Hypocreales Family: Nectriaceae Genus: *Fusarium* Species *F. oxysporum*	Filamentous mycelium, microconidia	Not ident.	MAT1 gene identified and expressed in *F. oxysporum*. A mixed distribution of MAT1-1 and MAT1-2 alleles in *Fusarium* species complex	Microconidia, macroconidia chlamydospores	*Fusarium* wilt on plant crops, Emerging cause of fusariosis in humans	*Fusarium* species complex are pathogenic especially to agriculture plants

Due to shortcomings of morphological characters for defining species and subgeneric groupings of the genus *Fusarium*, research focus has shifted to molecular tools for identification and determination of evolutionary relationships. These molecular tools include ribosomal spacer sequencing, Restriction Fragment Length Polymorphism (RFLP) and Random Amplified Polymorphic DNA (RAPD) markers. Interestingly, molecular phylogenetic studies revealed substantial genetic diversity among isolates, supporting the current view that *F. oxysporum* represents a species complex. In 1998, a pioneering study established that different field isolates of a f. sp. have polyphyletic origins, suggesting that the capacity to

infect a given plant host has arisen multiple times during evolution (O'Donnell et al., 1998). The genome sequence of the tomato pathogenic isolate *F. oxysporum* f. sp*. lycopersici* was published in 2010 (Ma et al., 2010). Since then, eleven additional *F. oxysporum* strains have been sequenced. The availability of the complete genome sequences, as well as of molecular tools and well-established pathogenicity assays has allowed to address the genetic bases and evolutionary origins of pathogenicity and host range in *F. oxysporum*.

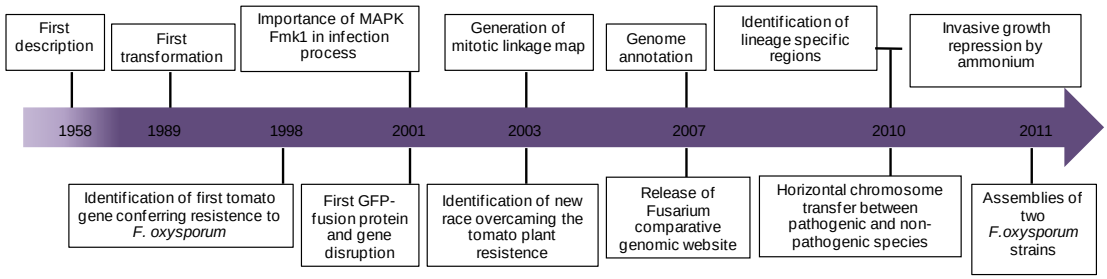

Figure 1. Key milestones in the history of *F. oxysporum* research.

1.3. Biology of *F. oxysporum*

F. oxysporum changes its morphology and color depending on the environmental conditions. The culture conditions affect growth rate, shape, size and abundance of conidia as well as number of septa and pigmentation (Booth, 1971). In general, aerial mycelium appears first in a white color and then turns to a variety of colors, ranging from pink to dark purple, depending on the isolate and the environmental conditions. The species produces three types of asexual spores: microconidia, macroconidia and chlamydospores (Figure 2) (Agrios, 1997).

Figure 2. Types of *Fusarium* conidia. (A) Macroconidia. **(B)** Microconidia. **(C)** Chlamydospores.

Microconidia are single-cell dispersal structures that are abundantly produced under most conditions. Macroconidia contain three to five cells and are gradually pointed and curved toward the ends and are commonly found on the surface of dead plants killed by the pathogen. Chlamydospores are thick-walled cells generally developed through the modification of hyphal and conidial cells. Their formation is induced by aging or unfavorable environmental conditions such as low temperatures or carbon starvation. Chlamydospores represent the principal structure for long-time survival during unfavorable periods in the soil, and play an important role as primary inoculum for plant root infection Chlamydospore germination is stimulated when carbohydrates are released from decaying plant tissue or from roots (Couteaudier and Alabouvette, 1990; Kono et al., 1995; Nelson, 1981b; Schippers, 1981b; Stevenson and Becker, 1972). The fungus can travel long distances within infected plants, soil or by wind in the form of microconidia. In short distances, *F. oxysporum* propagates mainly through water irrigation or contaminated equipment. Although it can infect fruit tissue and contaminate seeds, propagation rarely happens via the seed (Agrios, 1997).

1.4. Overview of the *F. oxysporum* genome

The genome sequencing, assembly and annotation of *F. oxysporum* f. sp. *lycopersici* was performed by the Broad Institute as part of the Fusarium Comparative Sequencing Project and can now also be accessed though the *EnsemblFungi* website (www.fungi.ensembl.org). A striking feature of the genome is that 28% corresponds to repetitive sequences, including many retroelements and short interspersed elements (SINEs) as well as class II transposable elements (TEs) (Table 2).

Table 2. Overview of the *F. oxysporum* genome data

Genome size (Mb)	61.36
Chromosomes	15
GC content (%)	48.4
Number of Genes	17708
Non-coding RNAs (tRNAs)	308
Introns	unknown

Avg. gene size/ intergenic region	1,3 kb
Transposons	28% of the genome identified as repetitive sequence; Retroelements (copia-like and gypsy-like, LINEs (long interspersed nuclear elements) and SINEs (short interspersednuclear elements). DNA transposons (Tc1-mariner, hAT-like, Mutator-like, and MITEs)
***S.cerevisiae* homologs**	Unknown
Mitochondrial DNA (kb)	34.48
References	(http://www.broadinstitute.org) (Takken and Rep, 2010)

Comparison of the *F. oxysporum* genome with those of *F. graminearum* and *F. verticillioides* led to the discovery of four supernumerary chromosomes that are enriched for TEs and for genes putatively related to host–pathogen interactions (Ma et al., 2010). These so-called lineage-specific (LS) regions contain more than 95% of all DNA transposons. Only 20% of the predicted genes in the LS regions could be functionally classified on the basis of homology to known proteins. Many encode predicted secreted effectors, virulence factors, transcription factors and proteins involved in signal transduction but less house keeping proteins. Recent data suggest that LS regions of *F. oxysporum* strains with different host specificities may differ considerably in sequence.

1.5. Plant infection cycle and development of vascular wilt by *F. oxysporum*

F. oxysporum can survive for long time periods as a saprophyte on plant debris in the soil , either as mycelium or conidia, but most commonly as chlamydospores (Agrios, 1997). *F. oxysporum* spores in the soil germinate in response to signals from the plant host and differentiate infection hyphae, which adhere to the plant roots and penetrate them directly without the need for specialized infection structures (Figure 4). Root penetration appears to occur predominantly through natural openings at the intercellular junctions of cortical cells, or through wounds (Perez-Nadales and Di Pietro, 2011). Once inside the root, hyphae grow inter- and intracellular to invade the cortex and cross the endodermis, until they reach the xylem vessels (Figure 3 B). The fungus then uses the xylem as avenue to colonize the host (Figure 3 C).

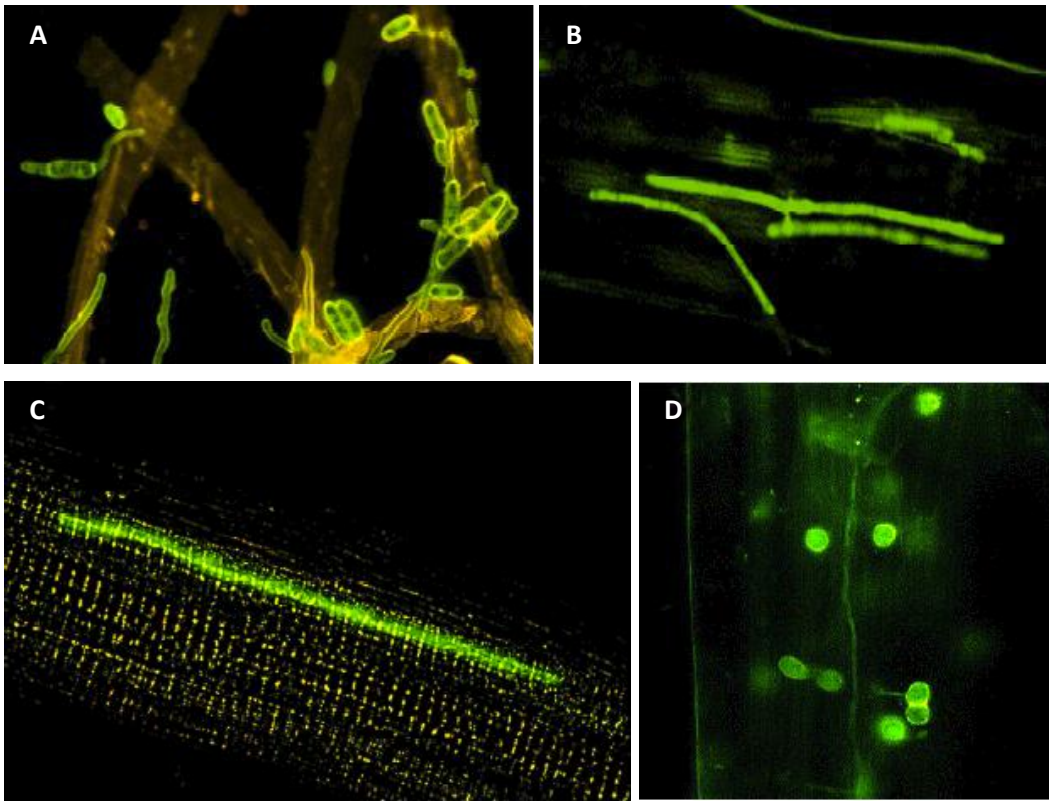

Figure 3. Penetration and colonization of tomato roots by *F. oxysporum*. A. Germinated microconidia and penetration hyphae of wild-type strain 4287 attaching to the root surface 24 h after inoculation**. B.** and **C.** Infection hyphae of wild-type strain 4287 growing in the root cortex, 5 days after inoculation **(B);** and in a root xylem vessel, 7 days after inoculation **(C)**. D. Chlamydospores of *F. oxysporum* wild-type strain produced on dying plant tissue. From (Di Pietro et al., 2001).

.

Vascular wilt is most likely caused by a combination of pathogen activities and plant defense responses. The former include accumulation of fungal mycelium in the xylem vessels and phytotoxin production, while the latter include production of vascular gels, gums and tyloses, and vessel crushing by proliferation of adjacent parenchyma cells (Beckman, 1987a). Ultimately, wilt symptoms are caused by severe water stress mainly due to vessel occlusion. Disease symptoms include wilting, chlorosis, necrosis, premature leaf loss, browning of the vascular system and stunting, which eventually will lead to plant death (Michielse and Rep, 2009b). Severely infected plants wilt and die, while plants affected to a lesser degree become stunted and lose productivity. Small oval-shaped microconida, falcate macroconidia and thick-walled chlamydospores (Figure 3 D) are formed on the dead plant tissue and in the

soil. *F. oxysporum* can survive in the soil for extended time periods, either as chlamydospores or by growing saprophytically on organic compounds until a new cycle of infection starts (Agrios, 2005b).

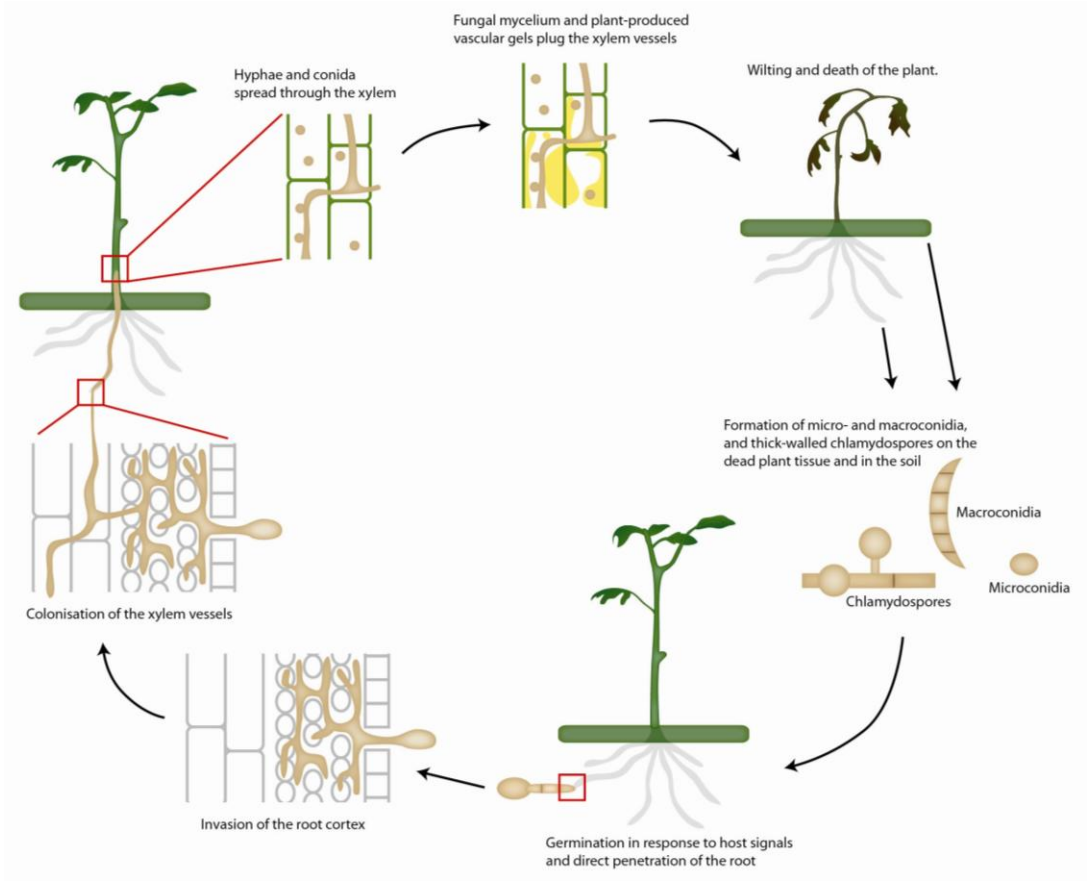

Figure 4. Life cycle of *F. oxysporum*. (A) Germination in response to host signals and direct penetration of the root. **(B)** Invasion of the root cortex**. (C)** Colonisation of the xylem vessels. **(D)** Hyphae and conidia spread through the xylem. **(E)** Fungal mycelium and plant-produced vascular gels plug the xylem vessels. **(F)** Wilting and death of the plant. **(G)** Formation of macro-microconidia and thick-walled chlamydospores on the dead plant tissue and in the soil (Perez-Nadales et al., submitted).

1.6. Management of *Fusarium* vascular wilt

The management of *Fusarium* wilt is achieved through resistant cultivars or chemical soil fumigation. However, the broad-spectrum biocides used to fumigate soil before planting, particularly methyl bromide, are environmentally damaging and are now banned in most

countries. The most environmentally safe and most cost effective method of control is the use of resistant plant cultivars, when available (Fravel 2003). Resistant tomato and melon cultivars are highly successful in conferring resistance to certain races of *F. oxysporum* f.sp. *lycopersici* and *F. oxysporum* f.sp. *melonis*, respectively (Joobeur et al., 2004; Ori et al., 1997). In cases where there is no resistance against *Fusarium* wilt such as in banana, the disease can only be controlled by preventing the introduction of the pathogen through destruction of diseased plants. Under greenhouse and field conditions, studies on biological control of Fusariosis have been focused on the application of antagonistic bacteria or nonpathogenic strains of *F. oxysporum*. The mechanisms contributing to the biocontrol capacity of these biocontrol agents include competition for nutrients in the soil, affecting the rate of chlamydospore germination, competition for infection sites on the root or triggering of plant defense reactions and systemic resistance (Khan et al., 2006; Larena et al., 2002; Larkin and Fravel, 2002).

1.7. Plant-pathogen interactions

1.7.1. Virulence mechanisms

Pathogenic fungi have developed efficient strategies to invade and grow within plant hosts. In contrast to bacteria and viruses, multicellular fungi are able to actively penetrate plant surfaces. For example, the pea pathogen *F. solani* f. sp. *pisi* secretes cutinases for enzymatic degradation of the cuticle, the first barrier encountered by aerial plant pathogens (Maiti and Kolattukudy, 1979). Penetration of *F. oxysporum* through the roots does not require cutinases but relies on the secretion of cell wall-degrading enzymes such as cellulases and pectinases (Di Pietro, 2009). Some phytopathogenic fungi secrete enzymes for detoxification of plant antifungal compounds. One such enzyme in *F. oxysporum* is tomatinase, which degrades the plant saponin α-tomatine (Pareja-Jaime et al., 2008; Roldan-Arjona et al., 1999). *F. oxysporum* is able to use the degradation product of this hydrolysis to suppress induced plant defense responses by interfering with fundamental signal transduction processes (Bouarab et al., 2002).

1.7.2. Plant defence mechanisms

Plants have evolved efficient mechanisms to protect themselves against pathogens. Two types of plant resistance responses can be distinguished: nonhost and host or race/cultivar specific. In both cases, the biochemical processes involved in pathogen resistance are similar (Somssich, 1998). Resistance in plants, characterized by the inability of the pathogen to grow and spread, often takes the form of a hypersensitive reaction (Agrios, 1997) characterized by cell death at the site of infection resulting in confining of the pathogen to necrotic lesions at the site of infection (Van Loon, 1997). Tissues surrounding necrotic lesions undergo localized acquired resistance (Baker et al., 1997; Fritig et al., 1998; Hammond-Kosack and Jones, 1996) which lead to nonspecific resistance throughout the plant, known as systemic acquired resistance, thus providing long-term protection against new infections by a broad range of pathogens (Fritig et al., 1998; Ryals et al., 1996; Sticher et al., 1997; Van Loon, 1997). The metabolic alterations in localized acquired resistance include cell wall reinforcement by deposition and crosslinking of polysaccharides, glycoproteins and insoluble phenolics; stimulation of secondary metabolic pathways, some of which yield small compounds with antibiotic activity (the phytoallexins); defense regulators such as salicylic acid, ethylene and lipid-derived metabolites; and accumulation of broad range of defense-related proteins and peptides (Fritig et al., 1998; Hahn, 1996).

1.7.3. Plant-pathogen recognition

Plant-pathogen interaction is a complex process with several stages and levels of recognition that determine success or failure of the infection process (Callow, 1987). Pathogen detection is the first step for activation of plant defence mechanisms. Plants respond to attacks by pathogens at two levels (Jones and Dangl, 2006). First, the plant is able to recognize molecules commonly produced by all microbes, called pathogen-associated molecular patterns (PAMPS), including polysaccharides and glycoproteins present in fungal cell walls, and mounts an innate immunity response. Successful pathogens have evolved mechanisms to overcome this first layer of defense, either by evading detection or by suppressing the immune response by the means of secreted effectors. In these cases, the plant becomes a host for a given pathogen species, establishing a compatible interaction. However, plants

have acquired a second level of defense based on the capacity to recognize specific virulence factors called effectors, and to mount a hypersensitive response (Jones and Dangl, 2006). The gene-for-gene hypothesis established by Flor (Flor, 1947; Flor, 1971) proposed that for every avirulence gene (*avr*) in the pathogen there is a corresponding host resistance gene (*R*) and that the loss or mutation of an *avr* gene should lead to a loss of resistance mediated by the corresponding *R* gene (Farman et al., 2002). This gene-for-gene model was recently shown for *F. oxysporum* f. sp. *lycopersici*-tomato interaction. In this f. sp. there are three known races, named in order of discovery race 1, 2 and 3 (Table 3). These are defined by their capacity to produce vascular wilt on tomato cultivars carrying different resistance genes. Genes I-1, I-2 and I-3 confer resistance against race 1, 2 and 3, respectively (Beckman, 1987a). The tomato I-2 resistance gene as well as several avirulence genes from *F. oxysporum* have been cloned, providing molecular support for the gene-for-gene hypothesis in this pathogen-host interaction (Takken and Rep, 2010). One of these avirulence proteins is Six1 which is secreted during colonisation of the xylem and mediates recognition by resistance gene I-3. Strains defective in *six1* are thus virulent on I-3 plants, while those expressing the gene are not. However, loss of Six1 comes at a cost for the pathogen, causing a global reduction of virulence (Rep et al., 2004).

Table 3. Races and resistance genes described in the *F. oxysporum* f. sp. *lycopersici* – tomato interaction. From (Takken and Rep, 2010).

Race	Resistance genes in tomato cultivars		
	I-1	**I-2**	**I-3**
Race 1	Avirulent	Virulent /Avirulent	Virulent /Avirulent
Race 2	Virulent	Avirulent	Virulent /Avirulent
Race 3	Virulent	Virulent	Avirulent

1.7.4. Fungal genes required for pathogenicity on plants

The number of pathogenic isolates resistant to fungicides is increasing and causes a need for the development of new active principles for agriculture and human health. However, a deeper understanding of the molecular mode of infection is required to develop novel strategies for disease control. The information provided by fungal genomes sequencing is

aiding the identification of new genes and proteins that could be useful for the design of targeted drugs (Isaacson, 2002).

In *F. oxysporum* and in other fungal pathogens, two main strategies have been used to identify pathogenicity genes. The first is reverse genetics, involving targeted deletion of candidate genes whose products may be involved in known biological functions relevant for infection (Pietro et al., 2003). This strategy has been facilitated recently through the sequencing of the genome of *F. oxysporum* (Ma et al., 2010). A second strategy known as forward genetics involves generation of pathogenicity mutants by random insertional mutagenesis followed by identification of the affected genes in these mutants (Madrid et al., 2003). Methods used for random insertional mutagenesis include the use of transposable elements (Li Destri Nicosia et al., 2001; Lopez-Berges et al., 2009), *Agrobacterium tumefaciens* (ATMT)-mediated transformation (de Groot et al., 1998; Michielse et al., 2009) and restriction enzyme mediated integration (REMI) mutagenesis (Imazaki et al., 2007; Namiki et al., 2001). Genes that have a significant effect on pathogenicity are often regulatory genes such as those encoding signalling components and transcription factors (Table 4).

Table 4. *F. oxysporum* genes with an effect in pathogenicity. Adapted from (Michielse and Rep, 2009b).

Product/function	Effect of gene inactivation/deletion	Reference
Transporter of several compounds	Reduced virulence on tomato plants	(Lopez-Berges et al., 2012)
GATA transcription factor, activator of nitrogen catabolism	Reduced virulence on tomato plants	(Lopez-Berges et al., 2010)
Argininosuccinate lyase	Strongly reduced virulence, arginine auxotrophy	(Namiki et al., 2001)
Beauvericin-enniatin synthase	Reduced virulence on tomato plants	(Lopez-Berges et al., 2012)
Class II chitin synthase	Reduced virulence	(Martin-Urdiroz et al., 2008)
Chaperone-like protein	Reduced virulence	(Martin-Urdiroz et al., 2008)
Class V chitin synthase	Strongly reduced virulence, hypersensitive to α-tomatine and H_2O_2	(Madrid et al., 2003)
Class VII chitin synthase	Non-pathogenic, hypersensitive to Congo red and Calcofluor white	(Martin-Urdiroz et al., 2008)
Carboxy- cis, cismuconate	Non-pathogenic, reduced growth on	(Michielse et al., 2012)

cyclase	phenolic compounds	
Chloride channel	Reduced virulence, deficient in laccase activity, increased sensitivity to oxidative stress	(Canero and Roncero, 2008)
Transcription factor	Non-pathogenic	(Pareja-Jaime et al., unpublished results)
Transcription factor	Reduced virulence	(Michielse et al., 2009a)
Cell wall protein	Reduced virulence	(Michielse et al., 2009a)
F-box protein	Reduced virulence, impaired in root attachment and invasive growth	(De Miguel & Hera, unpublished results)
G-protein α-subunit	Markedly reduced virulence, decreased conidiation	(Jain et al., 2002)
G-protein α-subunit	Non-pathogenic, increased resistance to heat	(Jain et al., 2005)
G-protein β-subunit	Markedly reduced virulence, decreased conidiation	(Delgado-Jarana et al., 2005 ; Jain et al., 2003)
Histidin kinase	Reduced virulence on tomato plants	Rispail and Di Pietro, 2010)
Mitogen-activated protein kinase	Non-pathogenic, impaired in root attachment and invasive growth	(Di Pietro et al., 2001)
Transcription factor	Markedly reduced virulence, reduced ability to use secondary nitrogen sources	(Divon et al., 2006)
Mitochondrial carrier	Strongly reduced virulence, impaired in plant colonization	(Inoue et al., 2002)
Transcription factor	Non-pathogenic, impaired in invasive growth, not in root attachment	(Imazaki et al., 2007)
Hypothetical protein	Reduced virulence	(Michielse et al., 2009a)
Similar to chloride conductance regulatory protein	Markedly reduced virulence	(Kawabe et al., 2004)
F-box protein	Non-pathogenic, impaired in root colonization and penetration, impaired growth on various carbon sources	(Duyvesteijn et al., 2005; Jonkers et al., 2009)
Transcription factor	Reduced virulence (RNAi silencing)	(Ramos et al.,2007)
β-1,3-Glucanosyltransferase	Markedly reduced virulence, reduced growth on solid medium	(Caracuel et al., 2005)
bZIP transcription factor, regulator of iron homeostasis	Reduced virulence on tomato plants and non virulence on immunodepressed mice	(Lopez-Berges et al., 2012)
Regulator of secondary metabolites	Reduced virulence on tomato plants	(Lopez-Berges et al., 2009)
bZIP transcription factor, repressor of nitrogen katabolism	Reduced virulence on plants	(Lopez-Berges et al., 2009)
Transmembrane mucin-like protein	Markedly reduced virulence, reduced growth on solid media, increased sensitivity to cell wall stress.	(Pérez-Nadales and Di Pietro,2011)
Transcription factor	Increased virulence and transcription of acid-expressed genes	(Caracuel et al., 2003)

Peroxin	Reduced virulence, impaired in growth on fatty acids	(Michielse et al., 2009a)
Peroxin	Reduced virulence, impaired in growth on fatty acids	(Michielse et al., 2009a)
Monomeric G protein	Markedly reduced virulence, reduced growth on solid media	(Martinez-Rocha et al., 2008)
Transcription factor	Non-pathogenic, reduced conidiation	(Michielse et al., 2009b)
Tetraspan transmembrane protein	Markedly reduced virulence, reduced growth on solid media, increased sensitivity to cell wall stress.	(Pérez-Nadales PhD Thesis, 2010)
Small secreted protein	Reduced virulence, effect more pronounced on 4- to 5-week-old plants	(Rep et al., 2005)
Protein kinase involved in carbon catabolite repression	Markedly reduced virulence, reduced growth on complex carbon sources	(Ospina-Giraldo et al., 2003)
Transcription factor	Markedly reduced virulence, impaired in invasive growth	(Asuncion Garcia-Sanchez et al., 2009; Rispail and Di Pietro, 2009)
Regulator of G protein	Reduced virulence on tomato plants	Michielse *et al*., 2009
Tomatinase enzyme	Reduced virulence, reduced tomatinase activity, increased sensitivity to α-tomatine	(Pareja-Jaime et al., 2008)
Regulatory protein	Reduced virulence, altered development and reduced secondary metabolism	(López-Berges et al., 2013)
Regulatory protein	Reduced virulence, altered development and reduced secondary metabolism	(Lopez-Berges et al., 2009)

1.8. The molecular and methodological toolbox for *F. oxysporum*

F. oxysporum can be routinely transformed via enzymatic protoplastating (Di Pietro and Roncero, 1998). Gene replacement is performed through homologous recombination with exogenous DNA constructs generated by fusion PCR methodology (Szewczyk et al., 2006), typically using Phleomycin or Hygromycin B resistance cassettes, flanked by 1000 bp homology regions to the target site of insertion. To date, these methods have allowed the generation of *F. oxysporum* strains carrying reporter genes (GFP; ChFP), regulatable promoters and numerous gene deletion mutants. Forward genetic insertional mutagenesis screens with T-DNA or transposon tagging have also been applied in *F. oxysporum*, leading to the discovery of novel virulence factors (Lopez-Berges et al., 2009; Michielse et al., 2009).

Recently, a custom-made *F. oxysporum* microarray chip has been made by Agilent Technologies, allowing transcriptional profiling studies (Lopez-Berges et al., 2012). A great variety of laboratory assays have been developed to allow the study of invasive growth functions and plant pathogenicity in this species.

Table 5. Overview of molecular and methodological tools available in *F. oxysporum*.

Transformation	Protoplast & ATMT (Agrobacterium-mediated transformation)
Minimal homology for gene deletion	> 1000 bp
Episomal elements	self-replicative ARS *(active replicating system)* plasmid pFNit-Lam-Tlam, linear
Promoters **[c] constitutive** **[r] regulatable**	[r] Thiamine repressed sti35 promoter [c] gpdA promoter
Commonly used selection markers	Hygromycin B, Phleomycin
Reporter genes	GFP; ChFP
Fluorescent protein labels	GFP; ChFP
Cytochemical dyes	Calcofluor White, DAPI, FITC
Arrays	Custom made DNA microarray, Affymetrix.
Pathogenicity models	Plant models:Tomato plants, tomato fruits, apple fruits; Mammalian model: immunodepressed mice;. Invertebrate model: *Galleria mellonella*
Strains	*F. oxysporum* f. sp. *lycopersici* wild type 4287 (FGSC 9935)

The tomato root infection assay is performed by immersing the roots of two week-old seedlings in a microconidial suspension in distilled water, followed by planting in vermiculite and maintenance in a growth chamber at 28°C (Di Pietro and Roncero, 1998) (Figure 5A). More recently, severity of vascular wilt is plotted as percentage survival across time, by recording mortality each day for 30 to 45 days. This method allows statistical analysis of the samples: survival rates are estimated by the Kaplan-Meier method and compared among groups using the log-rank test (Lopez-Berges et al., 2012; Lopez-Berges et al., 2013). In planta quantification of fungal biomass is performed by extracting total genomic DNA from infected tomato roots and/or stems at 4, 7 or 10 days post-infection, followed by quantitative real-time PCR analysis (Pareja-Jaime et al., 2010) of the *Fusarium*-specific *six1* gene, and normalized to the tomato *gadph* gene. Quantitative evaluation of the rate of initial root penetration during the initial 12 to 24 h after inoculation is performed using scanning

electron microscopy (Perez-Nadales and Di Pietro, 2011). Finally, the ability of the fungal germlings to attach to the tomato roots is documented by incubating the tomato roots with fungal spores for prolongued times (24 hours) in potato dextrose broth diluted 1:50 with water and supplemented with 20 mM glutamic acid (Di Pietro et al., 2001; Prados Rosales and Di Pietro, 2008).

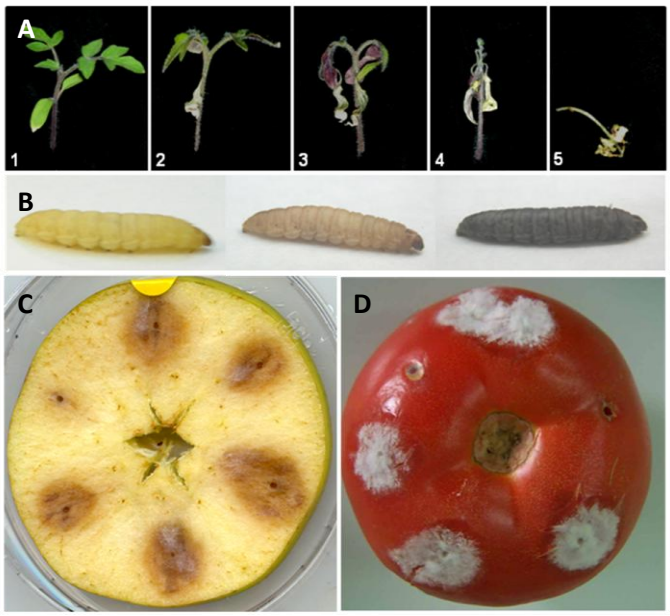

Figure 5. *F. oxysporum in vivo* virulence assays. (A) Tomato plant root assay. Two week old tomato seedlings (cultivar Moneymaker) were inoculated with *F. oxysporum* strains by immersing the roots in a microconidial suspension for 30 min, planted in vermiculite and incubated in a growth chamber at 28 °C. Evaluation is performed using a disease index for *Fusarium* vascular wilt going from 1= healthy plant to 5= dead plant. (1-5) **(B)** Larvae of the greater wax moth (*Galleria mellonella*) used to investigate virulence of *F. oxysporum.* Tipically, the infection is performed via micro-injection in the posterior pseudopod.progression of the fungal infection is associated with melanization of the larvae. **(C, D)** Invasive growth assay on living fruit tissue. Apple fruits **(C)** or tomato fruits **(D)** were inoculated with *F. oxysporum* strains and incubated in a humid chamber at 28°C for 3 days.

Rapid invasive growth assays on tomato or apple fruit tissue (Figure 5E-F) are performed by injecting a microconidial suspension into tomato fruits or apple slices, and evaluating invasive growth and maceration of the surrounding fruit tissue (Di Pietro et al., 2001). In the wild type strain, a dense mycelial growth is visible on the fruit surface 3 to 4 days post-infection (Di Pietro et al., 2001). The *in vitro* cellophane penetration assay has been shown to

correlate significantly with *in vivo* pathogenicity on tomato plants. For this assay, a fungal colony is allowed to grow on a cellophane membrane placed on a solid agar medium plate. The cellophane with the fungal colony is removed at day 2-4 after inoculation and the ability of the fungus to reach the underlying medium is evaluated. (Prados Rosales and Di Pietro, 2008). A mouse infection model has been established for the same *F. oxysporum* f. sp. *lycopersici* strain, making Fol 4287 the first fungal isolate to serve as a dual model for the study of fungal pathogenesis in plants and mammals (Ortoneda et al., 2004). Infection assays are performed with immunodepressed mice by injecting conidia into a lateral vein of the tail. Mortality of the animals is recorded each day for 15 d and survival rates are estimated as in the plant root infection assay. Fungal tissue burden in kidneys and lungs at 7 days post-infection is also evaluated using standard plating methods (Lopez-Berges et al., 2012; Lopez-Berges et al., 2013; Ortoneda et al., 2004). More recently, the greather wax moth *Galleria mellonell*a has been used as a novel non-vertebrate infection model for studying virulence mechanisms of *F. oxysporum* on animal hosts (Navarro-Velasco et al., 2011) The model provides valuable data without the need to use mammals for *in vivo* testing. *F. oxysporum* is able to proliferate inside the hemocoel of *G. mellonella* larvae and to kill and colonize the insects. Most genes required for full virulence on immunodepressed mice also play a significant role in *G. mellonella* infection (Navarro-Velasco et al., 2011).

1.9. Current research topics in *Fusarium*

1.9.1. Lineage specific chromosomes

Sequence characteristics of the genes present on the LS genome regions indicate a distinct evolutionary origin from the core genome, suggesting that they could have been acquired through horizontal transfer from another *Fusarium* species. This idea was experimentally supported by the finding that co-incubation of two strains of *F. oxysporum* can result in transfer of small LS chromosomes from a tomato pathogenic to a non-pathogenic strain, converting the latter in a pathogen. This led to the hypothesis that horizontal chromosome

transfer in *F. oxysporum* can generate new pathogenic lineages (Ma et al., 2010). The genetic and cellular mechanisms underlying these processes are currently subject to intensive study.

1.9.2. Secreted effectors and gene-for-gene system

In 2008, Houterman et *al.*, reported the identification of a fungal avirulence factor, Avr1 that suppresses disease resistance conferred by two *resistance* genes *I-2* and *I-3* but that triggers disease resistance when the host plant, tomato, carries a matching *R* gene *(*I *or* I-1) (Houterman et al., 2008). Host specificity in different races and cultivars of *F. oxysporum* f. sp. *lycopersici* is determined by a set of secreted effector genes called "Secreted In the Xylem" (*six*) genes. Interestingly, all *six* genes are located on a single LS chromosome (chromosome 14), also called the pathogenicity chromosome and are associated with chromosomal subregions enriched for DNA transposons (Ma et al., 2010). However, they are not functionally independent of the core genome, since their expression *in planta* requires the transcription factor *Sge1*, which is located on a core chromosome (Michielse and Rep, 2009a).

1.9.3. *F. oxysporum* as a model for trans-kingdom pathogenesis

Besides causing disease on plants, *F. oxysporum* is also an opportunistic pathogen of humans (Nucci and Anaissie, 2007). *F. oxysporum* causes invasive infections in immunosuppressed individuals, being the second most frequent species of the genus after *F. solani,* (Guarro and Gene, 1995; Nucci and Anaissie, 2007). Previous work established that a tomato pathogenic isolate of *F. oxysporum* f.sp. *lycopersici* can cause disseminated infection in immunocompromised mice (Ortoneda et al., 2004) and was the first fungal isolate shown to cause disease both in tomato (*Solanum lycopersicum*) plants and in immunodepressed mice. The ability to cause disease in both plants and mammals makes *F. oxysporum* a unique multihost pathogen for studying fungal infection across different host kingdoms (Ortoneda et al., 2004). Since then, a number of genes have been identified that are either required for pathogenicity on tomato but not on mice (Table x), including the *Fusarium* Fmk1 MAPK, the small G protein Rho1 and the glucanosyltransferase Gas1 (Caracuel et al., 2005; Di Pietro et al., 2001; Martinez-Rocha et al., 2008) or vice versa, such as the pH response factor PacC,

the light response factor White Collar-1 (Wc-1), or the secreted *Fusarium* Pathogenesis Related 1 (PR-1)–like protein Fpr1 (Caracuel et al., 2003; Prados-Rosales et al., 2012; Ruiz-Roldan et al., 2008). Collectively, these results suggested that fungal pathogenicity on plants and animals may have fundamentally distinct evolutionary origins. However, most of the *F. oxysporum* genes required for infection of mice have orthologues associated with virulence in the two well-established animal model pathogens *C. albicans* and *C. neoformans* (Csank et al., 1998; Davidson et al., 2003; Davis et al., 2000) thus confirming that the opportunistic pathogen *F. oxysporum* behaves as a "true" human pathogen. Recently HapX, a transcription factor that governs iron homeostasis, was characterized as the first virulence determinant required for both plant and animal infection in the same fungal strain (Lopez-Berges et al., 2012). Δ*hapX* mutants are significantly attenuated in their capacity to cause vascular wilt symptoms and mortality in tomato plants and were unable to efficiently colonize and kill immunodepressed mice (Lopez-Berges et al., 2012), confirming previous reports in the human pathogens *C. neoformans*, *A. fumigatus*, and *C. albicans* (Hsu et al., 2011; Jung et al., 2010; Schrettl et al., 2010). Similarly, the velvet protein complex, a conserved regulator of fungal development and secondary metabolism, contributes to infection of plants and mammals, in part by promoting biosynthesis of the depsipeptide mycotoxin beauvericin (Lopez-Berges *et al.*, 2013).

Table 6. *F. oxysporum* genes studied both in plant and animal models.

Mutant	Phenotype in Plant	Phenotype in Mouse	Reference
Δ*fgb1*	Avirulent	Virulent	(Delgado-Jarana et al., 2005; Prados-Rosales et al., 2006)
Δ*fmk1*	Avirulent	Virulent	(Di Pietro et al., 2001; Ortoneda et al., 2004)
Δ*fmk1*/Δ*fgb1*	Avirulent	Avirulent	(Delgado-Jarana et al., 2005; Prados-Rosales et al., 2006)
Δ*chsV*	Avirulent	Virulent	(Madrid et al., 2003; Ortoneda et al., 2004)
Δ*pacC*	Virulent	Avirulent	(Caracuel et al., 2003; Ortoneda et al., 2004)
Δ*fpr1*	Virulent	Avirulent	(Prados-Rosales et al., 2012)
Δ*rho1*	Avirulent	Virulent	(Martinez-Rocha et al., 2008)
Δ*wc1*	Virulent	Avirulent	(Ruíz-Roldán et al., 2008)
Δ*hapX*	Avirulent	Avirulent	(Lopez-Berges et al., 2013)
Δ*laeA*	Avirulent	Avirulent	(Lopez-Berges et al., 2012)
Δ*veA*	Avirulent	Avirulent	(Lopez-Berges et al., 2012)
Δ*abc3*	Avirulent	Virulent	(Lopez-Berges et al., 2012)
Δ*beas*	Avirulent	Avirulent	(Lopez-Berges et al., 2012)
Δ*gas1*	Avirulent	Virulent	(Caracuel et al., 2005)
Δ*ureG*	Reduced	Reduced	This work
Δ*car1*	Reduced	Reduced	This work
Δ*ure1*	Reduced	Virulent	This work

1.9.4. The role of MAPK signaling cascades in virulence

The *F. oxysporum* MAPK (mitogen-activated protein kinase) Fmk1, an orthologue of the yeast Fus3/Kss1 MAPKs, was found to be essential for virulence on tomato plants (Di Pietro et al., 2001). Infection-related processes such as invasive growth, vegetative hyphal fusion and root adhesion (Di Pietro et al., 2001; Prados Rosales and Di Pietro, 2008) absolutely require Fmk1 and are negatively controlled by the nitrogen source ammonium (Lopez-Berges et al., 2010). Because this MAPK is widely conserved among fungi and determines pathogenicity in all plant pathogens studied so far (Rispail et al., 2009), a major effort has been directed towards elucidating the upstream and downstream components of this signalling cascade. The homeodomain transcription factor Ste12 was shown to function downstream of Fmk1 and to be required for invasive growth, the most critical of the Fmk1-regulated functions for plant infection (Rispail and Di Pietro, 2009). The mucin-like transmembrane protein Msb2 was recently characterized as an upstream component of the cascade (Perez-Nadales and Di Pietro, 2011).

In addition to the Fmk1 pathway, orthologues of the *S. cerevisiae* high osmolarity Hog1 and cell integrity Mpk1 MAPK signalling cascades have also been identified in *F. oxysporum* and are currently under investigation. The Rho-type GTPase Rho1 functions upstream of Mpk1 and was found to be essential for morphogenesis and pathogenicity (Martinez-Rocha et al., 2008). Future studies will address how signalling through different MAPK cascades is orchestrated to control infectious growth in *F. oxysporum*. From the MPK1 pathway which is involved in cell wall integrity of *S. cerevisiae,* to date only the Rho-type GTPase Rho1 has been characterized in *F. oxysporum*. Rho-type GTPases regulate polarized cell growth through the reorganization of the actin cytoskeleton as well as through signalling pathways that control the expression of cell wall biosynthesis genes (Levin, 2005). In 2008 the *rho*1 mutant of *F. oxysporum* revealed non-pathogenicity on tomato plants and a higher resistance to cell-wall degrading enzymes, probably due to higher chitin content (Martinez-Rocha et al., 2008).

2. Material and Methods

2.1. Material

2.1.1. Strains and Plasmids

F. oxysporum and *S. cerevisiae* strains, plasmids, plant cultivars and animal species used in this work are listed in the tables below.

Table 1. Fusarium *oxysporum* f. sp. *lycopersici* strains used in this study.

Strain	Background	Genotype	Reference
4287 (FGSC 9935)	wild type		J. Tello, University of Almeria, Spain
Δ*fmk1*	4287	*fmk1::PHLEO*	(Di Pitro et al., 2001)
Δ*msb2*	4287	*msb2::HYG*	(Perez-Nadales and Di Pietro, 2011)
Δ*meaB*	4287	*meaB::HYG*	(Lopez-Berges et al., 2010)
Δ*meaB+ meaB*	Δ*meaB*	Δ*meaB:: HYG; meaB; PHLEO*	(Lopez-Berges et al., 2010)
Δ*mebB*	4287	*mepB::HYG B*	(Segorbe-Luke, unpublished)
Δ*mepB+ mepB*	Δ*mebB*	Δ*mebB:: HYG;mepB; PHLEO*	(Segorbe-Luke, unpublished)
Δ*areA*	4287	*areA::HYG*	(Lopez-Berges et al., 2010)
Δ*snf1*	4287	*snf1::HYG*	
Δ*hxk1*	4287	*hxk1::HYG*	
ΔFOXG_04361	4287	FOXG_04361*::HYG*	this study
ΔFOXG_08976	4287	FOXG_08976*::HYG*	this study
ΔFOXG_15235	4287	FOXG_15235*::HYG*	this study
ΔFOXG_00769	4287	FOXG_00769*::HYG*	this study
ΔFOXG_00769 +FOXG_00769	ΔFOXG_00769	ΔFOXG_00769*::HYG;* FOXG_00769; PHLEO	this study
ΔFOXG_09776	4287	FOXG_09776*::HYG*	this study
ΔFOXG_ 08666	4287	FOXG_ 08666*::HYG*	this study
ΔFOXG_10398	4287	FOXG_10398*::HYG*	this study
ΔFOXG_12838	4287	FOXG_12838*::HYG*	this study
ΔFOXG_13832 (Δ*ureG*)	4287	*ureG::HYG*	this study
Δ*ureG+ ureG*	Δ*ureG*	Δ*ureG::HYG; ureG; PHLEO(1)*	this study
ΔFOXG_01071 (Δ*ure1*)	4287	*ure1::HYG*	this study
ΔFOXG_12915 (Δ*car1*)	4287	*car1::HYG*	this study

(1) Hygromycine cassette replaced with phleomycin cassette

Table 2. *Sacchamomyces cerevisiae* strains used in this study.

Strain	Genotype	Reference
Y2HGold Yeast Strain	*MATα*	Clontech, Cat. 630498
Y187 Yeast Strain	*MAT*α	Clontech, Cat. 630457

Table 3. Plant and fruit cultivars and animal species used in this study

Species	Cultivar/Species	Origin
Tomat (*Lycopersicon esculentum*)	Seeds: Monika /Money maker	
Apple (*Malus pumila*)	Golden Delicious	
Geather wax moth (*Galleria mellonella*)		Animal center, s.c.p., Valencia (Spain)
Mice (*Mus musculus*)	BALB/c; Oncins France	Harlan, United Kingdom Charles River, Criffa S.A

Table 4. Plasmids used in this study

Plasmid	Origin/Features	Reference
pGEM®-T	Derived from plasmid pGEM®-5Zf(+), linearized with *Eco*RV and with a T added in both 3' ends	Promega
pAN7-1	Derived from pUC18; A.nidulans gpdA promoter; phosphotransferase hygromicin B gene from Streptomyces spp. (hph); A. nidulans trpC terminator	(Punt et al., 1987)
pAN8-1	Derived from pUC18; A.nidulans gpdA promoter; phleomycin resistance gene; A. nidulans trpC terminator	(Mattern et al., 1988)
msb2-pGemT	*msb2* locus (FOXG_09254.2, 5.9 Kb) from *F. oxysporum* 4287 strain, including endogenous promoter and terminator sequences, cloned into pGemT.	Perez-Nadales and Di Pietro ., 2011
(1)pGBKT-7 (DNA-BD Vector)	Express any protein as a GAL4 DNA-BD fusion, Kan^r for selection in *E. coli* and the *TRP1* nutritional marker for selection in yeast	Clontech Cat. No. 630489
(2) pGADT7 -Rec (DNA-AD Vector)	Express any protein as a GAL4 DNA-AD fusion, Amp^r for selection in *E. coli* and the *LEU* nutritional marker for selection in yeast	Clontech, Cat. No. 630442
p-GADT7-Lam	Express lamin C as GAL4 DNA-BD fusion (contol vector)	Clontech
pGBKT7-53	Express murine p53 as a GAL4 DNA-BD fusion (contol vector)	Clontech
pGADT7-T	Gal4 AD fused with SV40 large T-antigen(contol vector)	Clontech

(1) Yeast Two-Hybrid DNA-BD plasmid pGBKT7 were used in this study for the expression of various proteins as a GAL4 DNA-BD fusion protein and was named according the name of the gene; e.g.: pGBKT7 gene name-BD .

(2) Yeast Two-Hybrid DNA-AD plasmid pGADT7-Rec were used in this study for the expression of various proteins as a GAL4 DNA-AD fusion protein including the cDNA llibrary of *F. oxysporum*. For single proteins this plasmid was named according the name of the gene; e.g.: pGADT7 gene name-AD.

2.1.2. Synthetic oligonucleotides

Oligonucleotides used in amplification and sequencing reactions were designed with the software Oligo (version 6.65; Molecular Biology Insights, Inc. USA), analyzing internal stability, duplex and hairpin formation and different physicochemical parameters (Tm, %G+C, %A+T) in each case. Oligonucleotides were synthesized by the company Eurofins Operon.

Oligonucleotides used in this work are listed in table 5. Underlined nucleotides do not belong to the original sequence and were introduced to generate M13 (Hyg/Phleo fusion –PCR) or Yeast plasmid (pGBKT7 and pGADT7) complementary sequences.

Table 5. Oligonucleotides used in this study. Added restriction sites not present in the orginal DNA sequence are indicated in italics. Underlined nucleotides indicate plasmid homologue vector sequences used for homolog recombination during *S. cerevisiae* transformation or sequences complementary to M13 primers. All primers are designed with an annealing temperature of 64°C. Only exceptions are indicated.

Gene/Name	Sequence (5`- 3`)
Msb2-CT_for	ACACCACTTGATCTTTCATCATGCGACGATACAAGCGCAAGAAG
Msb2-CT_rev	AAAGGGGGATCACGAGCATCA
Msb2-CT primer containing enzyme restriction sides to clone into the bait plasmid pGBKT7	
Msb2-F2 (*Eco*RI)	*GAATTC*CGACGATACAAGCGCAAGAAG
Msb2-R1 (*Pst*I)	*CTGCAG*GTTCCATCCAAGAGAGTTCTC
M13for	CGCCAGGGTTTTCCCAGTCACGAC
M13rev	AGCGGATAACAATTTCACACAGGA
PHL	Agttgaccagtgccgttccg
LEO	Gccacgaagtgcacgcagtt
Gene-knockout primer (corresponding gene names in chapter 3)	
UreG_Prom_for	CCGGCTACCATCGACTCTCT
UreG Prom_rev	GGGTTTCTGTCTCCACCCACagcggataacaatttcacacagga
UreG Term_for	gtgactgggaaaaccctggcgTCGCCATCAGCTTGCACTGC
UreGTerm_rev	GAGCCAGCTCCACCAAGTCA
Car1_prom_F	CCTACGTCAGTCCTTCATTCC
Car1_prom_R	GTCGTGACTGGGAAAACCCTGGCGCCCCATTTGTATTCGGAGGTC
Car1_term_F	TCCTGTGTGAAATTGTTATCCGCTGGCACATTCGGTACTGAGACA
Car1_term_R	CCAGTTAGAGCCATCGCAAAG
4361 prom F	TCGAGGCGGAGGTTCGTACT
4361 prom R	GTCGTGACTGGGAAAACCCTGGCGCGTGGAAGAAGCGGTGATGG
4361 term F	TCCTGTGTGAAATTGTTATCCGCTTGTGGACTAGGGAGGGCCAA
4361 term R	AACAGGCACCAAGGTCGTCG
14173 prom F	GCTTCGTTACAGCCACCCAG
14173 prom R	GTCGTGACTGGGAAAACCCTGGCGCCTATGAACTGCGCGACTTTG
14173 term F	TCCTGTGTGAAATTGTTATCCGCTCATGCCACGAGCACGAGCTT
14173 term R	CGGCATCCTCCTGATGAAGC
08666 prom F	CCCCTATTGCGATGTCTTTGG
08666 prom R	GTCGTGACTGGGAAAACCCTGGCGAAACGAATGGACAGTTGAGGGT

08666 term F	TCCTGTGTGAAATTGTTATCCGCTCCCTCAACCCATAGAAGCATC
08666 term R	GCTGGTCGAGACCTCTCATC
08976 prom F	CGCACGCACTGGGATGATTG
08976 prom R	GTCGTGACTGGGAAAACCCTGGCGAGAGACTATCTCGCCGCACG
08976 term F	TCCTGTGTGAAATTGTTATCCGCTGCGGTTGGGATTGTTGGGAG
08976 term R	CGGCACAGTCGAAGAAGACG
09776 prom F	GGGGACAGCCATACAAGCTC
09776 prom R	GTCGTGACTGGGAAAACCCTGGCGTGACAAGAGGGTGATGTAGCG
09776 term F	TCCTGTGTGAAATTGTTATCCGCTCAATCAAGATCTCAGGTGGCC
09776 term R	GAATCTGATTGGCTGTTGGCC
10398 prom F	CAGCGGACTTGGCAAGATTGA
10398 prom R	GTCGTGACTGGGAAAACCCTGGCGTTCGGTGTTTTCACCGCACGA
10398 term F	TCCTGTGTGAAATTGTTATCCGCTCTCGTCGAGTCGATATATGCC
10398 term R	TGGTGTGGGTATTGTTGTGGC
12838 prom F	TGGTGCCGTCGTCGTTCATG
12838 prom R	GTCGTGACTGGGAAAACCCTGGCGGCTAGTAGGAGAGCGAAGTGA
12838 term F	TCCTGTGTGAAATTGTTATCCGCTCAAAAGCTCAGGTTCTGACTAC
12838 term R	AGCCCATCACGTTTTCTACTCT
00231 prom F	TCAGCCATCTGAACAGAGTCAT
00231 prom R	GTCGTGACTGGGAAAACCCTGGCGTGACGATAGAGCTGAGGTTAAG
00231 term F	TCCTGTGTGAAATTGTTATCCGCTGTCACGCTCCACGAATTACAAA
00231 term R	ATACAGTATCTTGCAGAGCACG
15235 prom F	ACATGGTGCCGTAGATGATGG
15235 prom R	GTCGTGACTGGGAAAACCCTGGCGTTCTTGTCGTGTAAGACGCCG
15235 term F	TCCTGTGTGAAATTGTTATCCGCTGGCTACCCTAATCTATTTCTCTT
15235 term R	CTGCCAAACACCATTGCAGCA
Verification primer (ver) for diagnostic PCR of gene knockout mutants	
ureG_2.5_ pF	AGCAAGAGACGGAGAACGCAA
Car1_prom_ver_F	CCCATCCGAAACAATCGAGAG
Car1_term_ver_R	GCCATGCTTCGTAACTTCGTC
Ure1_co_P_F	AGTTCGCCCTTGTCACCTACA
Ure1_co_T_R	ATGAACCTGGTCCTTCCTACG
13832 prom_F_ver	ATGGTGCAGGTGTTGCTGTTAA
UreG_ver_rev	TGACCGTTGACCCTGAAGAG
4361 prom F ver	GTAAACGGCGGGAAGTTTTTGA
4361 term R ver	ACAAGCTATCGAATACGGTACG
14173 prom F ver	TGGTATGCTGGATGGTGAAGG

14173 term R ver	GAGGACATATCAAGTCTGACTG
08666 prom F ver	CAGCAGAACACAATGATGGTAAA
08666 term R ver	AAGCTACTACGGTGGACTTCTT
08976 prom F ver	TTCCGAGATGCCAAAGAATGGT
08976 term R ver	CAGCAGTAGAGGAACGTCAGT
09776 prom F ver	CATGAGAGAATCAAAGCGACCA
09776 term R ver	TAGATAGTGGCGAAGTGTTTGC
10398 prom F ver	ATGTCTATCACCGCTAACGGAA
10398 term R ver	GGCCATTTGGAACGTAGCCAT
12838 prom F ver	CCCTAACCAGCATGTAGTCAAA
12838 termR ver	TTACTGCACTATGACTACAGGC
00231 prom F ver	TGTCTTTCTGCGGGGCATCC
00231 term R ver	GGCAGTGTATCATGACTTCAAC
15235 prom F ver	ACCAATAACAATACCAGTGAAGG
15235 term R ver	CCGTTTGTTTTTGCATGTAGATG
Real-time primer (InEx)	
Actin primer act-2	GAGGGACCGCTCTCGTCGT
Actin primer act-q6	GGAGATCCAGACTGCCGCTCAG
GallFor	AGATCGCTTTCATAGTCGCAATA
Gallrev	CTCTCTCCAACTTCTACCTACT
Six1-1	ATAGCATGGTACTCCTTGGCG
Six1-2	CCTGATGGTGACGGTTACGAA
09795-for (*fpr1*)	CCCAAGAAGAACCCTGCTCC
09795-rev (*fpr1*)	GAGTAGGGGTTGGAGCCGC
10398 inEx_for	AGTCGTGACATGGACTCCTGT
10398 inEx_rev	GGAGCAGGTCTTTTCGATCTC
Primer for genes involved in urea cycle (Real-time; InEx)	
13832 inEx_for	CCACTCGCATGAGATCCTTGA
13832 inEx_rev	GGGTGAAGATGTCGTTCGTCA
urease2: Ure2_InEx_F	GGCCCATGGAAAGAAGCTCAA
urease2: Ure2_InEx_R	CCAACGGATGGAAGTCTGCTT
putative urea transporter: Dur3_InEx_F	ACTTGGGCTGCTACCCTTCTT
putative urea transporter: Dur3_InEx_R	GCGAAGATGAGGATGATGACG
urease1:Ure01071 inEx_F	ATATCGGAGTCAAAGAGGGCAT
urease1:Ure01071 inEx_R	GCAGACCCTCAGGAGAACTAT
nitrate transporter: 00635_InEx_F	GTGATCTGTATGGACCTCGAC
nitrate transporter: 00635_InEx_R	GCAGACCAAGGGGACAATGAA

glutamine synthetase: 05182_InEx_F	CGATGGCACTCCCAACAAGTA
glutamine synthetase: 05182_InEx_R	AAGAATCGTGAAACCCAAAGTTG
argininosuccinate lyase: 01957_InEx_F	TTGGTTTCAGCGGAATCACTCT
argininosuccinate lyase: 01957_InEx_F	CATAGTGGCGATAACCCCGTT
Arginase: 12915_InEx_F	CGGACATCAACACTCCTGAGA
Arginase: 12915_InEx_R	CACGCTCTCGCAGATGAAATC
ornithine aminotransferase: 09346_InEx_F	TTCTACAACGATGTCTTCCCCA
ornithine aminotransferase: 09346_InEx_R	TCGCAGATGAAAGCAGCAGTC
ornithine decarboxylase: 07603_InEx_F	TGTCCTCGACACCTACAATCAT
ornithine decarboxylase: 07603_InEx_R	ACAGACTTGACGTATCGGACAT
nit1-For	CGGCTACTGGGGTGAGAAGG
nit1-Rev	GGAACACTTCTCGGTCTGCG
Yeast Two Hybrid primer	
Amplimer 5`	CTATTCGATGATGAAGATACCCCACCAAACCC
Amplimer 3`	GTGAACTTGCGGGGTTTTTCAGTATCTACGAT
BD insert For	tcatcggaagagagtagt
BD insert Rev	agagtcactttaaaatttgtat
Primer tail for homologues recombination in pGADT7 plasmid	
AD tail for_primer	GAGGCCAGTGAATTCCACCCAAGCAGTGGTATCAACGCAGAGTGG
AD tail rev_primer	TCCCGTATCGATGCCCACCCTCTAGAGGCCGAGGCGGCCGACATG
Primer for pGADT7 plasmid (always with AD tail for/rev)	
Msb2-CT_pGAD_For	AD tail for+ CGACGATACAAGCGCAAGAAG
Msb2-CT _pGAD_Rev	AD tail rev+ TTCCATCCAAGAGAGTTCTC
Sho1_pGAD7_for	AD tail for+ ATGGATCACTCAAGAATGTATGG
Sho1_pGAD7_rev	AD tail rev+ TCATAACAAGATGAGGTAGTTGC
Cdc42_pGAD7_F	AD tail for+ ATGGCTGTTGTCGCAACTATTA
Cdc42_pGAD7_R	AD tail rev+ TTATAGGACAAGGCACTTGTGT
00769_pGAD_for	AD tail for+ ATGGTTGTCCATGACGGTCACGA
00769_pGAD_rev	AD tail rev+ GTAACATGACTACTTGGATTGCT
04361_pGAD_for	AD tail for+ ATGTCTCGGGACCGGCGTG
04361_pGAD_rev	AD tail rev+ TTAGTTTTCATGTAGCAGTCTGG
14173_pGAD_for	AD tail for+ ATGCCTCCAGGTAAGATTCTCTT
14173_pGAD_rev	AD tail rev+ TTACAGGCTATCCTCGAGTTCG
08666_pGAD_for	AD tail for+ ATGGTCGACCATGACATGTACG
08666_pGAD_rev	AD tail rev+ CTAGAAATCGGCTGCGTCAAAG
09776_pGAD_for	AD tail for+ ATGACCGTCTTTAACATCGACG
09776_pGAD_rev	AD tail rev+ TTAGTGCTTTCCATTCGGCTTC

10398_pGAD_for	AD tail for+ ATGACGTACCCCCGTCCCGA
10398_pGAD_rev	AD tail rev+ TTATTTCACCCTGTTGTAGTAAGC
12838_pGAD_for	AD tail for+ ATGAATCGTCCCTATCGTCCC
12838_pGAD_rev	AD tail rev+ CTACCGAGCCCATGAGCCC
00231_pGAD_for	AD tail for+ ATGGCTGCCATGTTCAGCCAG
00231_pGAD_rev	AD tail rev+ CTAATCCTTCTTCAAGGGCAAGA
15235_pGAD_for	AD tail for+ ATGCCTCTACCGTCTCGGG
15235_pGAD_rev	AD tail rev+ CTAGTAAATGCCTGTAAAATCTAA
13832_pGAD_for	AD tail for+ ATGTCGCACTCTCACGACGGT
13832_pGAD_rev	AD tail rev+ TTACTCCAGCTGCTCCAGACC
Primer for genes of the velvet complex	
veA_pGAD_For	AD tail for+ ATGGCTACACCATCCTCGATTC 66º
veA_pGAD_Rev	AD tail rev+ CTACTCGTCATAATACCGGTTGA 66º
velB_pGAD_For	AD tail for+ ATGAATTCTGCCTATCACTCGC
velB_pGAD_Rev	AD tail rev+ TCAGTTCTGATCGTACATCTCTT
velC_pGAD_For	AD tail for+ ATGCCACATCCACACCCGAC
velC_pGAD_Rev	AD tail rev+ TCACTATCGCGCCGAACGG 62º
laeA_pGAD_For	AD tail for+ ATGGTTGTAATGCCTCCTCAAAA
laeA_pGAD_Rev	AD tail rev+ TTACTGTTGAGGTCCGGGCTT
areA_pGAD_For	AD tail for+ ATGAGCACATCTGTCTCAATCA 62º
areA_pGAD_Rev	AD tail rev+ TCACAGGCTCATCGTCAGCC
Primer for pGBKT7 plasmid (plasmid tails are underlined)	
UreG _pGBKT7_For	GCATATGGCCATGGAGGCCGAATTCATGTCGCACTCTCACGACGG
UreG _ pGBKT7_Rev	TGCGGCCGCTGCAGGTCGACGGATCCTTACTCCAGCTGCTCCAGACC
10398 _pGBKT7_For	GCATATGGCCATGGAGGCCGAATTCATGACGTACCCCCGTCCCGA
10398_ pGBKT7_Rev	TGCGGCCGCTGCAGGTCGACGGATCCTTATTTCACCCTGTTGTAGTAAGC
veA_pGBKT7_For	CATGGAGGCCGAATTCATGGCTACACCATCCTCGATTC 66º
veA_ pGBKT7_Rev	GCAGGTCGACGGATCCCTACTCGTCATAATACCGGTTGA 66º
velB_ pGBKT7_For	GCATATGGCCATGGAGGCCGAATTCATGAATTCTGCCTATCACTCGC
velB_ pGBKT7_Rev	TGCGGCCGCTGCAGGTCGACGGATCCTCAGTTCTGATCGTACATCTCTT
velC_ pGBKT7_For	GCATATGGCCATGGAGGCCGAATTCATGCCACATCCACACCCGAC
velC_ pGBKT7_Rev	TGCGGCCGCTGCAGGTCGACGGATCCTCACTATCGCGCCGAACGG 62º
laeA_ pGBKT7_For	GCATATGGCCATGGAGGCCGAATTCATGGTTGTAATGCCTCCTCAAAA
laeA_ pGBKT7_Rev	TGCGGCCGCTGCAGGTCGACGGATCCTTACTGTTGAGGTCCGGGCTT
areA_ pGBKT7_For	GCATATGGCCATGGAGGCCGAATTCATGAGCACATCTGTCTCAATCA62º
areA_ pGBKT7_Rev	TGCGGCCGCTGCAGGTCGACGGATCCTCACAGGCTCATCGTCAGCC

2.1.3. Media and culture conditions

All media were prepared with Milli-Rho deionized water and sterilized either by autoclaving at 120 °C for 20 min or by filtration (0.22 µm pore size, Millipore).

Table 6. Media and buffer solutions used in this work

Media and solutions	Ingredients and preparation (1 l)
Potato Dextrose Broth (PDB)	Boil 200 g of peeled potatoes in 0.6 l of water for 60 min. Stir and add 20 g of glucose and deionized water up to 1 l. Sterilize by autoclaving
Potato Dextrose Agar (PDA)	3.9% potato dextrose agar (w/v) (Scharlau Microbiology). For culturing *F. oxysporum* transformants add hygromycin B (55 µg/ml) or phleomycin (5.5 µg/ml-1) after autoclaving.
YPD /YPDA (Yeast extract Peptone Dextrose/Agar)	Yeast extract (3g), peptone (10g) and glucose (20g). Add bactoagar (15 g) for solid medium.
Puhalla's minimal medium (MM) (Puhalla, 1968)	$MgSO_4$ x .$7H_2O$ (0.5g), KH_2PO_4 (1g); KCl (0.5g), $NaNO_3$ (2g) and sucrose (30g). Add oxoid agar (20g) for solid medium. Urea was adding after autoclaving (final conc. 0, 05 M).
Regeneration minimal medium	$MgSO_4$ x $7H_2O$ (0.5g), KH_2PO_4 (1g), KCl (0.5g), $NaNO_3$ (2g), glucose (20g), sucrose (200g) and oxoid agar (12.5 g/l for Petri dishes and 4 g/l for top agar).
PBS (1x)	8 g/l NaCl, 0,2 g/l KCl, 1, 44 g Na_2HPO_4, 0,24 g/l KH_2PO_4, adjust pH 7,4 add H_2O until 1 l autoclave and store at room temperature
1M Tris pH 7,4	12, 11 g Tris in 80 ml H_2O, add 7 ml HCl, adjust pH 7, 4 and add H_2O until 100 ml
Buffer TE	10 mM Tris, 1 mM EDTA,pH 7,8
pH buffer for MM media	(A) 0.1 M Citric acid (B) 0.1 M Sodium citrate For 50 ml MM media use 25 ml of following mix pH 3: (A) 46.5 ml + (B) 3.5 ml pH 4: (A) 33 ml + (B) 17 ml pH 5: (A) 20.5 ml + (B) 29.5 ml pH 6: (A) 9.5 ml + (B) 41.5 ml

2.1.4. *Escherichia coli* growth conditions

Escherichia coli strain XL1Blue were culturing in Luria-Bertoni medium (Sambrook et al., 1989) and incubated at 37°C. For selection of recombinant *E. coli* cells either the antibiotics ampicillin (100 µg/ml) or kanamycin (15µg/ml) was added to the media after autoclaving. The screening of pGEM-T (Promega) plasmids was performed by ampicillin resistance and blue-white selection with X-gal and IPTG. Screening of recombinant *E. coli* containing Yeast-

Two Hybrid plasmids pGBKT7 or pGADT7-Rec were performed by using kanamycin or ampicillin, respectively.

2.1.5. *S. cerevisiae* media and culture condition

S. cerevisiae culturing was followed appropriate as described in Matchmaker® Gold Yeast Two-Hybrid System User Manual (Clontech). In short, YPDA broth (Clontech) or SD (synthetically defined medium, Clontech) minimal media was used to grow *S. cerevisiae* at 30°C. The media was prepared by dissolving pouch contents in ddH_20 and autoclaved for 15 min at 121˚C. Dropout supplements (Clontech) were used to select positive Yeast transformants. SD/–Trp dropout supplement was used to select for the bait (pGBKT7) and SD/–Leu dropout for the prey plasmid (pGADT7-Rec) transformed in the yeast strains Gold and Y187, respectively. SD– Leu/–Trp dropout supplement was used to select for diploid cells after yeast mating containing the bait and prey plasmids. To determine positive protein interaction in a Yeast-Two Hybrid assay X-a-Gal and Aureobasisin A (final concentration of 200 ng/ml) was added to the SD– Leu/–Trp media (DDO/X/A) after autoclaving. To increase the selection of strong protein interaction positive clones were confirmed on high stringency media SD– Leu/–Trp/-His/-Ade/+X/+Aur (QDO/X/A) media. For long time storage and stocks Freezing Medium were added to the yeast cells consists of 2x YPDA broth + 25% glycerol.

2.1.6. *F. oxysporum* growth conditions

F. oxysporum strains were cultured in rich (PDB and YPD) or nutrient limiting minimal media (MM), according to specific requirements and experimental designs. For microconidia production or extraction of DNA cultures were grown in liquid PDB at 28°C with orbital shaking at 170 rpm for 4- 5 days. For transformants which contain a antbiotic resistant cassette, appropriate antibiotics (hygromicin B at 55 µg/ml or phleomycin at 5.5 µg/ml) were added to the culture medium. For preparation of challenge inocula, microconidia were obtained by filtration through a nylon filter (Monodur; mesh size 10 µm) as described previously (Di Pietro and Roncero, 1998) and harvested by centrifugation /12000g for 15 min). The conidia concentrations were adjusted with a hemocytometer to the wanted

density. For long-term storage microconidia from 4-5 day-old cultures were collected by filtration; resuspended in sterile deionized water with 30% glycerol (v/v) and stored - 80ºC. These suspensions were used for later inoculation to obtain fresh microconidia.

2.2. Molecular methodology

2.2.1. Restriction mapping and subcloning

Restriction mapping, subcloning and plasmid DNA extraction from *E. coli* were carried out according to standard methods (Sambrook et al., 1989), and using the reagents according to the manufacturer´s instructions. *E. coli* competent cells were transformed with purified plasmids by the heat shock method described by (Hanahan, 1985). Restriction enzymes were provided by Roche (Barcelona, Spain). Ligations were carried out using T4 DNA ligase from Roche. DNA fragments were isolated from TAE electrophoresis gels using the QIAquick Gel extraction Kit (QIAGEN) following the manufacturer´s instructions or the "glass milk" extraction. For the latter DNA was cutting from a 1% of Low melting temperature agarose gel (NuSieve^R GTG^R Agarose/LONZA), transferred in a 2 ml Eppendorf centrifuge tube with 700 µl (3V) of NaI 6M buffer (1) and incubate 5 minutes at 55 °C. The tube was vortex during this incubation time until the agarose was completely dissolved. 15 µl of "glass milk" (2) solution was added and incubate for 10 minutes on ice with vortexing every 1minute. After centrifuging for 1 minute at full speed, the pellet was resuspended in 500 µl "new washing buffer" (3). The washing step was performed three times. After drying the pellet through an additional centrifuge step the pellet was resuspended in 20 µl ddH_2O and incubated for 5 minutes at 55 °C. The mix was centrifuged for 1 minute at full speed and the supernatant containing the DNA was transferred to a new Eppendorf centrifuge tube.

(1) NaI 6M buffer: dissolve 90 g NaI; 1, 52 g Na2SO3 in 100 ml H2O, sterile filtrate and store at 4 ªC.

(2) Glass milk: 100 mg/ml silice powder (Sigma S5631) in PBS 1x (0,8 g NaCl; 0, 02 g KCl; 0,144 g Na_2HPO_4, adjust pH 7,4 add H_2O until 100ml and autoclave)

wash with PBS (1x), let it sediment and resuspend in TE-Buffer (10 mM Tris, 1mM EDTA, pH 7,8).

(3) New washing buffer: 20 mM Tris pH 7,4; 1mM EDTA; 100 mM NaCl (1 ml 1M Tris pH 7,4; 100 µl 0,5 M EDTA; 1 ml 5 M NaCl; 47,9 ml H_2O until all is dissolved, then add 50 ml EtOH 100%), store at -20ºC

2.2.2. Nucleic acid (gDNA/RNA) extraction from *F. oxysporum*

During this work two different protocols to isolate genomic DNA from *F. oxysporum* were used. Genomic DNA was extracted from *F. oxysporum* mycelium using the CTAB method (Torres et al., 1993), to obtain a high concentration of clean DNA e.g for verification PCRs after single sporing of transformants or for Southern-blots. Briefly, approximately 100 mg of mycelium were ground to a fine powder in a mortar and pestle under liquid nitrogen and transferred to a 2 ml Eppendorf centrifuge tube with 1 ml of CTAB extraction buffer (1) and vortexed. 4 µl of β-mercaptoethanol (Merck) and 500 µl of a chloroform: octanol 24:1 (v/v) solution were added quickly, the mix was vortexed and incubated at 65ºC for 30 minutes. After incubating at room temperature for 15 minutes the tube was centrifuged for 5 minutes at 10000 g. The supernatant was then precipitated with 1 ml of 100% ice-cold ethanol and incubated at -20ºC for at least 10 minutes (optional over night), followed by centrifugation for 5 minutes at 7500 g and two consecutive washes with 1 ml 75 % ethanol. Finally, the pellet was resuspended in 50-100 µl of sterile deionised water with 4 µl de RNase (10 mg/ml) and incubated at 37°C for 30 minutes.

(1) CTAB extraction buffer: 12.1 g/l Trizma base; 7.44 g/l EDTA; 81.8 g/l NaCl y 20 g/l and 20 g/l Cetyltrimethylammonium bromide. Heat to 60 °C to dissolve and adjust to pH 8.0 with NaOH. Keep at 37 ºC to avoid precipitation.

The second DNA extraction method used in this work was the “Glass Beads” gDNA method which allows isolating gDNA from *F. oxysporum* mycelium growing on solid media. This method was used for fast DNA extraction from putative mutants growing on PDA masterplate after transformation. This DNA was exclusively used for a diagnostic PCR screening. Briefly, with a sterile spatula approximate 0, 5 mm^2 of mycel were cut from the

plate transferred to a 2 ml Eppendorf centrifuge tube containing 500 µl Lysis Buffer (1). The mycel were homogenized with the T 10 basic ULTRA-TURRAX (IKA®) or optional mycel can be grounded manually with glass beads (0, 5 mm) and a spatula. After centrifugation at 7500 g for 2 minutes the supernatant was transferred to a new 2 ml Eppendorf centrifuge tube containing 275 µl 7M Ammonium acetate (2) and incubated 5 minutes at 65°C. After incubating 5 minutes on ice, 500 µl chloroform was added, the mix was vortexed and centrifuged at 7500 g for 3 minutes. The supernatant was transferred to a new Eppendorf centrifuge tube containing 1 ml Isopropanol and the DNA was precipitated by a 5 min incubation step at room temperature followed by centrifugation for 5 minutes at 7500 g and two washes with 1 ml 70 % ethanol. After drying the pellet was resupended in 20 µl deionised water with 4 µl de RNase (10 mg/ml) and incubated at 37ºC for 30-60 minutes.

(1) Lysis Buffer : 100mM Tris pH 8.0; 50 mM EDTA; 1% SDS

(2) 7 M Ammonium acetate ($NH_4C_2H_3O_2$): 27 g Ammonium acetate in 50 ml deionised water

For RNA extraction, approximately 100 mg of frozen mycelium were ground to a fine powder in a mortar and pestle under liquid nitrogen and transferred to a pre-chilled 2 ml Eppendorf centrifuge tube with 1 ml (4 volumes) of TRIzol Isolation Reagent (Life Technologies™), followed by vortexing and incubation for 5 minutes on ice. After centrifugation for at 12000 g for 10 minutes at 4ºC the supernatant was transferred to a new vial. 200 µl of chloroform per 1 ml of TRIzol were added and the mix was vortexed for 15 seconds at low vortex power. After incubated on ice for 3 minutes the centrifugation at 4ºC for 20 minutes at 12000 g results in the formation of three phases. The upper clear phase with high-quality RNA was remove and transferred to a new clean 1, 5 ml Eppendorf centrifuge tube pre-chilled with 750 µl Isopropanol. The tube was mixed by inversion followed by incubation on ice for 10 minutes and centrifugation at 4°C for 20 minutes and 12000 g to precipitate RNA. The pellet was washed with 1 ml of 75% ethanol (v/v) and centrifuged at 4°C for 5 minutes and 7500 g. The pellet was air dried for 5-10 minutes and resuspended in 20-50 µl of RNase-free water.

2.2.3. Nucleic acid quantification

DNA and RNA were quantified in a Nanodrop® ND-1000 spectrophotometer at 260nm and 280 nm wavelengths, respectively. In addition, the quality of the DNA and RNA obtained was monitored by electrophoresis in a 0.7% and 1% agarose gel (w/v), respectively.

2.2.4. DNA isolation form *S. cerevisiae*

For PCR analysis a fast DNA extraction was performed. A yeast cell was picked with a toothpick and transferred into a 1, 5 ml Eppendorf centrifuge tube with 50 µl of NaOH (0, 02 M). The tube was incubated for 20 minutes at room temperature during this time the tube was mixed several times. Then the Eppendorf centrifuge tube was cooked in a microwave for 2 minutes at maximal strength. The mix was spin down at 7000 rpm. 5 µl of the supernatant was used as a template for a PCR reaction with V_{fin}: 50 µl.

2.2.5. Plasmid isolation from *S. cerevisiae* cells

Plasmid isolation from Yeast cells was performed using the plasmid isolation kit (Roche). Briefly, a 5 ml over night culture of *S. cerevisiae* was centrifuged at 3000 rpm for 5 minutes. After discarding the supernatant the cell pellet was resuspended in 250 µl suspension buffer 1 (Roche) transferred to Eppendorf centrifuge tube and kept on ice. Add 2/3 volume glass beads (0, 5 mm) and shake 3x 20 seconds on a Mini BeadBeater-8 (BioSpec Products). Between these steps tubes were incubating on ice for 1 minute. After centrifugation at 13.200 rpm for 5 minutes at 4°C the supernatant was transferred to a clean Eppendorf centrifuge tube. 250 µl lysis buffer 2 was added and the tube was inverted gently 5 times and incubate for 2 min on ice. 350 µl chilled binding buffer 3 was added, mixed by gently invertion (5 times) and incubated on ice for 5 minutes. After centrifugation at 13.000 rpm for 10 minutes at 4°C the supernatant (700 µl) was apply to a column and centrifuged at 13.000 rpm for 1 minute at 4°C. The flow though was discarded and the column was washed with 700 µl washing buffer 5. After discarding washing buffer column was cleaned and dried by an additional centrifugation step for 1 minute. The plasmid was eluted by adding 30 µl elution

buffer 6 to the column and additional centrifugation as described before. 20 µl of the elution was used to transform competent *E. coli* cells.

2.2.6. Southern blot analysis

Southern analysis and probe labelling were carried out as described (Di Pietro and Roncero, 1998) using the non-isotopic digoxigenin labelling kit (Roche Diagnostics SL, Barcelona, Spain).

2.3. Amplification reactions

2.3.1. Standard PCR

PCR amplifications were performed in a termocycler using the thermostable DNA polymerase of the Roche Expand High Fidelity PCR System. Each reaction contained 300 nM primers, 2.5 mM de MgCl2, 0.8 mM dNTPs mix and 0.05 U/µl of polymerase. Genomic DNA was added at 20 ng/µl and plasmid DNA at 2 ng/µl. PCR cycling conditions were: an initial step of denaturation (5 min, 94ºC) followed by 35 cycles of 35 s at 94ºC, 30 s at the calculated primer annealing temperature and 35 s at 72ºC (or 68ºC for templates larger than 3Kb), and a final extension step at 72ºC (or 68ºC) for 10 minutes. PCR for screening procedures were done with the Velocity DNA Polymerase (Bioline) following the manufacturer´s instructions. For PCR amplification of fragments higher than 7 Kb and/or with high GC, the more robust iProof High-Fidelity DNA Polymerase (BioRad) was used, following the manufacturer´s instructions.

2.3.2. Colony PCR from *S. cerevisiae* and *E. coli* cells

To determine the insert after Yeast or Bacterial transformation, with a sterile toothpick a small colony was picked and used directly for a PCR reaction or for more PCR reactions a bigger colony was picked and transfer into a PCR tube containing 10 µl of ddH_2O. From this mix 5µl was used for a PCR with V_{fin} 50µl. The PCR reaction was performed as described in section 2.3.1.

2.3.3. Reverse transcriptase PCR

Prior complementary DNA (cDNA) synthesis, the RNA was treated with DNaseI (Fermentas). Therefore 1 µg of total RNA was mixed together with 1 µl DNAse and 1 µl of DNAse buffer (Fermentas) and ddH_2O to V_{fin}: 10µl. After 30 minutes of incubation at 37°C, 1 µl EDTA (25 mM) was added and incubate for 10 minutes at 65°C. For the following first strand cDNA was synthesized different protocols were used. Briefly, 1 µl oligodT primer (100 pmol) and 1 µl dNTPs (0.4 mM) were added and incubate 10 minutes at 65°C. Next, the tube was transferred to ice for 5 minutes. After a short spin 4 µl 1x First Strand Buffer (Invitrogen), 2 µl of 0, 1 M dithiothreitol (DTT) and 1 µl of 4 U/µl of RNAsas RNasin® Plus RNase Inhibitor (Promega) were added and incubated for 2 minutes at 37°C. Then, 1µl retrotransciptase (10 U/µl) was added followed by a 50 minute incubation at 37ºC and a final 15 minute incubation at 70°C to inactivate the enzyme. 30 µl ddH_2O were added to a V_{fin} 50 µl. 5 µl were used for a quantitative real-time PCR (qPCR) reaction. Optinal distinct qRT-PCR Kits were used. The "Transcriptor Universal cDNA Master" (Roche**)** or **"**Transcriptor First Strand cDNA Synthesis Kit" (Roche) following the instructions of the manufacturer.

2.3.4. Real-time quantitative PCR

Quantitative real-time PCR reactions (qPCR) were performed in an iCycler apparatus (BioRad, USA) using iQ SYBR Green Supermix (BioRad, USA), 400 ng cDNA template and 300 nM of each gene-specific primer in a final reaction volume of 15 µl. All primer pairs amplified products of 160 – 200 bp. The following PCR program was used for all reactions: an initial step of denaturation (5 min, 94°C) followed by 40 cycles of 30 s at 94°C, 30 s at 60°C, 30 s at 72°C, and 20 s at 80°C for measurement of fluorescence emission. A melting curve program was run for which measurements were made at 0.5°C temperature increments every 5 s within a range of 55 – 95°C.

Once Ct values were obtained (Ct=number of cycles required for the fluorescent signal to cross the threshold), comparison of multiple samples was performed using relative quantification by the 2-ΔΔCt method (Livak and Schmittgen, 2001; Pfaffl, 2001). For this, the wild type strain was chosen as the calibrator and the expression of the target gene in all

other strains was expressed as an increase or decrease relative to the calibrator. To determine the relative expression of a target gene in the test sample and calibrator sample, a reference gene (actin) was used as the normalizer.

2.3.5. Fusion PCR

Fusion PCR or overlap extension represents a new approach to genetic engineering (Ho et al., 1989; Yang et al., 2004) and is schematically represented in Figure x. Complementary oligodeoxyribonucleotide (oligo) primers and the polymerase chain reaction are used to generate two DNA fragments with overlapping ends. In this PCR (PCRI) reaction a ~1, 5 kp fragment upstream (prom) of the target gene and a ~1, 5 kp fragment downstream (term) of the target gen is amplified. For the prom region the primer pair X_prom_F/X_term_R and for the term region the primer pair X_term_F/X_term_R were used, where X stands for the target gene (table x). The primer X_term_R and X_term_F contain a tail which is homologue to the hygromycin resistance cassette which was amplified in parallel using the M13F/M13R primer (A). These fragments are combined in a two subsequent 'fusion' reaction (Fusion PCRI, prom+hyg and term+hyg) in which the overlapping ends anneal, allowing the 3' overlap of each strand to serve as a primer for the 3' extension of the complementary strand (B). The resulting fusion product was used as a template for the next PCR reaction (Fusion PCRII). Primers were added to amplify the fusion product produced in the first fusion PCR (C). In this work, this technique was used for the generation of gene knockout constructs, where part of the ORF of the gene was replaced with the hygromycin resistance cassette. The fragments were either purified with the commercial GENECLEAN Turbo Nucleic Acid Purification kit or the “glass milk method” or precipitated before used for transformation. For PCR fusion of final fusion fragments larger than 5 Kb, the more robust iProof High-Fidelity DNA Polymerase (BioRad, Madrid, Spain) was used, following the manufacturer´s instructions. Gene knockout was performed by homologous recombination (E) after replacing the target gene with the two fusion PCR products (D). All primers used to make the construct and confirm positive knockout mutants are indicated in figure 1.

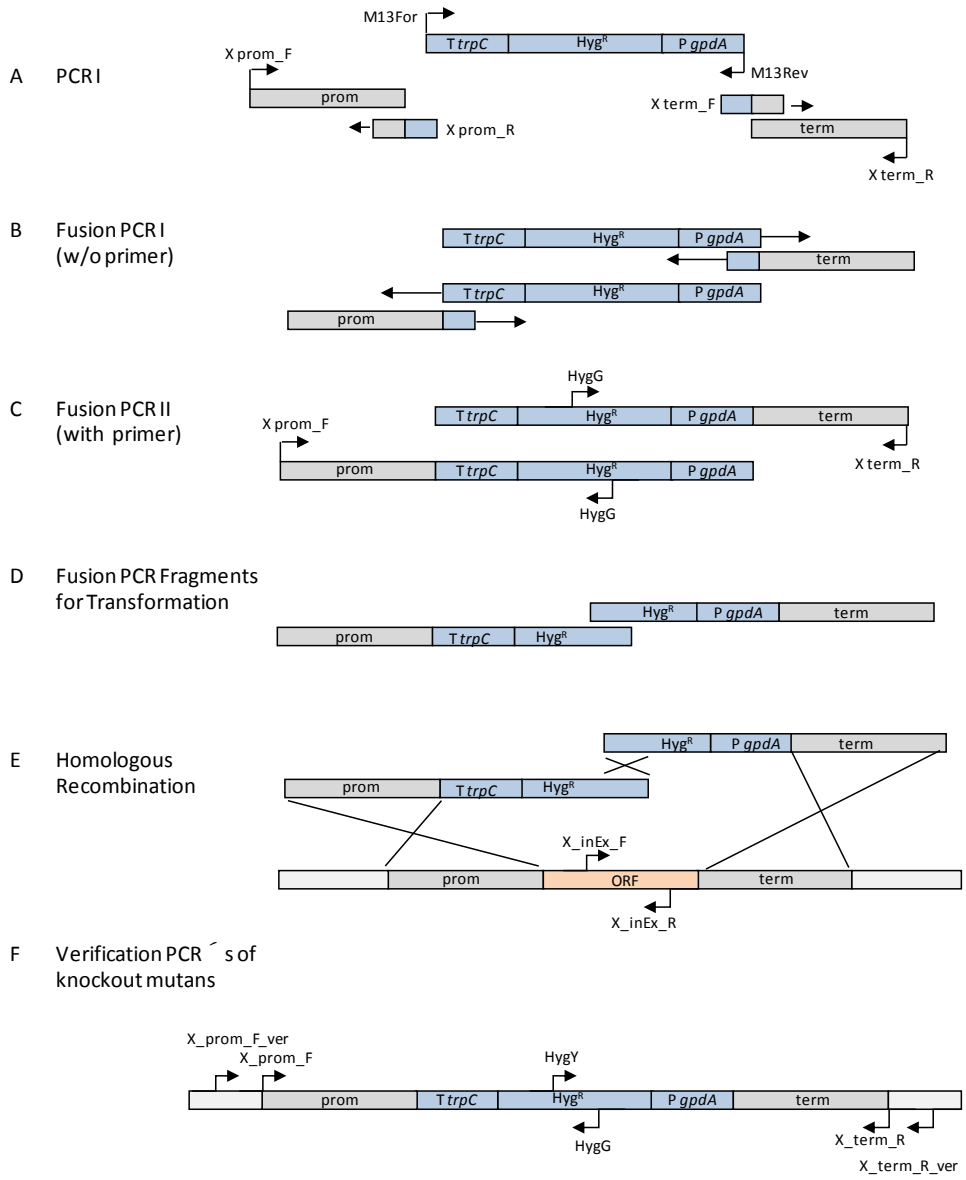

Figure 1. Schematic representation of the Fusion PCR technique used to generate split-maker for gene knockout in *F. oxysporum* via homologous recombination. Amplifiaction of the upstream (prom region) and downstream region (term region) of the target gene with primer which contain homolgoues tails to the Hygromycin resistance cassette. The PCR products obtained are used as templates for a PCR reaction with no oligos (PCR2), resulting in annealing of complementary template sequences and extension by the polymerase. The final reaction (PCR3) uses the PCR2 product as a template for amplification with the external primer and the primer set inside the Hyg cassette. Transformation with the two PCR fragments resulting in homologous recombination and reconstruction of the complete Hyg cassette inside the target gene locus.

2.3.6. Generation of a *F. oxysporum* cDNA library

The cDNA for the library was generated by using the SMART™ technology (Matchmarker™ Library Construction& Screening Kits User Manual, Clontech) following the manufacturer´s instructions with some modeifications. Complete RNA were extracted (as described in section x) of *F. oxysporum* growing in liquid MM media. The first strand synthesis was performed using CDS III primer (hybridize to the 3`-end of poly A^+RNAs) following the manufacture protocols for the SMART™ technology but with 20 reactions (total volume 320 µl first strand synthesis). From the first-strand cDNA 160 µl were used for the Long-Distance PCR with a total volume of 3200 µl aliquoted in 64 PCR tubes with V_{fin}: 50 µl. The Long-Distance PCR was performed by using the Expant High Fidelity Polymerase (Roche) and 22 PCR cycles where the number of thermal cycles used based on the amount of RNA used in the first-strand synthesis and fewer cycles are better to avoid nonspecific PCR products. The cDNA was precipitated to V_{fin}: 200 µl. After agarosegel confirmation Nanodrop measurement reveal a concentration of 4700 ng/µl cDNA. A total volume of 100 µl was loaded through CHROMA SPIN™ TE-400 Columns to fractionate and select for cDNA > 200 pb and resulted in Vfin: 200 µl cDNA with a concentration of 260 ng/µl. This cDNA was diluted for test transformation before used for the yeast library construction.

2.4. Protein methods

2.4.1. Protein purification from *F. oxysporum* mycelia

For analysis of cytosolic proteins in whole cell extracts 200 to 500 µl of ice-cold protein extraction buffer A or B (B for urease activity assay) dependent on the experimental procedure was added to approximately 100 mg of frozen mycelium and homogenized with the T 10 basic ULTRA-TURRAX (IKA®) followed by strong vortexing. After centrifuging at 4°C to pellet cell debris the supernantant was either quantified and used in subsequent experiments (B) or stored at -80°C (A).

(A) 10% glycerol, 50 mM Tris-HCL pH7.5, 150 mM NaCl, 0.1 % SDS, 1% Triton, 5 mM EDTA, 1 mM PMSF and Protease inhibitor cocktail (Sigma, P8215).

(B) 40 mM Tris-HCl, 20 mM dithiothreitol [DTT], 4% Triton X-100, 1 mM EDTA, 2 mM phenylmethylsulfonyl fluoride [PMSF], protease inhibitor cocktail (Sigma, P8215), pH 9

2.4.2. Protein purification from *F. oxysporum* culture supernatants

For detection of the urease activity in culture supernatants, germlings from PDB were obtained as described in section x, washed twice in sterile water, transferred to liquid MM + 50 mM urea and incubated at 28ºC at 170 rpm. Culture supernatants were harvested after 7 h of incubation, sterile filtered (0.22 µm pore size) and dialyzed in pre-treated cellulose membranes ((A) Sigma) against various changes of distilled water for 24h at 4°C and lyophilized. Samples were resuspended in protein extraction buffer B (see above) and ammonia secretion was measured spectrophotometrically over time (see below).

(A) Cellulose membranes have to be pre-treated before using by boiling for 10 minutes in 2% sodium bicarbonate EDTA solution (B) followed by washing steps (rinse twice in H_2O) and followed by a second boiling for 10 minutes in 1 mM EDTA, pH 8.2 (C). After cooling down cellulose membranes were stored in a fresh and sterile 1 mM EDTA solution pH 8.2 at 4°C

(B) 20g Sodium bicarbonate; 2 ml EDTA, pH 8.2 in 1 l H_2O

(C) 800 µl EDTA, pH 8. 2 in 800 ml H_2O

2.4.3. Determination of protein concentration

Protein concentration of cell extracts was determined photospectrometrically (959 nm) with the Bio-Rad protein assay reagent, using bovine serum albumin as standard and following the manufacturer´s instructions.

2.4.4. Western blot analysis

For western blot analysis, 100 µg of total protein was resuspended in protein loading buffer (1) and separated in 5 to 20% gradient SDSpolyacrylamide gels (Laemmli, 1970) at constant voltage, using Tris-HCl/glycine/SDS as running buffer (2). The gel was transferred to

nitrocellulose membranes (Bio-Rad) using the Mini Trans-blot® Cell (Bio-Rad) and a transfer buffer (3) at constant voltage (100 V at room temperature for 2 hours). For Western blot analysis, membranes were blocked using 5% non-fat skimmed milk for 1 h. p44/42 MAP kinases were detected using the Phospho Plus p42/p44 MAP Kinase (Thr202/Tyr204) Antibody kit (Cell Signaling Technology, Beverly, MA) according to the manufacturer´s instructions, except that ECL Plus immunoblotting reagent (GE Healthcare, Barcelona, Spain) was used for detection. Monoclonal α-actin antibody from Sigma (A3853) was used as a loading control.

(1) 50 mM Tris-HCl, pH 6, 8; 8% glycerol (v/v); 1,6% SDS w/v; 4% β- mercaptoetanol (v/v); 0,1% bromophenol blue

(2) 50mM Tris-HCl, 400 mM glycine, 0.02%, SDS

(3) 48mM Tris-HCl pH 7.5, 39 mM glycine, 0.0375% SDS, 20% methanol

2.4.5. Protein interaction using small-scale Yeast Two -Hybrid

To determine protein-protein interaction, the Y2H approach was used following the manufacturer´s instructions (Matchmarker™ Gold Yeast Two-Hybrid System User Manual, Clontech). Briefly, the cDNA of the proteins of interest were raised for full-length of the sequences by amplification using gene specific primer containing a homologous tail to the bait vector, pGBKT7-BD or the prey vector, pGADT7-Rec-AD of the Match-Marker Gold Yeast-Two Hybrid system (Clontech). The cDNA`s were inserted via homologous recombination during transformation into the pre-linearized bait and prey vectors into the yeast strains Gold and Y187, respectively. Positive transformants were obtained on selection media according the nutritional marker of the plasmid and transfomation efficiency was calculated. The correct in-frame cloning of the required gene in the bait and prey vectors was confirmed by sequence analysis before proceeding. Analysis of the interaction between target proteins were carried out by yeast mating in a small-scale format and preformed according to the manufacturer`s protocol with little modification. In brief, a 2-3 mm colony of each strain was picked and placed into one 1,5 ml Eppendorf centrifugation tube containing 500 µl 2x YPDA and mixed by vortexing. The mating of the positive and negative control strains provided by

the kit was performed always in parallel. The mating was performed by incubating on a shaker (200 rpm) at 30 °C over night (20-24h). From this mated culture 100 µl of several dilutions was spread on selection plates. On SD-Trp the survival of the bait and on SD-Leu the survival of the prey plasmid was calculated. The colonies on the mating media SD-Trp/-Leu (double-drop-out media without tryptophane and leucine) were used to calculate the mating efficiency. The positive protein interactions were obtained via blue colonies on DDO/X/A (without tryptophan, leucine, adenne, and histidine and with or without aureobasidine A and X-α-Gal) selective-media agar plates for screening of positive clones. Optional several dilutions were done with colonies from the mating media (SD-Trp/-Leu) and spotted on selection media to confirm or exclude protein interactions.

2.5. Genetic transformations

2.5.1. Competent cells S. cerevisiae

Competent Yeast cells were prepared using the LiAc method as described in "Matchmarker™ Library Construction & Screening Kit User Manual" (Clontech) with some changes. Briefly, 3 ml YPDA was inoculated with one colony of *S. cerevisiae* growing on YPDA plates (fresh streaked from -80 stocks) and incubated at 30°C with shaking. After 8 h 50 µl of these pre-culture was transferred into 50 ml YPDA (250 ml flask) and incubated on a shaker at 30°C over night (14-16h). When the OD_{600} reached 0, 15-0, 3 the cells were centrifuged for 5 minutes at 700 g at room temperature. After discarding the supernatant the pellet was resuspended in 100 ml of YPDA media and incubated additional 3-5 h at 30°C with shaking until OD_{600} 0,4- 0,5. (Important: not to overgrow the culture) After centrifugation for 5 minutes at 700 g the supernatant was discarded and the cells were washed with 60 ml H_2O. After, cells were resuspended in 3 ml of fresh prepared 1.1xTE/LiAc (1) solution split into two Eppendorf centrifuge tube and centrifuged 15 sec. at high speed. Supernatants were discarded and each pellet was resuspented in 600 µl of 1.1xTE/LiAc solution.

(1) Prepare always fresh: 1.1 ml of 10x TE with 1.1 ml of 1M LiAc (10x), add H_2O until 10 ml

2.5.2. Transformation of *S. cerevisiae*

Transformation was performed as described in the "Yeastmaker TM Yeast Transformation System 2 User Manual" (Clontech) and using the competent *S. cervisiae* cells as described above. Briefly, for transformation in a "small scale" (in contrast to Libray scale) in a pre-chilled tube were mixed 125 ng plasmid DNA (pre-linearized pGBKT7/pGADT7) together with 166 ng cDNA (amplified with primer who added a tail for homologous recombination) and 5 µl Yeastmaker Carrier DNA (denaturated by heating at 95°C-100°C for 5 minutes, cooled on ice and repeated again just before adding). 50 µl of the competent Yeast cells were added and mixed gently by pipetting before 500 µl of PEG/LiAc were added and mixed gently. The transformation mix was incubated at 30°C for 30 minutes and mixed by gently vortexing every 10 minutes. Then 20 µl of DMSO was added and incubated at 42°C for 15 minutes with gently mixing every 5 minutes. After the cells were centrifuged at high speed for 15 sec, the supernatant was removed and cells were resuspented in 1 ml YPD Plus media (optional 2x YPDA medium) and incubated 30-60 minutes at 30°C. After centrifugation the cells were resuspended in 1 ml of 0, 9% (w/v) NaCl solution (optional H_2O). 100 µl of the transformation mix (diluted 1/10 and 1/100) was spread on the appropriate selection media and incubated upside down at 30°C until colonies appear after 3-5 days. For transformation with the pGBKT7 plasmid SD/-Trp and for the pGADT7 plasmid SD/-Leu were used. Transformation efficiency (TE) was calculated as described below (2).

(1) PEG/LiAc (always fresh prepared): mix 8 ml of 50% PEG 3350 with 1 ml of 10x TE Buffer and 1 ml of 1M LiAc (10x)

(2) TE= (cfu x suspension volume (ml) / volume plated (ml) x amound of DNA (µg)) x dilution factor

2.5.3. Construction of the *F. oxysporum* cDNA library in *S. cerevisiae*

After generation of the cDNA (SMART™ technology) followed the manufacturer´s instructions (Matchmaker™ Library Contruction & Sceening Kits, User Manual, Clontech) and descriped in section x, the library construction was performed following the manufacturer´s instructions (Make Your Own "Mate and Plate™" Library System User Manual, Clonetech)

with some aberrations. It is important to calculate the transformation efficiency to determine the number of independent clones in the cDNA library. To cover a large part of the *F. oxysporum* expressed genes, the library should contain >1 million independent clones. The first "library scale" transformation did not reveal the minimum of independent clones to screen the complete genome of *F. oxysorum.* Therefore we tested different concentration of cDNA together with plasmid DNA for the optimal transformation efficiency to reveal the desired library titer which is necessary to have > 1 million independent clones in our library. This value depends on the transformation efficiency when constructing the library. Instead of a transformation in a "library scale" we made 24 transformation aliquots in a "small scale". Transformation was performed using the total amount of 3 µg of pGADT7-Rec together with 3984 ng cDNA aliquoted in (24 x (125 µg pGADT7-Rec, 166 ng cDNA, 5 µl Yeastmaker Carrier DNA, 50 µl competent Y187 Yeast cells, 500 µl PEG/LiAc, 20 µl DMSO)) 1, 5 Eppendorf centrifugation tubes and following the transformation protocol (see section x). The transformation mix was resuspended in 1 ml 0, 9 % (w/v) NaCl, incubate for 90 minutes at 30 °C with shaking and 100 µl (1:1 dilution with 0, 9 % (w/v) NaCl) were plated on SD-Leu plates (480 plates). The expected transformation efficiency after transformation with 3 µg pGADT7-Rec together with recommended 2-5 µg cDNA should reveal ≥ $1x10^6$ transformants to have a library which contains >1 million independent clones. The transformation efficiency after transformation of 3 µg pGADT7-Rec and 3,984 µg cDNA revealed an efficiency of 1, 759 x 10^6 cfu/µg and was determined by spreading several dilutions after transformation of the library on SD-Leu plates. The same dilutions were used to calculate the number of 7 million independent clones in the library. After 3 days, the colonies on the plates were harvest using 2 ml freezing media per plate and pooled together in a flask, mixed well and 1ml aliquot were performed to store at -80 °C.

The calculation revealed that one library aliquot had a cell density of 6, 25 x 10^9 cells/ml, therefore a volume of 50 µl (~3 $x10^8$ cells) of the yeast library aliquot was used for screening procedure with via yeast mating with a bait protein.

2.5.4. Screening against a cDNA library of *F. oxysporum* by Yeast Two-Hybrid

The Y2H of msb2-CT-BD and msb2-ORF-BD (transformed into the Gold strain) against the cDNA library of *F. oxysporum* was performed following the manufacturer´s instructions (Matchmaker™ Gold Yeast Two-Hybrid System User Manual, Clontech). Before, different concentration of the bait protein and the library was tested by in a small scale and library scale for the best result of mating efficiency. The bait Gold (msb2-CT-BD and msb2-ORF-BD) was cultures until the OD_{600} reaches 0.8 (16-20h). After centrifugation (1000 g for 5 minutes) the pellet was resuspended to a cell density of 2 $x10^8$ cells/ ml. From this culture 5 ml ($1x10^9$ cells) was used for yeast mating.

After mating the library titer was recalculate to confirm it remains > $1x\ 10^7$cfu/ml. The number of screened clones was calculated by counting the colonies from the SD-Leu/-Trp plates. It is imperative that at least 1 million diploids are screened, since less will result in less chance of detection genuine interaction on Aureobasidin A plates (selection media: DDO/X/A). The number of screened clones: cfu/ml of diploids x resuspension volume (ml) = 1,573 x 10^6. Next, the mating efficiency should be more that 2% to screen more than 1 million calculated with the no. of cfu/ml of diploids (1, 43 x 10^5 cells/ml) divided through the strain with the lower viability (limiting partner, here the prey library= 7, 4 x 10^5 cells /ml) multiplied by 100. The calculation revealed a mating efficiency of 19, 32%

No. of cfu/ml on SD-Leu = viability of the prey plasmid (cDNA library): 7, 4 x 10^5

No. of cfu/ml on SD-Trp: =viability of the bait (msb2-CT):2,744 x 10^8

No. of cfu/ml on SD-Leu/ Trp= viability of diploids: 1, 43 x 10^5

2.5.5. Generation of *F. oxysporum* protoplasts

Protoplasts were obtained following the protocol described by (Powell and Kistler, 1990), with some modifications. Briefly, $5x10^8$ microconidia were inoculated into 200 ml of PDB and incubated for 14 h at 28°C with 170 rpm. After, germlings were harvested by filtration with a monodur and washed first with 500 ml of dd H_2O and after with 200 ml MgP solution (1). A sterile spatula was used to tranfer germlings from the monodur to a sterile 50 ml Falcon tube, containing 20 ml of MgP with 0.5% (w/v) Glucanex® (Novozymes) as the protoplasting

enzyme. The protoplasts were incubated in the enzyme solution for 45 minutes at 30°C with slow shaking (60 rpm), and protoplast accumulation was monitored under the microscope. When optimal number and quantity of protoplasts were achieved, the sample was filtered through a double layer of monodur nylon filters and washed with 400 ml of STC solution (2). The flow-through containing the protoplasts was collected in pre-chilled ice-cold 50 ml centrifuge tubes. Filtrates were centrifuged at 4°C and 1500 g for 15 minutes to collect protoplasts, which were carefully resuspended in 1 ml STC and counted. The protoplast suspension was adjusted to a final concentration of 2 x 10^7 protoplasts and stored as 100 µl aliquots in Eppendorf tubes to be used directly for transformation. For long-term storage at -80°C, 10% of PEG (3) (v/v) and 1% DMSO (Merck) (v/v) were added.

(1) MgP solution: 1.2 $MgSO_4$; 10 mM Na_2HPO_4, pH 5.8-6.0 adjusted with orthophosphoric acid .

(2) STC solution: 0.8 M sorbitol; 50 mM $CaCl_2$ y 50 mM Tris-HCl, pH 7.5.

(3) PEG solution: 60% polyethylene glycol MW 4000 (p/v) in 0.6 M MOPS.

2.5.6. Transformation of *F. oxysporum*

Transformation was performed as described (Malardier et al., 1989), with slight modifications. 2-3 µg of transforming DNA were mixed with 10 µl of 0.1 M aurintricarboxylic acid (ATA), a potent inhibitor of nucleases, in a final volume of 60 µl with TEC solution (1). For cotransformation experiments, 1, 5 µg of the DNA construct conferring antibiotic resistance was added. For the negative transformation control 50 µl of TEC was mixed with 10 µl of ATA in an additional tube and treated like the transformation mix in the following procedure. The 2 mixes were incubated on ice for 20 minutes in parallel with 2 tubes of 100 µl protoplasts (2x 10^7) generated as described above. Next, protoplasts and DNA solutions were carefully mixed and incubated a further 20 minutes on ice. Then, 160 µl of PEG solution were added and mixed carefully, followed by 15 minute incubation at room temperature before 1 ml of STC solution (described above) was added. The tube was centrifuged for 5 minutes at 3000 rpm to pellet protoplasts, which were resuspended in 200 µl of STC. Next, 50 µl aliquots were mixed with 3 ml of top agar (2) at 45°C and spread onto plates containing

25 ml of solid regeneration minimal medium (3). Four transformation controls were made. To calculate the protoplast regeneration 10 µl of the negative control mix was diluted 10^{-4} and 10^{-5} with STC and spread on plates without antibiotic. A 10^{-5} dilution made with H_2O leads to burst of the protoplasts and allows the determination of conidia which inhibits the transformation efficiency. The antibiotic control was performed by spreading the rest of the negative control (190 µl) on regenerations media containing the appropriate antibiotic. Plates were incubated at 28°C for 2 hours or 16 hours before addition of 3 ml of top agar containing 2 mg of hygromycin B or 160 µg of phleomycin, respectively. Incubation at 28°C was prolongued for 4-5 days until transformant colonies became were visible. Colonies were transferred to PDA plates with selective medium, and transformants were submitted to two consecutive rounds of single monoconidial purification on selective PDA plates.

(1) TEC solution: 10 mM Tris-HCl, pH 7.5; 1 mM EDTA and 40 mM CaCl2.

(2) Top agar: 0.4% agar (Oxoid) (w/v) in regeneration minimal medium.

(3) Regeneration minimal medium (1 l): 0.5g $MgSO_4$ x $7H_2O$; 1g KH_2PO_4; 0,5g KCl; 2 g $NaNO_3$; 20 g glucose, 200g sucrose and 12,5 g oxoid agar (12.5 g/l for Petri dishes and 4 g/l for top agar).

2.5.7. Generation and confirmation of *F. oxysporum* knockout strains

The *F. oxysporum* gene disruption constructs were generated by the fusion PCR technique. As described in section x. A ~1500 bp upstream fragment and a ~1500 bp downstream fragment relative to the *F. oxysporum* gene open reading frame (ORF) were amplified from genomic DNA using PCR with primer pairs X_prom_for and X_prom_rev and X_term_for and X_term_rev, respectively, where the X stands for the individual gen name (Table 1). The hygromycin B resistance gene, under the control of the *A. nidulans* gpdA promoter and trpC terminator (Punt et al., 1987) cloned into the pGEMT vector was amplified with the universal primers M13-For and M13-Rev. The three obtained PCR fragments were used for a final fusion PCR (Figure x). For targeted gene knockout, the *F. oxysporum* gene fusion constructs were used to transform protoplasts of *F. oxysporum* wild type strain 4287. Hygromycin-resistant transformants were selected and purified by monoconidial isolation as described

above. Gene knockout was confirmed by diagnostic PCR analysis. Therefore different primer combinations were used. By using the primer pair X_promF_ver/X_termR_ver which binding by encompassed the entire knockout construct, should give a fragment in the wt and knockout situation. A successful gene knockout was confirmed by differentiation of the fragment size, where the knockout band was bigger when the gene was smaller than the hygromycin cassette. In the case of an ectopic integration of the knockout construct we obtained the two amplicons in the gel. Additional PCR`s were done to confirm the successful integration of the fusion PCR constructs. With the primer pair X_promF/HygG and X_termR/HygY, which should amplified only in transformants, were confirmed the integration of the promoter and terminator region, respectively. A negative control was performed by using the primer pair X_InEx_F/X_InEx_R which binds within the gene and gave an amplicon only in the genomic wt situation.

2.5.8. Generation of gene complemented strains

A PCR fragment encompassing the entire gene to complement the corresponding gene knockout was obtained by a PCR amplification from genomic DNA with primers X_prom_for and X_term_rev which was introduced into protoplasts of the knockout strain by cotransformation with the phleomycin resistance cassette amplified from plasmid pAN8-1 (Punt et al., 2008) with the universal primers M13-For and M13-Rev. Phleomycin-resistant transformants were isolated as described before. The integration of the gene construct in the corresponding knockout mutant was confirmed by different diagnostic PCR`s. The primer pair X_prom_F/InEx_R and X_term_R/InEx_F gave an amplicon when the complementation construct was integrated into the knockout genome. Optional the primer pair X_InEx_F/X_In_Ex_R was used which amplified a small fragment within the gene. Whereas the primer pair X_prom_F_ver/InEx_R and X_term_R_ver/InEx_F gave an amplicon only in these transformants where the construct was integrated into the gene locus by replacing the hygromycin cassette.

2.6. Phenotypical assays

2.6.1. Vegetative growth assay

For phenotypic analysis of colony growth, drops of water containing several microconidia concentration were spotted onto YPD or MM agar plates and plates were incubated at 28°C for 3 days. For cell wall stress assays 30 µg/ml Calcofluor white (Sigma) were added to 50 mM MES (10, 66 g/l) -buffered SM agar, pH 6.5 (Ram and Klis, 2006). The pH indication Bromcresol purple (stock solution 5 ml/l) was added to MM media 0, 5% (v/v). Preparation of stock solutions from these compounds is summarized in Table 7. All experiments included three replicates and were performed at least three times with similar results.

Table 7. Preparation of stock solutions for fungal and bacteria media.

Component/Company	Preparation	Storage
Calcofluor white (CFW); Sigma	1% (w/v) with 0.5% (w/v) KOH and 83% glycerol (v/v), Stock: 10 mg/ml	-20 C in the dark
Urea (Merk, Cas:5 7-13-6)	Sterile filtrated stock solution (0,5 M)	Room temperature
Arginine (Sigma)	Sterile filtrate stock solution (0,5 M)	4°C
Bromcresol Purple	Stock (0,09g/10 ml)	Room temperature
Hygromycin	Stock (50 mg/ml)	-20 °C
Phleomyin	Stock (20 mg/ml)	-20 °C
Ampicillin	Stock (50 mg/ml)	-20 °C
Kanamycin	Stock (50 mg/ml)	-20 °C

2.6.2. Cellophane penetration

For cellophane invasion assays (Prados-Rosales and Di Pietro, 2008) autoclaved cellophane sheets were placed on MM plates and the centre of each plate was inoculated with 5 µl of 2 x 10^7 microconidia per ml. After 3 days at 28°C, the cellophane sheet with the fungal colony was removed carefully. The presence or absence of fungal mycelium on the underlying medium was recorded after incubation of the plates for an additional 24 h at 28°C. All experiments included three replicates and were performed three times with similar results.

2.6.3. Culture condition for ammonia secretion and pH assays

F. oxysporum (5x 10^8) microconidia were inoculated in 100 ml PDB and incubated for 14 h with shaking (170 rpm) at 28 °C. Germlings were washed with sterile ddH_2O and shifted in

liquid 50 ml MM media (time point T=0) containing the different nitrogen or carbon sources and incubated on a shaker (170 rpm) at 28°C. At different time points 600 µl aliquots were taken, centrifuged and the supernatant splited into two tubes. The pH was measured directly with a pH electrode for microsamples (<100 µl, 5028 Crison). The second tube was stored at -80 to measure ammonia and/or glucose concentration.

For ammonia measurement of the protein extracts against the supernatants, all samples were adjusted to the same volumes to calculate the ammonia concentration according to the initial culture volume of 50 ml. The ammonia assay was done in Multilabel Microplates with following volumes. 160 µl of the protein extract or supernatant (either directly after dialysis or after lyophylization and 10x concentrated) was added to 20 µl of 10x urease reaction buffer (1) and 20 µl of urea (0, 5 M) mixed well and incubated at 37 °C. 5 µl of the reaction mix was taken every 30 minutes, absorbance was measured and used to calculate ammonia production over time as describe below.

(1) Urease reaction buffer (1x): 10 mM potassium phosphate, 10 mM lithium chloride, 1 mM EDTA, pH 8.2

2.7. Ammonia measurement

Ammonia was determined with the Ammonia Assay Kit (Sigma) following the manufacture instruction with following modifications. The measurements were done in multi-well plates and absorbance at 340 nm was determined in a Multilabel Microplate Reader (Spectrafluor Plus, TECAN). 5 µl of the culture supernatants (diluted 1:25) was incubated with 100 µl of the Ammonia Assay Reagent for 5 minutes and absorbance were measured at 340 nm. After adding 10 µl of the enzyme L-Glutamate Dehydrogenase (1:10 diluted with 50 mM PO_4 buffer, pH 7, 4) the plate was incubated for 5 minutes and measured again. The absorbance was calculated with a standard curve (NH_4NO_3 in a concentration rage from 2, 5 mM- 0, 0625 mM). For the standards, absorbance at 340 nm was ploted (nm; y axis) vs. concentration of ammonia (mM; x axis) and the concentration of ammonia (mM) was calculated using the standard curve formula and multiplied by the dilution factor in sample preparation.

2.8. Glucose measurement

Glucose concentrations were determined with the Glucose (GO) Assay Kit (Sigma) following the manufacture instruction with following modifications. The measurements were done in multi-well plates and absorbance at 540 nm was determined in a Multilabel Microplate Reader (Spectrafluor Plus, TECAN). Therefore, 40 µl of the culture supernatants (1: 500 diluted) were mixed with 80 µl of fresh prepared Assay Reagent (A) and incubated 30 minutes at 37°C. After 30 minutes the reaction was stopped by adding 80 µl of H_2SO_4 12N. The absorbance was calculated with a standard curve (80 mg- 10 mg) using the provided glucose standard. For the standard absorbance at 540 nm (nm; y axis) was plotted vs. the concentration of glucose (mg, x axis) and the concentration of glucose (mg) was calculated using the standard curve formula and multiplied by the dilution factor in sample preparation.

(A) Glucose Oxidase/Peroxidase Reagent was prepared by adding 39, 2 ml of H_2O. O-Dianisidine Reagent was resuspended in 1 ml of H_2O. The Assay Reagent was always prepared fresh as a 1: 50 dilution of o-Dianisidine Reagent and Glucose Oxidase/Peroxidase Reagent.

2.9. Infection assays

2.9.1. Fruit infection

Invasive growth assays on apple slices (cultivar Golden Delicious) were carried out as described (Di Pietro et al., 2001; Sánchez López-Berges et al., 2009), using three replicates. Briefly, apple slides were inoculated with 5 µl of a freshly obtained microconida suspension (2×10^7 microconidia per ml) and incubated in a humid chamber for 3 days at 28°C. Invasive growth was documented either by scanning the apple slides or by measuring the diameter of the infected tissue area.

2.9.2. Plant root infection

Tomato root infection assays were performed in a growth chamber as described (Di Pietro and Roncero, 1998), using the susceptible cultivar Money Maker (Syngenta Seeds, Almeria,

Spain). Briefly, two week-old tomato seedlings were inoculated with *F. oxysporum* strains by immersing the roots in a microconidial suspension (2, 5 x 10^8/50 ml H_2O) planted in vermiculite and maintained in a growth chamber. Ten days after inoculation, severity of disease symptoms was recorded with indices ranging from 1 (healthy plant) to 5 (dead plant) (Huertas-González et al., 1999). The dates of termination of plants were used to determine survival after challenge. Survival was calculated by the Kaplan-Meier method with the software GraphPad Prism 5. Ten plants were used for each treatment.

2.9.3. Gene expression in infected roots

For analysis of gene expression in *F. oxysporum* during infection of tomato plants, roots of 2 week old plants of the susceptible cultivar Money Maker (Syngenta Seeds, Almeria, Spain) were immersed into microconidial suspensions of the different strains in sterile water (2.5 x 10^6 ml^{-1}) for 48 h at 28°C. Roots with adhering mycelium were collected, frozen in liquid nitrogen and processed as normal mycelium for RNA extraction.

2.9.4. *Galleria mellonella* infection

G. mellonella infection was performed as described in Navarro-Velasco et al. 2011. Briefly, *G. mellonella* larvae in the final larval stage were obtained from the company animal center, s.c.p., Valencia (Spain) maintained in glass bottles with sterile artificial diet in the dark and used within 2 days from the day of shipment. Larvae between 0.2 and 0.3 g in weight were employed in all assays. 15 randomly chosen larvae per treatment were used in each experiment. A Burkard Auto Microapplicator (0.1–10 ll; Burkard Manufacturing Co. Limited, Hertfordshire, UK) with a 1 ml syringe (Terumo Medical Corporation, Somerset, NJ) was used to inject 8 µl of microconidial suspension in (2x 10^7 microconidia/ml in 1x PBS) into the hemocoel of each larva through the last left proleg. Before injection, the area was cleaned using an alcohol swab. Larvae injected with 8 µl PBS served as controls. After injection, larvae were incubated in glass containers at 30 °C, and the number of dead larvae was scored daily. Larvae were considered dead when they showed melanisation (Figure 2C) and displayed no movement in response to touch. The Kaplan–Meier test was used to assess statistical significance of differences in survival among groups using Graph Pad Prism 5. Differences

indicated with a P value of less than <0.05 were considered significant. Each experiment was performed at least three times with similar results.

Figure 2. Inoculation with *F. oxysporum* wt microconidia leads to melanisation (B) and death (C) of *G. mellonella* larvae.

2.9.5. In vivo gene expression in infected *G. mellonella*

For determination of fungal gene expression, groups of 10 insects were injected with 2 x 10^4 microconidia per larva and incubated at 30 °C as described above. Forty eight hours after infection, three randomly chosen larvae per group were sacrificed, homogenized individually in liquid nitrogen and RNA isolation was performed as described in X. *F. oxysporum* gene sequences for qRT-PCR were determined by BLAST search with the corresponding sequence from *Rhizophagus intraradices* (Fellbaum et al., 2011) against the BROAD Fusarium Database (http://www.broadinstitute.org/). Sequence data can be found in the *Fusarium* Genome Database under following accession numbers: *nt*: nitrate transporter (FOXG_ FOXG_00635); *gs1*: glutamine synthetase 1 (FOXG_05182); *al*: argininosuccinate lyase (FOXG_01957); *car1*: arginase (FOXG_12915); *oat*: ornithine aminotransferase (FOXG_09346); *odc*: ornithine decarboxylase (FOXG_07603); *ureG*: urease asseccory protein G (FOXG_13832); *ure1*: urease1 (FOXG_01071); *nit1*: nitrate reductase (FOXG_04181); *ure2*: urease2 (FOXG_ FOXG_17146); *Dur3*: urea transporter (FOXG_12291); *MepB*: ammonia permease (FOXG_00462)

2.9.6. Mice infection

All animal experimentation was done in accordance with UK Home Office regulations and was approved by both the UK Home Office and the University of Aberdeen ethical review committee. Female BALB/c mice (Harlan, UK; 6-8 weeks old) were maintained in groups of

up to 6 animals per cage. All mice were fed sterilized laboratory chow and water *ad libitum*. Each animal was individually marked and was weighed daily. Immunosuppression was performed by intraperitoneal injection of 150 mg cyclophosphamide (Sigma) per kg body weight, which was repeated every 3 days thereafter. For preparation of challenge inocula, microconidia were obtained by filtration as described previously (Di Pietro and Roncero, 1998) harvested by centrifugation, washed, and resuspended in sterile physiological saline. The conidia concentration was adjusted with a hemocytometer to the desired density. The actual inoculum level was confirmed by plating serial dilutions on potato dextrose agar plates (PDA; Sigma) and incubating for 24 h at 28°C. Mice were infected by intravenous injection of 0.2 ml of a conidia suspension into a lateral tail vein. Mice were observed for up to 28 days post-challenge and were humanely terminated when they showed signs of severe illness and/or their body weight reduced by more than 20% of their initial body weight. Animals culled due to severe illness were recorded as having died on the following day. Data was used to construct Kaplan-Meier survival curves, with differences determined by log rank statistics using GraphPad Prism 5.

2.9.7. Tissue burden and histopathology

When mice were culled the hearts, lungs, kidneys, spleens and livers were aseptically removed, and one half of each organ was weighed and homogenized in 0.5 ml sterile saline. Ten fold serial dilutions of this homogenate were spread onto PDA. Plates were incubated at 28°C, colonies were counted after 48 h and CFU per gram for each organ were calculated. Fungal colony counts were converted to Log_{10} and data were analysed with the software GraphPad Prism 5. The remaining halves of the organs were embedded in Cryo-M-bed (Bright Instruments, UK) and flash frozen. Sections (8 µm) were stained with Periodic acid-Schiff (PAS)-hematoxylin and examined by light microscopy. In addition, samples of spleen tissue from infected immunocompetent mice were homogenized, treated with KOH and stained with 25 µg ml^{-1} Calcofluor White (CFW) to visualize fungal structures.

2.10. *F. oxysporum* macrophage phagocytosis assay

2.10.1. *F. oxysporum* staining using Fluorescein Isothiocyanate (FITC)

To visualize *F. oxysporum* during phagocytosis assays, germlings were havested and stain with 0, 5 ml of fresh prepared FITC (Sigma, UK) in 1 mg/ml in 0.05 M carbonate-bicarbonate buffer (pH 9.6) for 20 min at room temperature in the dark. Unbound FITC was removed by washing *F. oxysporum* in 1 ml 1 x PBS. After centrifuging at 3,000 × g for 5 min the supernatant was removed and the pellet washed for three times in 1 ml 1 x PBS before the pellet was finally resuspended in 1 x DMEM medium (Lonza, Slough, UK).

2.10.2. *F. oxysporum* culture preparation for microscopy imagine

Murine J774.1 macrophages (2x 10^5m/ml) were cultured in 12 well cell culture plate (Cell star from Greiner bio-one) in DMEM media at 37°C with 5% CO_2 over night. Macrophages were co-cultured with FITC-stained *F. oxysporum* germlings as follows. *F. oxysporum* (6x 10^5 c/ml) microconidia were germinating for 8h in 1 ml DMEM media at 37 C with 5% CO_2 in multi-well plates. The germlings were stained with FITC (as described above). The DMEM media from the pre-cultured macrophage cultures was removed and the fresh DMEM media containing the FITC stained *F. oxysporum* germlings were added at a 3:1 ratio for co-incubating at 37°C with 5% CO_2. After 2h; 4h; or 8h of co-incubation the cell cultures were fixed with 4% Paraformaldehyde (2). Therefore the DMEM media was removed; 1 ml of Paraformaldehyde was added and incubated for 5 minutes in the dark. After the Paraformaldehyde was removed the cell culture plate containing *F. oxysporum* and the macrophages was washed with PBS and stored in 1 ml PBS at 4°C in the dark until microscopy investigation. Before microscopying, the *F. oxysporum* germlings were stained with CFW (25 µg/ml) by adding 25 µl of Fluorescent Brightener 28 (1mg/ml) to the culture. Fungal cells stained with CFW obtain blue and are attached or ouside the macrophaes. CFW can not enter the macrophages and phagocytosed FITC labelled fungal germlings appeared green.

(2) Dissolve 1.2g Paraformaldyde in 19 ml PBS and heat to 60 °C (add 10 µl of 5M NaOH until it is dissolve). Add 10 ml PBS and adjust pH 7.2 (approx. 5µl of 5M HCl). V_{fin} 30 ml. Sterile filtrate and store at 4°C until use.

2.10.3. Preparation and culturing of the J774.1 mouse macrophage cell line

J774.1 macrophages cell cultures were maintained in 75 cm^2 tissue culture flasks in DMEM medium supplemented with 10% (v/v) fetal calf serum (FCS), 200 U/ml penicillin/streptomycin and 2 mM L-glutamine at 37 °C with 5% CO_2. (The preparation of primary macrophages is described in detail in McPhillips et al., 2009; Erwig et al., 2006). J774.1 cells were scraped from the tissue culture flask and transfered to a 50 ml Falcon tube and centrifuged at 600 × g for 5 min to obtain a cell pellet. Supernatant was removed and the pellet was resuspended in 10 ml pre-warmed supplemented DMEM medium. Cells were counted using a haemocytometer.

2.10.4. Macrophage cell preparation for live-cell imagine

1×10^6 J774.1 macrophages were plated in 2 ml supplemented DMEM medium in a 35 mm glass-based Iwaki imaging dish (VWR, Leistershire, UK) and incubated overnight at 37 °C, 5% CO_2. Prior imaging, replace supplemented DMEM medium with 2 ml pre-warmed supplemented CO_2-independent medium (with 10% (v/v) fetal calf serum (FCS), 200 U/ml penicillin/streptomycin and 2 mM L-glutamine) containing 1 µM LysoTracker Red DND-99 (Invitrogen, Paisley, UK) (Erwig et al., 2006).

2.10.5. Phagocytosis assay using live cell video microscopy

For live-cell imaging the DeltaVision Core microscopy (Applied Precision, Washington, USA) including point-revisiting and time-lapse features with an environmental control chamber was used for the long term experiment of the live cell video of the *F. oxysporum* macrophage phagocytosis assay. The microscope setup included an inverted stage and video microscopy was conducted at an environmental chamber heated to 37 °C and excitation/emission filters for the chosen stains (FITC and TRITC). The imaging dish was mounted on the microscope

stage and the focus was adjusted to find the J774.1 macrophages. The appearance was optimized for TRITC and DIC images by adjusting the percentage of transmitted light and exposure times.

Phagocytosis assay with *F. oxysporum* was performed using a protocol previously described for *C. albicans* (Lewis et al., 2012a; Rudkin et al., 2013). F. *oxysporum* microconidia (6 x 10^5 c/ml) were germinated for 8 h in DMEM media at 37 °C with 5% CO_2, stained with FITC (as described above) and added at a 3:1 ratio to glass-based Iwaki imaging dish containing macrophages stained with LysoTracker Red (described above) in supplemented CO_2-independent medium. Video microscopy was performed at 37°C with a DeltaVision Core microscope (Applied Precision, Washingtom, USA) and images captured at 1 min intervals for 6 h by an EMCCD camera.

2.10.6. Analysis of live cell video microscopy movies

Murine macrophages were selected from eleven movies and analysed individually at 1 min intervals throughout the 6 h phagocytosis assay. Measurements taken included *F. oxysporum* uptake, defined as the number of *F. oxysporum* germlings taken up by an individual phagocyte (n=190) over the 6h period.

The rate of engulfment of *F. oxysporum* cells by macrophages (n=219) were determined by the time points at which a *F. oxysporum* cell was fully engulfed, defined as the time taken from establishment of cell-cell contact to complete ingestion of a *F. oxysporum* cell (Lewis et al., 2012a). A fungal cell was considered to have been fully ingested when the FITC fluorescent signal was diminished, indicating that the fungal cell was inside the macrophage. The percentage of macrophage killing s was defined as the percentage of macrophages (n= 194) that had been killed by specific time points over a 6 h period. Counting was used to calculate the percentage of macrophages killed by *F. oxysporum* in relation to the defined number of phagocytosed germlings over a 6 h period. Macrophage migratory responses to the presence of *F. oxysporum* were determined by tracking directional and distance components of movement between 1 minute intervals for the first 30 minutes of live video microscopy movies, as this represents a period of elevated migratory activity (Lewis et al.,

2012a). Volocity 6.3.0. software (PerkinElmer, Massachusetts, USA) was used to track and analyse 50 macrophages from 3 representative movies.

2.11. Microscopic and binocular analysis

Microscopic imagings of *F. oxysporum* were performed using the Zeiss Imager M2 from Axio Zeiss. For High-resolution three-dimensional and fluorescence imaging were performed by the stereomicroscopy (SteREO Lumar. V12, Zeiss).

For Fluorescent Microscopy of the *F. oxysporum* macrophage assays the Zeiss Axio Observer Z1 inverted microscope with motorised filter sets (DAPI, FITC) was used for imaging. For live-cell imaging the DeltaVision Core including point-revisiting and time-lapse features with an environmental control chamber was used for the long term experiment of the live cell video of the *F. oxysporum* macrophage phagocytosis assay.

2.12. Bioinformatic analysis

2.12.1. Sequence retrieval and Phylogenetic analysis

The corresponding gene sequence of putative *F. oxysporum* Msb2 interactor proteins and of putative UreG homologoues for amino acid alignments (Software: BioEdit) with other organisms were identified by BLAST search in the Fusarium Comparative Database of the Broad Institute (http://www.broadinstitute.org) and the NCBI genome Database (http://www.ncbi.nlm.nih.gov/). The phylogenetic tree was perfomed using the online program Phylogeny (http://www.phylogeny.fr) with following modulation of Tree Rendering: TreeDyn; Tree style: Cladogram (ignore branch lengths); Display branch support values in %.

2.12.2. Software

Data management and processing was performed using different software products listed in Table 8.

Table 8. Software products used in this work.

Program	Application
LaserGene (DNA-Star)	Sequence editor
	SeqBuilder ORF and restriction sites analyzer
Vector NTI ®(Invitrogen)	Sequence edition, visualize maps, cloning strategy
BioEdit	Sequence alignment
Oligo 6	Synthetic oligonucleotides design
Phylml	Phylogenetic trees computation
AxioVision	Edition and analysis of binocular and microscope Images
Fujifilm Image Reader	Obtaining, edition and analysis of chemiluminescence Images
Kodak 1D Image Analysis	Obtaining, edition and analysis of DNA and RNA gel
Espson Scan	Image scanning
Bio-Rad iQ5	Obtaining and analysis of real time RT-PCR data
Microsoft Office	Word Word processing
	PowerPoint Image presentation and processing
	Excel Data processing
EndNote	Reference and bibliography editor
Adobe Photoshop	Elements Image processing
Adope Illustrator	Elements Image processing
GraphPad Prism 5	Calculation of survival by the Kaplan-Meier method
ImageJ	Image and Live cell video processing
Carl Zeiss Vision (AxioVision 4.7)	Imaging and Image analysis
Velocity Demo (PerkinElmer)	Live cell microscopy imaging and image analysis

Chapter 1

Murine model for *Fusarium oxysporum* invasive fusariosis reveals organ-specific structures for dissemination and long-term persistence

Summary

The soil-borne plant pathogen *Fusarium oxysporum* causes life-threatening invasive fusariosis in immunocompromised individuals. The mechanism of infection in mammalian hosts is largely unknown. In the present study we show that the symptoms of disseminated fusariosis caused by *F. oxysporum* in immunosuppressed mice are remarkably similar to those reported in humans. Distinct fungal structures were observed inside the host, depending on the infected organ. Invasive hyphae developed in the heart and kidney, causing massive colonization of the organs. By contrast, chlamydospore-like survival structures were found in lung, spleen and liver. Systemically infected mice also developed skin and eye infections, as well as thrombosis and necrosis in the tail. We further show that *F. oxysporum* can disseminate and persist in the organs of immunocompetent animals, and that these latent infections can lead to lethal systemic fusariosis if the host is later subjected to immunosuppressive treatment.

The work of this chapter has been performed at the Institute of Medical Sciences, University of Aberdeen (UK), under the supervision of Professor Neil A.R. Gow and Dr. Donna MacCallum.

The results of this chapter have been published:

Schäfer K, Di Pietro A, Gow NA, Maccallum D. **Murine Model for *Fusarium oxysporum* Invasive Fusariosis Reveals Organ-Specific Structures for Dissemination and Long-Term Persistence**. PLoS One. 2014 Feb 27;9 (2)c:e89920. PMID: 24587124.

1. Introduction

Fungi of the genus *Fusarium* are important plant pathogens commonly found in soil, water and decaying organic matter (Naggie and Perfect, 2009). In addition, *Fusaria* can cause a broad spectrum of diseases in humans, ranging from superficial or localized infections in healthy hosts to lethal disseminated fusarioses in immunocompromised patients (Dignani and Anaissie, 2004).

Today, *Fusarium* is the second major cause of mould infections in immunocompromised patients after aspergillosis, and the incidence is increasing (Nucci and Anaissie, 2007). *Fusarium* species are among the most drug resistant fungal pathogens (Anaissie et al., 1991; Reuben et al., 1989; Rotowa et al., 1990) and thus associated with high morbidity and mortality rates (de Pauw and Meunier, 1999; Walsh et al., 1996). Rapid diagnosis is essential for successful antifungal therapy and survival of the patient. In many cases the entry sites of disseminated *Fusarium* infections remain unclear, but reported portals of entry include onychomycosis, the respiratory tract (particularly paranasal sinuses), the gastrointestinal tract, and the central venous lines.

However, few model systems for evaluating virulence and pathogenesis of this group of fungi have been described. Here we developed a murine infection model and use it to demonstrate that the infection symptoms caused by disseminated *Fusarium* infection in immunosuppressed mice are remarkably similar to those reported in humans (Dignani and Anaissie, 2004; Nucci and Anaissie, 2002; Nucci and Anaissie, 2007). One of the most frequent symptoms of infection by *Fusarium* species is the development of skin lesions, which are most commonly found on the extremities. They are described as painful subcutaneous nodules that can result in thrombosis and tissue necrosis (Fan et al., 2010). Skin lesions are often the only source of diagnostic material, because blood cultures remain negative in many cases, in spite of blood dissemination (Nucci and Anaissie, 2006). Therefore, it is of interest to characterize the clinicopathological features of skin lesions and their role in *Fusarium* infection and to establish them in the diagnosis and management protocols of fusariosis. Previous studies suggest that *Fusarium* can cause skin lesions even in immunocompetent individuals, and that upon immunosuppression these foci can lead to the

development of invasive and disseminated fusariosis (Boutati and Anaissie, 1997). It has been recommended that patients to undertake severe immunosuppressive therapy should undergo a thorough skin evaluation before initiation of therapy (Nucci and Anaissie, 2002).

Soil-borne *Fusarium oxysporum* is the causal agent of vascular wilt, a devastating disease affecting a large variety of economically important crops worldwide (Beckman, 1987c). *F. oxysporum* also causes invasive infections in immunosuppressed individuals, being the second most frequent species of the genus after *Fusarium solani,* (Guarro and Gene, 1995; Nucci and Anaissie, 2007). The incidence of invasive fungal infections leading to significant morbidity and mortality is rising because of the increase of the pool of immunocompromised patients caused by a dramatically increase number of solid organ transplants and the use of newer and more potent chemotherapeutic agents (Low and Rotstein, 2011). This is coupled with an increase in the number of reports of severe cases of invasive fusariosis often with lethal outcomes, due to the broad resistance to antifungal drugs (Boutati and Anaissie, 1997; Odds et al., 1998). *F. oxysporum* infections are often misdiagnosed as a result of the histopathological similarities with *Aspergillus* or non-*Aspergillus* hyalohyphomycoses (Boutati and Anaissie, 1997; Dignani and Anaissie, 2004; Nelson et al., 1994; Silveira and Husain, 2007).

Previous work established that a tomato pathogenic isolate of *F. oxysporum* f.sp. *lycopersici* can cause disseminated infection in immunocompromised mice (Ortoneda et al., 2004). The ability to cause disease in both plants and mammals makes *F. oxysporum* a unique multihost pathogen for studying fungal infection across different host kingdoms. To date several knockout mutants have been tested for virulence in immunosuppressed mice (Lopez-Berges et al., 2012; Lopez-Berges et al., 2013; Martinez-Rocha et al., 2008; Ortoneda et al., 2004; Prados-Rosales et al., 2012).

In the present study we used the *F. oxysporum*-mouse model to investigate infectious growth of *F. oxysporum* in mammals. We found that *F. oxysporum* develops distinct invasive structures, including hyphae, microconidia and chlamydospores, depending on the infected organ. We further show that *F. oxysporum* can cause thrombosis and necrosis in the tails of immunosuppressed mice, which can serve as model to study fungal skin infection in

mammals. Finally we present strong evidence for dissemination of *F. oxysporum* in immunocompetent animals. Our results suggest that latent organ infections without macroscopic disease symptoms can initiate lethal systemic fusariosis, if the host is later subjected to immunosuppressive treatment.

2. Results

2.1. Effect of inoculum size and timing of immunosuppressive treatment on the severity of *F. oxysporum* systemic infection

The effect of inoculum size on systemic infection by *F. oxysporum* in immunosuppressed mice was investigated. Intravenous inoculation with 2 x 10^7 microconidia led to rapid development of systemic infection, with all mice becoming severely ill within 24 h (Figure 1A). An inoculum of 2 x 10^6 microconidia also caused 100% mortality, however disease progression was significantly slower (p = 0.0016, with all mice dying within 5 days. Finally, inoculation with 10^6 microconidia caused a significant drop in mortality, with only two of the six infected mice succumbing to infection within the 20 d observation period (p = 0.0024).

We next tested the effect of timing of immunosuppression on disease severity. When the immunosuppressive treatment was initiated 3 d prior to infection (day -3) and repeated every 3 days thereafter, all mice succumbed to infection (Figure 1A & B). By contrast, a delay in the start of the immunosuppression (day 0) led to a significant reduction in mortality (p = 0.0009) (Figure 1B). Fungal burdens in the heart, lung and liver declined by 1-2 orders of magnitude over 18 days following inoculation, but remained at the same level in the kidneys and declined only slightly in the spleen (Figure 1C).

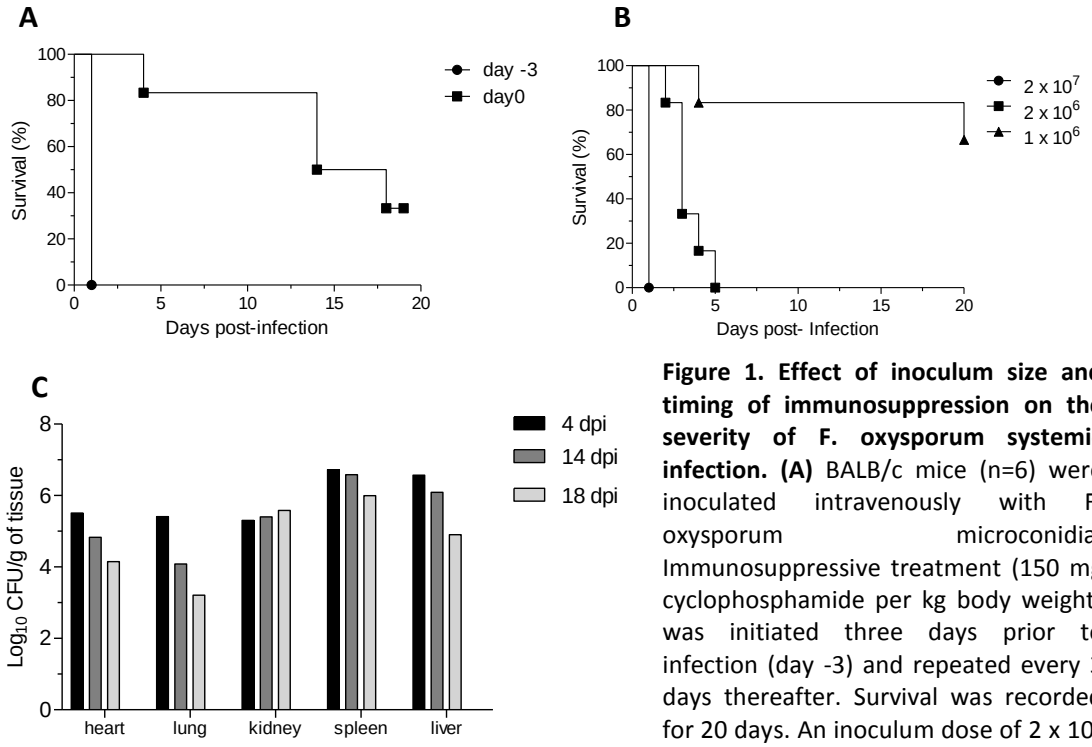

Figure 1. Effect of inoculum size and timing of immunosuppression on the severity of F. oxysporum systemic infection. (A) BALB/c mice (n=6) were inoculated intravenously with F. oxysporum microconidia. Immunosuppressive treatment (150 mg cyclophosphamide per kg body weight) was initiated three days prior to infection (day -3) and repeated every 3 days thereafter. Survival was recorded for 20 days. An inoculum dose of 2 x 10^6 microconidia caused significantly lower mortality than 2 x 10^7 microconidia (p = 0.0016); 10^6 microconidia caused significant lower mortality than 2 x 10^6 microconidia (p = 0.0024). **(B)** BALB/c mice (n=6) were inoculated with 2 x 10^7 microconidia, and immunosuppressive treatment was initiated either on day -3 or on day 0, and repeated every 3 days thereafter. Survival was recorded over 20 d. **(C)** Fungal burdens in mice immunosuppressed on day 0 and inoculated with 2 x 10^7 microconidia. On each of the indicated days post-infection (dpi), one animal was sacrificed and organ homogenates quantified.

2.2. *F. oxysporum* displays distinct invasion strategies in different organs of the host

Variations in the fungal burdens observed (Figure 1C) prompted us to conduct a histopathological analysis of the invasive growth of *F. oxysporum* in mice subjected to immunosuppressive treatment on day 0, and every 3 days thereafter. PAS-hematoxylin-staining of tissue sections revealed striking differences in fungal development between different organs. At 24 h post inoculation, a significant number of microconidia had germinated in the heart and kidney (Figure 2A & D), whereas only ungerminated microconidia were observed in lung, spleen and liver (data not shown). After 4 d post-inoculation (dpi), branched fungal hyphae had developed in the heart and kidney (Figure 2B

& E), leading to the production of large mycelial colonies and the complete invasion of the infected tissue area at 16 dpi (Figure 2C & F). Invasive growth was particularly aggressive in the kidneys (Figure 3), where the fungal biomass was detectable macroscopically on the surface of the organ (Figure 3A & C). By contrast, invasive growth was not detected in the lung, spleen and liver. Instead, *F. oxysporum* developed chlamydospore-like structures, which were detected at 4 dpi and remained visible at 16 dpi (Figure 2G, H & I).

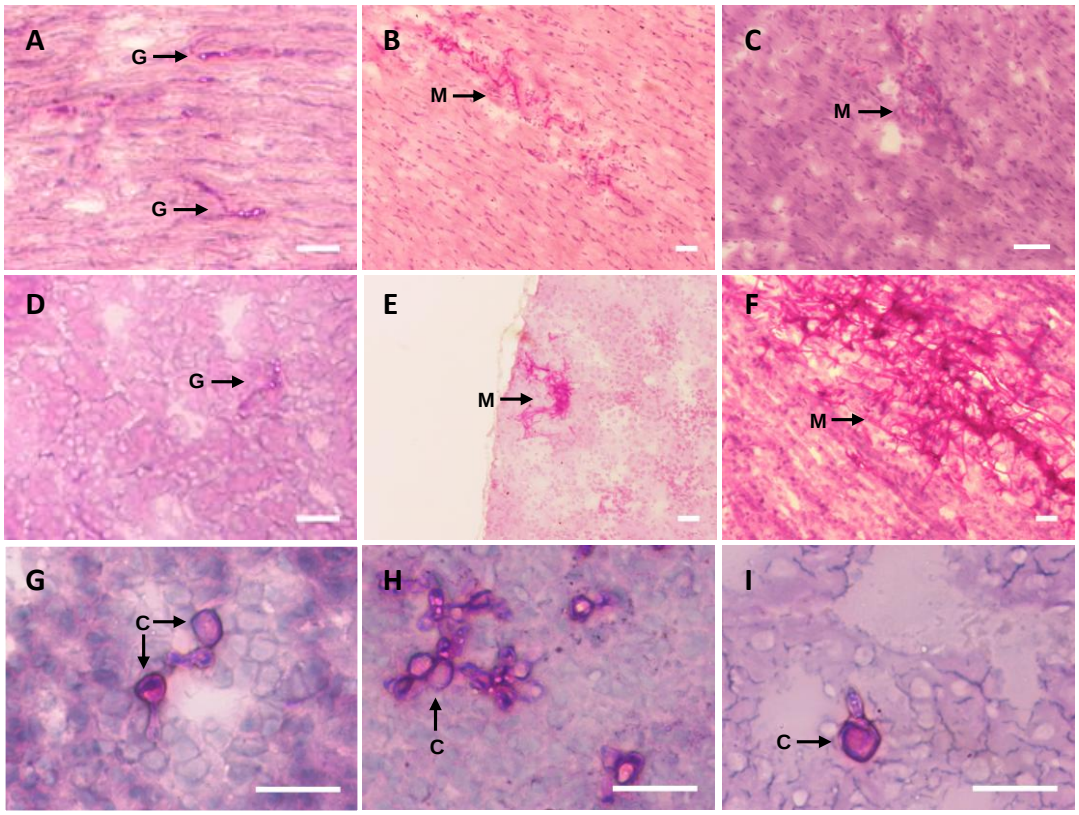

Figure 2. *Fusarium oxysporum* displays distinct growth morphologies in different organs. PAS-hematoxylin-staining of tissue sections from organs of immunosuppressed mice, on day 1 **(A, D)**, 4 **(B, E, G, H, I)** or 14 **(C, F)** post-infection with 2 x 10^7 microconidia: heart **(A-C)**, kidney **(D-F)**, lung **(G)**, spleen **(H)**, liver **(I)**. Fungal structures are indicated by arrows. G, microconidial germlings; M, mycelium; C, chlamydospores. Scale bar = 50 µm.

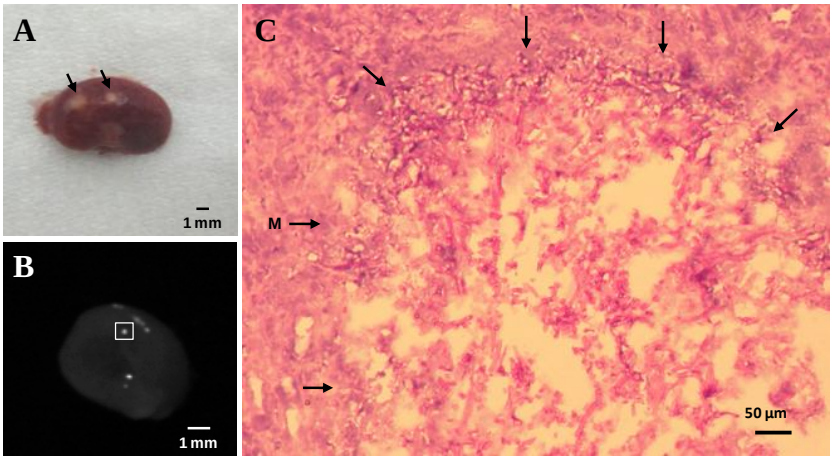

Figure 3. Invasive growth of *F. oxysporum* in the kidney. **(A)** Fungal biomass on the surface of an aseptically removed kidney from an immunosuppressed mouse, obtained 20 d after infection with 1 x 10^6 microconidia. Visible fungal lesions are indicated by arrows. **(B)** Kidney cross section from an immunosuppressed mouse infected with 1 x 10^6 microconidia and sampled at 20 dpi. Bright areas correspond to fungal biomass stained with the chitin-binding dye Calcofluor White (CFW). The white box indicates the area used for the tissue section shown in C. **(C)** PAS-hematoxylin staining of a tissue section. The area of invasive mycelial growth is surrounded by arrows. M, mycelium. Scale bars are indicated.

2.3. *F. oxysporum* causes thrombosis and necrosis in tails and infections in eyes of immunosuppressed mice

We noted that the immunosuppressed mice infected with *F. oxysporum* developed bulges and swellings which appeared at multiple sites along the tail, not restricted to the site of inoculation (Figure 4B). Some of these swellings subsequently turned into open lesions (Figure 4C & E). In addition, some mice displayed macroscopic symptoms of necrosis at the tail. The necrotic tissue was initially visible as a black region at the tip (Figure 4D & E) which spread upwards along the tail, in some cases leading to loss of the tip (Figure 4F). Calcofluor white (CFW) staining of tissue samples obtained from the open wounds revealed the presence of chlamydospores and hyphae of *F. oxysporum* (Figure 4 G & H).

Another observation associated with the presence of *F. oxysporum* in the immunosuppressed mice was the development of infection symptoms around and within the eye (Figure 4I-M). The presence of fungal structures in the infected eye tissue was confirmed microscopically (Figure 4N).

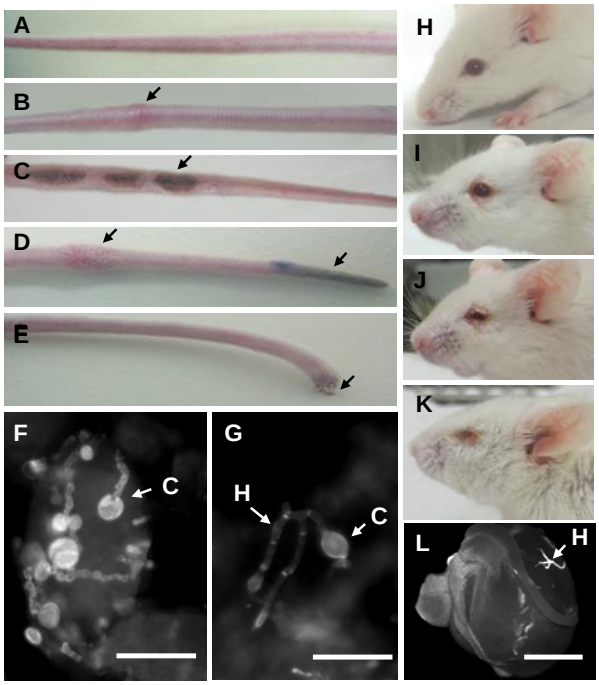

Figure 4. *F. oxysporum* causes infection in the tails and eyes of immunosuppressed mice. (A) Tail of a non-infected immunosuppressed BALB/c mouse. **(B-E)** Tails of immunosuppressed BALB/c mice intravenously inoculated with 1 x 10^6 conidia at 10 d post-infection. Macroscopic symptoms are indicated by arrows: swellings **(B,D)**, open lesions **(C)**, necrosis **(D,E)**, and loss of the tip **(E)**. **(F, G)** CFW staining of tissue samples taken from the lesion shown in **(C)**. Fungal structures are indicated by arrows. H, hyphae; C, chlamydospores. **(H-L)** Infection of the eye tissue in immunosuppressed mice infected with *F. oxysporum*. **(H)** Uninoculated mice; **(I-K)** mice inoculated with with 1 x 10^6 conidia at 10 dpi . **(L)** CFW staining of an eye removed from a immunosuppressed mice infected with *F. oxysporum.* H, hyphae. Scale bar = 50 µm **(F, G)**; 1 mm **(L)**.

2.4. *F. oxysporum* disseminates and persists in immunocompetent mice

Inoculation *F. oxysporum* typically leads to 70-100% mortality in immunosuppressed mice, whereas immunocompetent animals fail to display detectable signs of illness ((Ortoneda et al., 2004) and this work, data not shown). Thus, we investigated whether *F. oxysporum* was able to disseminate and persist in an immunocompetent host. Strikingly, fungal burdens at 4 dpi in immunocompetent mice inoculated with 2 x 10^7 microconidia were similar or only slightly lower than in animals subjected to immunosuppressive treatment on day 0, and every 3 days thereafter (Figure 5A). *F. oxysporum* microconidia and germlings were observed in the heart, lung, kidney, spleen and liver of immunocompetent animals (Figure 5C-F). At 11 dpi the fungal burdens in immunocompetent animals had declined by approximately two orders of magnitude in most of the organs, but remained relatively high (~10^5 CFU per g tissue) in the spleen (Fig 5B). Indeed, PAS-hematoxylin and CFW staining confirmed the presence of chlamydospores, as well as germinated and ungerminated microconidia in different organs of infected animals at 4 and 11 dpi (Figure 4G).

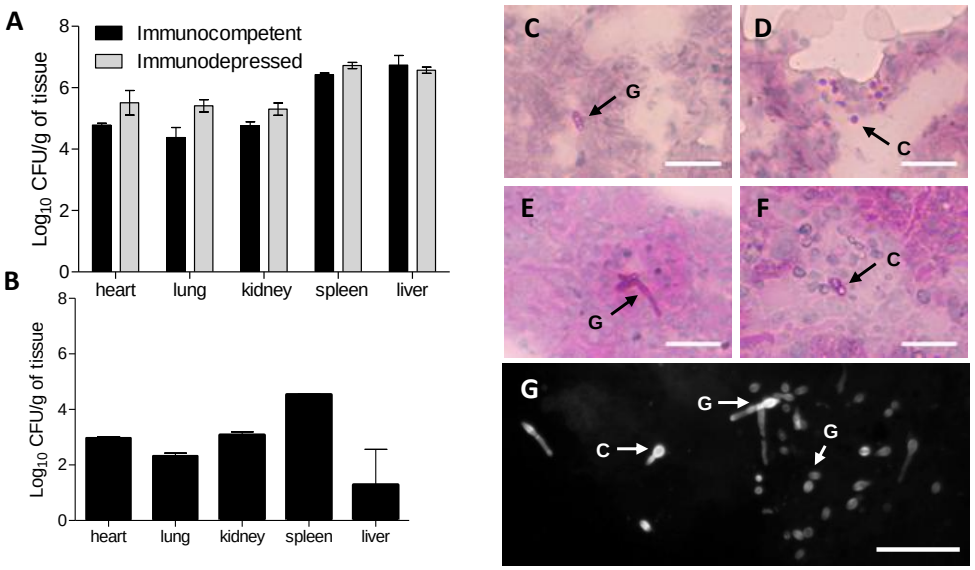

Figure 5. *F. oxysporum* disseminates and persists in immunocompetent mice. (A) Fungal burdens were determined at day 4 post-infection for groups of 3 BALB/c mice, either immunocompetent or immunosuppressed on day 0, and intravenously infected with 2 x 10^7 microconidia. **(B)** Fungal burdens in infected immunocompetent mice sacrificed at 11 d post-infection. **(C-F)** PAS-hematoxylin-staining of tissue sections obtained from different organs of immunocompetent mice sacrificed at 4 d post-infection. **(C)** heart, **(D)** lung, **(E)** kidney, **(F)** liver. **(G)** Spleen sample from an infected immunocompetent mice sacrificed at 11 d post-infection was homogenized, KOH-treated and stained with CFW to visualize fungal structures (indicated by arrows). G, microconidial germlings; C, chlamydospores. Scale bar = 50 µm.

2.5. Persistence of *F. oxysporum* in the immunocompetent host can lead to subsequent systemic infection upon immunosuppressive treatment

The presence of fungal propagules in the organs of immunocompetent mice even at >10 dpi suggests that *F. oxysporum* can develop resting structures such as chlamydospores, but also actively growing mycelium to persist within the immunocompetent host. Such a host might subsequently become susceptible to invasive fusariosis if the immune system is disrupted. When immunocompetent mice inoculated with *F. oxysporum* were subjected to immunosuppressive treatments starting at either 3 or 7 dpi and repeated every 3 days thereafter, one mouse in each group died at 16 and 15 dpi, respectively (Figure 6A). Fungal burden was determined in different organs from one of the killed mice, revealing high counts

of fungal propagules (Figure 5B). Tissue sections confirmed the presence of invasive mycelial growth in multiple organs, including heart, kidney spleen and liver, indicative of systemic fusariosis (Figure 5C-F).

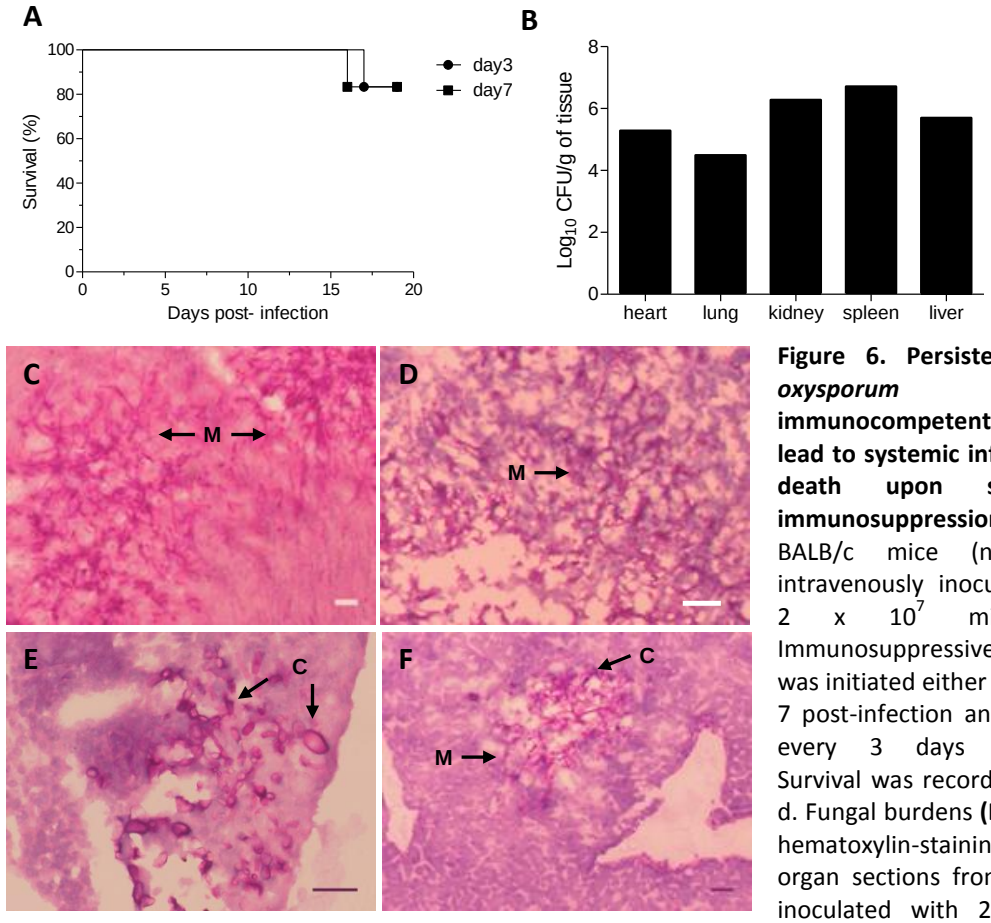

Figure 6. Persistence of *F. oxysporum* in immunocompetent mice can lead to systemic infection and death upon subsequent immunosuppression. (A) BALB/c mice (n=6) were intravenously inoculated with 2 x 10^7 microconidia. Immunosuppressive treatment was initiated either on day 3 or 7 post-infection and repeated every 3 days thereafter. Survival was recorded over 20 d. Fungal burdens **(B)** and PAS-hematoxylin-staining **(C-F)** of organ sections from a mouse inoculated with 2 x 10^7 *F. oxysporum* microconidia and subjected to immunosuppressive treatment starting at 7 dpi. The mouse that died was culled at 16 dpi. Organs: heart **(C)**, kidney **(D)**, spleen **(E)**, liver (F). M, mycelium; C, chlamydospores. Scale bar = 50 µm.

3. Discussion

Fungi of the genus *Fusarium* are common soil inhabitants and notorious plant pathogens, and have long been recognized as etiologic agents of focal infections of the skin, nails, and cornea of humans (Paul and Cecilia, 1994). Moreover, invasive *Fusarium* infections in immunosuppressed patients are associated with high mortality rates (de Pauw and Meunier, 1999; Walsh et al., 1996). Rapid antifungal therapy, achieved by a prompt diagnosis, is essential for survival of these patients. A critical step is the identification of *Fusarium,* which is often made difficult by some histopathological similarities with *Aspergillus.* Infections caused by both *Fusarium* and *Aspergillus* are characterized by hyaline branching septate hyphae at acute angles, which invade the blood vessels causing thrombosis and tissue infarction (Patterson et al., 2009; Silveira and Husain, 2007). Therefore, a detailed characterization of the invasive behaviour of *Fusarium* within the host, including growth and development of fungal structures formed by the pathogen and associated with disease, is required and will have important consequences for the diagnosis and management of fusariosis. Here we used the mouse model to investigate *Fusarium* infection in mammals. The usefulness of the animal model is highlighted by the finding that the disease symptoms observed in mice are remarkably similar to those reported in human fusariosis (Dignani and Anaissie, 2004; Nucci and Anaissie, 2002; Nucci and Anaissie, 2007).

3.1. *Fusarium oxysporum* displays distinct growth morphologies in different organs

A key result of this study is that *F. oxysporum* displays distinct invasion strategies in different organs of mice. While the fungus initiated hyphal growth 24 h after inoculation in the kidney and the heart, no such growth was detected in the spleen, liver or lung. Instead, chlamydospore-like structures were formed in these organs. This novel finding represents an important advance in our understanding of *Fusarium* infections in mammals. Chlamydospores are thick-walled cells generally developed through the modification of hyphal and conidial cells. Their formation is induced by aging or unfavorable environmental conditions such as low temperatures or carbon starvation. Chlamydospores represent the

principal structure for long-time survival during unfavorable periods in the soil, and play an important role as primary inoculum for plant root infection (Couteaudier and Alabouvette, 1990; Kono et al., 1995; Nelson, 1981a; Schippers, 1981a; Stevenson and Becker, 1972). Our findings highlight the importance of detailed histopathological analysis of infection structures, in addition to routine determination of fungal burden. For example, kidneys contained reduced fungal burdens compared to the spleen, but microscopic analysis revealed massive mycelial invasive growth in this organ, which in some instances was even visible macroscopically on the organ surface. Thus, although fungal burden is a useful parameter for assessing fungal dissemination in the host, it fails to provide detailed information on the impact of filamentous pathogens on the infected organs. It was reported previously that during *F. solani* or *A. fumigatus* infection, quantitative culture led to underestimation of absolute fungal burden as compared to non-culture-based methods such as quantitative PCR or determination of galactomannan levels by enzyme immunoassays (EIAs) (Gonzalez et al., 2013; Marr et al., 2004; Musher et al., 2004; Sheppard et al., 2006). In an inhalational rat model of invasive pulmonary aspergillosis (IPA), both real-time nucleic acid sequence-based amplification (NASBA) and qPCR showed a progressive increase of fungal biomass in lung tissue, whereas CFU counts were stable over time (Zhao et al., 2010).

3.2. *F. oxysporum* causes infection in the tails and eyes of immunosuppressed mice.

A frequent symptom associated with *Fusarium* infections is the development of superficial skin lesions, described as subcutaneous nodules that can result in thrombosis and tissue necrosis (Fan et al., 2010). In more than 60% of disseminated *Fusarium* infections skin biopsies of affected patients revealed necrosis of skin papules (Bodey et al., 2002) and microvessel thrombosis associated with fungal hyphae (Fan et al., 2010). Here we found that infection of immunosuppressed mice by *F. oxysporum* led to macroscopic symptoms in the tail, including necrosis of the skin, swellings and wounds and even loss of the tail tip. Microscopic analysis of the skin lesions confirmed that the nodules contained both chlamydospores and hyphae of *F. oxysporum*. CFW staining proved to be highly useful for

detection of progressive systemic fusariosis in the mouse system, and could therefore be used as a rapid diagnostic tool in immunocompromised patients. Because skin lesions often appear during early stages of *Fusarium* infection before the disease spreads to the trunk and the extremities, they are crucial for the diagnosis and management of fusariosis, allowing rapidly initiation of a specific treatment in order to prevent progression of skin lesions and further necrosis.

F. oxysporum keratitis is one of the most important causes of corneal ulcers, ocular morbidity and visual loss in developing nations (Bharathi et al., 2003). It is also a common type of infection caused by *F. solani* in immunocompetent individuals worldwide (Foster, 1992; Gugnani et al., 1976; Ishibashi, 1982; Jones et al., 1970; Liesegang and Forster, 1980; Polack et al., 1971). A previous study on disseminated *F. solani* infection via inoculation of microconidia in the lateral tail vein of immunocompetent mice reported disease symptoms both in intra-ocular structures and in neighbouring muscles (Mayayo et al., 1999) Here we provide evidence for the presence of fungal biomass around and within the eyes of immunosuppressed mice, associated with disseminated *F. oxysporum* infection. This result supports the view that fungal keratitis should be established as part of the diagnostic protocol for disseminated *Fusarium* infections in order to prevent a delay in diagnosis or inadequate treatment, which may lead to loss of the affected eye. Further, we observed that mice affected by disseminated *F. oxysporum* infection showed a “twister” phenotype indicating a possible infection of the brain. Supporting this idea, analysis of fungal burden in the brain of an animal displaying a twister phenotype showed the presence of fungal biomass (data not shown), suggesting that *F. oxysporum* is able to enter the mouse brain.

3.3. Persistence of *F. oxysporum* in immunocompetent mice can lead to systemic infection and death upon subsequent immunosuppression

Initiation of immunosuppressive treatment at day -3 led to death of all infected animals, while mortality was significantly lower when immunosuppression was started in parallel to infection. Thus, the immune status of the host has a major effect on the severity of infection

by *F. oxysporum*. Importantly, we show here for the first time that *F. oxysporum* can also disseminate and persist in immunocompetent individuals. Unexpectedly, fungal burdens in immunocompetent mice at 4 dpi were only slightly lower than in immunosuppressed animals, with microconidia and germlings observed in the heart, lung, kidney, spleen and liver of immunocompetent animals even after more than 10 dpi. The finding that *F. oxysporum* can persist in an immunocompetent mammalian host is highly relevant, because these fungal foci could lead to subsequent systemic infection upon immunosuppressive treatment. Indeed, one mouse in each group later succumbed to fungal infection. We conclude that invasive fusariosis in these animals was caused by chlamydospore-like structures which had persisted in the organs, suggesting that latent fungal survival structures have the potential to initiate invasive mycelial growth once the immune system is no longer effective.

Chapter 2

Hyphal growth of phagocytosed *Fusarium oxysporum* causes cell lysis and death of macrophages

Summary

Fusarium oxysporum is an important plant pathogen and an opportunistic pathogen of humans. Here we investigated phagocytosis of *F. oxysporum* by murine macrophages using live cell video microscopy. J774.1 macrophages avidly migrated towards *F. oxysporum* germlings and were rapidly engulfed after cell-cell contact was established. *F. oxysporum* germlings continued hyphal growth after engulfment by macrophages, leading to escape and associated macrophage lysis. Macrophage killing depended on the number of fungal cells engulfed by the phagocytes. After engulfment *F. oxysporum* inhibits macrophages completing mitosis, resulting in large multinucleated daughter cells fused together by means of a *F. oxysporum* hypha. These results shed new light on the initial stages of *Fusarium* infection and the innate immune response of the mammalian host.

The work of this chapter has been performed at the Institute of Medical Sciences, University of Aberdeen (UK), under the supervision of Professor Neil A.R. Gow and Professor Lars Erwig.

Results of this chapter have been submitted for publication.

1. Introduction

Fusarium species cause devastating diseases on a wide variety of economically important crops worldwide (Dean et al., 2012). In addition, *Fusaria* can cause a broad spectrum of diseases in humans, ranging from superficial or localized infections in immunocompetent hosts to lethal disseminated fusarioses in immunocompromised patients (Nucci and Anaissie, 2007). Previous work established that a tomato pathogenic isolate of *F. oxysporum* can cause disseminated infection in immunosupressed mice (Ortoneda et al., 2004; Schäfer et al., 2014). Multiple knockout mutants have been examined for virulence in the mouse model (Lopez-Berges et al., 2012; Lopez-Berges et al., 2013; Martinez-Rocha et al., 2008; Ortoneda et al., 2004; Prados-Rosales et al., 2012). However the early events of the infection process and host defence mechanisms are currently unknown.

The mammalian immune response against the two major human fungal pathogens *Candida albicans* and *Aspergillus fumigatus* relies mainly on phagocytosis of the fungus by cells of the innate immune system (Gow, 2012; Mech et al., 2011). Phagocytic clearance of fungal pathogens can be classified into distinct stages (reviewed in (Brown, 2011)): recognition of pathogen-associated molecular pattern (PAMPs) and migration towards fungal cells; cell-cell contact and engulfment of fungal cells bound to the phagocyte cell membrane; phagosome maturation and processing of engulfed cells within the phagocyte; and killing of the phagocyte by the fungus. In *C. albicans,* phagocyte killing is associated with hyphal growth within the macrophage (Lewis et al., 2012a; McKenzie et al., 2010). The invasive properties of fungal hyphae promote the escape from immune cells resulting in death of the phagocytes (Ghosh et al., 2009; Lorenz et al., 2004; McKenzie et al., 2010), whereas the yeast form promotes dissemination in the bloodstream (Kumamoto and Vinces, 2005). Murine macrophage phagocytosis displays strong preferences based on genus, species and morphology. For example, *C. albicans* yeast cells are engulfed preferentially over hyphal cells (Keppler-Ross et al., 2010; Lewis et al., 2012a).

In this study we investigated phagocytosis of the filamentous fungus *F. oxysporum* by J774.1 murine macrophages. Hyphae of this pathogen have been shown to penetrate mammalian

tissues and to cause invasive fusariosis in different organs of immunosupressed mice (Schäfer et al., 2014). Here we used live cell video microscopy coupled with image analysis tools to obtain detailed insights into all stages of the phagocytosis process, including migration, recognition, engulfment and phagocyte killing. This detailed step-by-step analysis has been reported previously only for *C. albicans* (Lewis et al., 2012a). We found that *F. oxysporum* germlings undergo rapid recognition and uptake by murine macrophages, once cell-cell contact is established. Fungal hyphae continue growth after phagocytosis, ultimately leading to their escape from the macrophages and to host cell lysis.

2. Results

2.1. *F. oxysporum* maintains hyphal growth after engulfment, resulting in lysis of phagocytes and fungal escape

To investigate the interaction between *F. oxysporum* and macrophages, we established a macrophage phagocytosis assay using live-cell video microscopy, as previously described for *C. albicans* (Lewis et al., 2012a; Rudkin et al., 2013). We found that the murine macrophages efficiently take up *F. oxysporum* germlings (Figure 1A-D). Here we examined all stages of the phagocytosis assay consisting of migration, recognition, engulfment and fungal escape, followed by macrophage cell lysis (presented in snapshots Figure 2B-F).

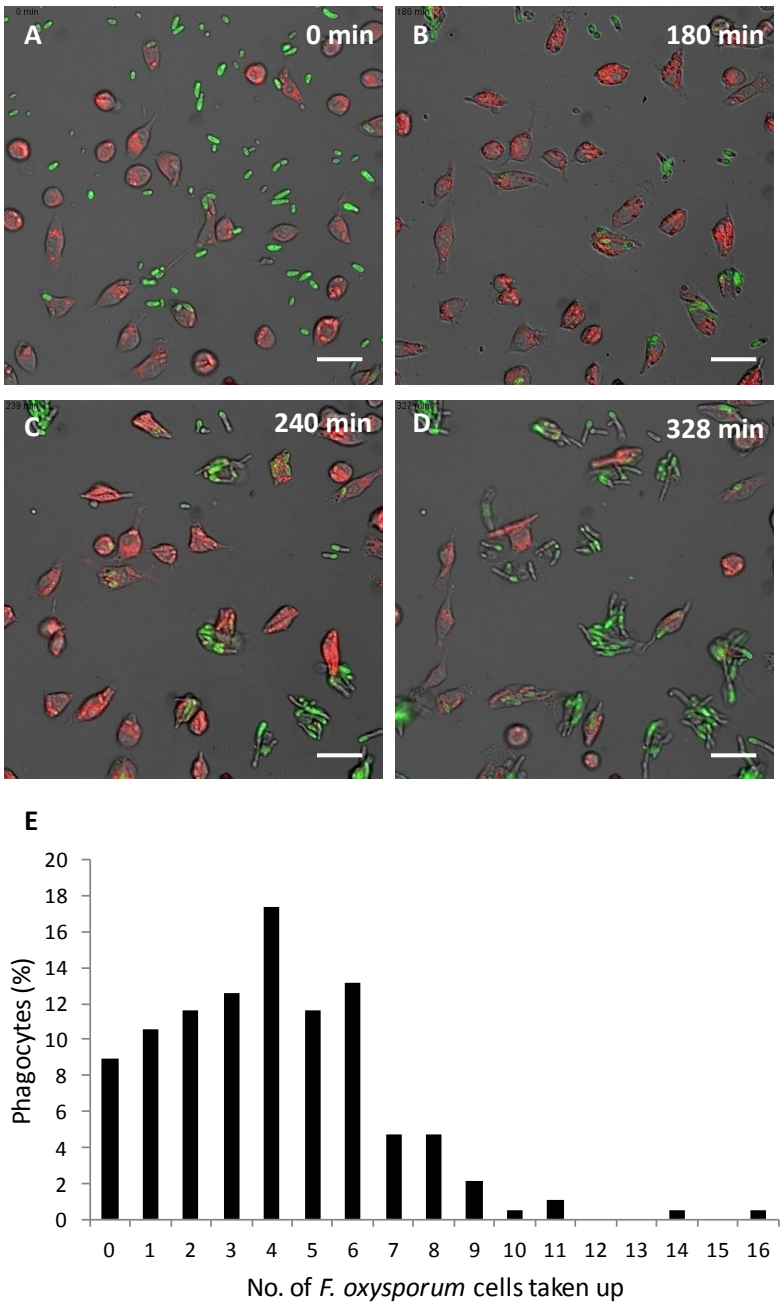

Figure 1. Overview of the uptake of *F. oxysporum* by J774.1 murine macrophages. (A-D) Snapshots from live-cell microscopy experiments following the phagocytosis of live *F. oxysporum* germlings (green) by macrophages (red) at 0 min, 180 min, 240 min and 328 min. The *F. oxysporum* cell/phagocyte ratio was a 3:1. The majority of *F. oxysporum* germlings were engulfed rapidly by macrophages once cell-cell contact was established. **(E)** Numbers of *F. oxysporum* cells ingested by macrophages. Bars represent percentace of macrophages that engulfed a defined number of *F. oxysporum* cells at the end of the phagocytosis assay. Scale bar, 20 µm.

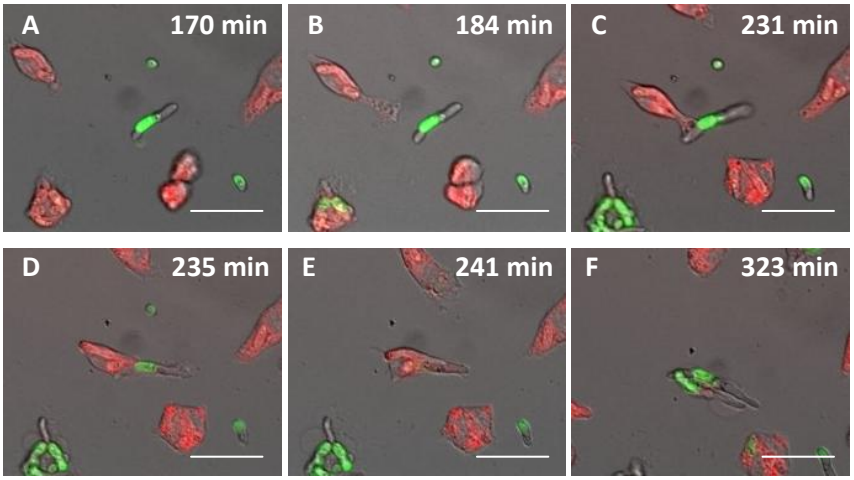

Figure 2. Engulfment of a *F. oxysporum* germling by a macrophage, followed by fungal outgrowth and macrophage lysis. (A-F) Snapshots taken from live cell video microscopy capturing the engulfment process. A macrophage (red) and a *F. oxysporum* germling (green) are shown prior to cell-cell contact **(A)**; at recognition **(B)**; during cell-cell contact **(C)**; during phagocytosis **(D)**; after engulfment **(E)**; and after outgrowth of *F. oxysporum* leading to macrophage cell lysis (F). Scale bar, 20 µm.

Efficient uptake of fungal cells requires migration of phagocytes towards the target (Lewis et al., 2012a). The migration kinetics of 50 macrophages was determined and the tracks plotted relative to their starting position (Figure 3) to indicate directionality and distance traveled assessed in 1 minute intervals. Track data were used to calculate mean track velocity which was 1.22 µm min^{-1} above including baseline random migration of macrophages (macrophages not subsequently engulfing fungi). Previous studies have defined the baseline velocity of the same macrophage cell line as 1.8 µm min^{-1} in the absence of fungal particles (Lewis et al., 2012a), therefore excluding baseline values, thus he mean track velocity of macrophages in response to *F. oxysporum* is 3.1 µm min^{-1}. Figure 4 A-R shows exemplary events of migration of a macrophage towards a *F. oxysporum* germling and its subsequent engulfment.

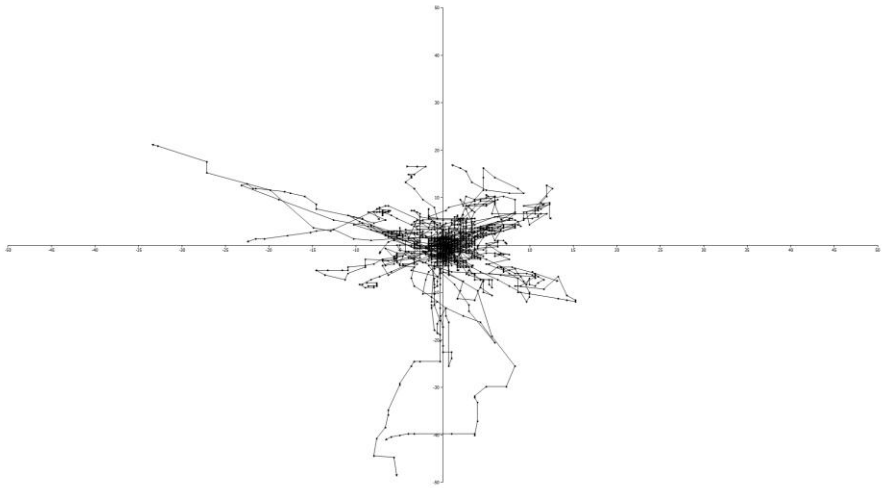

Figure 3. Magrophage migration towards *F. oxysporum* germlings. Tracking diagram shows a detailed dissection of macrophage migration dynamics illustrating the distances travelled, directionality and velocity of J774.1 macrophages cultured with *F. oxysporum* germlings. Tracks represent the movement of individual macrophages (n= 50) relative to their starting position and symbols indicate the location at 1 min intervals.

Macrophage migration towards fungal particles is necessary to establish fungal cell contact, the rate of engulfment, defined as the time elapsed between the establishment of cell-cell contact and the complete uptake of the fungus (Lewis et al., 2012a). We used live cell video microscopy and subsequent image analysis of to generate a detailed minute-by-minute account of the engulfment process. *F. oxysporum* was rapidly phagocytosed by macrophages, once cell-cell contact was established, the average engulfment time for engulfment being 6.74 min (Figure 4S). The vast majority (93%, n=219) of *F. oxysporum* cells that became bound to a macrophage were taken up within the first 11 min. None of the germlings were internalized within less than 2 min or more than 25 min (Figure 4S).

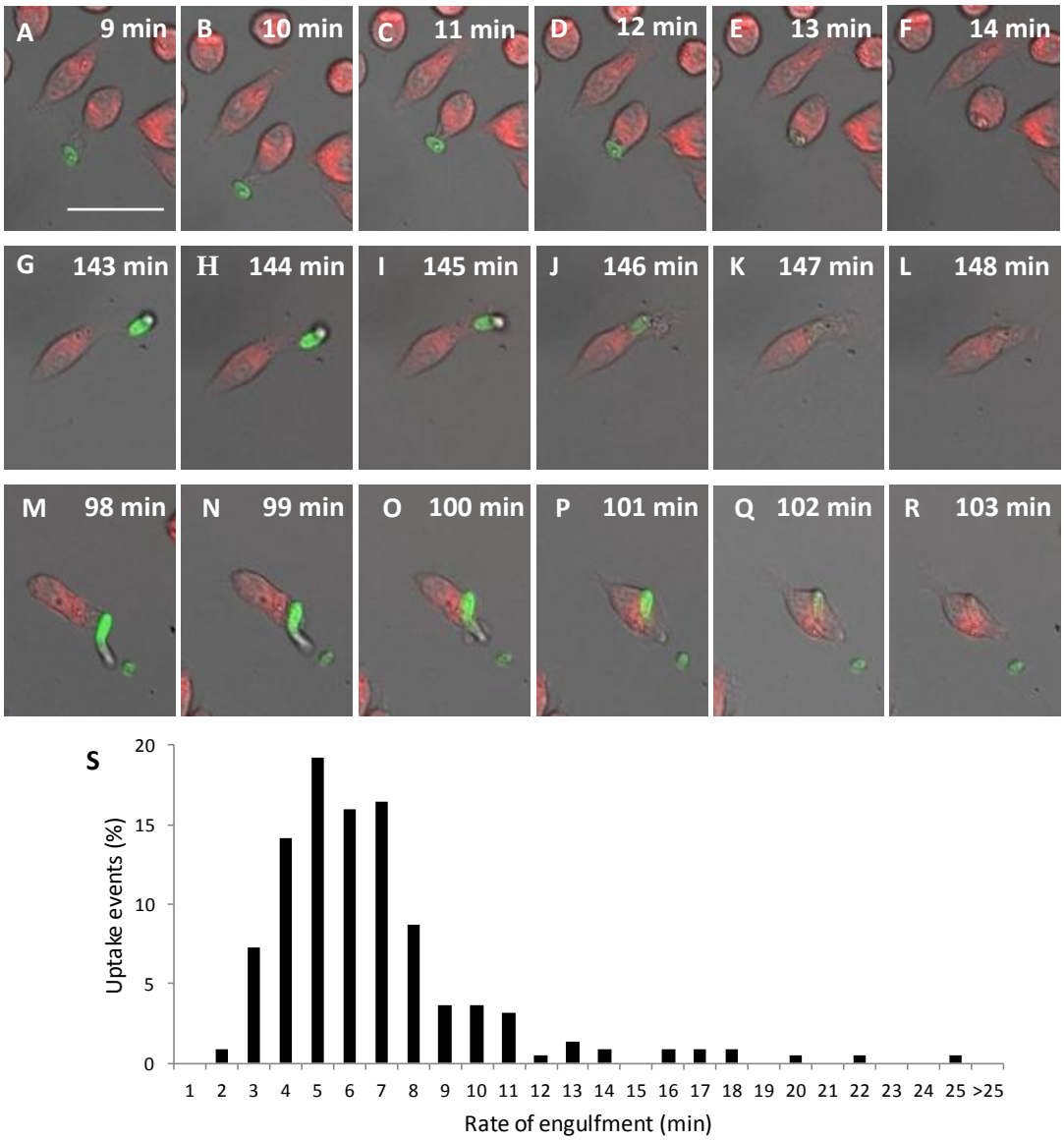

Figure 4. Time of macrophage engulfment of live *F. oxysporum* germlings. (A-F) Snapshots of live-cell video microscopy showing 3 events **(A-F; G-L; M-R)** of various stages of *F. oxysporum* phygocytosis by murine macrophages during phagocytosis assay. **(A, G, M)** Macrophages (red) and *F. oxysporum* germlings (green) establishing cell-cell contact, **(B-E; H-K** and **N-Q)** initializing of fungal cell engulfment; **(F; L and R)** *F. oxysporum* inside the macrophages after engulfmet. The times in the Figures **A-F**; **G-L** and M-R showing the time (min) taken for J774.1 macrophages to ingest *F. oxysporum* cells following cell-cell contact. **(S)** Times taken for phagocytosis of *F. oxysporum* germlings by macrophages. The rate of engulfment was defined as the time taken from first cell-cell contact to complete ingestion of *F. oxysporum* cells by the phagocytes. Bars represent the percentace of uptake events. Scale bar, 20 µm.

The total number of *F. oxysporum* cells taken up by individual macrophages was recorded over a 6 h period. An uptake event was defined as the complete engulfment of one *F. oxysporum* germling by one macrophage cell following cell-cell contact. Most of the macrophages (80.5%, n=190) ingested more than one fungal cell (Figure 1E). Following engulfment, growth of hyphal filaments within the macrophage was observed. The membrane of the macrophage frequently failed to restrain hyphal expansion, resulting in rupture and lysis of the phagocyte. At this point, the fluorescence of the FITC labeled fungal germlings became visible again. Macrophage cell lysis was accompanied by rapid appearance of a bubble-like structure, followed by extensive hyphal growth of *F. oxysporum* and disappearance of the macrophage. After escaping from a macrophage fungal hyphae were recognized by other macrophages, which initiated engulfment until they were lysed themselves by the fungal hyphae.

2.2. The rate of macrophage killing increases with the number of internalized *F. oxysporum* cells

F. oxysporum initialized phagocyte lysis 3 h after engulfment (Figure 5A). Lysis increased over time, causing death of 71% of the macrophages after 6 h. We observed a linear increase in phagocyte killing in relation with the number of internalized fungal cells (Figure 5B). A very high fraction (93.4%) of the macrophages that took up 4 or more fungal germlings was killed within the 6 h of observation. By contrast, mortality was less than 50% among macrophages which took up 3 or less fungal cells (Figure 5B). Interestingly, a small fraction (13.8%) of the macrophages survived 6 h even after ingesting up to 9 fungal germlings, although almost all of them died before 8 h. Thus, the number of engulfed fungal cells plays a crucial role in killing of the macrophages.

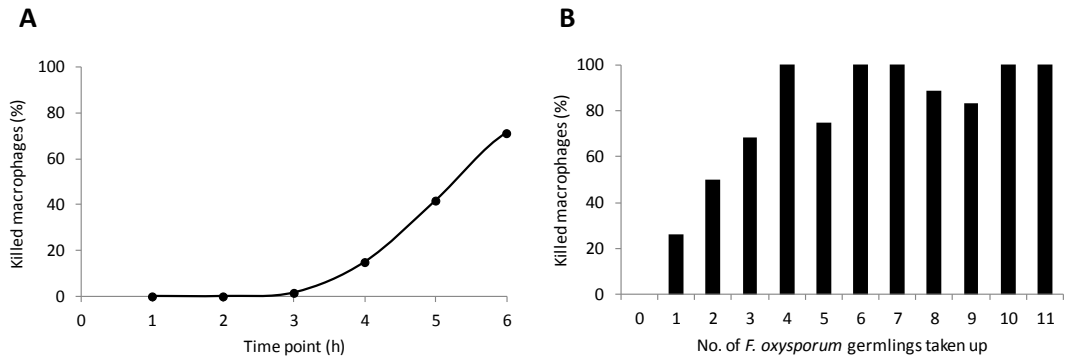

Figure 5. *F. oxysporum* mediated J774.1 murine macrophages killing. (A) Percentage of macrophages killed by *F. oxysporum* germlings over a 6 h period. The viability was defined as the percentage of macrophages that had been killed by specific time points. **(B)** Percentage of macrophages killed by *F. oxysporum* in relation to the defined number of phagocyted germlings over a 6 h period.

2.3. Macrophages with phagocytosed *F. oxysporum* germlings inhibit mitosis

We used live cell video microscopy to follow the dynamics of macrophage mitosis. During the observation period, almost 10% of the macrophages with phagocytosed *F. oxysporum* germlings initiated mitosis (n=384). This is lower as in previous studies which showed that 30.8% of the same macrophage cell line underwent mitosis in the absence of fungal cells (Lewis et al., 2012b). Mitosis was successfully completed in 74% of the cases, as determined by the appearance of two separate daughter cells (Figure 6A-D). After completing mitosis, the daughter cells continued engulfment of fungal cells until they were lysed by the phagocytosed germlings. In the remaining 26% of the macrophages that had initiated mitosis, the two daughter cells remained together by means of a *F. oxysporum* hypha spanning both cells, and subsequently fused back into a single cell (Figure 6E-H).

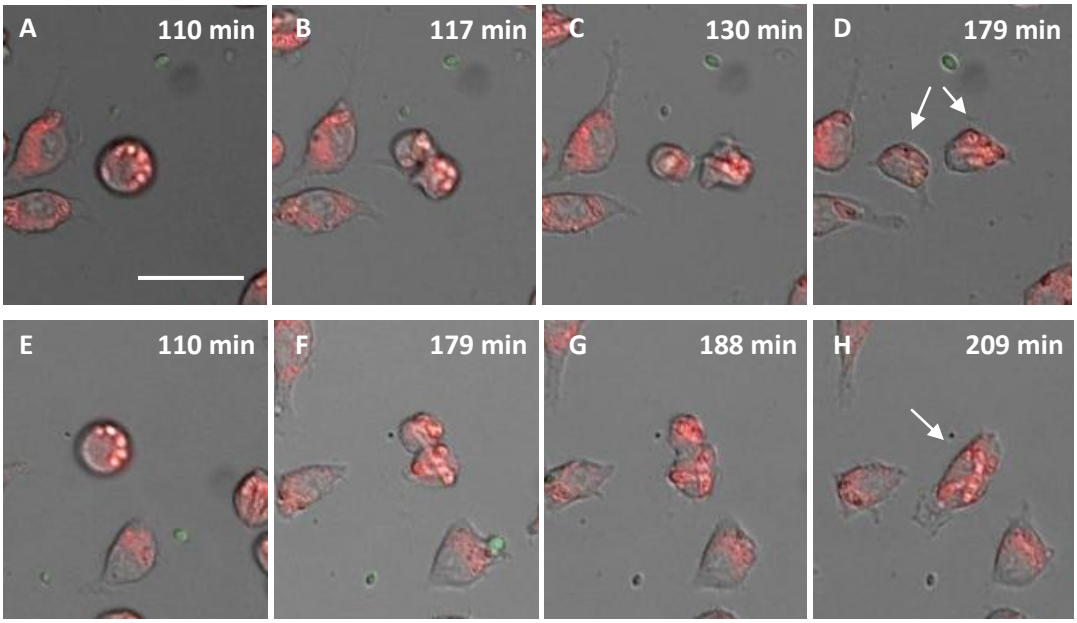

Figure 6. Successful and failed mitosis of macrophages after engulfment of *F. oxysporum*. The macrophages (**A** and **F**) initiated mitosis with phagocytosed *F. oxysporum* germlings (**B** and **F**). This resulted either in successfully completed mitosis with the appearance of two separated daughter cells **(C-D)**, or to failure of the macrophages to complete cell separation **(F-H)**. In the latter case, the macrophages initiated mitosis **(F)** but instead of completely separating, the daughter cells remained fused together **(G)** by means of a *F. oxysporum* hypha spanning both cells (**F** and **G**). Then the two daughter cells fused back to a single cell **(H)**. Scale bar, 20 µm.

3. Discussion

A key aspect of virulence in filamentous fungal pathogens is the capacity for penetration and dissemination, which is a prerequisite for systemic infection. Macrophages are key components of the innate immune response in mammals and provide an important line of defense against fungal invaders by directly engulfing and destroying fungal cells (reviewed in (Brown, 2011)).

Both, *F. oxysporum* and the air-borne fungus *A. fumigates* are opportunistic human pathogens characterized by filamentous hyphal growth. *A. fumigates* conidia are inhaled and exposed to the attack by alveolar macrophages (AMs), the major phagocytes present in lung alveoli along with polymorphonuclear neutrophiles (PMNs) (Brakhage, 2005; Latge, 1999; Sole et al., 2005; Wald et al., 1997). *Aspergillus* conidia that escape from AM can then germinate, but are attacked by PMNs which kill the hyphae through production of reactive oxygen species and degranulation (Braedel et al., 2004; Hube, 2004; Jahn et al., 2002; Kullberg et al., 1999; Latge, 2001; Netea et al., 1999; Newman et al., 2005).

In contrast to *Aspergillus*, *Fusarium* enters the human body mostly through skin infections, before reaching the bloodstream (Nucci and Anaissie, 2002). Here we analyzed the interaction between *F. oxysporum* germlings and murine macrophages. To our knowledge, this is the first detailed analysis of the phagocytosis process in the important opportunistic pathogen *Fusarium*.

3.1. *F. oxysporum* germlings hyphal growth after engulfment by macrophages leading to escape and associated macrophage lysis.

Our results demonstrate that murine macrophages efficiently migrate towards, recognize, and internalize *F. oxysporum* germlings. The use of video microscopy allowed a detailed dissection of the engulfment process, revealing remarkable similarities with the results previously reported for *C. albicans* (Lewis et al., 2012a). However the migration velocity of

macrophages at 3.1 µm min^{-1} is faster compared to those values obtained previously for J774.1 macrophages responding to *C. albicans* strains, ranging from 2.2-2.7 µm min^{-1} (Lewis et al., 2012a).. The average engulfment time of *F. oxysporum* (6.74 min) was almost identical to that reported in *C. albicans* (6.7 min). Likewise, the fraction of fungal cells bound to a macrophage that were taken up after 15 min was also very similar (96% and 95% for *F. oxysporum* and *C. albicans*, respectively (Lewis et al., 2012a). We found that the number of engulfed fungal germlings crucial affects the survival of the macrophage. A very large fraction (93.4%) of the macrophages that internalized 4 or more germlings were killed by *F. oxysporum* whereas less than 50% of those were killed that engulfed less than 4 germlings. Since most of the macrophages (61.8%) ingested more than 3 germlings, a large fraction of these eventually got killed by the fungus.

F. oxysporum hyphae that had escaped from the killed macrophage were subsequently engaged and engulfed, often by multiple macrophages (video S2). In spite of multiple macrophages simultaneously trying to engulf , phagocytosis of large hyphae was frequently frustrated, suggesting a limitation for successful phagocytosis with increasing hyphal length, similar to what has been reported for *C. albicans* (Lewis et al., 2012b).

3.2. *F. oxysporum* inhibits macrophages completing mitosis

Mitosis of tissue-derived macrophages plays an important role in macrophage proliferation. Inhibition of macrophage cell division was previously reported for the fungal pathogens *Cryptococcus neoformans*, *Candida krusei* and *C. albicans* (Garcia-Rodas et al., 2011; Lewis et al., 2012b; Luo et al., 2008). Here we found that in the presence of *F. oxysporum,* mitosis of macrophages was unsuccessful in approximately 25% of the cases. This proportion is similar, although somewhat lower than that reported in *C. albicans* (35,9%) (Lewis et al., 2012b). Strikingly, the percentage of macrophages underwent mitosis in presence of *F. oxysporum* (9.9%) was lower than previously reported for the same macrophages cell line in the absence of fungal particles (30.8 %) or cultured with *C. albicans* (29.5%) (Lewis et al., 2012b). It has been suggested that interference of the fungus with macrophage cell division may inhibit the

formation of new uninfected macrophages. On the other hand, however, successful mitosis of macrophages carrying fungal cells may also contribute to the spreading of the pathogen within the host (Lewis et al., 2012b).

Although phagocytosis of *F. oxysporum* may be crucial to protect the host, the mechanisms and molecules involved in this process remain still unknown. Recognition and phagocytosis of *C. albicans* by macrophages is dependent on the glycosylation status and specific components of the fungal cell wall (McKenzie et al., 2010). Likewise, conidial germination in *A. fumigatus* is associated with an increase of β1,3-glucan in the outer cell wall. Because β1,3-glucans are targeted by the pattern-recognition receptor Dectin-1 which is expressed in macrophages, monocytes, neutrophils and a subset of T cells (Hohl et al., 2005; Taylor et al., 2002), germ tubes are recognized more efficiently than ungerminated conidia (Luther et al., 2007) leading to phagocytosis and synthesis of different proinflammatory cytokines (Gersuk et al., 2006). Currently, little is known about the cell wall components of *F. oxysporum* modulating recognition and uptake by macrophages, as well as the role of these surface molecules in the ability of the fungus to evade destruction by immune cells. Our results highlight the need for more detailed studies on the interaction between *F. oxysporum* and the mammalian immune system, which will lead to a better understanding of the early molecular events during *Fusarium* infection. (Alkan et al., 2008).

Chapter 3

The signalling mucin Msb2 in *Fusarium oxysporum*: Identification of putative interaction partners by Yeast Two-Hybrid assay

Summary

Fungal pathogenicity on plants requires a conserved mitogen-activated protein kinase (MAPK) cascade homologous to the yeast filamentous growth pathway. In the soilborne vascular wilt pathogen *Fusarium oxysporum,* the orthologous MAPK Fmk1 controls invasive growth and virulence on tomato plants. We recently found that full phosphorylation of Fmk1 requires the transmembrane protein Msb2, a member of the family of signalling mucins that have emerged as novel virulence factors in fungal plant pathogens. *F. oxysporum* mutants lacking either *msb2* or *fmk*1 share characteristic phenotypes related to invasive growth and virulence on tomato plants. Moreover, Δ*msb*2 mutants also show *fmk*1-independent phenotypes suggesting additional roles of Msb2 in distinct pathways.

The exact signalling mechanism of fungal transmembrane mucins is currently unknown. Our aim is to find new Msb2 interaction partners with a role in the MAPK signalling cascade. A Yeast Two-Hybrid screen against a cDNA library from *F. oxysporum* yielded eleven candidates interacting with the Msb2 cytoplasmic tail. To test the role of these genes in MAPK signalling, a knockout approach was designed, followed by phenotypic analysis of the mutants.

1. Introduction

1.1. The MAP kinase modules in *F. oxysporum*

One of the most broadly conserved pathogenicity mechanisms in fungi involves a mitogen-activated protein kinase (MAPK) cascade (Pathogenicity MAP Kinase PMK1 cascade) homologous to the Fus3/Kss1 mating/ filamentation cascade of *S. cerevisiae* (Qi and Elion, 2005). In *F. oxysporum* the orthologous MAPK (*Fusarium* MAPK1) pathway became in focus of interest since 2001, when the MAPK Fmk1 which is part of a signal transduction pathway was shown to be essential for pathogenicity on tomato plants (Figure 1). (Di Pietro et al., 2001).

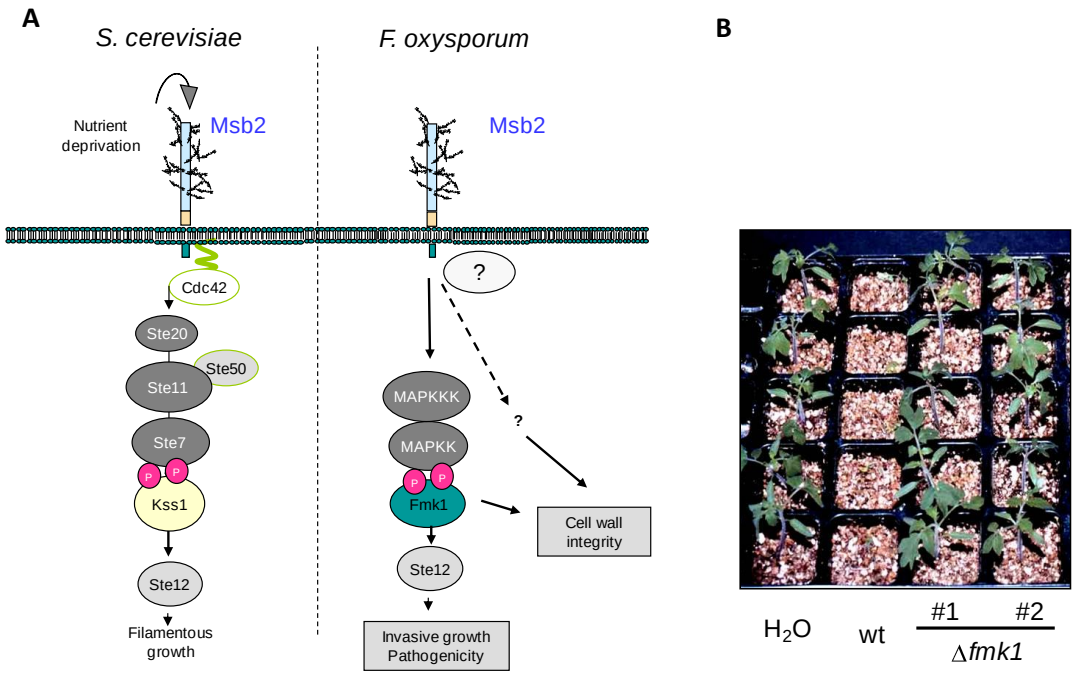

Figure 1. The Fmk1 MAPK signalling pathway is essential for virulence of *F. oxysporum* on tomato plants. **(A)** Schematic diagram of the Kss1-MAPK signalling cascade in *S. cerevisiae* (left) and the orthologous Fmk1 pathway in *F. oxysporum* (right); Figure adapted from the PhD thesis of E. Perez-Nadales, 2010. **(B)** The MAPK Fmk1 is a pathogenicity factor of *F. oxysporum* on tomato plants (Figure taken from Di Pietro et al., 2001).

Fmk1 is required for multiple virulence-related functions such as root attachment and penetration, secretion of pectinolytic enzymes, invasive growth on living plant tissue and

infection of tomato (*Solanum lycopersicum*) plants (Delgado-Jarana et al., 2005; Di Pietro et al., 2001). Fmk1 is dispensable for vegetative growth and conidiation in culture, suggesting that it plays specific role during the interaction of *F. oxysporum* with the plant host and is not required under conditions encountered by the fungus in culture (Di Pietro et al., 2001). Fmk1 is also required for vegetative hyphal fusion, an ubiquitous process in filamentous fungi whose biological role remains poorly understood (Prados Rosales and Di Pietro, 2008).

Invasive growth, the most critical of the Fmk1-regulated functions for plant infection, is mediated by the homeodomain transcription factor Ste12 (Rispail and Di Pietro, 2009). Δ*ste*12 and Δ*fmk*1 mutants of *F. oxysporum* share phenotypes related to invasive growth but not other Fmk1-regulated functions such as pectinolytic activity, vegetative hyphal fusion or root adhesion. Yet, both Δ*ste*12 and Δ*fmk*1 mutants have dramatically reduced virulence, suggesting that invasive growth is the main virulence function controlled by the Fmk1 MAPK in *F. oxysporum*, and that this control is exerted through the Ste12 transcription factor.

1.2. The mucin like transmembrane protein Msb2 in *F. oxysporum*

Msb2 is a highly glycosylated mucin-type membrane protein. The genome sequences of ascomycetes including plant and human pathogens contain putative Msb2 orthologs (Rispail et al., 2009) displaying a similar domain architectures as *F. oxysporum* Msb2 (Perez-Nadales and Di Pietro, 2011). While *S. cerevisiae* and *Ashbya gossypii* have two paralogs, Msb2 and Hkr1, other ascomycetes including *F. oxysporum* contain a single Msb2 orthologue.

Msb2 acts upstream of the Fmk1 MAPK pathway and triggers a rapid and transient increase in Fmk1 phosphorylation levels by contact with a solid surface (Perez-Nadales and Di Pietro, 2011). In addition, Msb2 contributes to maintenance of cell wall integrity (Figure 2B) through a distinct pathway (Perez-Nadales and Di Pietro, 2011). Msb2 promotes invasive growth and plant infection via the Fmk1 MAPK cascade. The Δ*msb*2 and Δ*fmk*1 mutants share characteristic phenotypes such as defects in hyphal growth under poor nitrogen conditions, penetration of cellophane membranes, colonization of living fruit tissue, root penetration,

and virulence on tomato plants (Perez-Nadales and Di Pietro, 2011). Besides Fmk1 phosphorylation, Msb2 also regulates the expression of two Fmk1-regulated genes, *fpr*1, which encodes a secreted PR-1-like protein, and *chs*V, which encodes a class V chitin synthase essential for plant infection (Madrid et al., 2003).

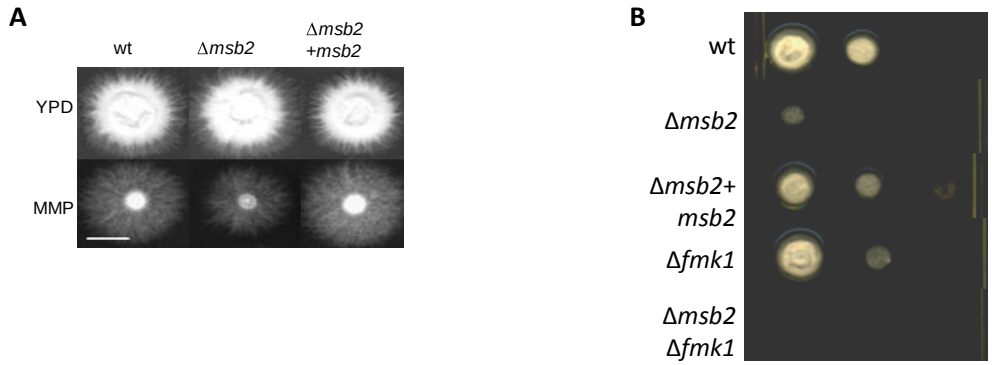

Figure 2. Msb2 is an upstream component of the Fmk1 signalling pathway and contributes to hyphal growth under conditions of nutrient limitation and cell integrity stress. **(A)** Colony phenotype of the indicated strains grown on full nutrition medium(YPD) and on minimal medium(MM). **(B)** Colony growth on MM mediumsupplemented with 40 µg/ml Clacofluor White (CFW). Figure adapted from (Perez-Nadales and Di Pietro, 2011).

In *S. cerevisiae,* Msb2 also functions as an osmosensor in combination with Sho1 (synthetic high osmolarity sensitive) (Tatebayashi et al., 2007), in the high osmolarity glycerol pathway (HOG) MAPK pathway which mediates responses to hyperosmotic shock (Hohmann et al., 2007). However, *F. oxysporum* Δ*msb*2 mutants had no growth defect in the presence of osmotic or oxidative stress. Instead, they showed increased sensitivity to Congo Red (CG) and Calcoflour White (CFW) (Perez-Nadales and Di Pietro, 2011), two compounds affecting cell wall biosynthesis and composition (Roncero and Duran, 1985). It has been suggested that Msb2 and Fmk1 promote cell wall integrity of *F. oxysporum* through independent pathways, since the Δ*fmk1* Δ*msb2* double mutant is more sensitive to CFW than the single mutants (Perez-Nadales and Di Pietro, 2011).

Msb2 (*FOXG_09254*) in *F. oxysporum* encodes a protein of 1129 amino acids which includes the N- terminal signal sequence (20 amino acids); a large extracellular domain (amino acids 21-991; including the mucin homolgy domain, MHD: amino acids 106 to 836 and a positive

regulatory domain, PRD: 176 amino acids) which is predicted to be highly glycosylated; a single transmembrane domain (TM; 22 amino acids); and a short cytoplasmic tail (CT; 95 amino acids) (Perez-Nadales and Di Pietro, 2011). (Figure 3).

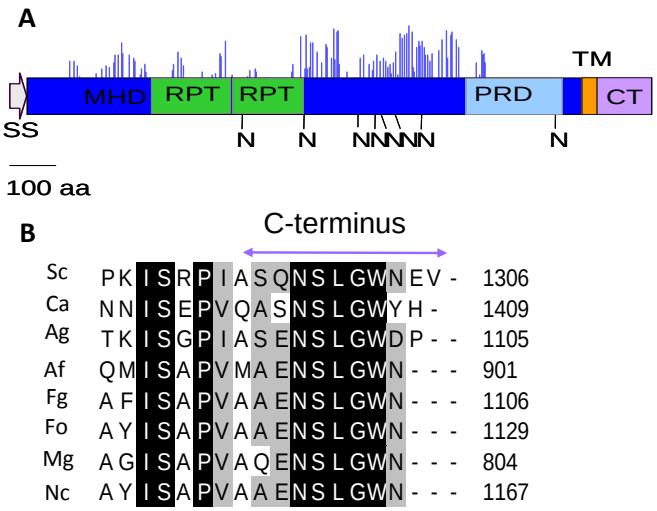

Figure 3. The cytoplasmic tail (CT) of *F. oxysporum* Msb2 is highly conserved. (A) Schematic representation of the F. oxysporum Msb2 (ORF open reading frame: 1129 aa) protein. Shown are the N-terminal signal sequence (SS), the extracellular mucin homology domain (MHD) with imperfect repeats (RPT), the positive regulatory domain (PRD), the transmembrane domain (TM), and the cytoplasmic tail (CT).**(B)** Amino acid sequence alignment of C-terminal intracellular region (Msb-CT cytoplasmic tail) of putative Msb2 orthologs of *S. cerevisiae* (Sc), *C. albicans* (Ca), *A. gossypii* (Ag), *A fumigatus* (Ag), *F. graminearum* (Fg), *F. oxysporum* (Fo), *M oryzae* (Mg) and *N. crassa* (Nc). Highly concserved residues are shaded in black; moderately conserved residues are shaded in gray. Figures are adapted from (Perez-Nadales and Di Pietro, 2011).

Together with the transmembrane mucin Msb2, the plasma membrane tetraspan protein Sho1 serves as stress sensor in many fungal systems (Boisnard et al., 2008; Krantz et al., 2006; Ma et al., 2008; Norice et al., 2007; Roman et al., 2009; Roman et al., 2005) and functions upstream of several MAPK cascades (Cullen, 2007; Seet and Pawson, 2004). In *S. cerevisiae*, Msb2 and Sho1 interact to regulate signalling cascades involved in osmotic stress response and pseudohyphal growth and are required for activation of filamentous growth and agar invasion in response to nutrient limitation (Chen and Thorner, 2007; Cullen et al., 2004; Vadaie et al., 2008). Msb2 interacts with Cdc42, and it has been hypothesized that this complex provides sensory capacity in the filamentous growth pathway, transmitted via the PAK kinase Ste20 (Cullen et al., 2004). Nothing is known about the interaction between Msb2 and other proteins in *F. oxysporum* (Perez-Nadales et al., unpublished).

1.3. Aim of this work

Msb2 has a dual function in *F .oxysporum.* First it is required for surface-induced phosphorylation of Fmk1 and promotes functions related to invasive growth and virulence upstream of Fmk1. Second Msb2 contributes to maintenance of cell integrity through a distinct pathway (Perez-Nadales and Di Pietro, 2011). This suggests that Msb2 interacts with unknown proteins to regulate distinct functions in *F. oxysporum* (Figure 4).

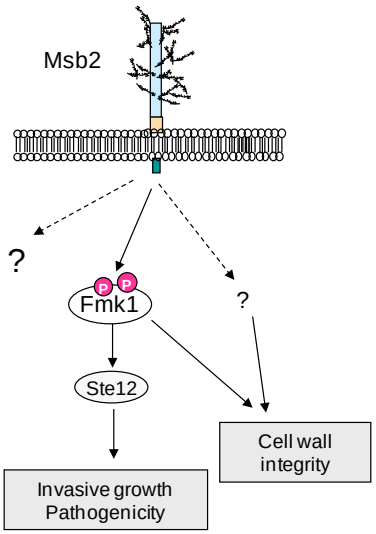

Figure 4. The transmembrane protein Msb2 has a dual function in *F .oxysporum.* First Msb2 is required for surface-induced phosphorylation of Fmk1 where it promotes functions related to invasive growth and virulence upstream of Fmk1 and second Msb2 contributes to maintenance of cell integrity through a distinct pathway (Perez-Nadales and Di Pietro, 2011).

The aim of this study was to identify new interaction partners of Msb2 to elucidate its mechanism of signalling in *F. oxysporum*, using a Yeast Two-Hybrid (Y2H) screen with Msb2 as a bait.

2. Results

2.1. Construction of a cDNA library of *F. oxysporum* in a Y2H vector

After generation of cDNA using the SMART^{TM} technology, library construction was performed following the manufacturer´s instructions (Make Your Own "Mate and Plate^{TM}" Library System User Manual, Clontech, 2010) usinf RNA optained from minimal medium growth condition. Since the first "library scale" transformation did not generate the minimum of 1 million independent clones required to screen the complete genome of *F. oxysporum,* we tested different concentration of cDNA together with plasmid DNA for optimal transformation efficiency, and calculated the library titer required to obtain > 1 million independent clones from our library. Instead of a single transformation on a "library scale", we performed 24 transformations at a "small scale". Dilution on SD-Leu and subsequent calculation (3 µg pGADT7-Rec and 3,984 µg cDNA) revealed a transformation efficiency of 1.759×10^6 cfu/µg and 7 million independent clones in our library.

2.2. Yeast Two-Hybrid with Msb2 against the *F.oxysporum* cDNA libraray

The cytoplasmic tail of *msb2* (msb2-CT=95 amino acids) was cloned in the bait plasmid pGBKT7 and transformed in the yeast strain "Gold". Msb2-CT is expressed in yeast cells fused to the Gal4 DNA-binding domain (BD). We confirmed in-frame cloning of *msb2-CT* cDNA with the Gal4 DNA-binding domain (BD) in the bait plasmid and the absence of toxicity and of autoactivation in absence of a prey protein. The cDNA library of *F. oxysporum* described above was cloned in the plasmid pGADT7-Rec, transformed into the yeast strain Y187 and expressed as a fusion protein with the Gal4 transcriptional activation domain (AD). The Y2H screen was performed via yeast mating (Figure 1) before plating on selection medium(quadruple-drop-out (QDO) mediumwithout tryptophan, leucine, adenine and histindine). After mating of the bait Gold-pGBKT7-msb2-CT-BD against the cDNA library, the

number of screened clones was calculated, which should be at least 1 million of diploids to detect genuine interactions on the selection plates which can be only achieved by a mating efficiency of 2-5%.

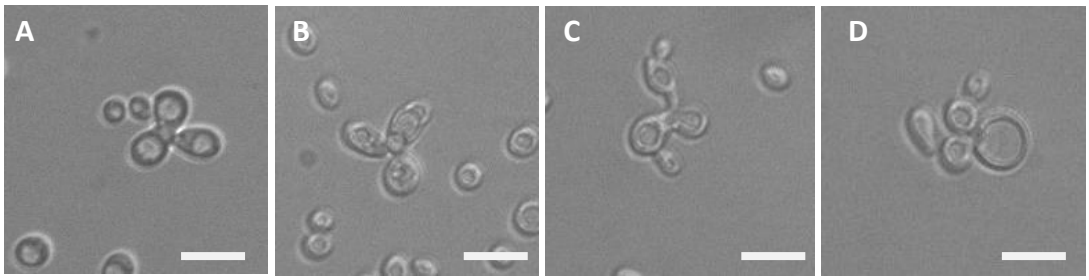

Figure 1. A typical yeast zygote during yeast mating showed a 3-lobed structure. The lobes represent the two haploid parental cells and the budding diploid cell. Some zygotes resemble a clover leaf **(B and C)**, while others have a shape similar to a "Mickey Mouse" face **(A and D)**. Scale bar= 5 µm.

Viability colony counts after mating on the appropriate selection plates revealed a percentage of diploids (mating efficiency) of 19.32% and a number of screened clones of 1,573 x 10^6. The screen revealed in the first screen 134 colonies which were re-plated on high stringency mediumafterwards (QDO mediumsupplemented with the drug aureobasidin A and 5-bromo-4-chloro-3-indolyl-α-D-galactopyranoside (X-α-Gal)) (Figure 2). In a second Y2H screen performed in parallel with the complete open reading frame of Msb2 (Msb2-ORF-BD), no clones were obtained on the protein-protein-interaction selection plates.

Figure 2. Y2H analysis with the cytoplasmic tail of Msb2 (Msb2-CT) against the cDNA library of *F. oxysporum* revealed 134 positive interactions. The cDNA of *msb2-CT* was cloned into the bait plasmid (pGBKT7) and transformed into the yeast strain Gold. The cDNA library of *F. oxysporum* was cloned into the plasmid pGADT7-Rec and transformed into the yeast strain Y187. Positive interactions were obtained after yeast mating and screening first on selection medium(SD-Leu/-Trp/X/A) followed by replating on a high stringency master plate (SD-Leu/-Trp/_Ade/-His/+X-α-Gal/+Aureobasidin).

After re-plating the 134 candidates on high stringency selection plates, 35 clones which displayed a strong growth and deep blue color were selected for further analysis. The plasmids from the selected 35 clones were isolated, the cDNAs amplified by PCR with the primer pair (Amplimer 3`/Amplimer 5`), purified from an agarose gel and sequenced. A BLAST search of the complete genome database of *F. oxysporum* (http://www.broadinstitute.org/) with the corresponding nucleotide sequences identified 11 different coding regions containing at least one of the positive clones (Table 1).

Table 1. Sequencing of positive Y2H clones revealed 11 candidate proteins interacting with Msb2-CT. The pGADT7-Rec plasmids from the positive clones were isolated and the inserts amplified and sequenced. A BLAST search against the *F. oxysporum* database identified 11 different genes.

Number of clones	Gene	BLAST result (Broad Institute)	BLAST result (NCBI)
20	*FOXG_13832*	urease accessory protein ureG	
1	*FOXG_04361*	ubiquitin-conjugating enzyme	
4	part of *FOXG_00769*	2421676- 2421848	glycoside hydrolase family 63
1	*FOXG_14173*	predicted protein	Ident. 45% heterochromatin protein one *Magnaporthe oryzae*
1	*FOXG_08666*	conserved hypothetical protein	vacuolar carboxypeptidase Cps1
1	*FOXG_08976*	Formamidase	
1	*FOXG_09776*	Acetyltransferase	
2	*FOXG_10398*	conserved hypothetical protein	glycoside hydrolase family 2 sugar binding protein
2	*FOXG_12838*	hypothetical protein similar to vesicle fusion factor NSFI	
1	*FOXG_00231*	20S proteasome subunit beta 6	
1	*FOXG_15235*	conserved hypothetical protein	C6 transcription factor (Ctf1B)

2.3. Mutational analysis of the candidate genes by systematic deletion

To investigate the 11 candidate interaction partners of Msb2 obtained from the Y2H screen, targeted deletion of the corresponding genes in the *F. oxysporum* genome was performed and the mutants were examined for known Δ*msb2* phenotypes. We failed to obtain deletion mutant of the genes *FOXG_14173* and *FOXG_00231* suggesting that these genes are

essential in *F. oxysporum.* The *FOXG_00231* orthologue is reported as an essential gene in *S. cerevisiae* (www.yeastgenome.org).

2.3.1. Growth assays

It was reported previously that colonies of the Δ*msb2* mutants displayed slower growth than those of the wt strain on solid minimal medium(MM) containing the non-preferred nitrogen source NO_3, but not on nutrient-rich medium (YPDA) (Perez-Nadales and Di Pietro, 2011). Therefore the 9 different *F. oxysporum* deletion mutants were tested for colony growth on MM + NO_3 and on YPDA (Figure 3) and compared with the wt and the Δ*fmk1* and Δ*msb2* mutant strains.

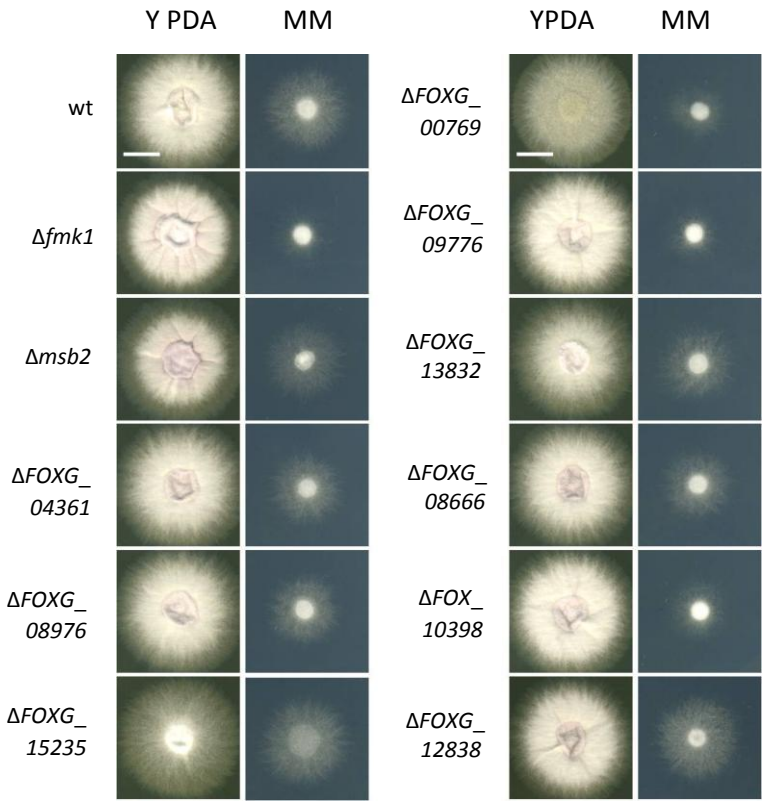

Figure 3. Growth assay of the nine *F. oxysporum* mutants on MM medium containing NO_3 as a nitrogen source. Colony phenotype of the indicated strains grown on yeast peptone dextrose agar (YPDA) or Minimal Medium(MM) plates. 10^5 microconidia from each strain were spot-inoculated and scanned after 3 days of incubation at 28 °C. Scale bar= 1cm.

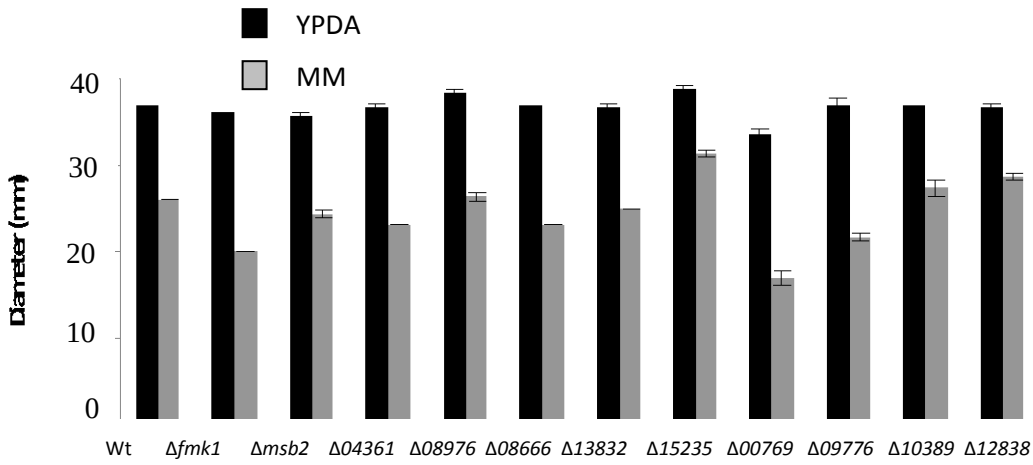

Figure 4. The analysis of the colony diameter growth showed differences in growth between Δ*msb2* and some of the indicated strains. To test the growing and germination ability of the mutants for further growth assays, same amount of microconidia of the indicated strains were spotted on YPDA or MM mediumand incubated in 28°C. Colony diameter of the indicated strains was measured after 3 days. Bars represent standard errors calculated from 3 technical and 2 biological replicates.

Colony diameter measurements showed significantly reduced growth on MM in the Δ*FOXG_00769* deletion mutant, similar to Δ*msb2* or Δ*fmk1* (Figure x). A different colony phenotype on YPDA media, but no effect on diameter was observed for mutants in genes *FOXG_15235* and *FOXG_00769,* but not Δ*msb2* or Δ*fmk1*.

2.3.2. Cellophane penetration

The Δ*fmk1* mutant fails to penetrate cellophane membranes (Lopez-Berges et al., 2010; Prados Rosales and Di Pietro, 2008) whereas the Δ*msb2* mutant displays reduced ability (Perez-Nadales and Di Pietro, 2011). We tested cellophane penetration ability of the gene deletion mutants on MM agar (Figure).

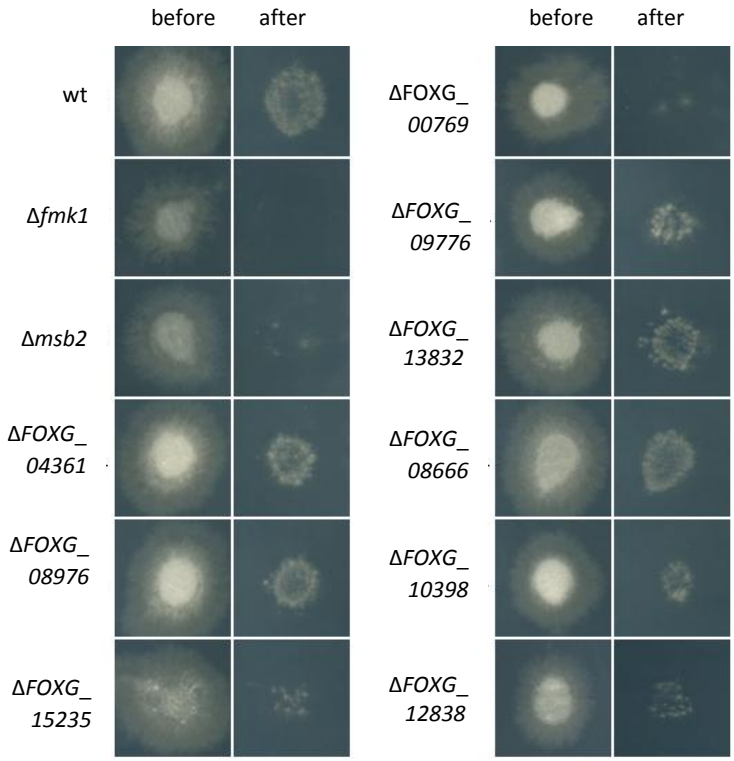

Figure 5. Assay of deletion mutants for ability to penetrate cellophane membranes. 5µl of a microconidial suspension (10^7 con/ml) were spot-inoculated on MM agar plates covered with a cellophane membrane. To determine the penetration of the membranes, the cellophane sheets with the fungal colony were removed after 4 days (before) and the plates were incubated for an additional day at 28 °C (after).

After removing the cellophane membranes, the deletion mutants Δ*FOXG_04361*, Δ*FOXG_08976*, Δ*FOXG_09776*, Δ*FOXG_13832*, Δ*FOXG_08666* and Δ*FOXG_10398* had penetrated like the wt strain. However, reduced penetration was observed for the Δ*msb2* mutant as described (Perez-Nadales and Di Pietro, 2011) and for the mutants Δ*FOXG_15235*, Δ*FOXG_00769* and Δ*FOXG_12838*. The Δ*fmk1* mutant failed to penetrate the cellophane as described previously (Lopez-Berges et al., 2010; Prados Rosales and Di Pietro, 2008).

2.3.3. Cell wall stress

In previous studies it was shown that the Δ*msb2* mutant, but not the Δ*fmk1* mutant, is hypersensitive to cell wall targeting compounds (Perez-Nadales and Di Pietro, 2011). Figure 6

shows the colony growth of the wt and the different mutant strains. We confirmed that the Δ*msb2* mutant, but not the Δ*fmk1* mutant is more sensitive to CFW. None of the tested deletion mutants showed reduced growth as the Δ*msb2* mutant. However, Δ*FOXG_00769* showed a distinct colony phenotype on medium containing CFW.

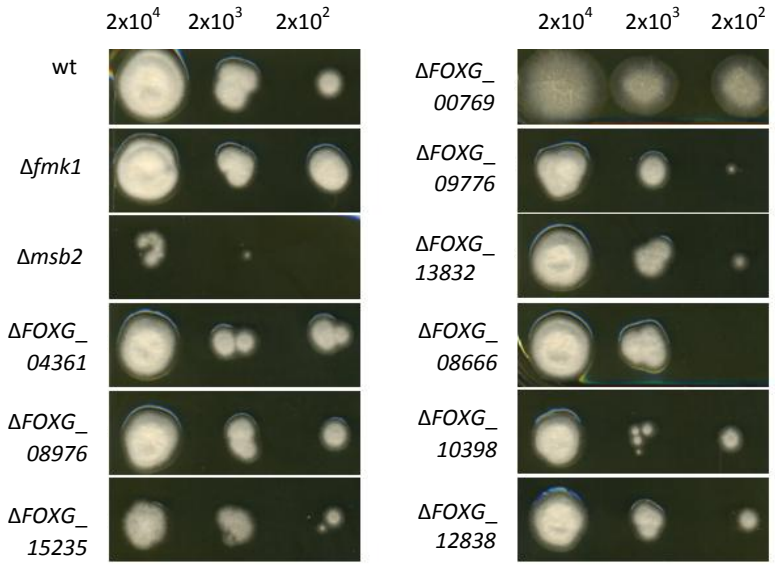

Figure 6. None of the deletion mutants shows increased sensitivity to cell wall stress like Δ*msb2*. Dilutions of microconodia ($2x10^4$; $2x10^3$; $2x10^2$) of the indicated strains were spotted on YPD-MES supplemented with 30 µg/ml Calcofluor White (CFW), incubated at 28°C for 3 days and scanned. Shown is one representative result from three biological replicates.

2.3.4. *fpr1* expression

To investigate a possible role of the candidate proteins in the Fmk1 pathway we examined expression of *fpr1*. *Fpr1* encodes a secreted protein with an SCP-PR-1-like domain that was shown to be transcriptionally regulated by the Fmk1 MAPK cascade (Prados-Rosales and Di Pietro, unpublished). Previous work has shown that Msb2 acts as an upstream component of Fmk1 (Perez-Nadales and Di Pietro, 2011) where the Δ*msb2* mutant showed ten-fold lower *fpr1* transcript level than the wild type and the Δ*fmk1*Δ*msb2* double mutant even a hundred-fold lower level (PhD thesis, E. Perez-Nadales, 2010). In this work (Figure 7) we could confirm the lower expression of *fpr1* in the Δ*fmk1* mutant and Δ*msb2* mutant strains. A reduced expression in comparison to the wt expression was determined in the mutants with the

deletions of the genes *FOXG_04361*, *FOXG_08976*, *FOXG_08666* and *FOXG_09776*. Slightly reduced was the *fpr1*-expression of the deletion mutants lacking the genes *FOXG_00769*, *FOXG_12838* and *FOXG_15235*. No significant difference was detected in the mutants of the genes *FOXG_13832* and *FOXG_10398*.

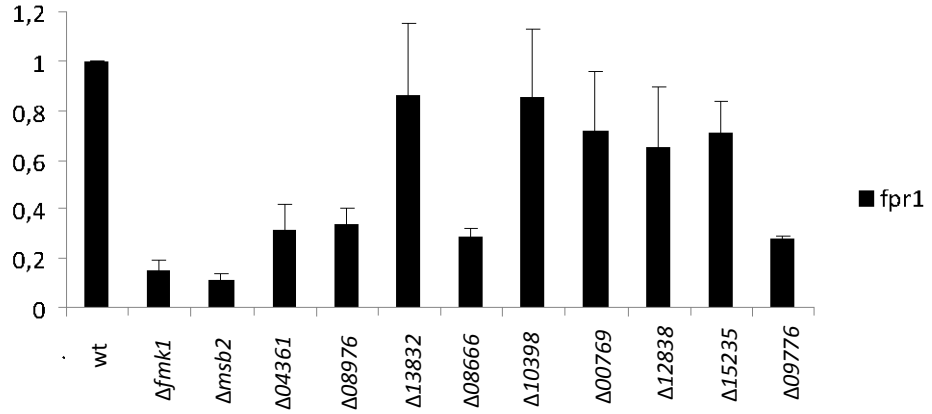

Figure 7. Reduced *fpr*1 mRNA abundance in some of the candidate mutant strains. cDNA derived from RNA isolated from invasive growth condition (15 h germination in PDB, transfer and incubation for 4h on solid MM+ $NaNO_3$). Relative expression levels optained by quantitative real-time PCR represent mean values normalized to the *actin* gene expression levels and relative to the expression in the wild type strain. Bars represent standard errors calculated from 4 technical replicates.

2.3.5. Phosphorylation of Fmk1

Previous work has shown that that Msb2 is required for the transient phosphorylation of Fmk1 upon contact with solid surface (Perez-Nadales and Di Pietro, 2011). Recently, we found that the phosporylation of Fmk1 is pH dependent. (Segorbe-Luke et al., unpublished). We confirmed with Western blot analysis using commercial α-phospho-p44/42 MAPK antibody a transient increase of Fmk1 phosphorylation levels in the wild type strain 30 min after changing the pH in the liquid PDB culture form pH 5 to pH 7 whereas Fmk1 was under-phosphorylated in the Δ*msb2* mutant (Figure 8). Fmk1 was under-phosphorylated in the deletion mutants lacking the genes *FOXG_08976*, *FOXG_00769* and *FOXG_15235* and was hyper-phosporylated in the mutants of the genes *FOXG_04361*, *FOXG_12838* but no difference in fmk1 expression level was observed in the strains *FOXG_08666*, *FOXG_13832*, *FOXG_09776* and *FOXG_10398*.

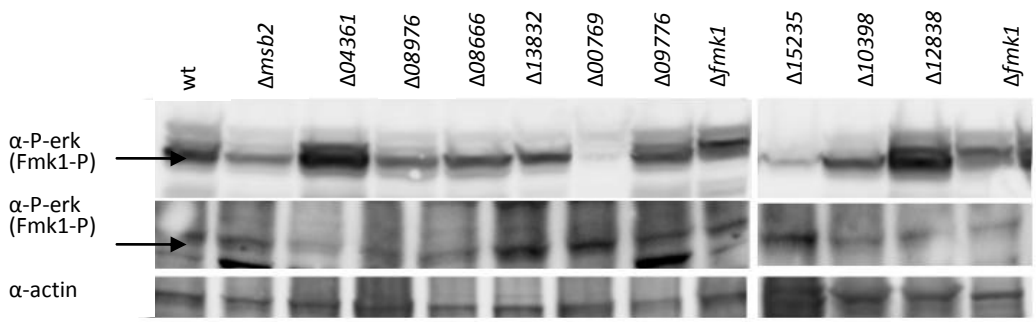

Figure 8. Determining phosphorylation levels of the MAPK Fmk1 by Western-blot. Increase in pH of the mediumproduces a transient increase in Fmk1 phosphorylation and Msb2 is required for full level of Fmk1 phosphorylation (Perez-Nadales and Di Pietro, 2011). Total protein extracts from the indicated strains (15h germination in PDB with pH 7, change for 20 min to pH 5, increase the pH for 30 min to pH 7) were used for hybridisation with commercial anti-phospho-p44/42 MAPK antibody (α-P-erk), or anti p44/p42 MAPK antibody (α-ERK). The loading control was detected using α- *S. cerevisiae*-actin monoclonal antibody.

2.3.6. Tomato plant root infection assay

Tomato plants inoculated with the wild type strain showed a continuous increase in wilt disease symptoms, and most of the plants were dead 34 days after infection (Figure). Plants inoculated with the Δ*fmk1* mutant failed to develop any disease symptoms (Di Pietro et al., 2001) and the deletion of Δ*msb2*, who controls Fmk1-regulated invasive growth functions and virulence of *F. oxysporum* on tomato plants, was significantly reduced in virulence (Perez-Nadales and Di Pietro, 2011). We tested the nine gene deletion mutants for virulence on tomato plants where the mortality rates of plants infected with the mutants lacking the genes *FOXG_08666*; *FOXG_13832*; *FOXG_15235*; *FOXG_00769*; *FOXG_10398*; *FOXG_12838* were significant reduced (p<0.05) than those plants infected with the wilt type or the deletion mutants lacking the genes *FOXG_04361*; *FOXG_08976* or *FOXG_09776* (Figure 9).

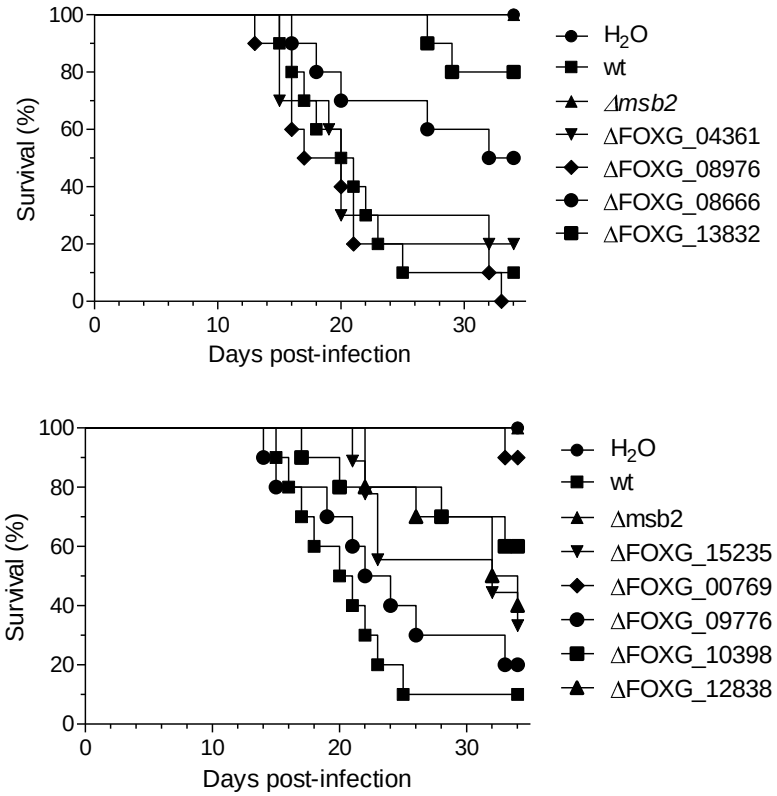

Figure 9. The nine deletion mutants showed dispersal in virulence on tomato plants. Groups of 10 two week old tomato seedlings (cultivar Money Maker) were inoculated with *F. oxysporum* strains by immersing the roots in a suspension of 5 x 10^6 freshly obtained microconidia ml $^{-1}$ of the indicated fungal strain for 30 min, planted in minipots containing vermiculite and incubated in a growth chamber at 28 °C. Evaluation was done using the disease index of *Fusarium* vascular wilt (1= healthy plant, 5= dead plant). Per cent of survival was recorded for 35 days. Mortality rates of plants infected with the mutants Δ*msb2*; as well those mutants lacking the genes *FOXG_08666*; *FOXG_13832*; *FOXG_15235*; *FOXG_00769*; *FOXG_10398*; *FOXG_12838* were significant lower (P<0.05) than those of plants infected with the wilt type or the deletion mutants lacking the genes *FOXG_04361*; *FOXG_08976* or *FOXG_09776*.

2.4. Yeast mating to verify protein-protein interaction from the Msb2-CT screen

2.4.1. Verification of the putative Msb2 interaction candidate proteins

The clones obtained by the Y2H screen as putative Msb2-CT interactors do not contain the complete ORF of the corresponding annotated gene. This is due to the cDNA library generation by using the SMART™ technology (Clontech). The CDS III primer which were used to amplify the RNA hybridize to the 3`-end of poly $A^+$RNAs and sequences close to the 5`end

of the transcript are therefore underrepresented. Table 2 shows the cDNA size (bp) of the pGADT7-Rec inserts in the Y2H clones and the size (bp) of the complete ORF`s obtained by a BLAST search of the Broad Institute Database (http://www.broadinstitute.org). To confirm the protein interaction of the candidate proteins and Msb2-CT, the cDNA of the complete ORF`s of the corresponding genes were cloned in the prey plasmid pGADT7-Rec, so that the entire protein is expressed as a fusion protein with GAL4 DNA-activation domain. Positive interactions were determined by yeast mating with the Gold strain expressing msb2-CT fused to the DNA-binding domain as it was used for the first screen against the cDNA library. The diploid cells were obtained on mating medium(SD-Leu/-Trp) and replated for positive interaction on high stringency selection medium(-Leu/-Trp/-His/-Ade/X-α-Gal/+Au).

Table 2. Verification Yeast Two- Hybrid (Y2H) assay with the complete ORF`s of the corresponding genes of the clones obtained as putative Msb2-CT interaction partner. The table shows the size of the cDNA (bp) obtained in the clones after the Y2H screen and the predicted size after BLAST search of the Broad institute database (http://www.broadinstitute.org). (+) indicates the unknown start or stop region of the indicated genes. The cDNA´s of the complete ORF´s of the candidate genes were amplified via PCR and cloned in the prey plasmid (pGADT7-Rec) to verify positive interaction by Y2H with Msb2-CT.

Gene	BLAST (Broad Institute)	BLAST (NCBI)	AD clone (bp)	Complete ORF (bp)
FOXG_13832	urease accessory protein ureG		525	810
FOXG_04361	conserved hypothetical protein	ubiquitin-conjugating enzyme	634	702
FOXG_00769	2421676- 2421848	glycoside hydrolase family 63		
FOXG_14173	predicted protein		214	336
FOXG_08666	conserved hypothetical protein	vacuolar carboxypeptidase Cps1	522	2015
FOXG_08976	formamidase		723	1233+
FOXG_09776	acetyltransferase		525	705
FOXG_10398	conserved hypothetical protein	glycoside hydrolase family 2 sugar binding protein	721	2247+
FOXG_12838	hypothetical protein similar to vesicle fusion factor NSFI		600	2319
FOXG_00231	proteasome component C5		689+	1064+
FOXG_15235	conserved hypothetical protein	C6 transcription factor (Ctf1B)	558+	2040+

The Y2H approach between Msb2-CT and the complete ORF`s of the candidate proteins (Table 2) confirmed two positive interactions. The Y2H using these two confirmed interactors

against the complete open reading frame of *msb2* (msb2-ORF-BD) fail to detect any interaction. The negative results with confirmed msb2-CT interacting proteins, implies that the complete ORF of the transmembrane protein Msb2 can not be used in an Y2H assay. The corresponding genes interacting with Msb2 in the Y2H control are *FOXG_10398* (glycoside hydrolase family 2) and *FOXG_13832* (urease accessory protein ureG). The corresponding deletion mutants were chosen for further investigations. Because of the interesting phenotypes of the deletion mutant of the gene *FOXG_00769*, this mutant was included as well in the following phenotypic investigation.

2.5. Phenotypical analysis of three candidates

Before analysing further phenotypes, the ability of the mutant strains Δ*FOXG_10398*, Δ*FOXG_13832* and Δ*FOXG_00769* to germinate and growth in standard culture media, defined minimal (MM) mediumand two nutrient rich mediumPDB and YPG, were tested and compared to the wt and the mutant strains Δ*msb2* and Δ*fmk1*. Defined number of microconidia were inoculated in the liquid cultures to determine the mycel dry weight after 15 h of incubation and revealed that none of the tested mutant strains showed a significant change in the ability to grow and germinate in any of the three *F. oxysporum* standard medium(Figure 10). However non of the mutant strains displayed aberrant growth in liquid cultures, Δ*FOXG_00769* showed a slight increase of fungal biomass in YPG.

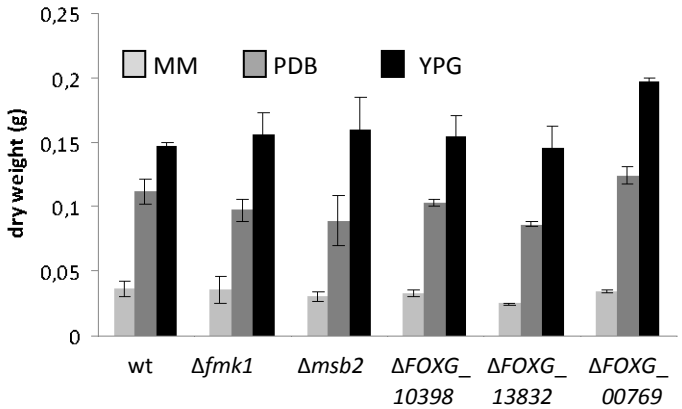

Figure 10. The analysis of the mycel-dry weight showed no significant differences in growth and germination between the indicated strains. To test the growing and germination ability of the mutants for further growth assays, 6,25x10^7 microconidia of the indicated strains were germinated and incubating for 24h either in 25 ml of PDB, YPG or MM media. Germlings were harvest, vacuum dried and weight. Bars represent standard errors calculated from 3 technical replicates.

2.5.1. *Fpr1* expression

To investigate a possible role of the candidate proteins in the Fmk1 pathway we examined expression of *fpr1* as it was performed in section 2.3.4. The lower expression of *fpr1* in the Δ*fmk1* mutant could be confirmed. No significant difference was detected in the mutants Δ*FOXG_13832*, Δ*FOXG_10398* or Δ*FOXG_00769*.

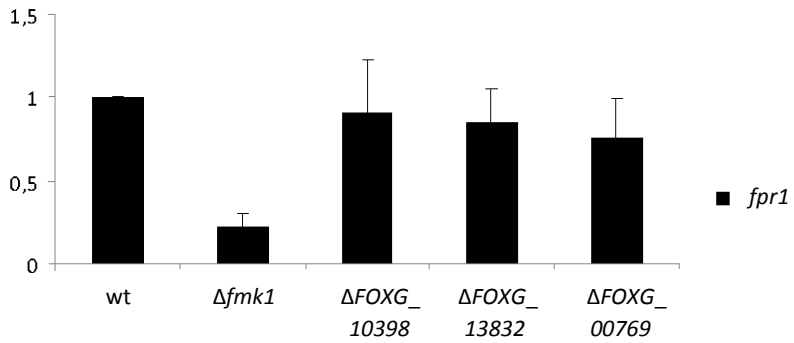

Figure 11. *fpr*1 mRNA abundance measurement by quantitative real-time PCR revealed no differences between the indicated strains. cDNA derived from RNA isolated from invasive growth condition (15 h germination in PDB, transfer and incubation for 4h on solid MM+ $NaNO_3$). Relative expression levels represent mean values normalized to the *actin* gene expression levels and relative to the expression in the wild type strain. Bars represent standard errors calculated from two biological and 4 technical replicates.

2.5.2. Determination of candidate genes expression in Δ*msb2* and Δ*fmk1* mutant strains

Quantitative real-time PCR was performed in the Δ*fmk1* and the Δ*msb2* mutant strains to determine if the expressions of the three candidate genes are regulated by the Fmk1 pathway via Fmk1 or Msb2 (Figure 12). Whereas no significant differences in gene expression levels were found in the Δ*fmk1* mutant comparing to the wt expression level, the expression of the candidate genes were significant reduced in the Δ*msb2* mutant. However, expression of Δ*FOXG_00769* which could not be confirmed in the Y2H assay was reduced in the Δ*msb2* mutant as well.

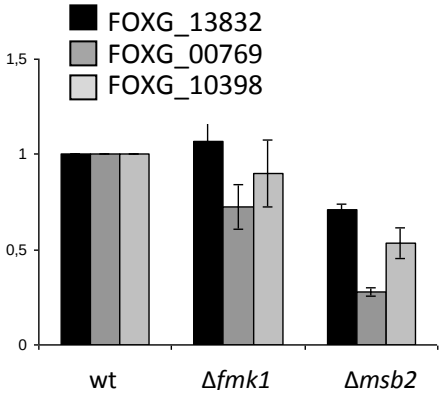

Figure 12. Reduced mRNA abundance of the three candidate genes in Δ*msb2*. mRNA abundance of the indicated genes was determined by quantitative real-time PCR. cDNA derived from RNA isolated from the indicated strains on invasive growth condition (15 h germination in PDB, transfer and incubation for 4h on solid MM+ $NaNO_3$). Relative expression levels represent mean values normalized to the *actin* gene expression levels and relative to the expression in the wild type strain. Bars represent standard errors calculated from 4 technical replicates.

2.6. Verification of Msb2 protein-protein interaction by switching the yeast plasmids and strains

2.6.1. *FOXG_10398* self-activates reporter gene expression

A further Y2H control was performed to confirm the two putative Msb2 interaction proteins. Therefore the plasmids and the yeast strains were switched. The cDNA of *msb2* was cloned into the pGADT7-Rec plasmid and transformed into the yeast strain Y187 where it is expressed as a fusion protein with the GAL4 DNA-activation domain (AD) and the cDNA of the two candidates (*FOXG_10398* and *FOXG_13832*) were cloned into the bait plasmid pGBKT7, transformed into the Gold yeast strain where they were expressed fused to the GAL4 DNA-binding domain (BD). The positive interaction were obtained after yeast mating and plating several dilution on yeast mating medium(-Leu/-Trp) and on selection medium(Q/+X-α-Gal/+Aur). In parallel the yeast mating with the distribution of the first Y2H screen was plotted as a confirmation. Negative controls were served either by the empty bait plasmid pGBKT7 or the prey plasmid containing the PCR fragment SV-40 Large T as an insert which encodes SV largeT-antigene (Clontech). The positive control was provided by the pGBKT7-53 encoding for a fusion between the GAL4 DNA-BD and murine p53 which interacts in the Y2H assay with SV40 largeT-antigen (Clontech). The Y2H confirmed the protein interaction between Msb2 and FOXG_10398 when cloned either in the bait or prey plasmid (Figure x), however expression of the reporter genes were self activated in diploid

cells when *FOXG_10398* was expressed as a fusion protein with the DNA-binding domain (bait plasmid pGBKT7 transformed into the Gold strain) in presence of the fusion protein of the negative control SV40 Large T (Figure 13).

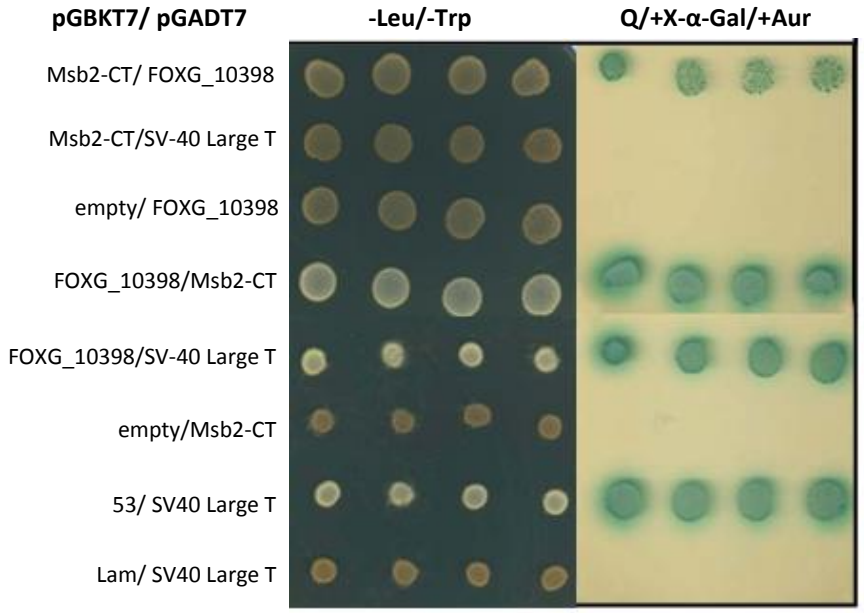

Figure 13 . The gene FOXG_10398 self activates the transcrition of the reptorter genes when fused to the DNA binding domain (pGBKT7 bait plasmid). FOXG_10398 was identified in a Y2H screen using the cytoplasmic tail (CT) of Msb2 as a bait against a cDNA library of *F. oxysporum*. The ORFs of *msb*2 CT and FOXG_10398 cDNA were either cloned into the plasmids pGBKT7 (expressed as a fusion protein with the Gal4 DNA-binding domain) and pGADT7 (expressed as a fusion protein with the Gal4 activation domain) and transformed in the yeast strains Gold or Y178, respectively. Drop test shows, that FOXG_10398 expressed the reporter gene expression when when its fused to AD-domain as well to the BD-domain in the presence of the apropriate Msb2-CT fusion protein. But FOXG_10398 is self-activating when fused to the DNA binding domain and activates the transcrition of the repoter genes in presence of the negative controle fusion protein SV40 Large T-AD . Protein interaction in the dipoid cells after yeast mating were determined via drop test of different dilutions spotted on mating control medium(SD–Leu/-Trp) and selection medium(SD-Leu/-Trp/-Ade/-His/+ X-α-Gal/+Aureobasisin).

2.6.2. The cytoplasmic tail of Msb2 interacts with UreG in a Yeast Two-Hybrid assay

The same controlles were performed to confirm the protein interaction btween Msb2 and FOXG_13832. First the entire cooresponding cDNA sequence was cloned either in the bait

plasmid (pGBKT7) and transformed in the Gold strain and as well in the pGADT7-Rec plasmid which was transformed into the Y187 strain. Our results show that *FOXG_13832* leading reporter gene expression when when fused to AD-domain as well when fused to the BD-domain only in the presence of the apropriate Msb2-CT fusion protein, but not in presence of the negative bait controle pGBKT7-BD-empty or prey controle pGADT7- SV40 Large T-AD. Through switching the plasmids and the yeast strains we confirmed the positive protein interaction between Msb2-CT and the protein of the gene *FOXG_13832* in the Y2H assay (Figure 14).

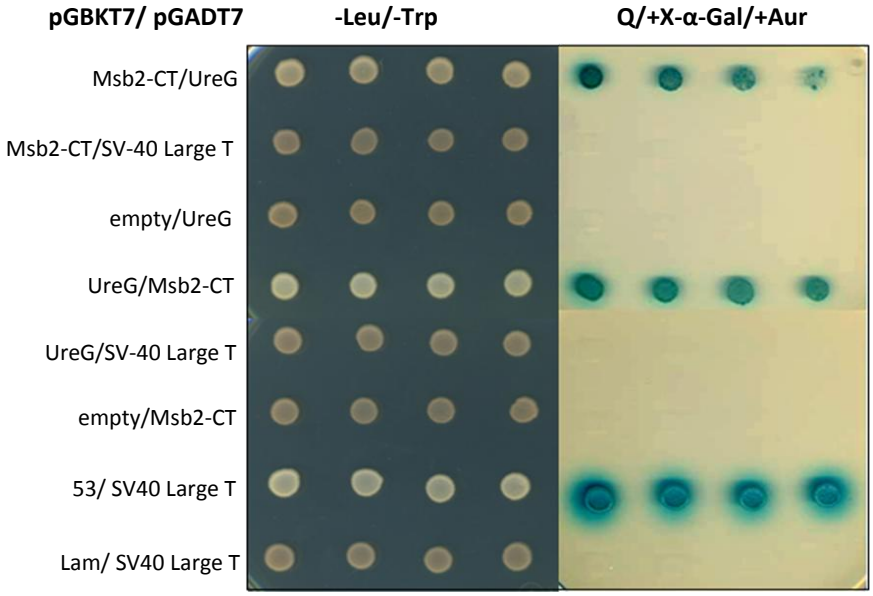

Figure 14 . The Msb2-CT interacts with FOXG_13832 in a Yeast Two-Hybrid (Y2H) assay. *FOXG_13832* was identified in a Y2H screen using the cytoplasmic tail (CT) of Msb2 as a bait against a cDNA library of *F. oxysporum*. The ORFs of *msb*2 CT and *FOXG_13832* cDNA were either cloned into the plasmids pGBKT7 (expressed as a fusion protein with the Gal4 DNA-binding domain) and pGADT7 (expressed as a fusion protein with the Gal4 activation domain) and transformed in the yeast strains Gold or Y178, respectively. Drop test shows, reporter gene expression when *FOXG_13832* is fused to AD-domain as well when fused to the BD-domain only in the presence of the apropriate Msb2-CT fusion protein but not in presence of the negative bait controle pGBKT7-BD-empty or prey controle pGADT7- SV40 Large T-AD. Protein interaction in the dipoid cells after yeast mating were determined via drop test of different dilutions spotted on mating control medium(SD–Leu/-Trp) and selection medium(SD-Leu/-Trp/-Ade/-His/+ X-α-Gal/+Aureobasisin).

2.7. Δ*FOXG_00769* phenotypes were not reproducible

To confirm the Δ*FOXG_00769* phenotypes, growth assays and virulence related assays were performed with two independent Δ*FOXG_00769* deletion mutants (Δ*FOXG_00769*#2; Δ*FOXG_00769*#10) and two complemented Δ*FOXG_00769*+ *FOXG_00769* strains (Δ*FOXG_00769*+ *FOXG_00769*#1; Δ*FOXG_00769*+ *FOXG_00769*#6).

2.7.1. Vegetative and invasive hyphal growth phenotypes are not reproducible

Vegetative growth on MM and YPDA and cellophane penetration assay displayed the aberrant growth and impaired cellophane penetration of the mutant Δ*FOXG_00769*#2. This phenotype could not be confirmed by the independent Δ*FOXG_00769*#10 mutant. In addition these phenotypes were still present in two complemented strains (Figure 16).

The same observations were made concerning the ability of invasive growth on living plant tissue. Only the Δ*FOXG_00769*#2 but not the Δ*FOXG_00769*#10 mutant strain showed reduced invasive growth on apple slides in comparison to the wt just as well two independent complemented strains didn't restore this phenotype (Figure 15). Our results suggesting that the recorded phenotypes we observed where not caused by the deletion of the gene *FOXG_00769*.

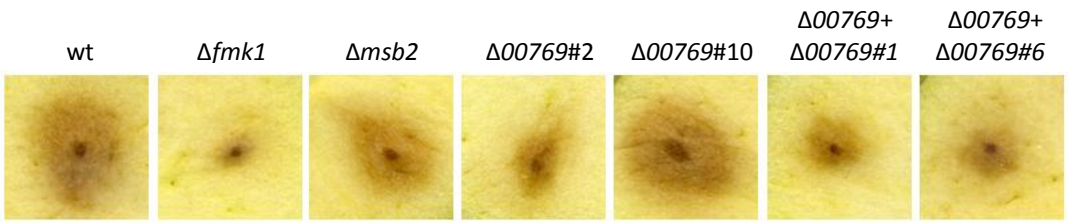

Figure 15. Reduced invasive growth on living fruit tissue of Δ*FOXG_00769* is not reproducible and is not restored after gene complementation. Apple fruits were inoculated with 5µl of 10^7 con/ml (5x 10^4) microconidia of the indicated strains and incubated in a humid chamber at 28°C for 3 days. Experiments were designed with 4 replicas. Data shown are from one representative experiment.

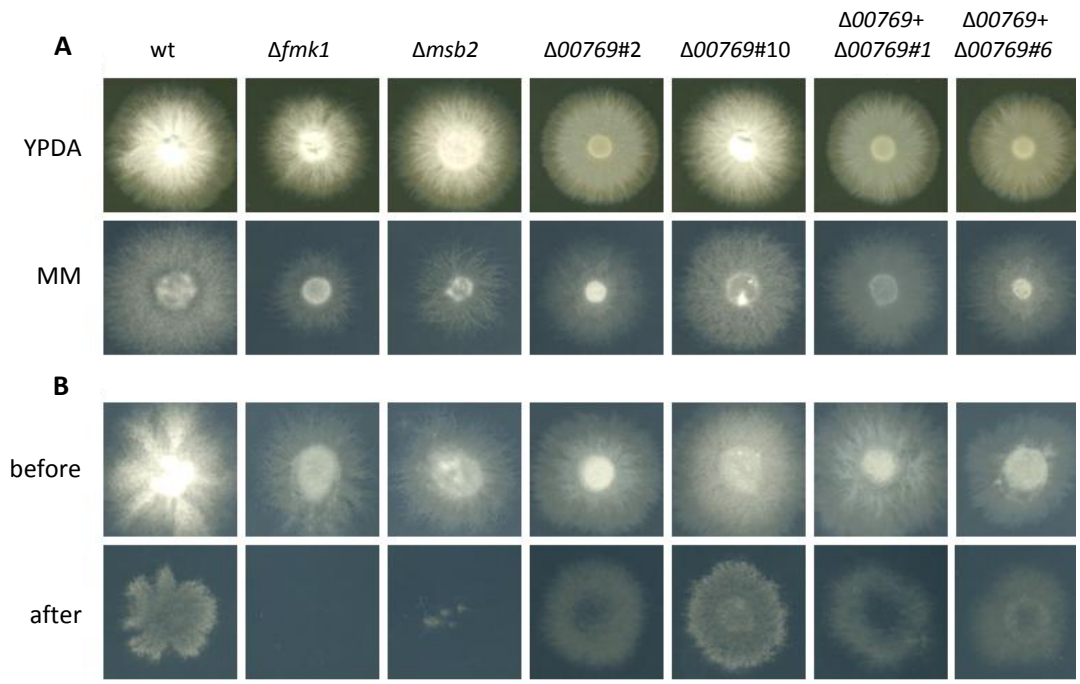

Figure 16. Different phenotypes on YPDA and MM medium(A) and invasive Cellophane penetration (B) are not reproducible by using independent *FOXG_00769* deletions. (A) 5µl of a microconidia suspension (10^7 con/ml) was spot-inoculated on MM or YPDA agar plates and incubated 3 days at 28°C. **(B)** 5µl of a microconidia suspension (10^7 con/ml) was spot-inoculated on MM agar plates covered with a cellophane membrane. To determine the penetration of the cellophane membranes the cellophane sheets with the fungal colony were removed after 4 days (before) and the plates were incubated for an additional day at 28 °C (after).

2.7.2. Sothern-blot analysis of Δ*FOXG_00769* and gene complementation

The distinct phenotypes of the deletion mutants and their complemented strains prompted us to perform a southern-blot analysis. The results confirmed a successful gene deletion of the two mutants *FOXG_00769*#2 and *FOXG_00769*#10. Further it confirmed the genetically integration of the *FOXG_00769* gene in the two complemented strains Δ*FOXG_00769*+ *FOXG_00769*#1 and Δ*FOXG_00769*+ *FOXG_00769*#6. These results clearly confirmed that the observed phenotypes of the mutant strain *FOXG_00769*#2 is not causes by the deletion of the gene *FOXG_00769*.

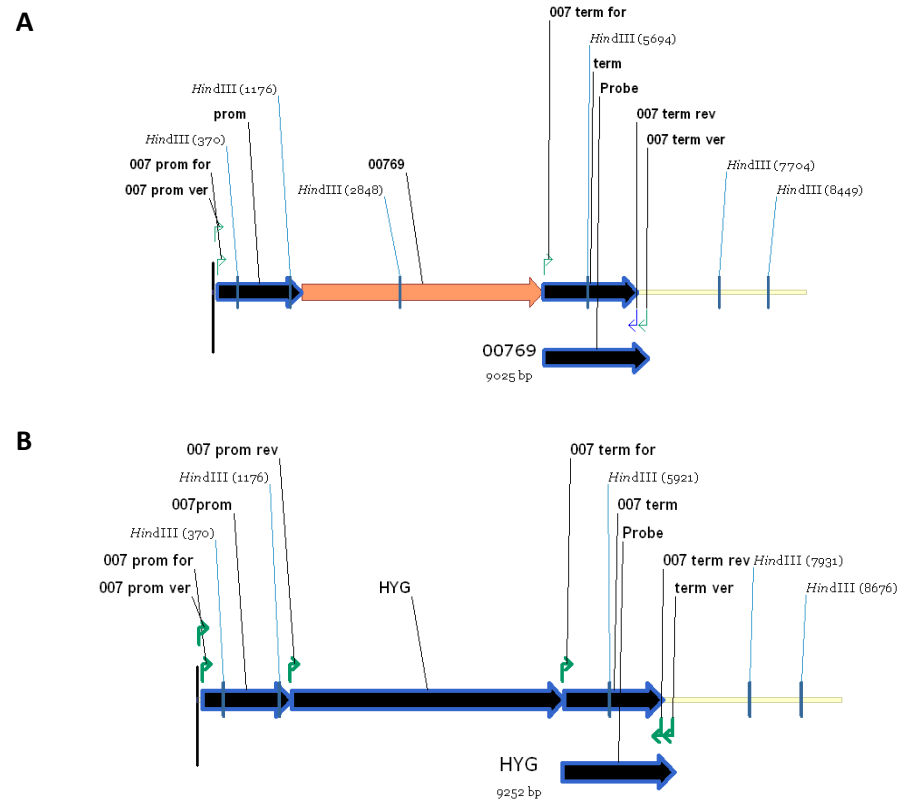

Figure 17: Southern-Blot hybridisation analysis confirmed two genetically successful deletions of the gene *FOXG_00769* and two complemented strains. Genomic maps of the gen locus of *FOXG_00769* in the wild type **(A)** and after introducing of the gene replacement construct **(B)**. The position of the primers used for generation of the split-marker construct as well for PCR analysis of the transformants and complemented strains are indicated. Genomic DNA was digested with *Hind*III and hybridized with a probe consist of the terminator region which is indicated as an arrow. **(C)** Southern-blot analysis showing the wild type strain 4287 and two successful deletion mutants of the gene *FOXG_00769* (#2 and #10), ectopic integration (ect1 and ect2) and two successful complemented strains (#1 and #6) and a multiple integration of the *FOXG_00769* gene (#3). Molecular sizes of the hybridizing fragments are: wt: 2010 bp and 2846 bp; Δ*FOXG_00769* deletion: 2010 bp and 4745 bp.

2.8. Yeast Two-Hybrid approach to verify certain protein-protein interaction

2.8.1. Examination of protein-protein interaction of Msb2 with Sho1 and Cdc42

In *S. cerevisiae*, Msb2 has been shown to interact with the transmembrane protein Sho1 (Cullen et al., 2004). Further they demonstrate that Msb2 interacts with Cdc42 to provide a role in the Kss1 filamentous growth pathway. To investigate a possible interaction in *F. oxysporum* the Y2H approach was performed by using the Gold strain expressing either the Msb2 cytoplasmic tail as a Msb2-CT GAL4 DNA-BD fusion protein or the complete open reading frame of msb2 Msb2-ORF GAL4 DNA-BD. After yeast mating with the Y178 strain expressing the fusion protein Sho1-GAL4 DNA-AD or Cdc42-Gal4 DNA-AD diploid cells were confirmed on mating medium(SD-Leu/-Trp, Figure 18 A). No growth could be detected by re-streaking these colonies on protein interaction selection medium (Q/+X-α-Gal/+Aur, Figure 18 B) which confirmed that neither Msb2-CT nor Msb2-ORF is interacting with Sho1 or with Cdc42 in our Y2H assay.

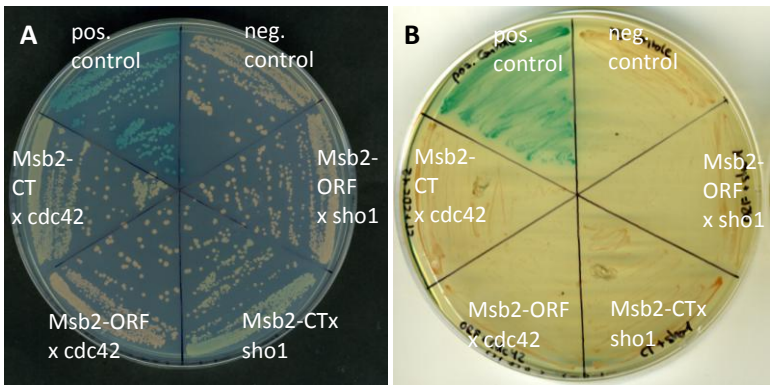

Figure 18. Msb2 (CT or ORF) is not interacting with Sho1 or Cdc42 in a Y2H assay. The cDNA of the transmembrane protein Sho1 and the small G protein Cdc42 were cloned in the prey plasmid pGADT7-Rec and transformed into the Y187 strain (expressed as a fusion protein with the Gal4 activation domain). Interaction were tested via yeast mating with the cDNA of the complete open reading frame of *msb2* (msb2-ORF) and the cytoplasmic tail (msb2-CT) cloned into the plasmid pGBKT7 (expressed as a fusion protein with the Gal4 DNA-binding domain). Protein interaction in the dipoid cells after yeast mating were determined on mating control medium (**A**: SD–Leu/-Trp) and selection medium (**B**: SD-Leu/-Trp/-Ade/-His/+ X-α-Gal/+Aureobasisin).

2.8.2. Examination of protein interaction with proteins from the velvet complex and AreA

Previous studies have demontrate that the heterotrimeric velvet complex co-ordinates fungal development and biosynthesis of secondary metabolites by modulating chromatin accessibility and gene expression (Bayram et al., 2008; Reyes-Dominguez et al., 2010). The member who belongs to the velvet protein family includes VeA, VelB, VelC and VosA. It was shown that in the absence of light, VeA and VelB interact and enter the nucleus (Bayram et al., 2008), where they assemble with the non-velvet protein LaeA, a global regulator of secondary metabolism (Bok and Keller, 2004; Bok et al., 2006). *F. oyxsporum* members of the velvet protein complex govern hyphal growth and conidiation, as well as virulence on tomato plants and immunodepressed mice (Lopez-Berges et al., 2013). By means of the Y2H approach we investigate protein interaction between members of the velvet complex in *F. oxysporum* (Figure 19). We show that in the Y2H the VeA protein can interact with both proteins VelB and VelC. We also detect a self-interaction VelB-VelB which was recently described in *A. nidulans* (Sarikaya Bayram et al., 2010). Further we detect the interaction between VelB and VelC and LaeA with VeA.

Controls were provided by using the SV40 largeT-antigen- GAL4 DNA-AD together with Gold-pGBKT7-53 GAL4 DNA-BD (positive control) or with Gold-pGBKT7-Lam GAL4 DNA-BD (negative control). A self activation of any of the tested proteins when expressed together either with the empty bait plasmid pGBKT7 or the prey plasmid containing the PCR fragment SV-40 Large T was not observed and all positive interaction were confirmed as well when plasmids and yeast strains were switched (data not shown).

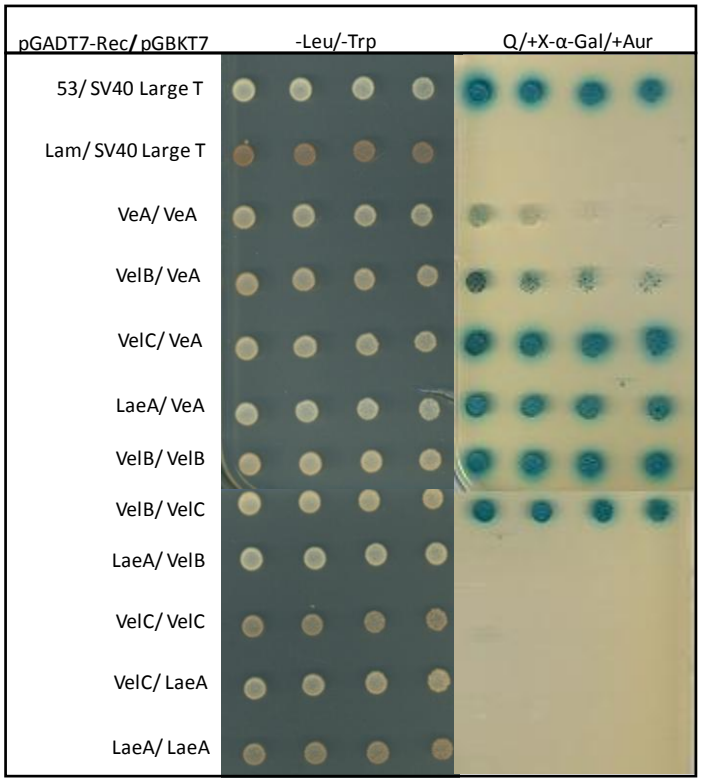

Figure 19. Member of the velvet protein complex interacting with each other in a Yeast Two-Hybrid (Y2H) assay. The ORFs of veA, velB, velC and laeA cDNA were either cloned into the plasmids pGBKT7 (expressed as a fusion protein with the GAL4 DNA-binding domain) and pGADT7-Rec (expressed as a fusion protein with the GAL4 activation domain) and transformed in the yeast strains Gold or Y178, respectively. Drop test shows a postitive protein interaction between VeA:VelB; VeA:VelC, VeA:LaeA; VelB:VelBVelC:VelB. None of the tested proteins showed a self activation in presence of the negative bait controle pGBKT7-BD-empty or prey controle pGADT7- SV40 Large T-AD (data not shown). Protein interaction in dipoid cells after yeast mating were determined via drop test of different dilutions spotted on mating control medium(SD–Leu/-Trp) and selection medium(SD-Leu/-Trp/-Ade/-His/+ X-α-Gal/+Aureobasisin).

In fungal organisms the nitrogen metabolite repression (NMR) mechanism ensures that genes required for the utilization of alternative nitrogen sources are only transcribed in the absence of preferred sources such as ammonium or glutamine. This depends on the wide domain nitrogen response regulator AreA/Nit2 (Arst and Cove, 1973; Marzluf, 1997). AreA belongs to the GATA factors, a class of transcriptional regulators present in fungi, metazoans and plants featuring a highly conserved DNA-binding motif comprising a Cys(4) zinc finger (Kudla et al., 1990; Scazzocchio, 2000). In *F. oxysporum*, AreA is also required for de-repression of NMR genes and a Δ*areA* mutant was shown to be deficient in nitrate-triggered upregulation of the *nit1* (nitrate reductase), *nii1* (nitrite reductase) and *mepB* (ammonium permease) genes (Lopez-Berges et al., 2010). Recently it was shown that velvet proteins and AreA function in parallel by promoting chromatin accessibility and transcription of nitrate metabolism genes, as well as secondary metabolite gene clusters encoding the ferricrocin

and BEA (Lopez-Berges et al., 2013). We therefore tested protein interaction between AreA and members of the velvet protein complex. However yeast two-hybrid experiments revealed a self-activation of AreA when fused to the DNA-binding domain, we were unable to confirm any interaction between AreA and members of the velvet complex proteins (Figure 20), suggesting that AreA and velvet have common, but physically separate functions in the regulation of chromatin structure and transcriptional activity of the ferricrocin and BEA gene clusters (Lopez-Berges et al., 2013).

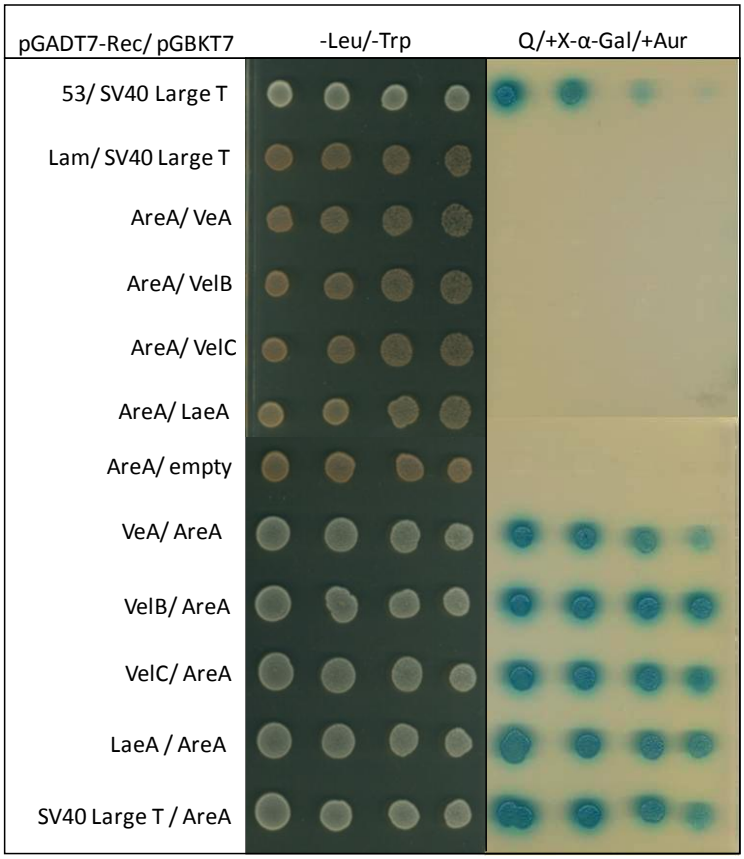

Figure 20 . AreA is not interacting physically with members of the velvet protein complex in a Y2H assay. The ORFs of areA and veA, velB, velC and laeA cDNA were either cloned into the plasmids pGBKT7 (expressed as a fusion protein with the GAL4 DNA-binding domain) and pGADT7-Rec (expressed as a fusion protein with the GAL4 activation domain) and transformed in the yeast strains Gold or Y178, respectively. Drop test shows no protein interaction between AreA with any member of the velvet protein complex. AreA showed a self activation when cloned into the bait plasmid (DNA-BD plasmid) in presence of the negative prey controle pGADT7- SV40 Large T-AD. Protein interaction in the dipoid cells after yeast mating were determined via drop test of different dilutions spotted on mating control medium(SD–Leu/-Trp) and selection medium(SD-Leu/-Trp/-Ade/-His/+ X-α-Gal/+Aureobasisin).

3. Discussion

3.1. The Y2H assay confirmed the interaction between FOXG_13832 and the cytoplasmic tail of Msb2

In the present work we performed the Y2H approach to confirm known and to find new protein interactions in *F. oxysporum*. Msb2 is an integral-membrane protein containing a presumptive and highly conserved cytoplasmic domain (Perez-Nadales and Di Pietro, 2011) therefore the Y2H library screen as well as direct two-hybrid analysis was performed using its cytoplasmic tail (Msb2-CT). In line with our hypothesis that the cytoplasmic domain provides an important part of interaction with certain intracellular proteins are previous reports from *S. cerevisiae* demonstrating that the cytoplasmic tail physically interacts with Cdc42 a component of the filamentous growth pathway or with Mig1 (see Discussion section x) a co-regulator of the filamentous growth pathway in response to glucose limitation (Cullen et al., 2004; Karunanithi and Cullen, 2012).

However we included the complete open reading frame of Msb2-ORF in our library screen and as well afterwards with confirmed protein interactors, detection of any protein interaction remain unsuccessful. Additionally, non growth after re-plating diploid cells on high stringency mediumsuggest that the Msb2-ORF is due to the transmembrane domain next to impossible to use for our purpose.

After the Y2H library screen, sequencing of the chosen 35 candidates out of 134 clones revealed eleven different candidate proteins interacting with the cytoplasmic tail of Msb2. As a first step to confirm the protein interaction we decided to perform deletion mutants of the corresponding genes to screen for known Δ*msb2* and/or Δ*fmk1* phenotypes. But phenotypical investigation of the mutant strains displayed a bride distribution between the mutant strains as well as in comparison to Δ*msb2* and/or Δ*fmk1*.

For example, a different colony growth phenotype on YPDA media, but not in diameter measurements, was observed of the mutant strains lacking the genes *FOXG_15235* and *FOXG_00769* but not with Δ*msb2* or Δ*fmk1*. In contrast a known phenotype of Δ*msb2* and

Δ*fmk1*, the impaired/non ability of cellophane penetration was observed with the mutants Δ*FOXG_15235*, Δ*FOXG_00769* and Δ*FOXG_12838*.

A role in the Fmk1 pathway should be determined by *fpr1* expression which is transcriptionally regulated by the Fmk1 MAPK cascade (Prados-Rosales and Di Pietro, unpublished). However a reduced *fpr1* expression was achieved in the Δ*FOXG_04361*, Δ*FOXG_08976*, Δ*FOXG_08666* and Δ*FOXG_09776* mutants. Fmk1 was under-phosphorylated in the deletion mutants lacking the genes *FOXG_08976*, *FOXG_00769* and *FOXG_15235* and was hyper-phosporylated in the mutants of the genes *FOXG_04361*, *FOXG_12838.*

Similar dispersal was obtained with the mortality rates of plants infected with the mutants, showing reduced virulence of Δ*FOXG_08666*; Δ*FOXG_13832*; Δ*FOXG_15235*; Δ*FOXG_00769*; Δ*FOXG_10398*; Δ*FOXG_12838* than those plants infected with the wilt type or the deletion mutants lacking the genes *FOXG_04361*; *FOXG_08976* or *FOXG_09776.* Importantly, none of the mutants displayed impaired growth on CFW, implying not be involved in the cell wall integrity pathway. Although the Δ*FOXG_00769* mutant showed a different colony phenotype on mediumcontaining CFW we further confirmed that this phenotype might not be caused by the deletion of this gene. We suggest that this strain might go through unknown defects during the transformation process.

Therefore we next confirmed the interaction of the putative candidates and Msb2-CT by performing the Y2H by cloning the complete ORF`s of the candidates. The cDNA library was generated (using the SMART$^{TM}$ technology; Clontech) with primer which amplify the RNA by hybridizing at the 3`-end of poly A^{+}RNAs therefore sequences close to the 5`end of the transcript are underrepresented. Unexpected, only two of the previous eleven interactions could be confirmed as an protein interactor of Msb2-CT. We suggest that a shorter version of some proteins may result in a different protein folding which may cause interactions however resulting in false positive. Switching of the plasmids and the corresponding yeast strains, an additional Y2H control, clearly confirmed the interaction of Msb2-CT with the encoding protein of the gene *FOXG_13832*. This gene is encoding for a urease accessory protein UreG. The function and role of this protein in *F. oxysporum* will be discussed in full length in the following sections.

3.2. Msb2 does not interact with Sho1 or Cdc42 in a Y2H assay

It has been reported that Msb2 physically interacts with certain proteins (Cullen et al., 2004; Karunanithi and Cullen, 2012). One of this interaction in *S. cerevisiae* was confirmed by co-immunoprecipitation determined a physical interaction with Sho1, however this physical interaction has been shown not be located at the cytoplasmic domain of Msb2 (Cullen et al., 2004). In *S. cerevisiae* Msb2 and Sho1 interacting to regulate signalling cascades involved in osmotic stress response and pseudohyphal growth and are required for activation of the MAPK Kss1 to regulate filamentous growth and agar invasion in response to nutrient limitation (Chen and Thorner, 2007; Cullen et al., 2004; Vadaie et al., 2008). Additionally, Msb2 in yeast interact with Cdc42, and it has been hypothesized that this complex provide sensory capacity in the filamentous growth pathway transmitted via the PAK kinase Ste20 (Cullen et al., 2004).

In *Ustilago maydis* attempts to visualize an interaction between Sho1 and Msb2 relying on epitope-tagged proteins and co-immunoprecipitation were unsuccessful and it has been suggested that interactions were only transient and may be restricted to appressoria (Lanver et al., 2010). Interestingly a Y2H approach revealed a physical interaction between Sho1 and Kpp6, the Kss1 orthologue in *U. maydis* (Mendoza-Mendoza et al., 2009).

Our Y2H screen using Msb2-CT as a bait against a cDNA library of *F. oxysporum* did not reveal any of the previously reported proteins, Sho1 or Cdc42. And the additional attempt to confirm the physical interaction by using direct protein-protein interaction approach was unsuccessful. This might be reasonable, since the MSb2-Sho1 interaction in yeast was determined by co-immunoprecipitation and has been shown not to be located at the cytoplasmic domain of Msb2. Although we can not exclude for both, Sho1 and Cdc42 that a putative interaction in vivo needs certain co-factors or stimuli or are only transient and may be restricted to certain environmental condition or development structure.

3.3. Members of the *F. oxysporum* velvet protein complex physical interact with each other

To determine the role of member belonging to the velvet protein family including VeA, VelB, VelC and VosA (Bayram et al., 2008) and the non-velvet protein LaeA, a global regulator of secondary metabolism (Bok and Keller, 2004; Bok et al., 2006) the yeast two-hybrid (Y2H) assay was used. Additionally we included the GATA factors AreA, a transcriptional nitrogen response regulator in *F. oxysporum* (Lopez-Berges et al., 2010). We systematically studied pairwise interaction where a single "bait" test protein was individually assayed in a Y2H system against a "prey" test protein (Fields and Song, 1989; Yu et al., 2004). An interaction was measured as a function of growth on selective mediumand confirmed by growth and color development on high-stringency selective media. However expressing *areA* as a DNA-BD fusion protein resulted in self-activation of the reporter gene expression, we could confirm interaction between members of the velvet protein complex. This results together with previous reports (Bayram and Braus, 2012) allowing a model for the role of members of the velvet complex in regulation of hyphal growth and development in *F. oxysporum*, where VeA forms a complex with VelB or VelC that have both overlapping functions in different development processes (Lopez-Berges et al., 2013). Further we confirmed the self-interaction of VelB-VelB which was recently described in *A. nidulans* (Sarikaya Bayram et al., 2010) as well as an interaction between VelB and VelC whose biological role is currently unknown.

Chapter 4

Components of the urease complex govern virulence of *Fusarium oxysporum* on plant and animal hosts

Summary

In the soilborne pathogen *Fusarium oxysporum,* a mitogen-activated protein kinase (MAPK) cascade homologous to the yeast filamentous growth pathway controls invasive growth and virulence on tomato plants. Full phosphorylation of Fmk1 requires the transmembrane protein Msb2, a member of the family of signalling mucins that have emerged as novel virulence factors in fungal plant pathogens. A yeast two-hybrid screen for proteins interacting with the Msb2 cytoplasmic tail identified UreG, a component of the urease enzymatic complex. UreG belongs to a set of accessory proteins needed to activate Apo-urease, which converts urea to yield ammonia and carbon dioxide. The *F. oxysporum* genome contains two structural urease genes, *ure1* and *ure2*. Mutants in *ureG* or *ure1* showed reduced growth on urea as the sole carbon and nitrogen source. Lack of urease activity in the mutants resulted in failure to secrete ammonia and to increase the extracellular pH; a mechanism strongly depends on the depletion of glucose.

The Δ*ureG* mutants caused significantly reduced mortality on tomato plants and on the animal model host *Galleria mellonella* as well in immunosupressed mice, while Δ*ure1* mutants only showed reduced virulence on tomato plants. Real-time qPCR analysis of key genes involved in nitrogen uptake and assimilation, as well as in the urea cycle, during infectious growth of *F. oxysporum* in *G. melonella* revealed increased transcript levels of arginase, which converts arginine to urea. The arginase knockout showed reduced virulence in plant and animal infection. Our results show that the urease accessory protein UreG plays an important role in pH modulation and fungal virulence on plant and animal hosts.

1. Introduction

1.1. Urea

Urea or carbamide ($CO(NH_2)_2$) is an organic compound consisting of two $–NH_2$ groups joined by a carbonyl (C=O) functional group. It occurs in nature as a by-product of animal metabolism of nitrogenous compounds, being the main nitrogen-containing substance in the urine of mammals (Smith, 2009). On the other hand, it is the world`s most common form of nitrogen fertilizer (http://faostat.fao.org), with a sustained increase in its use during the last four decades (Glibert, 2006). Consequently, its enzymatic hydrolysis is a process of great agriculture importance.

Urea was first discovered in human urine by Hillaire M. Rouelle in 1773. In 1798 it was recognized by Fourcroy and Vauquelin that ammonia in urine derives from the fermentation of urea and as a milestone in chemistry it became the first organic compound synthesized from inorganic materials (Wöhler, 1828). Urea is synthesized in many organisms as part of the urea cycle, either from the oxidation of amino acids or from ammonia. In the urea cycle, amino groups donated by ammonia and L-aspartate are converted to urea, with L-ornithine, citrulline, L-argininosuccinate, and L-arginine acting as intermediates. In animals, urea is produced in the liver, carried in the bloodstream to the kidneys and excreted in urine. Urea is highly soluble in water, practically non-toxic, neither acidic nor alkaline, and provides a vehicle for the body to transport and excrete excess nitrogen. The concentration of urea in the serum of healthy humans amounts to 1-10 mM (in blood of mice 1 to 3 mM (Mirbod-Donovan et al., 2006) and its concentration in urine is around 0, 5 mM (Burne and Chen, 2000; Collins and D'Orazio, 1993). Urea is able to pass across biological membranes and is evenly distributed in the subcutaneous adipose tissues, central nervous system (CNS), epithelial lining fluid, and blood serum (Ronne-Engstrom et al., 2001; Tyvold et al., 2007; Waring et al., 2008; Zielinski et al., 1999). 20-25% of all urea produced is estimated to remain in the intestinal tract. This renders urea readily available making the urinary and intestinal tracts to the most common site of ureolytic bacteria infections in human (Burne and Chen, 2000; Collins and D'Orazio, 1993).

Bacteria, fungi and plants are able to utilize urea as a nitrogen source, incorporating it into the cell through specific transporters. The first protein related to the sodium symporter superfamiliy which compromises more than hundred membrane proteins was ScDur3 described in *S. cerevisiae*. ScDur3 incorporates urea when the external concentration is below 0.25mM whereas at concentration above 0.5mM it enters the cell via facilitated diffusion (Cooper and Sumrada, 1975; Sumrada et al., 1976).

Plants can assimilate nitrogen in form of urea though the roots and higher plants posses various urea transport systems, both passive and active, which allow internally and environmental urea assimilation (Witte, 2011). In contrast to the external applied urea, intern urea originates from the breakdown of arginine and from purines and ureides (Goldraij and Polacco, 1999; Zonia et al., 1995) and accumulates in source leaves of older plants and in germinating seeds (Zonia et al., 1995). Urea is synthesized inside mitochondria during arginine degradation via arginase in the ornithine or urea cycle (Polacco, 1993b) and then exported to cytoplasm and hydrolyzed by urease (for details see section 1.4.2. and 1.12.1).

1.2. Urease

An un-catalyzed hydrolysis of urea has never been observed (Blakeley et al., 1982). In higher plants, some fungi and many prokaryotes, urea is hydrolyzed by urease which allows organisms to use externally and internally generated urea as a source of nitrogen (Mobley and Hausinger, 1989). In 1874 the first ureolytic microorganism *Micrococcus ureae* was isolated from urine by van Tieghem, and the first ureolytic enzyme was obtained in 1874 by Musculus from putrid urine. Miquel in 1890 proposed the name urease.

Urease (urea amidohydrolase EC 3.5.1.5) enzymes are widespread among plants, bacteria, fungi, algae and invertebrates, but absent in mammals. The activity of urease is strongly dependent on pH. The enzyme is active in a pH range of 4.5 to 10.5, with the optimum activity at pH 7-8 (Krajewska, 2009).

Both urea and urease represent landmark molecules in early scientific investigations. In 1926, the crystallization of urease from jack bean (*Canavalia ensiformis*) by James B. Sumner

(Sumner, 1926), showed for the first time that enzymes are proteins that can be crystallized and was awarded the Nobel prize in chemistry in 1946. Jack bean urease was also the first enzyme shown to contain nickel ions at the active side that are essential for enzymatic activity (Dixon et al., 1975).

Prokaryotic ureases are generally encoded by three genes (Mulrooney and Hausinger, 2003). *UreA, ureB* and *ureC* encode the structural subunits of urease (α,β and γ, respectively), which associate in an αβγ stoichiometry to form the apo-enzyme (Jabri et al., 1995). By contrast, in plants and fungi the structural urease protein is encoded by a single gene that comprises homologues of the three bacterial subunit genes (Follmer, 2008; Jabri et al., 1995).

Urease catalyzes the hydrolysis of urea to yield ammonia and carbamate (Mack and Villars, 1923; (Blakeley et al., 1969a; Sumner and Kirk, 1931). The latter compound spontaneously decomposes to yield another molecule of ammonia and carbonic acid (Scheme 1). In solution, the released carbonic acid and the two molecules of ammonia are in equilibrium with their deprotonated and protonated forms, respectively. The net effect of these reactions is an increase in pH.

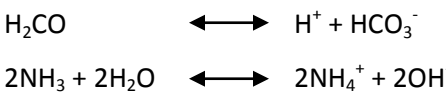

Scheme 1. Urease reaction. Enzymatic hydrolysis of urea to carbamate catalysed by urease and subsequent non-enzymatic decay of carbamate. Two mol ammonia and one mol carbon dioxide are generated from urea by these reactions.

Functionally, ureases belong to the superfamily of amidohydrolases and phosphotriesterases (Holm and Sander, 1997). All ureases studied so far required nickel as a cofactor for enzymatic activity (Carter et al., 2011). A common feature of these enzymes is the presence of metal centres at the active site, whose task is to activate the substrate and water for the reaction. Among dinuclear metallohydrolases in this superfamily, ureases are unique in that they possess nickel ions in the active site. During *in vivo* urease activation, accessory proteins

are absolutely required for GTP-hydrolysis-dependent incorporation of CO_2 and nickel into the apo-urease (Soriano and Hausinger, 1999).

Urease is generally assumed to be cytosolic because it does not contain an apparent subcellular targeting peptide, and several proteins required for urease activation appear to be cytosolic as well. However, evidence from studies on both plant and bacterial ureases suggest that the active enzyme may also be cell surface associated (Cambui et al., 2009; Dunn et al., 2001; Millanes et al., 2004). For *Helicobacter pylori* it was shown that the urease enzyme is released upon lysis of some bacterial cells and then associates with the surface of intact cells, where it can account for up to 30% of the total activity, (Krishnamurthy et al., 1998), followed by absorption of the enzymatically active protein to intact, viable bacteria (Dunn and Phadnis, 1998). A similar process has been suggested during the parasitic cycle of *Cryptococcus posadasii* where urease has been immunolocalized to the spherule cytoplasm and vesicles and the large vacuole (Mirbod-Donovan et al., 2006). The parasitic cells (spherules) lyse, releasing active urease. Subsequently the enzyme associates with the surface of intact endospores and the spherule outer wall fraction, which is produced in abundance during in vitro growth of the parasitic phase (Hung et al., 2000; Hung et al., 2002). Recently, a partial cell wall and membrane localization of urease has been suggested in bromeliad species (Aguetoni Cambui et al., 2009). Interestingly, in certain lichens a polygalactosylated urease acts as cell wall-associated algal receptor for the recognition of adequate fungal partners by binding a fungal lectin that is related to arginase (Vivas et al., 2010).

Although originally believed to be absolutely urea-specific, ureases are now known to hydrolyze a number of substrates albeit at a much lower rate (Krajewska, 2009). These alternative substrates can be classified into two distinct groups, the urea analogues and the phosphoric acid amides and esters. Most of them are considered to act both as enzyme substrate and as inhibitors (see Section 1.9.).

1.3. Structure of urease

All ureases form a basic trimeric structure. In most bacteria, each unit of the homotrimer is itself a heterotrimer of UreA, UreB and UreC subunits (Carter et al., 2009). Bacterial ureases are composed of three distinct subunits, one large (α, 60-76 kDa) and two small (β, 8-21 kDa and γ, 6-14 kDa), forming (αβγ) trimers, resulting in the enzyme molar mass between 190 and 300 kDa (Benini et al., 1999; Jabri et al., 1995). By contrast, the urease of *Helicobacter* species are composed of two subunits, α (61-66 kDa) and β (26-31 kDa) (Clayton et al., 1990; Dunn et al., 1990; Evans et al., 1991; Ha et al., 2001; Hu and Mobley, 1990; Labigne et al., 1991; Lee and Calhoun, 1997; Mobley et al., 1988).

In contrast plant and fungal (eukaryotic) urease are made up of identical subunits and he UreA, UreB and UreC subunits of bacterial ureases are fused in a collinear fashion to make up a single polypeptide chain typically around 90 kDa. Eukaryotic ureases form trimers and two trimeric units can also associate to a hexameric structure (Balasubramanian and Ponnuraj, 2010; Polacco and Havir, 1979).

Remarkably, though composed of different types of subunits, ureases from bacteria to plants and fungi exhibit high homology of amino acid sequences and structure (Balasubramanian and Ponnuraj, 2010; Follmer, 2008; Witte et al., 2005). Moreover, the active site in all known ureases are always located in the α subunit. Collectively, this suggests that all ureases are evolutionary variants of one ancestral enzyme (Krajewska, 2009; Navarathna et al., 2010).

1.4. Occurrence and function of ureases

Ureases are widespread in nature, are synthesized by numerous organisms and are also present in soils as a soil enzyme (see below). The substrate urea is readily available, arising mainly from urine excretion by animals, from the decomposition of N- compounds from dead organic matter (Wang et al., 2008), or from its application as a fertilizer. Thus ureases play a prominent role in the overall nitrogen metabolism in nature where their key function is to provide organisms nitrogen in the form of ammonia.

1.4.1. Soil urease and ammonia volatilization

Of great importance in agriculture is the ureolytic activity of soils (Krogmeier et al., 1989; Mulvaney, 1981) which is derived maily from soil urease rather than from microorganisms (Mulvaney, 1981). The urease enzyme in residues of dead plant and microbial cells becomes extracellular and is highly stable thanks to the immobilization on clays and humic substances (Krajewska, 2009). The presence of this stable form of urease in soils allows urea to be used as an efficient nitrogen fertilizer. Due to its high nitrogen content, chemical stability and low cost in production, urea makes up over 50% of the total nitrogen fertilizer applied worldwide. The role of soil urease is to hydrolyse the urea to ammonia to make it available to plants. However, if the hydrolysis is too rapid it may result in unproductive loss of nitrogen by ammonia volatilization, while ammonia toxicity and alkalinity along with nitrite accumulation may induce damage to plants, thereby causing severe environmental and economic problems (Krogmeier et al., 1989; Mulvaney, 1981). Ammonia volatilization also causes problems in the management of livestock waste where the loss of nitrogen in the livestock slurry leads to a reduction in its value as fertilizer, and the source of pollution, ammonia, contributes to the adverse odour. Attempts have been made to recycle urine to use as flush water by suppressing urease activity to avoid ammonia emission (Ikematsu et al., 2007). In medical, agriculture and environmental settings where it is important to control the urease activity, the use of urease inhibitors has been proposed to avoid its negative effects (Krajewska, 2009).

1.4.2. Urease in plants

The first plant urease gene has been characterized from soybean (*Glycine max*). The soybean genome contains an embryo-specific urease encoded by the gene *Eu1* (Meyer-Bothling et al., 1987) and a ubiquitous urease encoded by *Eu4* (Torisky et al., 1994). The residual urease activity in *Eu1/Eu4* double mutants was explained by urease-producing bacteria living on the plant (Holland and Polacco, 1992). In contrast, potato (*Solanum tuberosum*), tomato (*Lycopersicon esculentum*) and other *solanaceous* species, as well as *Arabidopsis thaliana* possess only a single urease gene (Witte et al., 2005).

The urease enzyme plays an essential role in catalyzing urea assimilation after uptake into the plant cell (Wang and Köhler, 2008; (Kojima et al., 2006). Higher plants posses various urea transport systems, both passive and active, which allow them to optimize nitrogen assimilation depending on the form available in the environment or internally. Although plants can assimilate nitrogen in form of urea though the roots, uptake occurs mostly in the form of ammonia which generated from urea hydrolysis though soil ureases.

Besides hydrolyzing the urea acquired from the environment, ureases allows plants to recycle nitrogen from urea originating from two metabolic processes: the arginase-catalyzed breakdown of arginine (Zonia et al., 1995) and the degradation of purines and ureides (Todd et al., 2006; Winkler et al., 1988). However plants have the capacity to degradation purine and ureides without generating urea intermediate, leaving arginine catabolism as the only confirmed source of urea (Witte, 2011).

Because nitrogen availability is generally growth-limiting for plants (Bray, 1983), efficient recycling is likely to provide plants an ecological advantage. Urea is metabolized rapidly and does therefore not accumulate, however when constantly generated it may serve as a nitrogen source. Combined genetic and biochemical analyses revealed that urease enzyme activity is regulated by the global nitrogen regulatory system (Magasanik, 1988) acting through the nac (nitrogen assimilatory control) gene product (Bender et al., 1983, Macaluso et al., 1990). Under conditions of low nitrogen availability, urease activity is induced. Interestingly, it was suggested that besides their ureolytic enzyme activity, plant ureases may play a role in the plant defence system because urease exhibits insecticidial (Follmer et al., 2004) and antifungal properties (Becker-Ritt et al., 2007; Menegassi et al., 2008).

1.4.3. Metabolic sources and transport of urea in plants

In plants, urea is especially important during germination and originates from the breakdown of arginine (Zonia et al., 1995) and from purines or ureides (Todd et al., 2006; Winkler et al., 1988). Arginine is the most important single metabolite for nitrogen storage in plant seeds (Vanetten C.H, 1967) and its catabolism is central to the mobilization of nitrogen from tissues. The importance of urease for recycling arginine nitrogen during germination is highlighted by the fact that aged Arabidopsis seeds failed to germinate when urease was chemically

inhibited but could be rescued by an external nitrogen source (Zonia et al., 1995). First, mitochondrial arginase hydrolyses arginine to access the stored nitrogen in the guanidinium group, thereby generating ornithine and urea which are then converted by the mitochondrial ornithine metabolism to glutamate (Funck et al., 2008). Urea is exported to the cytosol by a passive transport, possibly through aquaporins (Soto et al., 2010) also called MIPs (major intrinsic proteins), which conduct selected low molecular solutes along a concentration gradient through a channel. In the cytosol urea is hydrolysed by urease, and the urea-derived ammonium is re-assimilated by cytosolic glutamine synthetase, using glutamate from ornithine catabolism as the substrate.

Through these reactions, all the nitrogen from arginine is incorporated into glutamine, while urease is required to mobilize half of the nitrogen stored in arginine (Figure 2). This is the only firmly established role of urease in plant metabolism, apart from hydrolyzing root-imported urea, and arginase is the only plant enzyme known to generate urea *in vivo.* In the second pathway, urea is produced by the catabolism of purines or ureides like allantoin and allantoate, which are used for example by leguminous species for long-distance translocation of nitrogen (Stebbins and Polacco, 1995).

However, urea does not only originate from arginine or purine breakdown but can also be taken up from the environment via urea transporters (Kojima et al., 2006) Wang et al., 2008). Plants possess a high affinity urea transporter (DUR3) that is involved in uptake of environmental urea while also mediating internal urea transport. In *A. thaliana* DUR3 was identified by its similarity to the urea transporter of *S. cerevisiae* (ScDUR3) (Liu et al., 2003). The protein is localized at the plasma membrane of root epidermal cells especially in nitrogen starved plants, and the gene expression is induced by urea in the absence of other nitrogen sources (Kojima et al., 2007; Merigout et al., 2008). A role of Dur3 in internal urea transport is indicated by the expression of At*DUR3* near the root xylem and in the shoots (Kojima et al., 2007; Liu et al., 2003).

1.5. Urease enzyme activation mechanism

1.5.1. Urease complex assembly and urease accessory proteins

Biochemically, bacterial ureases are better characterized than those from any other organism. In all bacterial organisms studied so far, activation of the urease apo-enzyme by nickel binding *in vivo* requires four accessory proteins: UreD, UreE, UreF and UreG (Lee et al., 1992; Mulrooney and Hausinger, 1990). In bacteria urease is generally a heterotrimer with a binuclear nickel (Ni^{2+}) centre. For assembly of the functional ap-oenzyme complex the accessory proteins UreD, UreE, UreF and UreG are required. In addition, to mediate metal ion uptake from the environment, high-affinity nickel transporter (Nic1) are required.

In the bacterium *Klebsiella aerogenes*, four urease accessory proteins (UreD, UreF, UreG and UreE) are required for urease activation involving the carboxylation of an active site lysine and the incorporation of two nickel ions per active site that are bridged by the carboxyl group of the modified lysine. The precise role of the urease accessory proteins in metallocentre assembly is not yet fully understood (Carter et al., 2009). Apo-urease (encoded by *ureA*, *ureB* and *ureC* on the urease operon of *K. aerogenes*) forms a complex with UreD, and the U–UreD (urease–UreD) complex can in turn bind UreF. The U–UreDF complex is competent to bind UreG, forming a stoichiometric U–UreDFG complex. This assembly occurs in the absence of nickel (Park and Hausinger, 1995). The nickel-binding protein UreE then joins the U–UreDFG complex and delivers the nickel (Soriano et al., 2000). After assembly of the U–UreDFGE complex, GTP hydrolysis by UreG is required for urease activation (Soriano and Hausinger, 1999) and the complex dissociates into its components, releasing active urease.

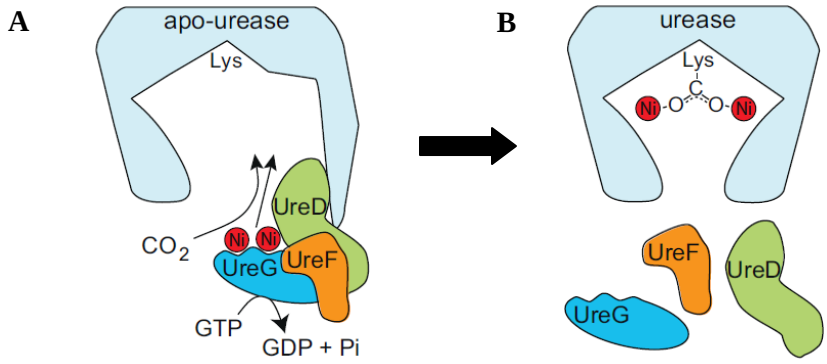

Figure 1. A model of urease activation in plants. (A) Hypothetical model of plant urease activation involving the binding of the three urease accessory proteins (UreD, UreF and UreG) to apo-urease, covalent modification of an active site lysine by nitrogen carboxylation, and specific incorporation of two nickel ions per active site. **(B)** The accessory proteins dissociate from urease after activation. Activation may require GTP hydrolysis mediated by UreG. Figure taken from (Witte, 2011).

In contrast to bacterial urease, plant and fungal ureases are homotrimers or homohexamers with nickel centres that requires only homologues of the three accessory proteins UreD, UreF and UreG for function (Mulrooney and Hausinger, 2003). In plants and fungi the UreG orthologue combines the functions of two of the bacterial accessory proteins (Fig. 1). The GPTase UreG contains the N-terminal histidine-containing region that is involved in nickel binding, apparently replacing the nickel-binding activity of the missing UreE homolog. All the three accessory proteins interact in a Yeast two hybrid (YTH) assay with the urease protein Ure1 and with each other and are essential for urease activity and growth on urea as a sole nitrogen source (Singh et al., 2013).

1.5.2. The urease accessory protein UreG

The accessory protein UreG belongs to the G3E family of P-loop GTPases (G3E family) (Leipe et al., 2002). Characterized members of the G3E family perform two roles in metallocenter assembly: 1) facilitating incorporation of the cofactor in an energy-dependent manner into the target protein`s catalytic site (insertase) and, 2) storage and delivery of a metal cofactor to a target metalloprotein (metallochaperone). G3E proteins have been found to function as

either metal-insertases or as a dual function metallochaperon/insertase (Haas et al., 2009). Structural studies of this protein family of GTPases have shown that they do not possess a rigid tertiary structure and belong to the class of intrinsically disordered proteins (IDP). UreG protein is the only naturally occurring enzyme showing an intrinsically disordered conformation, and the first documented case of intrinsically disordered enzymes displaying observable enzymatic activity while showing a largely disordered tertiary structure (Neyroz et al., 2006; Real-Guerra et al., 2012; Zambelli et al., 2012; Zambelli et al., 2007; Zambelli et al., 2005; Zambelli et al., 2009). In contrast to the ordered proteins with a relative stable three-dimensional structure which undergo cooperative first-order folding/unfolding transition between two distinct states, intrinsically disordered proteins exist as dynamic ensembles of conformers and typically undergo non-cooperative changes in their population (Uversky and Dunker, 2010). It has been proposed that disorder-to-order transition is a possible mechanism for UreG function *in vivo* and that the protein is activated by the interaction with other proteins partners (Zambelli et al., 2012). GTP hydrolysis is regulated at different levels in order to avoid unnecessary consumption of GTP. This regulation involves different effectors such as GTPase activating proteins (GAPs) and/or guanine nucteotide exchange proteins (GEPs). A possible GAP for UreG has been identified in UreF (Salomone-Stagni et al., 2007).

Intrinsically disordered proteins often act as hubs for protein-protein interaction networks, binding several partners in regulatory processes (Dunker et al., 2005). UreG is able to bind different protein partner and cofactors and is part of an activation network where this enzyme acts as a local hub or scaffold protein that coordinates multiple protein-protein or protein-cofactor interactions, acting as a switch represented by GTP hydrolysis to drive the process of Ni^{2+} ion trafficking towards urease activation. It has been suggested that native disorder represents a general mechanism for cells to regulate enzymatic activity, allowing UreG to interact and to be regulated by different protein partners (Zambelli et al., 2012).

The GTPase UreG is required for the assembly of the Ni^{2+}-dependent active side of urease, (Mulrooney and Hausinger, 2003; Zambelli et al., 2011) and proposed to catalyze, in the presence of CO_2, the formation of carboxyphosphate, a carbamylation agent for the metal-

binding lysine in the urease active site (Soriano and Hausinger, 1999). All UreG proteins contain a P-loop motif typically found in nucleotide-binding proteins. Site-directed mutagenesis of the P-loop motif in bacterial *ureG* resulted in inactive urease in the presence of nickel. In these cells the DFG complex was formed but failed to bind to the nucleotide-linked resin. All UreG proteins described so far were capable to bind GTP, although their GTPase activities were were very low or undetectable suggesting the requirement of co-factors to achieve their full activity (Moncrief and Hausinger 1997; Zambelli et al. 2005, 2007, 2009).

A Cys-Pro-His motif highly conserved among all UreG proteins is involved in the metal-binding property and was shown to participate in zinc binding in UreG from *H. pylori* and *K. aerogenes* (Zambelli et al. 2009; Boer et al. 2010). The formation of an UreG-UreE complex also involves binding of metal ions, as observed for the *H. pylori* (Bellucci et al. 2009) and *K. aerogenes* (Boer et al. 2010) proteins. UreG binds Ni^{2+} and Zn^{2+}, but the stoichiometry varies among proteins. *Bacillus pasteurii* UreG, a dimer in solution, appears to bind 2 Zn^{2+} or 4 Ni^{2+} ions per dimer (Zambelli et al. 2005). *H.pylori* UreG, a monomer in solution, binds 0.5 Zn^{2+} or 2 Ni^{2+} per monomer, where Zn^{2+} binding leads to protein dimerization (Zambelli et al. 2009). On the other hand, monomeric *K. aerogenes* UreG has been reported to bind one Ni^{2+} or Zn^{2+} per monomer, and neither metal ion is able to induce dimerization (Boer et al. 2010). In the plant *Glycine max,* UreG showed a different binding affinity for Ni^{2+} and Zn^{2+}, presenting a very tight binding for site for Zn^{2+}, but nor for Ni^{2+}. This suggests that Zn^{2+}may play a role in the plant urease assembly process, as suggested for bacteria (Real-Guerra et al., 2012). *G. max* encodes two structural genes for two different ureases (Meyer-Bothling and Polacco, 1987; Torisky et al., 1994). Mutation of *Eu3* encoding the urease accessory protein UreG orthologue from soybean, eliminated both urease activities (Freyermuth et al., 2000) and all further background activity proposed to be of bacterial origin (Meyer-Bothling et al., 1987). According to the genome sequence, soybean has two distinct genes for UreD, two for UreF and one for UreG.

In plants, the accessory protein UreG carries out two roles: Ni^{2+} storage and nucleotide hydrolysis. Plant UreG presents a poly-histidine stretch in its N-terminal that could fulfil the

function of bacterial UreE in Ni^{2+} trafficking (Freyermuth et al., 2000; Witte et al., 2001). A similar dual role has also been proposed for HypB, accessory proteins of the [Ni,Fe]-hydrogenase maturation system (Casalot and Rousset, 2001). Strikingly, comparing different accessory proteins from *A. thaliana* and *K. aerogenes* reveals that UreG is best conserved with an identity of 42.8% while UreD and UreF are only 21.8% and 19.4% identical, respectively (Witte et al., 2005). Null mutants of *A. thaliana* in UreD, UreF and UreG lack urease activity *in vivo* and were unable to grow on urea as the sole nitrogen source (Witte et al., 2005). GTPase activity of UreG is essential for metallocenter biosynthesis of urease (Mehta et al., 2003). In addition to the GTPase domain, UreG family members have a conserved, putative metal binding CXCC motif which is located in the Switch I region of the protein, suggesting that binding of CTP/GDP affects its conformation (Khil et al., 2004).

In the human pathogenic fungus *Cryptococcus neoformans* the incorporation of nickel into urease depends on the presence of UreG. As described for plants, UreG accessory protein combines the function of the two bacterial accessory proteins. It is the homolog of GTPase UreG and also includes an additional N-terminal histidine-containing region to bind nickel, replacing the bacterial UreE homolog. Mutagenesis of the key histidine residues reduced or abolished the ability of UreG to bind nickel as well as urease activity (Singh et al., 2013).

1.5.3. Regulation and activation mechanism of ureases in different organisms

In some some soil bacteria (Mobley and Hausinger, 1989) including *Bacillus pasteurii* (Morsdorf and Kaltwasser, 1989), *Sporosarcina ureae* (Kaltwasser et al., 1972) or the cyanobacterium *Anabaena variabilis* (Ge, 1990), urease is synthesized constitutively. However, ureases are mostly induced in response to environmental conditions by activation of transcription of the encoding genes through the global nitrogen control system. For example in the genus *Klebsella*, urease is not synthesized when cells are grown in presence of high quality nitrogen sources such as ammonia (Friedrich and Magasanik, 1977). In contrast, in presence of poor nitrogen sources such as arginine, proline or histidine, synthesis of urease is activated (Mulrooney et al., 1989). Nitrogen regulation of urease has been proposed to occur in a number of other ureolytic organisms. This control is dependent on

the nitrogen regulatory system (NTR) and ultimately the action of the positive regulator NAC (nitrogen assimilation control) at the level of urease transcription. In a second mode, urease expression in organisms such as *Proteus miranilis* is induced by the presence of the substrate urea (Rosenstein et al., 1980; Rosenstein et al., 1981). In organisms such the oral bacterium *Streptococcus salivarius,* where urease plays a role in protection from the acidic environment, the level of urease synthesis is regulated by pH (Sissons et al., 1992; Sissons et al., 1990).

In the fungus *C. neoformans* the level of urease expression and enzyme activity is regulated by the available nitrogen source (Singh et al., 2013). Although *ure1* transcript was also observed in cells grown in media supplemented with ammonium or proline as a sole nitrogen source, transcript levels were clearly more abundant in urea grown cells.

All ureases studied so far required nickel as a cofactor for enzymatic activity (Carter et al., 2011). Interestingly, no nickel-requiring metalloenzymes have been identified in vertebrates (Denkhaus and Salnikow, 2002; Mulrooney and Hausinger, 2003). In *S. pombe* where the urease is neither controlled by nitrogen repression nor by urea induction (Lubbers et al., 1996), the high affinity nickel permease Nic1 acts as a plasma membrane nickel transporter. The corresponding *S. pombe nic1* mutant was strongly impaired in Ni^{2+} uptake and contained only background activities of the nickel-dependent cytoplasmic enzyme urease. For *S. pombe* trace amounts of Ni^{2+} ion are sufficient for maximal urease activity and this activity was not stimulated by the addition of Ni^{2+} to the medium (Lubbers et al., 1996). Among a series of divalent transition metal cations tested (Cd^{2+}, Co^{2+}, Cu^{2+}, Mn^{2+}, and Zn^{2+}), only Co^{2+} caused considerable inhibition of Nic1-mediated Ni^{2+} uptake in *S. pombe* (Lubbers et al., 1996). In the human pathogen *C. neoformans* the nickel transporter Nic1 is required for urease activity and a defect by a gene knockout could be overcome if excess exogenous nickel was added to the medium (Singh et al., 2013). In vivo studies with mutants of *ure7* (ureG orthologue) or *nic1* both displayed greatly attenuated virulence and CFU in the brain were comparable to the *ure1* mutant strain (Cox et al., 2000).

Plant ureases and arginases are housekeeping enzymes in many if not all plant species (Brownfield et al., 2008; Witte and Medina-Escobar, 2001). Nickel-deprived plants do not contain an active urease and urea accumulates from arginine turnover, especially in

senescing tissues (Gerendas J., 1997; Gerendas J., 1999b). In plants it has been suggested that the urease activity is regulated by the global nitrogen regulatory system (Magasanik, 1988) acting through the NAC (nitrogen assimilatory control) gene product (Bender et al., 1983, Macaluso et al., 1990); thus, under conditions of low nitrogen availability, urease activity is expressed.

1.6. Urease assays

A number of assays are available for quantitification of urease activity and analysis of its kinetic behavior. Ammonia released during the reaction can be detect with phenol-hypocloride (Weatherburn, 1967), Nessler`s reagent (Sigma ammonia color reagent) or Bromocresol Purple to allow colometric determination of the activity. Alternative, ammonia released from urease action can be utilized by an NADH-dependent glutamate dehydrogenase so that the activity of the coupled system is easily monitored spectrophotometrically (Kaltwasser and Schlegel, 1966). In addition, ammonia ion-selective electrodes are available for monitoring ammonia release (Hamilton-Miller and Gargan, 1979; Katz, 1964; Montalvo, 1970). By using ^{14}C urea, bicabonate released from the reaction can be trapped and monitored by scintillation counting (McDonald et al., 1972). $^{14}CO_2$ released from this substrate and $^{13}CO_2$ (assayed by mass spectrometry) released from ^{13}C-urea have been used in breath tests to detect the presence of *H. pylori* urease in the human gastric mucosa (Bell et al., 1987; Graham et al., 1987). Since urease activity results in an increase of pH, several pH-dependent assay methods have been developed, including pH-sensitive dyes for use in spectrophotometric methods (Hamilton-Miller and Gargan, 1979; Ruiz-Herrera and Gonzalez, 1969), utilization of a pH stat (Blakeley et al., 1969b) and the analysis of changes by using a pH electrode (Bibby and Hukins, 1992). In addition several methods have been adapted to detect urease activity in native gels (Blattler et al., 1967; Fishbein, 1969; Martin de Llano et al., 1989; Shaik et al., 1980). Urease exhibits simple Michaelis-Menten-type kinetic behavior and in general, the K_m values determined for urease in cell extracts closely

match those measured for highly purified samples. Thus purified enzyme is not required for determination of th the K_m value.

1.7. Role of urease in virulence

1.7.1. Ureolytic bacterial infection

1.7.1.1 Urease in peptic ulcer disease caused by *Helicobacter pylori*

The primary ureolytic bacterium infecting the intestinal tract is *Helicobacter pylori* (Burne and Chen, 2000; Collins and D'Orazio, 1993; Dunn and Phadnis, 1998; McGee and Mobley, 2000). Urease is critical for *H. pylori* colonization of the human gastric mucosa. *In vitro*, the bacterium is sensitive to the effect of low pH (Hazel, 1985) unless urea is present (Marshall, 1988). Analysis of mutants has demonstrated that urease is required for mucosal colonization in the gnotobiotic piglet model (Eaton et al., 1991). This bacterium colonizes the mucosal lining of the stomach and increases the pH of the strongly acidic environment to 6-8, allowing it to grow and persist in the hostile condition. At the same time it causes damage in the host tissue, giving rise to gastritis and gastroduodental ulcers. Moreover, the highly toxic product monochloramine is derived from hydrogen peroxide resulting from the oxidative burst of the immune cells, which oxidizes chlorine ions that react with the ammonia liberated by *H. pylori* urease. This can induce mutagenic DNA damage which, in the case of chronic infection, is believed to contribute to the development of stomach cancer. The ammonium ion *per se* is not toxic; the damage results from the hydroxide ions generated by the equilibration of ammonia with water. Interestingly, *H. pylori* mutants lacking urease activity are phagocytosed more efficiently than the parental strain (Makristathis et al., 1998). Urease-containing *H. pylori* has been shown to activate monocytes (Mai et al., 1991), to cause the secretion of inflammatory cytokines (Craig et al., 1992) and to act as chemoattractant for leukocytes (Craig et al., 1992; Mai et al., 1992). Diagnosis of *H. pylori* infections in the upper intestinal tract is based on the urease reaction. Ingested ^{13}C- or ^{14}C-labelled urea is converted by *H. pylori* present in the stomach into isotope-labelled carbon dioxide, which is absorbed into the blood and exhaled in the breath where is can be detect

by mass spectrometer or scintillation counter (Granstorm M., 2008). Because of the importance of this enzyme in peptic ulcer disease, urease inhibitors and urease vaccines are currently being developed for clinical use.

1.7.1.2 Urease in urinary tract infection

Urinary tract infection increases the pH of urine (up to ca. 9, 2), which is typically neutral or slightly acidic, causing a number of complications such as necrosis of the kidney tissue and acute pyelonephritis. A more frequent symptom is the precipitation of normally soluble ions in urine leading to the formation of urinary stones often implicated in catheter encrustation. The most common bacteria responsible for their formation are *Proteus mirabilis* and *Ureaplasma urealyticum,* as well as bacteria belonging to *Pseudomonas*, *Klebsella* and *Staphylococcus* spp. (Burne and Chen, 2000; Rosenstein and Hamilton-Miller, 1984). Urinary stones are mainly composed of struvite ($MgNH_4PO_4x6H_2O$) and carbonate apatite ($Ca_{10}(PO_4)_6CO_3$) (Burne and Chen, 2000; Collins and D'Orazio, 1993; Rodman, 1999; Rosenstein and Hamilton-Miller, 1984). Ureolytic infection is estimated to contribute to 15-20% of all urinary stones. Performed in a controlled manner, the precipitation can be utilized for the phosphorus- and nitrogen recovery in wastewater and urine treatment processes (Maurer et al., 2006). Because human urine contributes to ca. 80% of the total N and ca. 45% of the total P in municipal wastewater (Wilsenach et al., 2007), the biological recovery of the two dominant nutrients together as struvite presents a interesting alternative to their chemical removal in urine recycling.

1.7.2. Role of urease in fungal pathogens

Urease activity has been reported in several genera of medically important fungal pathogens of humans including *C. neoformans*, *Coccidioides immitis*, *Histoplasma capsulatum*, *Sporothrix schenckii* and species of *Trichospora* and *Aspergillu*s. Urease activity is a major source of ammonia and an important virulence determinant for microbial pathogens (Bury-Mone et al., 2004). However, compared to the wealth of information available on ureases in plants and bacteria, little is known about their function in fungi (Mirbod-Donovan et al.,

2006). Among the medically important fungi, the urease enzyme and ammonia production have been associated with pathogenicity only in *Cryptococccus* and *Coccidioides* (Mirbod-Donovan et al., 2006; Osterholzer et al., 2009) (Cox et al., 2000; Olszewski et al., 2004).

1.7.2.1. *Cryptococcus neoformans*

C. neoforman, an opportunistic fungal pathogen and the primary cause of fungal meningoencephalitis in humans, is responsible for up to a million infections and approximately 600,000 deaths per year (Park et al., 2009). Known virulence factors include a polysaccharide capsule, melanin and a variety of extracellular proteins such as proteases, phospholipases and urease. The rapid detection of urease activity is one means of early identification of *C. neoformans* from clinical specimens (Canteros et al., 1996; Zimmer and Roberts, 1979). Although urease activity has no effect *in vitro* assays on known cryprococcal virulence mechanisms such as growth at 37°C, capsule size, phenoloxidase activity and melanin production, urease-negative strains are rarely to penetrate the central nervous system (CNS) and to cause disease (Cox et al., 2000). In a mouse model, urease activity is contributes to virulence of cryptococcosis. The primary role of urease is likely to convert urea into a usable nitrogen source in its ecological niche (Cox et al., 2000). Although urease was not required for virulence of *C. neoformans* when inoculation was performed directly into the brain of immunodepressed rabbit (Cox et al., 2000), it has been shown that urease enhances transmigration of *C. neoformans* into the mircrovasculature of the brain (Olszewski et al., 2004). Invasion of the mouse brain or transmigration into the blood-brain barrier (BBB) was severely impaired in urease-deficient *Cryptococcus* strains or in the presence of the urease inhibitor flurofamide (Shi et al., 2010).

While the exact role of the urease in BBB invasion is not known, it has been suggested that hydrolysis of extracellular urea to toxic ammonia may cause endothelial cell damage that leads to an increase in permeability. *In vivo* studies with *ureG* or *nic1* (nickel transporter) mutants revealed greatly attenuated virulence and a reduction of fungal CFU in the brain comparable to that in the *ure1* mutant strain. These results demonstrate that urease activity and not the ure1 protein itself is responsible for the role in pathogenicity (Cox et al., 2000). It

has been suggested that urease inhibition could provide therapeutic opportunities to decrease the number of *Cryptococcus* transmigration into the brain resulting in lower CFU counts and an increase in patient survival (Shi et al., 2010).

1.7.2.2. *Coccidioides immitis/posadasii*

Coccidioides is a dimorphic fungal pathogen that causes human respiratory disease known as coccidioidomycosis or San Joaquin Valley fever. The genus includes two morphologically indistinguishable species, *Coccidioides posadasii* and *Coccidioides immitis* (Fisher et al., 2002). The first urease gene cloned from a human pathogen was that of *C. immitis* (Yu et al., 1997). Both *C. immitis* and *C. posadasii* initiate infection in the lungs, and urease serves to promote pulmonary colonisation through alkalization, local tissue damage and inhibition of the immune response (Mirbod-Donovan et al., 2006). Disruption of the single urease gene of *C. posadasii* resulted in a marked reduction in the pathogenicity of the organism in the lungs of BALB/c mice and in reduced extracellular ammonia production (Mirbod-Donovan et al., 2006; Wise et al., 2013). Ammonia and enzymatically active urease released from parasitic cells of *C. posadasii* may thus contribute to host tissue damage and exacerbate the severity of coccidioidal lung infection (Mirbod-Donovan et al., 2006; Mirbod et al., 2002). Indeed, the pH at the site of infection was higher with the parental strain than with the urease knockout mutant (Mirbod-Donovan et al., 2006). Moreover, abscesses from BALB/c mice resulting from infection with the parental strain contained higher concentrations of urea than those produced by infection with the urease mutant strain (Mirbod-Donovan et al., 2006). Enzymatic urease present in the spherule exudate contributes to its alkalinity due to hydrolysis of extracellular urea. It was suggested that the high amount of urea detected at the site of infection is host derived, providing a substrate for intra-and extracellular urease resulting in localized high concentrations of NH_4^+/NH_3 (Mirbod-Donovan et al., 2006) causing a pH increase that could be damaging to the host tissue (Prusky et al., 2001).

1.8. Urease activity control and urease protein properties in immunity and plant defence

No nickel-requiring metalloenzymes have been identified in vertebrates (Denkhaus and Salnikow, 2002; Mulrooney and Hausinger, 2003) and targeting nickel-requiring process or enzymes can be used as a method to detect the pathogen, especially when a nickel-containing enzyme as the urease is a notable virulence factor. Urease inhibition by flurofamide in *C. neoformans* or by acetohydroxymic acid in *C. immitis* lead to improved survival of infected mice and reduction of fungal CFUs (Mirbod-Donovan et al., 2006; Shi et al., 2010). Nickel transporter mutants (Δ*nic1*) showed no urease activity, and since the human blood contains only very low amounts (0.5 nM) of nickel, inhibition of Nic1 may prove to be an effective strategy in combating urease-producing pathogens such as *Cryptococcus* (Denkhaus and Salnikow, 2002; Ragsdale, 2009).

Interestingly, recombinant urease from *C. immitis* was highly immunogenic in BALB/c mice (Li et al., 2001). The recombinant fungal protein and a mammalian plasmid vector containing the *ure1* gene were used to vaccinate BALB/c mice, resulting in significant protection against coccidioidal infection (Li et al., 2001).

Some ureases have antifungal properties. In soybean and other legumes, the highly active seed-specific ureases have no assimilatory role and may function in pathogen defence (Polacco, 1993a). Urease and urease-like proteins (canatoxin) exert a toxic effect on fungi and certain insects which is independent of the urease activity (Carlini, 2008; Follmer et al., 2004). The major jackbean urease, the embryo-specific soybean seed urease or a recombinant *H. pylori* urease impaired hyphal growth and/or germination of several filamentous fungi, including *F. oxysporum* at sub-micromolar concentrations (Becker-Ritt et al., 2007). Interestingly, the antifungal property of the proteins was not affected by treatment with an irreversible urease inhibitor, indicating that urease represents a plant defence mechanism against phytopathogens which is independent of ammonia release from urea. The effect of urease-treatment on *Penicillium herguei*, a maize pathogen, and revealed an effect based on fungal cell wall damage (Becker-Ritt et al., 2007).

1.9. Urease enzyme inhibitors

A promosing approach to control urea-related pathogenesis or excessive rates of ureolysis in soil is to use potent and highly specific urease inhibitors. These compounds are also of interest for providing insights into the molecular mechanism of urease action. A number of urease inhibitors have been reported (see review (Krajewska, 2009)). Acetohydroxamic acid, the most widely exploited inhibitor of the class of hydroxamic acids, is a slow-binding moderate strength inhibitor of ureases from plants (Blakeley et al., 1969a; Dixon et al., 1980b; Kobashi et al., 1971; Odake et al., 1992), bacteria (Blanchard et al., 1988; Kenny, 1983; Mobley et al., 1988; Odake et al., 1994; Pope et al., 1998), fungi (Creaser and Porter, 1985) and in soil (Qui-Xiang, 1994). Because of its low toxicity, acetohydroxamic acid is the most frequently used urease inhibitor for medical therapies and in ureolytic bacterial-induced pathological conditions (Andersen, 1975; Burne and Chen, 2000; Griffith et al., 1978; Rodman, 1999; Rosenstein and Hamilton-Miller, 1984).

Beta-mercaptoethanol, a compound of the thiol-group of inhibitors, can bind the urease by displacing all four water/hydroxyide molecules in the active site, resulting in a penta-coordination of the two nickel ions. Furthermore, amides and esters of phosphoric acid are known as slow-binding but very strong inhibitors. Their activity is based on diamidophosphate (DAP), a product of hydrolysis that replaces the cluster of four water molecules at the active site of the urease enzyme (see review (Krajewska, 2009)). Due to their efficiency, a variety of derivates of both phosphoric and thiophosporic acids have been intensively studied for retarding urease hydrolysis in soils and against ureolytic bacteria infections (see review (Krajewska, 2009)). Phosphate buffer has long been known to inhibit urease activity at neutral pH, based on the $H_2PO_4^-$ ion (Dixon et al., 1980a; Todd and Hausinger, 1989).

Boric acids represent rapidly-binding but weak urease inhibitors Moreover, heavy metal ions are worth to mention because of their importance in practical applications. Heavy metal ions inhibit both plant and bacterial ureases (Kenny, 1983) and have the following order of effectiveness: $Hg^{2+} \approx Ag^{+} > Cu^{2+} >> Ni^{2+} > Cd^{2+} > Zn^{2+} > Co^{2+} > Fe^{2+} > Pb^{2+} > Mn^{2+}$ (Zaborska et al., 2004), with Hg^{2+}, Ag^{2+} and Cu^{2+} nearly always listed as the strongest inhibitors (Kuswandi, 2003;

Toren and Burger, 1968; Zaborska et al., 2004)204). Urease inhibition by heavy metal ions is biologically important, since heavy metal pollution may reduce the level of urease activity in agricultural soils. On the other hand, urease inhibition-based sensing systems (Kuswandi, 2003) are used for *in situ* and real-time determination of trace levels of these ions for environmental monitoring, food control and biomedical analysis (see review (Krajewska, 2009)).

1.10. Urease-independent urea breakdown

Fungi exhibit a dichotomy with regard to urea utilization. Whereas all higher fungi use the nickel-containing urease, the *Hemiascomycetes* (yeasts and yeast-like fungi) lack the structural urease, as well as the accessory proteins and the attendant nickel transporter (Navarathna et al., 2010). *Hemiascomycetes* use an alternative urease-independent pathway for metabolising urea by possessing the urea amidolyase (*DUR1, 2*; Degradation of Urea). For example, in *S. cerevisiae* or *C. albicans*, urea is metabolised by urea amidolyase, a biotin-requiring enzyme consisting of domains with activities for both urea carboxylase and allophanate hydrolase to convert urea, ATP and bicarbonate to ammonia and carbon dioxide (Navarathna et al., 2010).

Urea amidolyase breaks down urea into ammonia and carbon dioxide in a two-step process (Scheme 2), in contrast to urease (EC 3.5.1.5) which ferforms the reaction in a one-step process (Navarathna et al., 2010). Urea is first carboxylated to allophanate in an ATP-dependent reaction by urea carboxylase and then allophanate is hydrolysed to ammonia and carbon dioxide by allophanate hydrolase (Altschul et al., 1997; Carter et al., 2009; Labadorf et al., 2010). Urea amidolyase is encoded by the DUR1,2 gene and was first characterised in the yeast *Candida utilis* now known as *Pichia jadinii* (Roon and Levenberg, 1972). This cytoplasmic enzyme (Roon et al., 1972) consists of a single polypeptide chain with regions for urea carboxylase (EC 6.3.4.6) and allophanate hydrolase (also known as amidase; EC 3.5.1.45) activity. Originally, two adjacent genes (*DUR1* and *DUR2*) were considered to

encode the two enzymes which were later renamed as a single gene, *DUR1, 2* (Cooper et al., 1980).

(1) Urea carboxylase: $urea + ATP + HCO_3^- \longrightarrow allophanate + ADP + P_i$

(2) Allophanate hydrolase (amidase): $allophanate \longrightarrow 2NH_3 + 2CO_2$

(3) Urease: $urea \longrightarrow 2NH_3 + CO_2$

Scheme 2. (1,2) Enzymatic hydrolysis of urea in a two step-process by Dur1,2. First urea is carboxylated to allophanate **(1)**, then allophanate is hydrolysed to ammonia and carbon dioxide **(2)**. By contrast, urea hydrolysis is performed in one single step by the urease enzyme **(3)**.

Interestingly, all *Sordariomycete* species (including *F. oxysporum*) except for *N. crassa* have both the urease and the urea amidolyase system (Strope et al., 2011).

1.11. Arginine

The amino acid arginine (2-amino-5-guanidinovaleric acid) was first isolated from lupin seedlings in 1886 and soon identified as a component of animal proteins. It was with the discovery of the ornithine cycle (urea cycle) by Krebs and Henseleit in 1932 that the prominent role of arginine in physiology and metabolic pathways was recognized. In the late 1930s and 1940s physiological and nutritional studies started a new era of arginine research. Arginine was found to be required for the synthesis of creatine, the precursor of creatinine, a clinical indicator of renal function (Reviewed in (Wu and Morris, 1998). Extensive studies in the 1950s to 1970s resulted in the initial classification of arginine as a dispensable (non-essential) amino acid for healthy adult humans (Rose et al., 1954), but as an essential amino acid for young, growing mammals and for carnivores (Reviewed in (Wu and Morris, 1998). Key studies reported that arginine is the precursor for mammalian nitrite/nitrate synthesis (Hibbs et al., 1987) and that nitric oxide (NO) is the endothelium-derived relaxing factor (Ignarro et al., 1987; Palmer et al., 1987). In 1988, NO was identified as the biologically active intermediate of the arginine-nitrite-nitrate pathway in macrophages (Hibbs et al., 1988;

Marletta et al., 1988) and endothelial cells (Palmer et al., 1988)(Reviewed in (Wu and Morris, 1998).

1.12. Arginase

The urea cycle enzyme arginase (L-arginine ureohydrolase, EC 3.5.3.1) hydrolyzes L-arginine to L-ornithine and urea (Kinne-Saffran and Kinne, 1999; Mendz and Hazell, 1996; Mendz et al., 1998). Arginases are highly conserved across the kingdom (Wu and Morris, 1998). Eukaryotic arginases usually have a high pH optimum (pH 9-11) and require manganese for optimum activity (Bach and Killip, 1961; Brown, 1966; Hirsch-Kolb et al., 1970; Jenkinson et al., 1996; Kuhn et al., 1995; Mohamed and Greenberg, 1945; Mora et al., 1965; Reczkowski and Ash, 1994). First discovered in 1904 by Kossel and Dakin in mammalian liver (Kossel A., 1904), arginase is not only involved in the urea cycle, but also serves to modulate cellular immune response during infection since arginine functions as a substrate for both arginase and inducible nitrite oxide synthase (iNOS).

Arginase is unique among the urea-cycle enzymes in vertebrates in that two distinct isoenzymes exist. Both catalyse the hydrolysis of L-arginine to urea and L-ornithine, but differ with regard to tissue distribution and subcellular localization. Arginase I is a cytosolic enzyme that is expressed in erythrocytes and in the liver. Arginase II is localized in the mitochondrial matrix and expressed in extrahepatic tissues like the small intestine, kidney, brain, monocytes and macrophages (Mori, 2007). Arginase II is synthesized as a pre-protein and imported to mitochondria where it is processed to the mature form (Cederbaum et al., 2004; Wu and Morris, 1998).

1.12.1 Role of arginase in plants

In plants, arginine catabolism by arginase occurs in the mitochondrial matrix and generates ornithine and urea. Mitochondrial ornithine metabolism then converts this compound to glutamate (Funck et al., 2008). On the other hand, urea is hydrolysed by urease in the cytosol (Soto et al., 2010) and the ammonium is re-assimilated by cytosolic glutamine synthetase

using glutamate from ornithine catabolism as a substrate. Through these reactions, all the nitrogen form arginine is incorporated into glutamine, whereby urease mobilizes half of the nitrogen stored in the arginine (Figure 2).

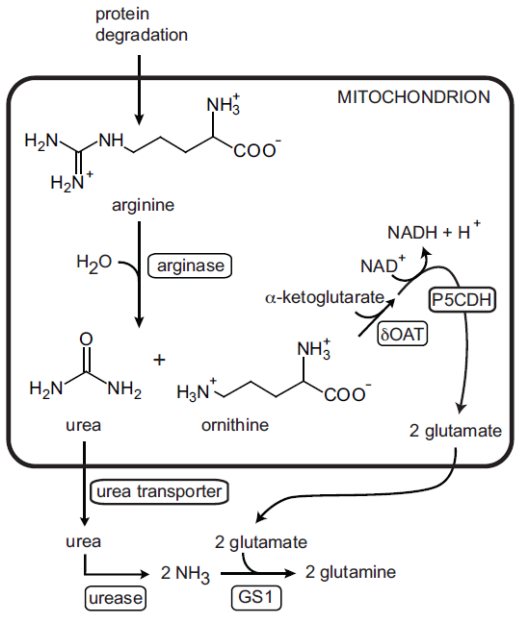

Figure 2. Arginine catabolism. Arginine is hydrolysed in the mitochondria by arginase into urea and ornithine. Urea exits the mitochondria where it is hydrolysed by cytosolic urease, and the released ammonia is re-assimilated by cytosolic glutamine synthetase (GS1). Mitochondrial δ-ornithine aminotransferase (δOAT) transfers the side chain amino group of ornithine to α-ketoglutarate, generating one molecule of glutamate and pyrroline-5-carboxylate which is oxydized to a second molecule of glutamate by pyrroline-5-carboxylate dehydrogenase (P5CDH). Glutamate can be exported from the mitochondria and serve as substrate for the cytosolic GS1-reaction. All four nitrogen atoms of arginine are thus incorporated into glutamine. Taken from (Witte, 2011).

Arginine catabolism is central to the mobilization of nitrogen from source tissues where arginase is the only plant enzyme known to generate urea *in vivo*. In many plant seeds, arginine is the most important single metabolite for nitrogen storage (Vanetten C.H, 1967). Upon seed germination, arginase activity rises (Cao et al., 2010; Flores et al., 2008; Goldraij and Polacco, 1999) in order to degrade arginine in the mitochondria (Goldraij and Polacco, 2000; Polacco, 1993a). High arginine concentrations also are found in underground storage organs of several plants (Reviewed in (Witte, 2011). The biosynthesis of arginine during seed/embryo development occurs in the plastids (Slocum, 2005). The importance of recycling arginine-derived nitrogen during germination is highlighted by the fact that aged Arabidopsis seeds failed to germinate when urease was chemically inhibited, but could be rescued by an external nitrogen source (Zonia et al., 1995). During senescence arginine is also subject to net degradation. In nickel-deprived plants which do not contain active urease,

urea accumulates from arginine turnover, especially in senescing tissues (Gerendas J., 1997; Gerendas J., 1999b)(Reviewed in (Witte, 2011).

1.12.2. Role of arginase in mammalian immune response

One of the enzymes competing with arginase for the substrate L-arginine is nitric oxide synthase (NOS). There are three types of nitric oxide synthases, the endothelial NOS, the neuronal NOS and the inducible NOS (iNOS). The latter is highly induced by lipopolysaccharide (LPS), lipoteichoic acid (LTA), and Type 1 cytokines like interferon gamma (IFNc), tumour necrosis factor alpha (TNF-a), interleukin 1 (IL-1), and IL-2. Nitric oxide (NO) contributes to a wealth of physiological processes, some of which are relevant to infection (Bogdan, 2001; Wu and Morris, 1998). Up-regulation of iNOS and nitric oxide (NO) is a major part of innate immunity in murine macrophages where NO is an effective antimicrobial agent against intracellular pathogens (Chakravortty and Hensel, 2003; Nathan and Shiloh, 2000). On the other hand the conversion of arginine to ornithine and urea via the arginase pathway can support the growth of bacterial and parasitic pathogens, and the polyamines produced by the arginase pathway down-regulate proinflammatory cytokine release. The cytokine profile after an infection is a key regulator of both iNOS and arginase induction and thus often determines the disease outcome (Das et al., 2010; Munder et al., 1999).

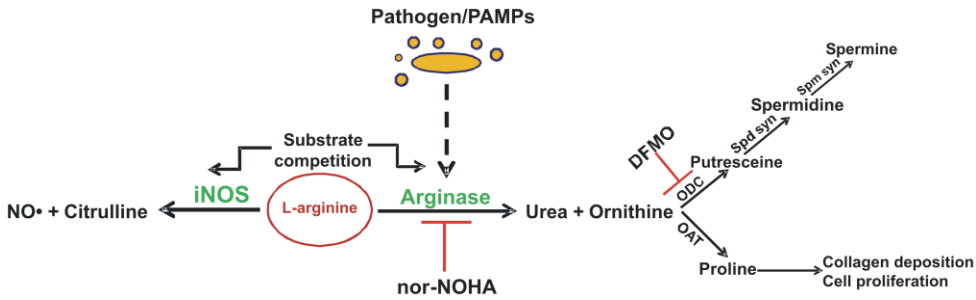

Figure 3. Simplified model of arginine substrate competition between arginase and iNOS. Only enzymes that directly use or produce arginine, ornithine, or citrulline are identified, and not all reactants and products are shown. DFMO, difluoromethyl ornithine; iNOS, inducible nitric oxide synthase; NO, nitric oxide; nor-NOHA, nor-N^{ω}-hydroxy-l-arginine; OAT, ornithine aminotransferase; ODC, ornithine decarboxylase; PAMPs, pathogen-associated molecular patterns; Spd Syn, spermidine synthase; Spm Syn, spermine synthase (Taken from: Das et al., 2010).

1.12.3. Role of arginase in microbial infection

The competition between iNOS and arginase for arginine can contribute to the outcome of microbial infections, when the availability of intracellular arginine is a rate-limiting factor in NO synthesis. Because arginase negatively regulates cellular NO production (Buga et al., 1996; Sonoki et al., 1997) it counteracts the biological effects of NO (Chang et al., 2001; Gobert et al., 2000). Interestingly, the extracellular arginine concentration has been shown to play a more important role in regulating NO synthesis than intracellular arginine (McGee et al., 1999).

1.12.4. Arginase in human fungal pathogens

Modulation of mammalian arginase by pathogens represents an evasion strategy from the immune system. *C. albicans*, for example, employs such a strategy to escape from macrophages after being ingested. Inside the macrophages *C. albicans* arginine biosynthetic genes are rapidly unregulated and arginine is metabolized by arginase to ornithine and urea. The resulting urea is degraded to CO_2 and NH_3 by urea amidolyase (Dur1, 2). CO_2 then activates adenyl cyclase and the cAMP-dependent protein kinase A pathway, triggering the yeast-to-hypha switch of *C. albicans* inside the macrophages and enabling its escape (Ghosh et al., 2009).

In vitro, macrophages respond to *C. posadasii* infection by a three-fold increase in the expression of the arginase I gene. On the other hand, the fungal arginase gene is expressed constitutively during the parasitic growth in the presence of urea (Mirbod-Donovan et al., 2006). The total arginase activity competes with iNOS in macrophages for the common substrate arginine, resulting in reduction of the level of nitrite oxide and an increase production of orithine and urea (Iniesta et al., 2002). Therefore it has been suggested that the high concentration of urea detected at the sites of coccidioidal infection is host derived. The urea available during infection provides a substrate for the urease from the pathogen, resulting in production and accumulation of ammonia and a pH increase (Mirbod-Donovan et al., 2006) that could damage the host tissue (Prusky et al., 2001).

1.12.5. Arginase in the bacterial pathogen *H. pylori*

The bacterium *H. pylori* is characterized by its production of urease which is absolutely essential for intestinal colonization (Eaton et al., 1991; Eaton and Krakowka, 1994). However, the substrate urea must be provided abundantly for the urease to work efficiently.

The bacterium directly stimulates murine macrophage NO production through the induction of iNOS expression, and macrophage-derived NO is a potent inhibitor of *H. pylori* growth (Gobert et al., 2001; Wilson et al., 1996). Upon infection with *H. pylori* mutants lacking the gene *rocF* encoding an arginase (McGee et al., 1999), a significant greater level of NO was released by macrophages, resulting in efficient killing of the Δ*rocF* mutants, suggesting that down-regulation of mammalian NO production by *H. pylori* arginase allows the pathogen to evade the host immune response (Gobert et al., 2001).

Additional studies have shown that the production of NO by macrophages is stimulated by the bacterial virulence factor urease. A mutant strain of *H. pylori* lacking urease failed to induce iNOS mRNA expression and production of iNOS protein or of NO (Gobert et al., 2002b). Since the concentration of urea in the stomach is very high (Kim et al., 1990; Schreiber et al., 2004), it has been suggested that the urea used as a substrate by *H. pylori* urease may derive from host arginase via direct release from the gastric epithelial cells, or may diffuse into the gastic juice from the blood-stream (Kim et al., 2011). Although *H. pylori* triggers the expression of murine gastric arginase II in the stomach (Gobert et al., 2002a), arginase II knockout mice were colonised to a similar extent by *H pylori* as wild-type mice, and even partial inhibition of host arginase I still permitted colonization of the Δ*rocF* mutant (Kim et al., 2011). In this case it is clear that the urea does not originate either from bacterial arginase or host arginase II. It has been suggested that urea may derive from the remaining host arginase I or from bacteria of the normal intestinal flora, or is produced by the alternative urea-generating enzyme agmatinase (Kim et al., 2011).

2. Results

Previously, Yeast Two-Hybrid screening against a *F. oxysporum* cDNA library, using the bait Gold_pGBKT7-msb2-CT-BD identifed a posive interaction with the hypothetical protein FOXG_13832 (chapter 3). Examination of the complete genome database of *F. oxysporum* (http://www.broadinstitute.org/) revealed that *FOXG_13832* encodes a putative urease G accessory protein. The gene has a size of 856 bp, contains one intron (nt 174- 219) and encodes a GTPase protein with a predicted size of 269 amino acids. Here we document the results of our investigations on the biological role of UreG in *F. oxysporum*.

2.1. UreG is a conserved urease accessory protein

A BLAST search with the amino acid sequence of the *F. oxysporum ureG* gene product FOXG_13832 against the complete genome database of NCBI (www.ncbi.nlm.nih.gov/pubmed) revealed high sequence identities with urease accessory proteins G from fungi, bacteria and plants (Table 1). No orthologue was found in the genome of *S. cerevisiae* (www.yeastgenome.org) known to lack urease and urease accessory proteins (Strope et al., 2011). While most analyzed organisms have only one UreG orthologue, two orthologues were found in *Arabidopsis thaliana* (Figure 2). The alignment shows the predicted GTP binding site at the P-loop motive (amino acid 58-65; GPVGSGKT: PROSITE accession number PDOC00017), the conserved NKDT motif which is involved in the guanine-specific recognition (guanine binding pocket, amino acid 263- 266), the motifs important for the conformational changes during GTP-binding the switch-I (DIFTRED) and switch-II (ESGGDNL) (Real-Guerra et al., 2012) and the putative region of nickel binding located at the histidine enrichted N-terminus (amino acid 2- 26). A histidine-enriched region was found in all eukaryotes but not in bacteria where an additional accessory protein named UreE is involved in nickel binding (Soriano et al., 2000). The *ureG* clone obtained from the YTH screen and containing the putative Msb2 interaction site encompasses the 3′-end of the of *ureG* gene (525 pb) corresponding to the C-terminus of the protein (amino acids 89-269) marked by a green box in Figure 1.

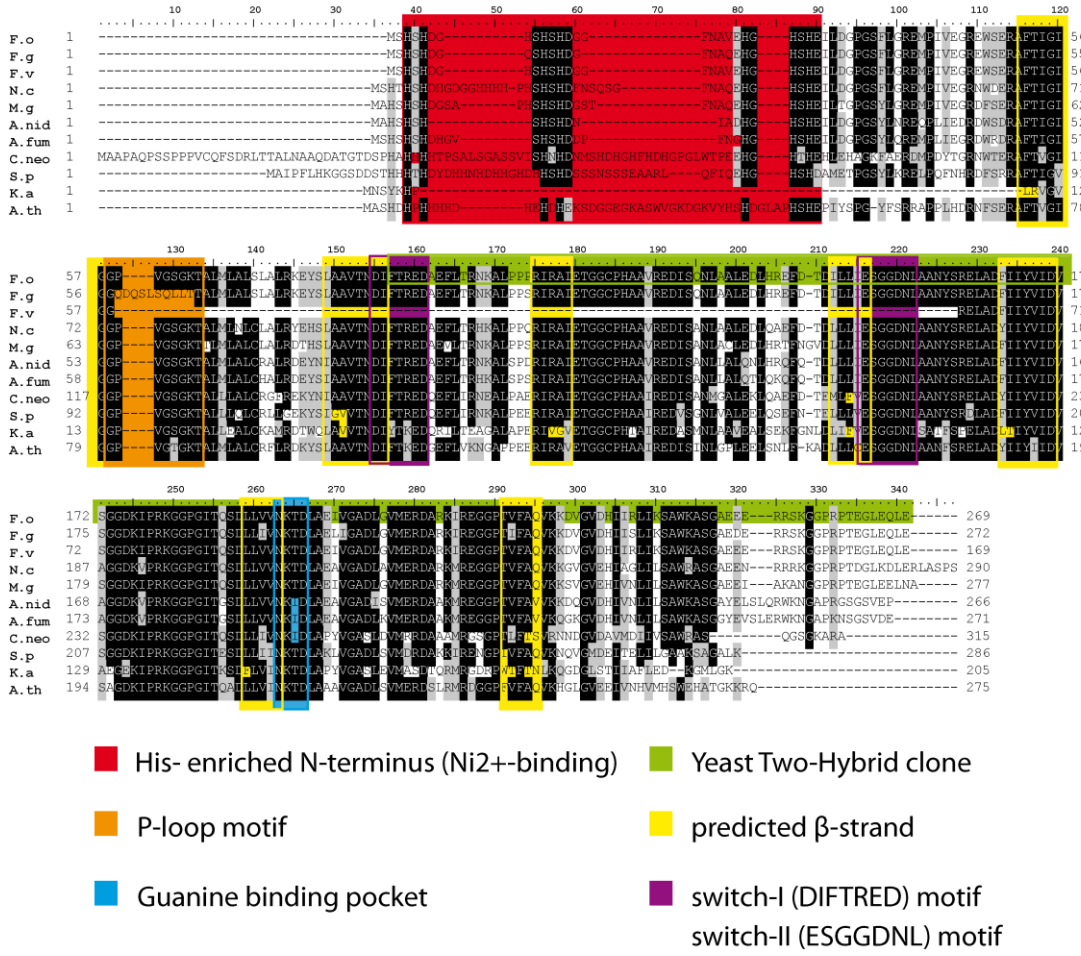

Figure 1. Amino acid sequence alignment of *F. oxysporum* UreG with fungal, plant and bacteria UreG proteins. The alignment shows the predicted amino acid sequence of UreG orthologues from fungal, plant and bacterial organisms. Highly conserved residues are shaded in black, moderately conserved residues are shaded in grey. The histidine-enriched N-terminus and the putative P-loop motive (PROSITE accession number PDOC00017) are highlighted in red. The NKTD motif corresponding to the guanine binding pocket is indicated in blue. The purple brackets represent the switch-I (DIFTRED) and switch-II (ESGGDNL) motifs important for the conformational changes during GTP-binding. The green box indicates the amino acids which correspond to the cDNA clone obtained from YTH analysis containing the putative interaction domain with Msb2. Fungi. Abbreviations and accession numbers: Fungi: F.o: *F. oxysporum* FOXG_13832; F.g: *Fusarium graminearum* FGSG_04402; F.v: *F usarium verticillioides* FVEG_11261; N.c: *Neurospora crassa* NCU01511; A.nid: *Aspergillus nidulans* ANID_00232; A.fum: *Aspergillus fumigatus* Afu2g12900; C.neo: *Cryptococcus neoformans* CNAG_00678; S.p: *Schizosaccharomyces pombe* SPCPB16A4; Bacteria: K.a: *Klebsiella pneumoniae* YP_001337096.1; Plants: A.th: *Arabidopsis thaliana* a: *A. thaliana* NP_180994.1.

Table 1. amino acid identities of *F. oxysporum* UreG (FOXG_13838) with fungal, plant and bacteria UreG proteins. Values represent identity score in % obtained after pair wise alignment assessed by a pair wise BLAST against the Broad Institute (http://www.broadinstitute.org) and NCBI (www.ncbi.nlm.nih.gov/pubmed) Database. Abbreviations as in Figure 1.

F.g	F.v	N.c	A.nid	A.fum	C.neo	S.p	K.a	A.th
92	100	88	79	77	70	72	56	66

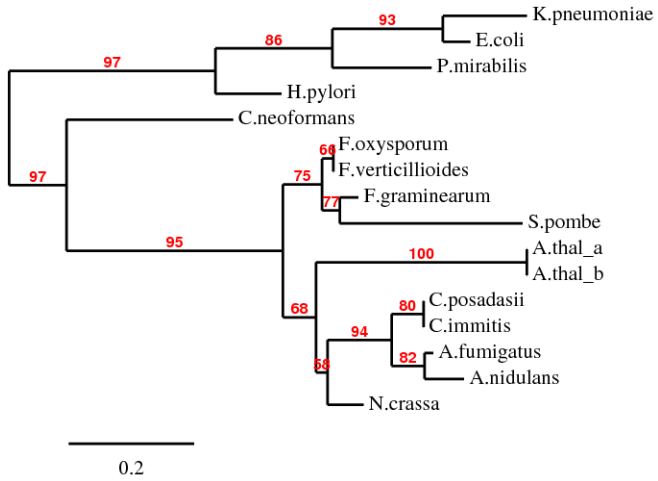

Figure 2. Phylogenetic tree with fungal, plant and bacteria UreG proteins. Shown are putative orthologues of the UreG protein in the indicated species. Tree Rendering: TreeDyn; Tree style: Cladogram (ignore branch lengths); Display branch support values in %. (http://www.phylogeny.fr). Abbreviations and NCBI /Broad Institute gene numbers: *F. oxysporum* FOXG_13832; *F. graminearum* FGSG_04402; *F. verticillioides* FVEG_11261; *N. crassa* NCU01511; *A. fumigatus* Afu2g12900; *A. nidulans* ANID_00232; *S. pombe* SPCPB16A4; *C. neoformans* CNAG_00678; *C. posadasii* CPAG_06968; *C. immitis* CIRG_05025; a: *A. thaliana* NP_180994.1 and b: NP_001031481.1; *K. pneumoniae* MGH 78578, YP_001337096.1; *E. coli* E110019, ZP_03051646.1; *H. pylori* jhp_0063; *P. mirabilis* YP_002153363.

2.2. Targeted deletion of *ureG* in *F. oxysporum*

To investigate the biological role of UreG (FOXG_13832) in *F. oxysporum*, targeted gene deletion was performed as follows. A Δ*ureG* allele was generated by replacing the open reading frame with the hygromycin resistance cassette (Figure 3A). The final deletion construct was obtained by fusion PCR and used to transform protoplasts of the *F. oxysporum* wild type (wt) strain. PCR analysis identified several transformants in which the 7 kb fragment corresponding to the knockout construct had been integrated in the homologous locus (Figure 3 B and C). Figure 3 C shows three several wt strains (1, 3, 4), one ectopic insertion (2) and three successful *ureG* knockout mutants which were named Δ*ureG*#5, Δ*ureG*#6, Δ*ureG*#7. For complementation of the Δ*ureG* mutation, a > 7 kb DNA fragment encompassing the complete *ureG* gene was amplified by PCR from wt genomic DNA and

introduced into the Δ*ureG*#5 mutant by co-transformation with the phleomycin resistance marker. Phleomycin-resistant transformants where selected and screened for amplification of a PCR product obtained from the wild type strain but not from the Δ*ureG* mutant. The results suggested that these strains named Δ*ureG*+*ureG* had integrated an intact copy of the *ureG* gene into their genome locus (Figure 3D).

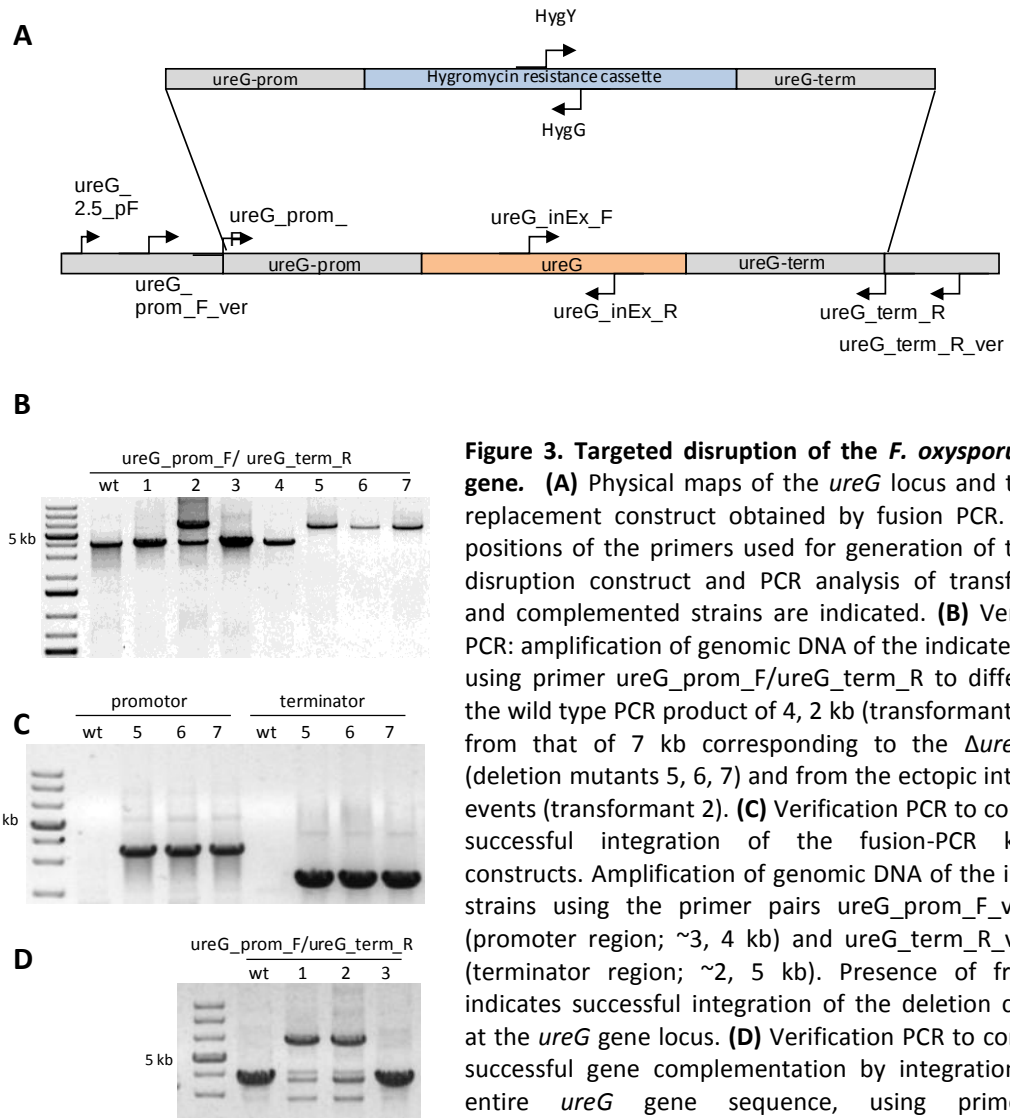

Figure 3. Targeted disruption of the *F. oxysporum ureG* gene. **(A)** Physical maps of the *ureG* locus and the gene replacement construct obtained by fusion PCR. Relative positions of the primers used for generation of the gene disruption construct and PCR analysis of transformants and complemented strains are indicated. **(B)** Verification PCR: amplification of genomic DNA of the indicated strains using primer ureG_prom_F/ureG_term_R to differentiate the wild type PCR product of 4, 2 kb (transformants 1, 3, 4) from that of 7 kb corresponding to the Δ*ureG* allele (deletion mutants 5, 6, 7) and from the ectopic integration events (transformant 2). **(C)** Verification PCR to control the successful integration of the fusion-PCR knockout constructs. Amplification of genomic DNA of the indicated strains using the primer pairs ureG_prom_F_ver/HygG (promoter region; ~3, 4 kb) and ureG_term_R_ver/HygY (terminator region; ~2, 5 kb). Presence of fragments indicates successful integration of the deletion construct at the *ureG* gene locus. **(D)** Verification PCR to control the successful gene complementation by integration of the entire *ureG* gene sequence, using primer pair ureG_prom_F/ureG_term_R. Presence of the single wild type PCR product (transformant 3) indicates the insertion of the entire *ureG* sequence in the *ureG* gene locus; the presence of additional fragments including the knockout fragment indicates multiple

copy integration besides the gene locus (transformants 1, 2). Sizes of molecular markers are indicated to the left.

2.3. Δ*ureG* knockout mutants display normal growth on different media

To test the role of UreG in vegetative hyphal growth and germination of *F. oxysporum*, colony diameter was measured on compelete (YPDA) or nutrient-limiting solid medium (MM) medium, and mycelial dry weight was determined from liquid cultures grown wither in PDB and YPG), or in nutrient-limiting liquid media (MM). For comparative purposes, the Δ*fmk1* and Δ*msb2* mutants were also included. No significant differences in hyphal growth and germination rates were observed between the Δ*ureG* mutants and the wt strain on solid YPDA or MM media or in liquid PDB, YPG or MM (Figure 4).

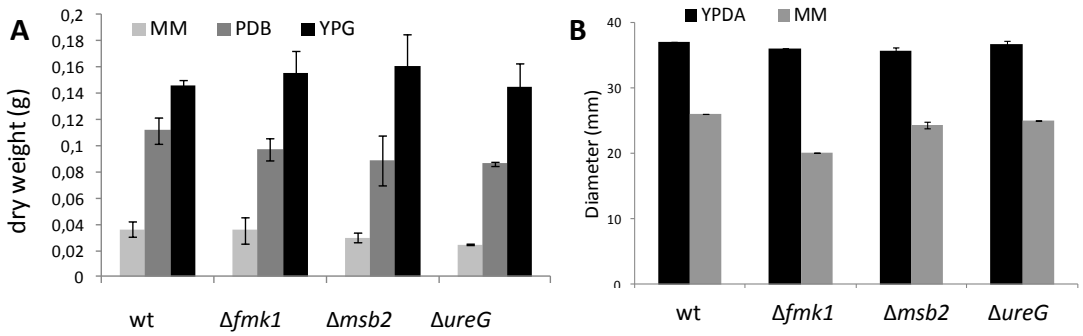

Figure 4. Analysis of mycelial dry weight and colony diameter of Δ*ureG* mutants and the indicated strains. (A) To measure growth, 6.25 x 10^7 microconidia of the indicated strains were germinated for 24 hours either in 25 ml PDB, YPG or MM. Mycelia were harvested, vacuum dried and weighed. **(B)** YPDA or MM agar plates were spot inoculated with 5 µl of a microconidia suspension (1x 10^7 /ml) and incubated at 28°C. Colony diameter was measured after 3 days. Bars represent standard errors calculated from 3 biological replicates.

2.4. The Δ*msb2* mutant displays reduced *ureG* gene expression

We next examined whether the mucin Msb2 regulates expression of *ureG* in *F. oxysporum*. Quantitative real-time PCR analysis revealed that *ureG* transcript levels were significantly reduced in the Δ*msb2* mutant compared to those in the wild type and the Δ*fmk1* strain (Figure 5A). To investigate a possible regulatory role of UreG in the Fmk1 MAPK pathway, we examined expression of *fpr1* encoding a secreted protein with an SCP-PR-1-like domain that

is transcriptionally regulated by the Fmk1 MAPK cascade. Previous work showed a five-fold reduction of *fpr1* transcript levels in the Δ*fmk1* mutant compared to the wild type strain (Prados-Rosales et al., 2012). Since Msb2 acts as an upstream component of Fmk1, Δ*msb2* mutants had ten-fold reduced *fpr1* transcript level whereas Δ*fmk1*Δ*msb2* double mutants had even hundred-fold lower levels (Perez-Nadales and Di Pietro, 2011). Here we also detected lower expression of *fpr1* in the Δ*fmk1* and Δ*msb2* mutants, but not in the Δ*ureG* mutants (Figure 5B). Thus, UreG is probably not involved in transcriptional regulation of *fpr1* and thus does not act upstream of Fmk1.

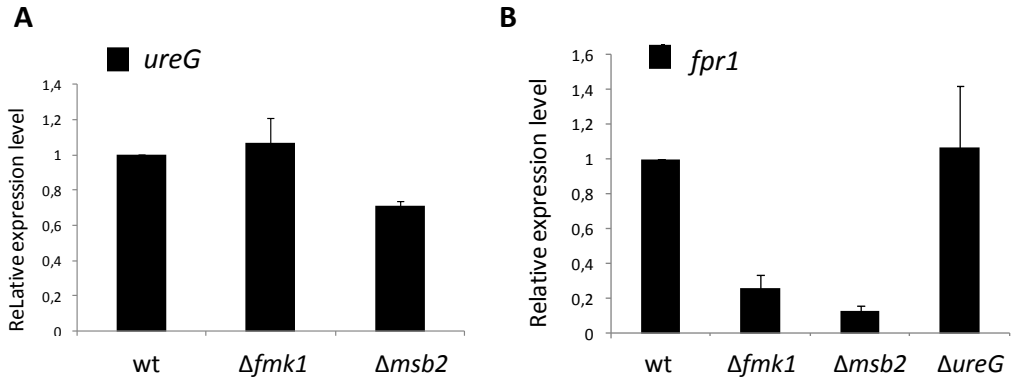

Figure 5. Msb2 is involved in transcriptional regulation of *ureG*. Measurement of *fpr*1 and *ureG* mRNA abundance by quantitative real-time PCR. cDNA derived from RNA isolated from invasive growth conditions (15 h germination in PDB followed by transfer for 4h on solid MM+ $NaNO_3$ medium). **(A)** Significantly reduced *ureG* gene expression in the Δ*msb2* mutant. **(B)** *fpr1* expression is not significant altered in the Δ*ureG* mutant. Relative expression levels represent mean values normalized to the *actin* gene expression levels and relative to the expression in the wild type strain. Bars represent standard errors calculated from two biological and 4 technical replicates.

2.5. Δ*ureG* knockout mutants can to utilize urea as a sole nitrogen source

Three independent Δ*ureG* mutants, but not Δ*msb2,* showed slightly reduced growth on MM medium when urea was the sole nitrogen and carbon source, suggesting that Δ*ureG* mutants are still able to utilize urea (Figure 6). To investigate if the growth reduction was specific for urea, we also tested vegetative hyphal growth on MM media containing different nitrogen sources in comparison to the wt, Δ*fmk1* and Δ*msb2* and Δ*ureG+ureG*. No differences in

growth of Δ*ureG* were observed under the tested conditions (MM medium with 25 mM NaGlu, Gln, $NaNO_3$, NH_4NO_3, ammonium tartrate $(NH_4)_2C_4H_4O_6$, $(NH_4)_2SO_4$, or 10 mM $NaNO_2$, Hypoxanthine or 5mM/25mM Thiourea; Supplementary Figure 1).

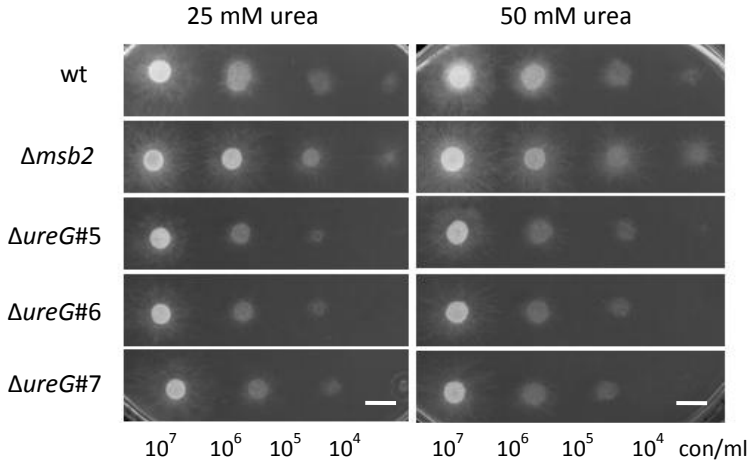

Figure 6. Δ*ureG* grows on urea as the sole nitrogen and carbon source. 2 µl microconidial suspension of the indicated strains was spotted on MM media containing 25 mM or 50 mM urea as a sole nitrogen and carbon source. Plates were incubated for three days at 28°C and scanned. Scale bar: 0.5 cm.

2.6. Δ*ureG* does not contribute to *in vitro* invasive growth functions

The components of the Fmk1 MAPK cascade, including Msb2, are required for *in vitro* virulence-related functions such as invasion of cellophane membranes (Prados-Rosales 2008, Pérez-Nadales and Di Pietro 2011), Since UreG was found to interact with Msb2 by Y2H, we tested its role of in virulence-related functions by systematically comparing the Δ*ureG* mutant to known phenotypes of the Δ*msb2* and Δ*fmk1* mutants. Our results confirmed the absence and the reduced cellophane penetration ability of Δ*fmk1* and Δ*msb2*, respectively (Perez-Nadales and Di Pietro, 2011), whereas three independent Δ*ureG* mutants displayed a similar penetration capacity as the wt (Figure 7). The same result was observed when performing the cellophane penetration assay on MM media containing urea as sole nitrogen and carbon source (Figure 8). Interestingly, even though all tested strains showed an improved growth when glucose was added as a carbon source in addition to urea, the cellophane penetration capacity was reduced under these conditions.

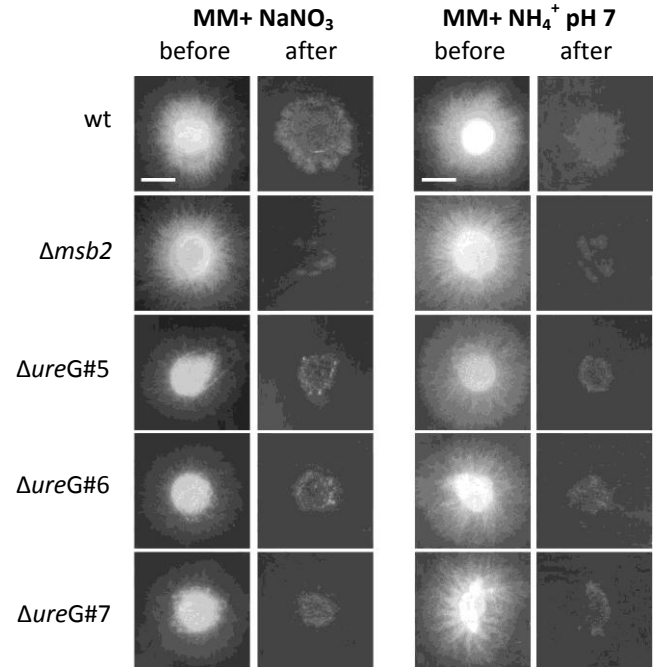

Figure 7. *Ure*G is not required for cellophane penetration on MM media containing $NaNO_3$ or NH_4^+ as the nitrogen source. 5µl of a microconidia suspension (10^7 con/ml) of the indicated strains were spot-inoculated on the indicated media covered with a cellophane membrane and incubated at 28°C. To determine penetration, the cellophane sheets with the fungal colony were removed after 4 days (before) and the plates were incubated for an additional day (after). Scale bar, 1 cm.

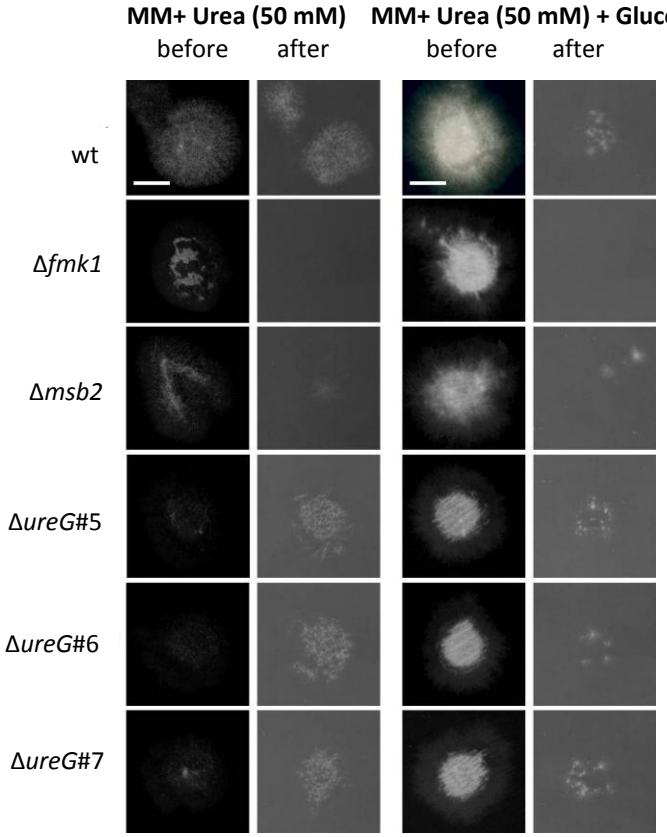

Figure 8. UreG is not required for cellophane penetration on MM media containing urea (w/o glucose) or urea with glucose. 5µl of a microconidia suspension (10^7 con/ml) of the indicated strains were spot-inoculated on the indicated media covered with a cellophane membrane and incubated at 28°C. To determine penetration, the cellophane sheets with the fungal colony were removed after 4 days (before) and the plates were incubated for an additional day (after). Scale bar, 1 cm.

To investigate the biological role of UreG for urease activation we also generated *F. oxysporum* urease mutants. A BLAST search in the Fusarium Genome Database (www.ncbi.nlm.nih.gov/pubmed) revealed two structural urease genes in *F. oxysporum* FOXG_01071 and FOXG_17146, named *Δure1* and *Δure2,* respectively. *Ure1* revealed higher sequence identities with ureases from other fungi, bacteria and plants and we generated the *F. oxysporum* Δ*ure1* gene knockout as performed for Δ*ureG* mutant described in section 2.2.

2.7. Urea is preferentially used as a nitrogen rather than a carbon source

The cellophane penetration assay (described in section 2.6.) revealed a reduced penetration ability of *F. oxysporum* when glucose was supplemented to the medium in addition to urea. This result prompted us to investigate the role of glucose in medium alkalization by *F. oxysporum.* To this aim, we compared growth and medium alkalinization on MM with urea alone or in combination of different carbon and/or nitrogen sources. Colony growth of the wt strain increased when an additional carbon source (glucose) or both a carbon and a nitrogen source ($(NH_4)_2SO_4$) was provided in addition to urea (Figure 9). Unexpectedly, a drastic growth reduction was observed when urea was provided together with $(NH_4)_2SO_{4.,}$ a condition where urea provides the only putative source of carbon. The Δ*ureG* mutant showed reduced growth on urea while the Δ*ure1* mutant was much less impaired. However all strains showed growth reduction on low pH, the medium pH does not have a major effect on the growth between the tested strains.

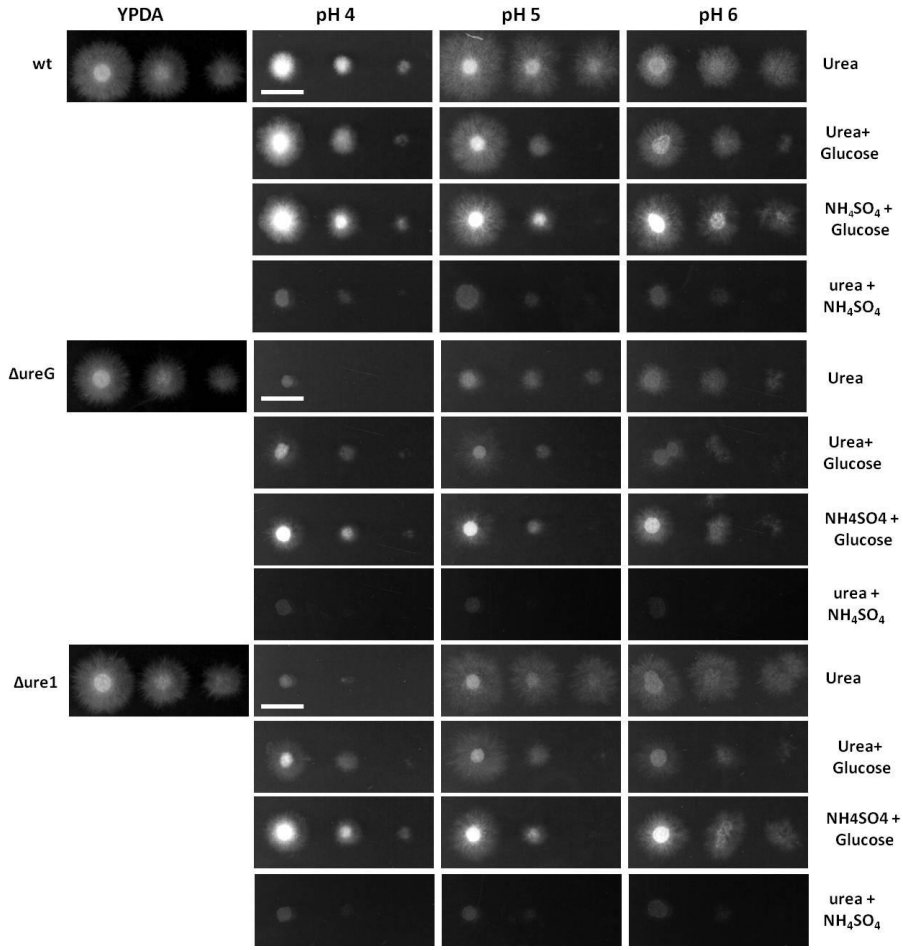

Figure 9. Utilization of urea as a nitrogen or carbon source by *F. oxysporum*. 2 µl of microconidia suspensions (10^5; 10^6; 10^7 conidia/ml) of the indicated strains were spotted on the indicated MM plates containing urea (50 mM) as a sole nitrogen and/or carbon source or on MM containing $(NH_4)_2SO_4$ (25 mM) and/or glucose (3%). Plates were incubated for three days at 28°C. Scale bar, 1 cm.

2.8. Δ*ureG* and Δ*ure1* mutants fail to secrete ammonia and alkalinize the medium when grown on urea

We next tested the capacity of the different strains to hydrolyze urea, as indicated by the ability to secrete ammonia and to alkalinize the surrounding medium. On MM + urea (50 mM) containing the pH indicator Bromocresol purple (BCP, 5',5''-dibromo-o-cresolsulfophthalein), media alkalization was detected as a colour change from yellow to purple in the wt, the complemented Δ*ureG*+*ureG* (Figure 10). In contrast, colonies of the Δ*ureG* and the Δ*ure1* mutants displayed a yellow colour indicative for an acidic pH (Figure

10). Strikingly, in highly buffered acidic urea medium only the Δ*fmk1* mutant showed a medium alkalization visible as a purple colour (Supplementary Figure 2).

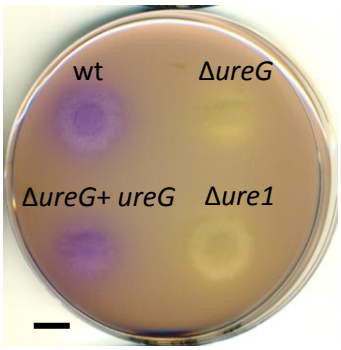

Figure 10. *UreG* and *ure1* are required for medium alkalinization during growth on urea. Microconidia of the indicated strains were inoculated on minimal medium (MM) containing 50 mM urea as the sole nitrogen and carbon source and the pH indicator Bromocresol purple. Urease activity was determined indirectly through the alkalinization of the medium represented by a colour change of the pH indicator (yellow <5.2; purple >6.8). Plates were incubated for 3 days at 28°C. Data shown are from one representative experiment. Experiments were performed three times with three technical repeats each, providing similar results. Scale bar: 1 cm.

To investigate whether the Δ*ureG* and Δ*ure1* mutants fail to alkalinize the medium because of the lack of secreted ammonia, we measured both pH and ammonia concentration in liquid MM medium containing urea (50 mM) as a sole nitrogen and carbon source over time (Figure 11A and B). The pH of the wt culture increased from 5 to 9 within the first 24 hours and thereafter increased only slightly until 72 hours (Figure 11A). Similar results were obtained with the Δ*fmk1* and Δ*msb2* mutant strains and Δ*ureG*+ *ureG.* Ammonia concentration in the culture increased concomitantly with pH over time, although some differences in the absolute amounts were detected between the strains (Figure 11B). Strikingly, the mutants Δ*ure1* and Δ*ureG* failed to increase extracellular pH above 7 and ammonia concentration after 72 hours was dramatically reduced compared to the wild type. Interestingly, this phenotype was more drastic in the Δ*ureG* than in the Δ*ure1* mutant. We conclude that *ureG* and *ure1* play a role in medium alkalisation caused by ammonia secretion in the presence of urea.

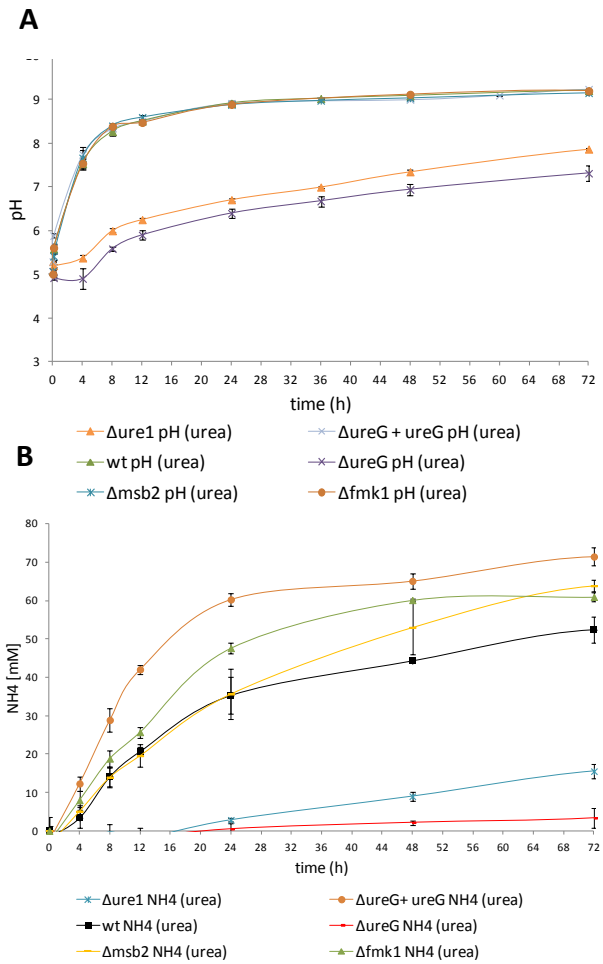

Figure 11. *UreG* and *ure1* are required for urease activity, determined by an increase in extracellular pH and secretion of ammonia. 2x 10^8 microconidia of the indicated strains were germinated for 14 h in 100 ml PDB, and the germlings were transferred to 50 ml liquid MM containing 50 mM urea as the sole carbon and nitrogen source. Samples of the culture supernatant were taken at the indicated time points to measure pH **(A)** and concentration of ammonia **(B)**. Mean values and standard errors were calculated from 3 biological repeats.

Microscopic examination of the MM+ urea cultures revealed the presence of struvite crystals in the supernatant of the wt (Figure 12A), the Δ*ureG*+ *ureG* (Figure 12C) and the Δ*msb2* mutant (data not shown). These structures started to appear after 72 h and were stable during the two weeks of the experiment. In contrast, the Δ*ureG* and Δ*ure1* mutant strains failed to produce the struvite crystals, and instead developed chlamydospore structures starting after 48 hours (Figure 12B and D).

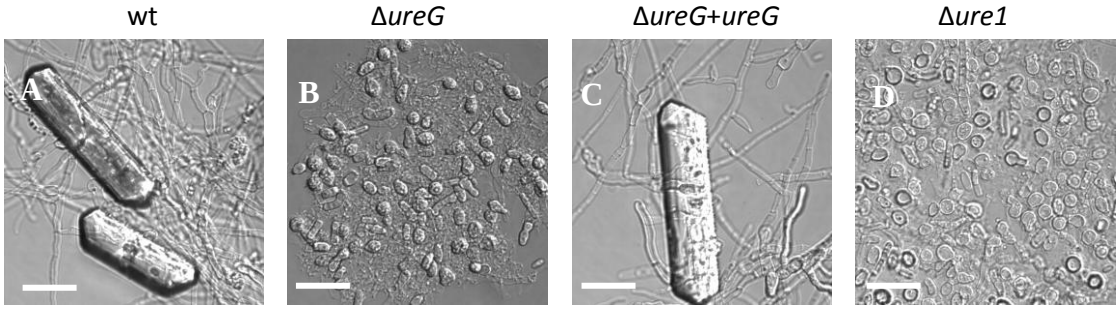

Figure 12. Production of struvite crystals and chlamydospores in MM + urea medium. Samples were taken from a two week old culture of MM containing 50 mM urea as a sole carbon and nitrogen source. Cultures of the wt **(A)** and the Δ*ureG*+ *ureG* complemented strain **(C)** as well as Δ*fmk1* and Δ*msb2* (data not shown) contained crystals of struvite (magnesium ammonium phosphate/$NH_4MgPO_4x\ 6H_2O$). The mutants Δ*ureG* **(B)** and Δ*ure1* **(D)** failed to produce crystals and developed thick-walled chlamydospores. Scale bar, 20 µm.

2.9. Glucose inhibits secretion of ammonia and medium alkalinization

We next examined the effect of glucose on urease-dependent media alkalization. When the wt strain was grown in urea containing liquid medium in the presence of 3% glucose, instead of a pH increase an initial decrease of the extracellular pH was observed (Figure 12A). This stage coincided with the absence of ammonia secretion into the medium (Figure 12B). After 24 hours, the pH started to increase concurrently with secretion of ammonia into the medium. The same pattern was observed for the Δ*msb2*, Δ*fmk1* and Δ*ureG*+*ureG* strains. By contrast, the Δ*ureG* and Δ*ure1* mutants only produced a slight increase in pH and failed to secrete ammonium (Figure 12B).

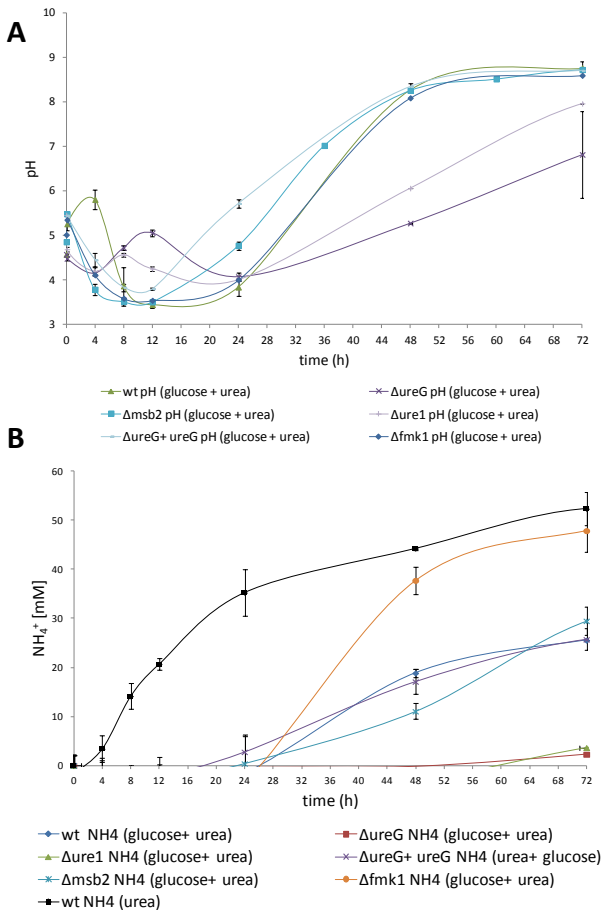

Figure 12. Glucose represses ammonia secretion and medium alkalization. 2 x 10^8 microconidia of the indicated strains were germinated for 14 h in 100 ml PDB and transferred to 50 ml liquid MM media containing 50 mM urea plus 3% glucose. Samples of the culture supernatant were taken at the indicated time points to measure pH **(A)** and concentration of ammonia **(B)**. Mean values and standard errors were calculated from 3 biological repeats

2.9.1. Ammonia secretion and medium alkalinization correlate with glucose depletion

We next monitored the concentration of glucose in the medium over time and found that the time of ammonia secretion and the consequent pH increase coincided with the depletion of glucose in the medium (Figures 13A, B). Ammonia secretion and media alkalization initiated after 24 hours when the glucose reached a concentration below 3g/l. Interestingly, the Δ*ureG* and Δ*ure1* mutants consumed glucose at a similar rate as the wt, but failed to secrete ammonia upon glucose depletion (Figure 13C). All these effects were fully restored in the complemented strains (Supplementary Figure 3). Unexpectedly, however the Δ*fmk1* mutant displayed the pH as the wt (Figure 13F), almost the double concentration of ammonia (47, 9 mM) compared to the wt (25, 5 mM) was secreted (Figure 13E).

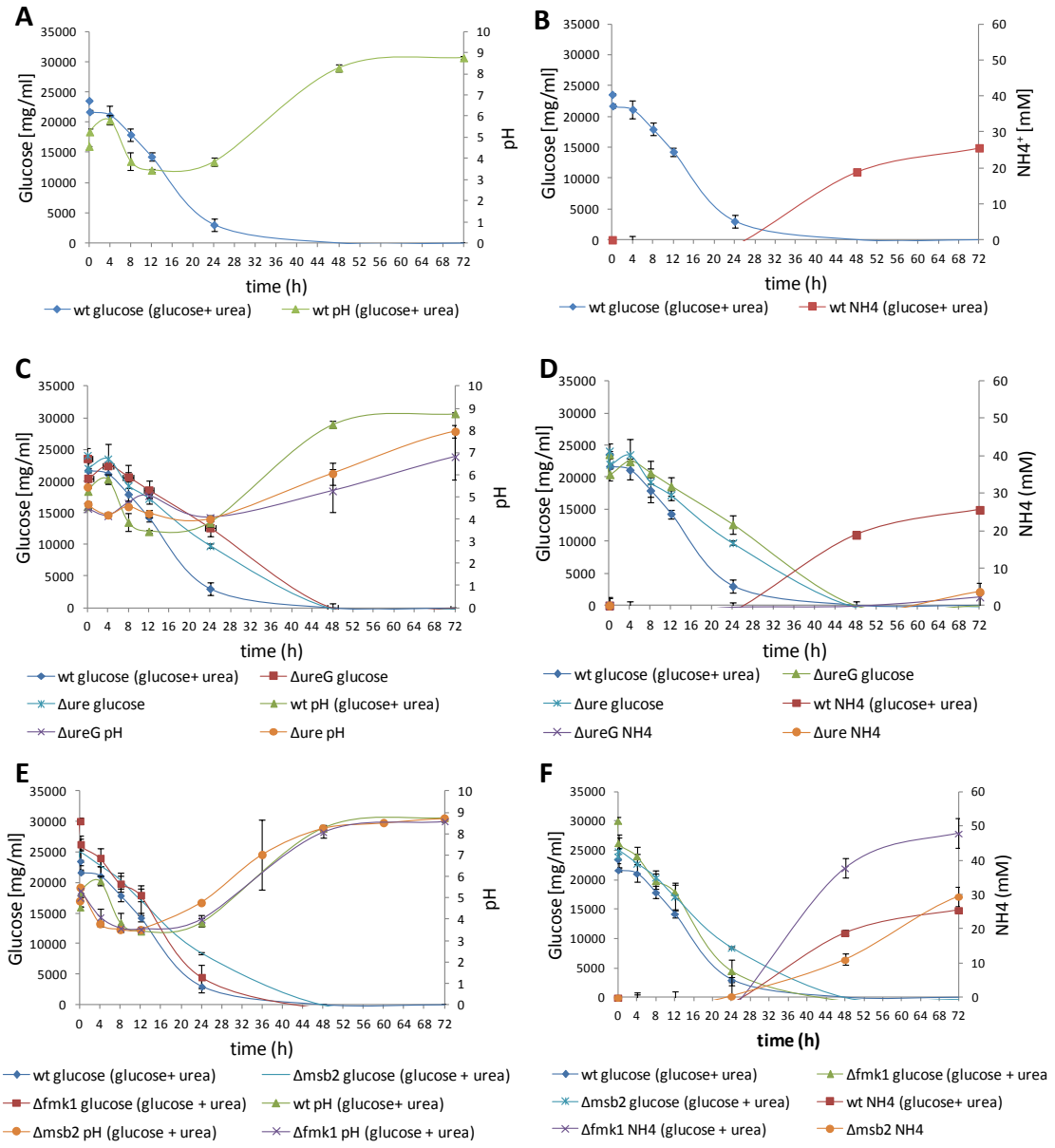

Figure 13. Ammonia secretion and medium alkalinization are triggered by glucose depletion. 2 x 10^8 microconidia of the indicated strains were germinated for 14 h in 100 ml PDB and transferred to 50 ml liquid MM media containing 50 mM urea plus 3% glucose. Samples of the culture supernatant were taken at the indicated time points to measure pH **(A,C,E)**, concentration of ammonia **(B,D,F)** or of glucose **(A-F)**. Mean values and standard errors were calculated from 3 biological repeats.

2.9.2. Carbon catabolite repression of ammonia secretion is specific for glucose

To investigate whether the repression of pH increase and ammonia secretion is specific for glucose, we tested a number of carbon sources. Galactose or glycerol failed to inhibit ammonium secretion and medium alkalinization in the wild type (Figure 14A, B). Thus, ammonium secretion is subject to carbon catabolite repression by glucose.

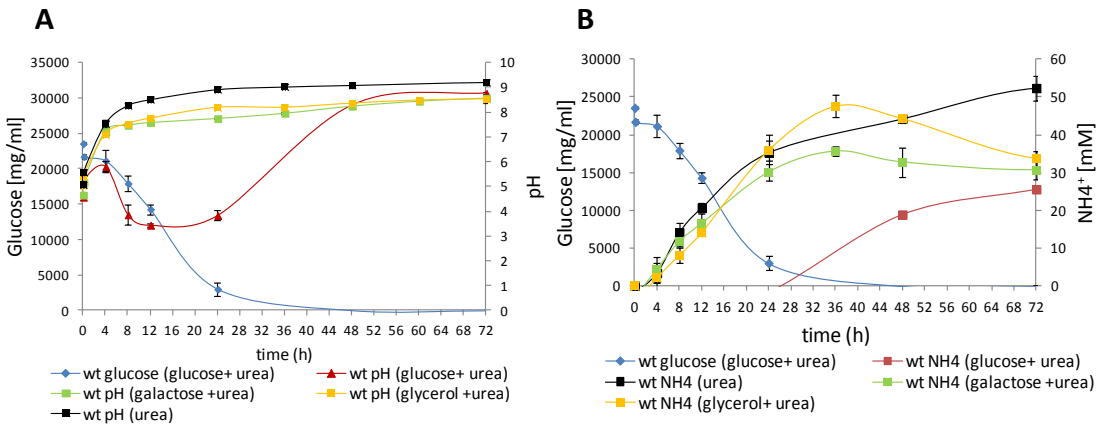

Figure 14. Carbon catabolite repression of ammonia secretion is specific for glucose. 2 x 10^8 microconidia of the indicated strains were germinated for 14 h in 100 ml PDB and transferred to 50 ml liquid MM media containing 50 mM urea, or urea plus either 3% glucose, galactose or glycerol. Samples of the culture supernatant were taken at the indicated time points to measure pH **(A)**, or concentration of ammonia **(B)**. Mean values and standard errors were calculated from 3 biological repeats.

2.9.3. Carbon catabolite repression of ammonia secretion also occurs on nitrogen sources other than urea

When casaminoacids instead of urea were used as a nitrogen source, ammonia secretion and pH increase were also observed as previously found on urea (Figure 15A, B). Moreover, the presence of glucose in the medium prevented both ammonium secretion and medium alkalinization. This suggests that the effect of carbon catabolite repression on ammonium secretion is not limited to urea as a nitrogen source.

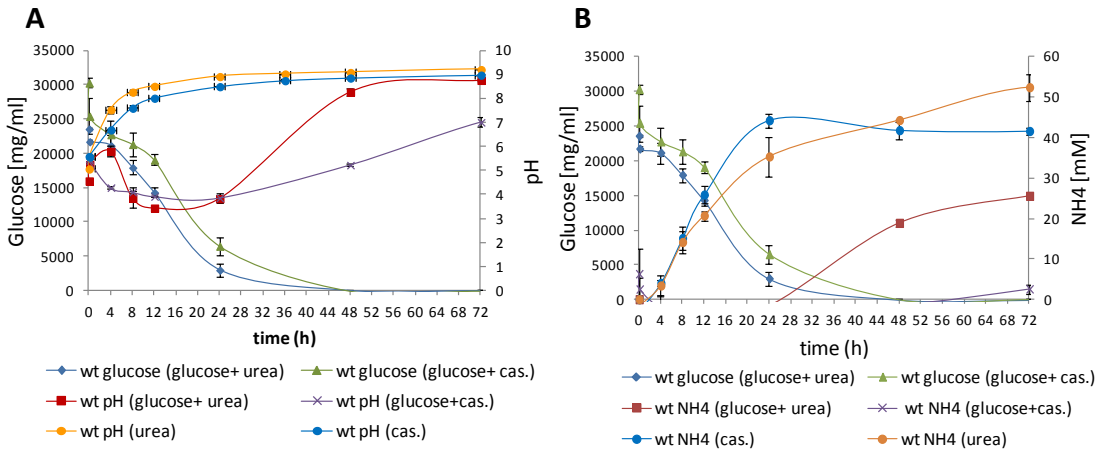

Figure 15. Carbon catabolite repression of ammonia secretion also occurs on nitrogen sources other than urea. 2 x 10^8 microconidia of the indicated strains were germinated for 14 h in 100 ml PDB and transferred to 50 ml liquid MM media containing 1% casaminoacids, or casamoinoacids plus 3% glucose. Samples of the culture supernatant were taken at the indicated time points to measure pH **(A)**, or concentration of ammonia **(B)**. Mean values and standard errors were calculated from 3 biological repeats.

2.9.4. The ammonium permease MepB and the nitrogen metabolism transcriptional regulators MeaB and AreA are required for carbon catabolite repression of ammonium secretion

In fungi, nitrogen metabolite repression (NMR) ensures that genes required for the utilization of alternative nitrogen sources are only transcribed in the absence of preferred sources such as ammonium or glutamine. NMR strictly depends on the nitrogen response GATA factor AreA/Nit2 (Arst and Cove, 1973; Marzluf, 1997). In *F. oxysporum* it was previously shown that AreA is required for de-repression of NMR genes (Lopez-Berges et al., 2010). Moreover, ammonium was shown to inhibit virulence-related functions in *F. oxysporum,* and this repression requires the bZIP protein MeaB (Lopez-Berges et al., 2010). Recent data suggest that *mepB,* encoding an ammonium permease that is subject to NMR, requires MeaB and AreA for transcriptional de-repression (Segorbe et al. unpublished).

We decided to examine the role of nitrogen metabolism regulation in urease-mediated ammonium secretion by testing the ability of different mutants to alkalinize the urea medium in present or absence of glucose. Strikingly, the inhibitory effect of glucose on

ammonium secretion and medium alkalinization was abolished in the Δ*mepB*, Δ*meaB*, and Δ*areA* mutants (Figure 16). The timing of ammonium secretion on urea + glucose in the mutants was comparable to that on urea in the absence of glucose (Figure 16C). Importantly, glucose concentration in the medium decreased over time in the mutants similar to the wt strain, demonstrating that they are not affected in glucose uptake or utilization. All these effects were fully restored in the complemented strains (Supplementary Figure 4). Interestingly, the Δ*areA* mutant displayed reduced ammonia secretion when grown on urea alone, but not on urea + glucose (Figure 16C), most likely due to the role of AreA in utilization of urea as a nitrogen source, as shown recently (López-Berges et al. 2014).

We also investigated the role of MepB in glucose repression of ammonium secretion on casaminoacids as the nitrogen source. Interestingly, in this condition glucose repression of ammonium secretion was still operating in the Δ*mepB* mutant (Figure 16D). We conclude that the role of MepB in carbon catabolite repression of ammonia secretion is specific for the nitrogen source urea.

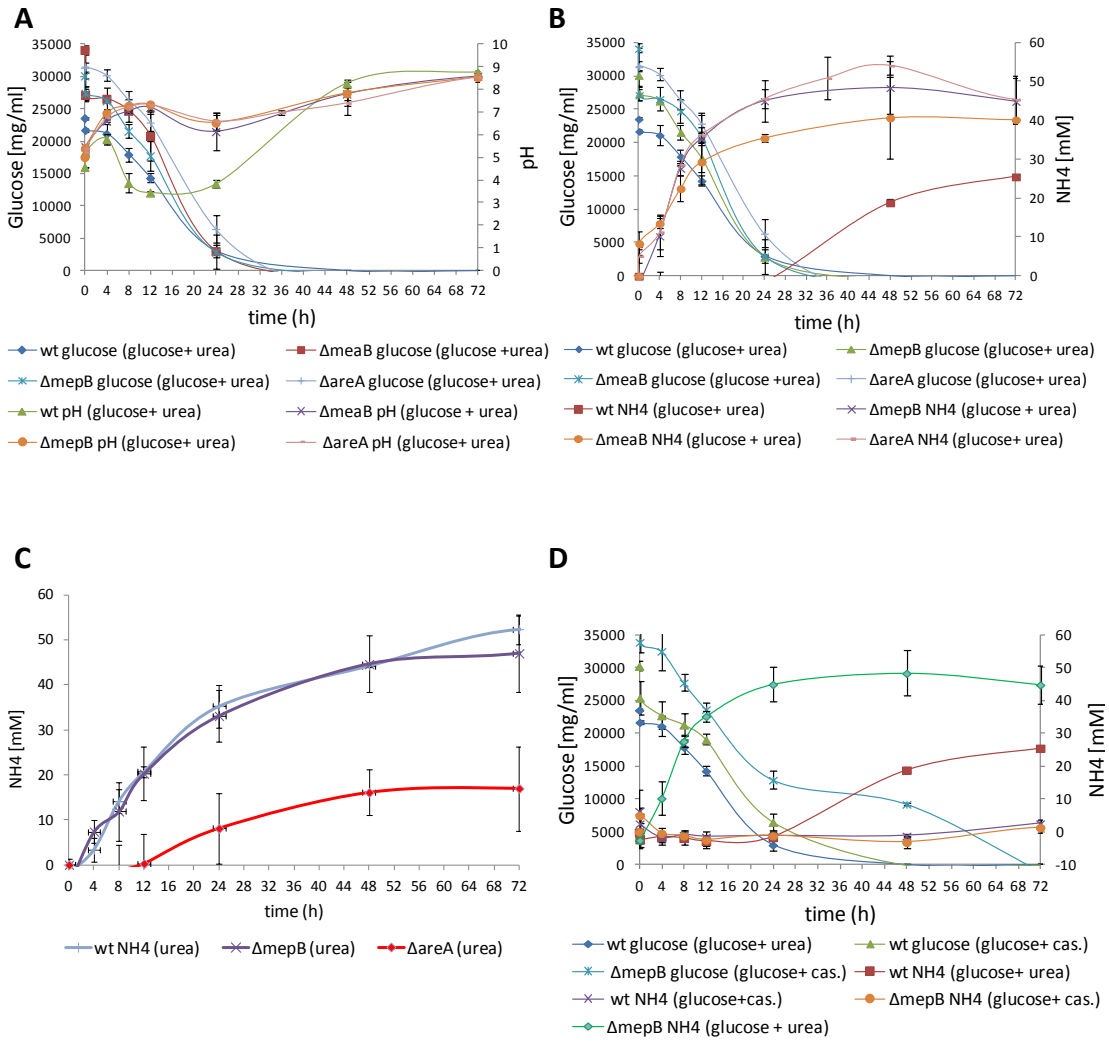

Figure 16. MepB, MeaB and AreA are required for carbon catabolite repression of ammonium secretion. 2 x 10^8 microconidia of the indicated strains were germinated for 14 h in 100 ml PDB and transferred to 50 ml liquid MM media containing either 50 mM urea, urea plus 3% glucose, 1% casaminoacids, or casamoinoacids plus 3% glucose. Samples of the culture supernatant were taken at the indicated time points to measure pH **(A)**, or concentration of ammonia **(B,C,D)** or glucose **(A,B,D)**. Mean values and standard errors were calculated from 3 biological repeats .

2.9.5. Urease dependent ammonium secretion and medium alkalization is partially controlled by the glucose sensing kinase Snf1

Carbon catabolite repression involves sensing of available carbon sources, whereby the presence of the preferred carbon source glucose prevents the utilization of non-preferred carbon sources as well as the function of different catabolic routes (Johnston, 1999; Rolland et al., 2002; Zaman et al., 2008). In *S. cerevisiae* two main glucose-responsive signaling pathways have been identified: a glucose induction pathway involving the membrane receptors Snf3 and Rgt2 and the transcription factor Rgt1; and a glucose repression pathway, mediated by the transcriptional repressor Mig1, where the Mig1-inactivating protein kinase Snf1 (sucrose non-fermenting 1) is required for de-repression of glucose-repressed genes. (for a review see (Carlson, 1999; Forsberg and Ljungdahl, 2001; Rolland et al., 2002; Santangelo, 2006). Following its uptake, glucose is phosphorylated to glucose 6-phosphate by the hexokinase Hxk2 before entering carbon metabolism. High glucose levels lead to inactivation of Snf1 complex. Inactive Snf1 cannot phosphorylate Mig1, which thus remains in the nucleus under high glucose levels, exerting repression of transcription of several genes. At low glucose concentrations Snf1 becomes active and phosphorylates Mig1, triggering its translocation to the cytosol and release of glucose repression (Christensen et al., 2009).

Previously it was shown that a *F. oxysporum* Δ*snf1* mutant had reduced expression of genes encoding cell wall-degrading enzymes, grew poorly on certain carbon sources and showed a delay in the progression of wilt symptoms on plants (Ospina-Giraldo et al., 2003). Here we tested the *F. oxysporum* Δ*snf1* and Δ*hxk1* (hexokinase 1; Gonzalez-Garcia et al., unpublished) mutants for glucose repression of ammonium secretion and environmental alkalization on urea medium (Figure 17). While the hexokinase mutant Δ*hxk1* was unaffected in this process, the Δ*snf1* mutant showed a reduction in the delay of glucose repression. Ammonia secretion in this mutant started already after 12h, meaning that repression was alleviated at a glucose concentration of 50 mM, double of that in the wt strain (Figure 17B). In urea medium urease activity was increased in the Δ*hxk1* mutant and reduced in the Δ*snf1* mutant (Figure 17C).

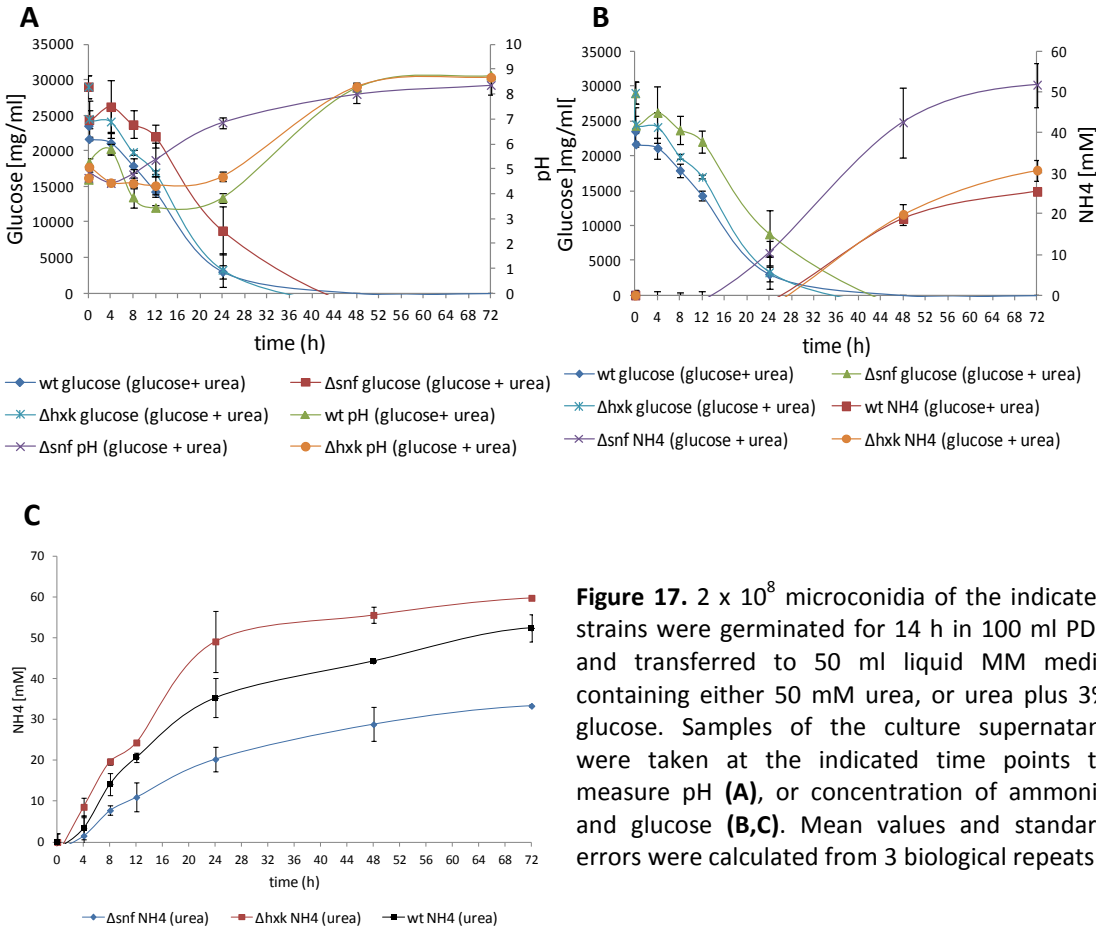

Figure 17. 2 x 10^8 microconidia of the indicated strains were germinated for 14 h in 100 ml PDB and transferred to 50 ml liquid MM media containing either 50 mM urea, or urea plus 3% glucose. Samples of the culture supernatant were taken at the indicated time points to measure pH **(A)**, or concentration of ammonia and glucose **(B,C)**. Mean values and standard errors were calculated from 3 biological repeats.

2.10. *ureG* but not *ure1* expression is up-regulated after glucose depletion

We next determined transcript levels of key genes at different time points of growth of *F. oxysporum* in urea + glucose. To this aim, mycelium was harvested for RNA extraction after 12, 24 and 48 hours of growth, representing the time points before, coinciding with, and 24 hours after glucose depletion, with medium pH values of 3,8, 3,7 and 7,2, respectively (Figure 18A). Real time qPCR with specific primers revealed low constitutive transcript levels of the genes *ure1* (urease) and *car1* (arginase which converts arginine to urea and ornithine), and a slight up-regulation of *mepB* (ammonia permease) expression after 24 hours (Figure 18B). No transcripts of the *FOXG_12291* gene encoding the putative *F. oxysporum* orthologue of the urea transporter Dur3 of *Aspergillus nidulans* were detected under the

conditions tested. Interestingly, in contrast to *ure1* whose expression did not change, the urease accessory protein gene *ureG* was highly up-regulated after 24 hours, coinciding with the time point of glucose depletion and the onset of ammonia secretion. Finally the transcript levels of *msb2* increased steadily from 12 hours until 48 hours correlating with the decrease of glucose and accumulation of secreted ammonia in the medium (Figure 18B).

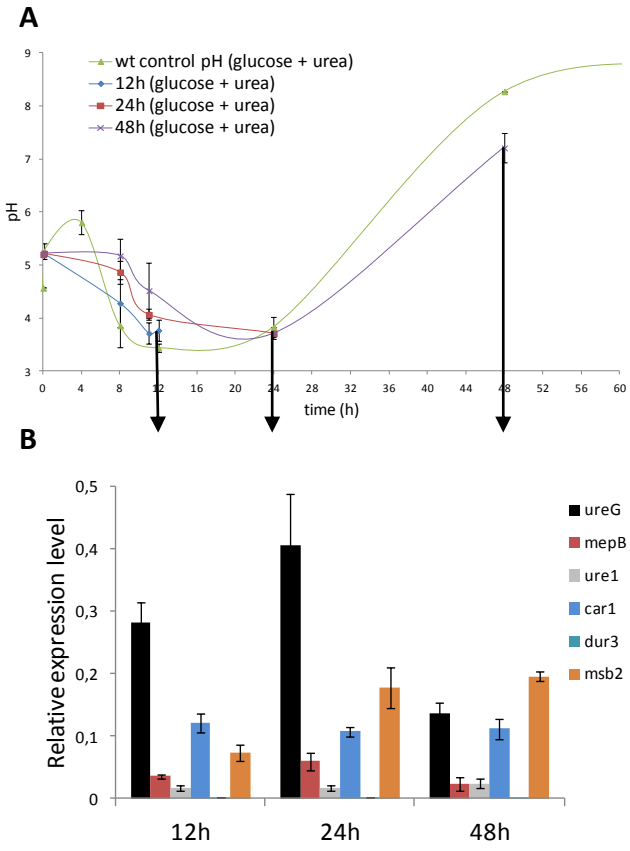

Figure 18. Transcript levels of *ureG* bud not of *ure1* are upregulated after depletion of glucose in urea medium. (A) 2 x 10^8 microconidia of the wt strain were germinated for 14 h in 100 ml PDB and transferred to 50 ml liquid MM media containing either 50 mM urea, or urea plus 3% glucose (time 0). Culture medium samples were taken at the indicated time points to measure pH **(A)**. Mean values and standard errors were calculated from 3 biological repeats. **(B)** Real-time qPCR of cDNA obtained from mycelia harvested at the time points indicated by arrows in **(A)**. Gene abbreviations: *ureG* (*FOXG_13832*, urease accessory protein G), *ure1* (*FOXG_01071*, urease1), *car1* (*FOXG_12915*, arginase), *dur3* (*FOXG_12291*, urea transporter), *mepB* (*FOXG_00462*, ammonia permease), *msb2* (*FOXG_09254*, mucin-like transmembrane protein). Relative expression levels represent mean values normalized to the *actin* gene expression levels. Mean values and standard errors were calculated from 3 biological repeats.

2.11. Lack of evidence for extracellular urease activity in *F. oxysporum* culture supernatants

Since we did not detect expression of the putative urea transporter Dur3 during growth of F. oxysporum on urea + glucose (Figure 19B), we tested the hypothesis that, in the absence of urea uptake into the cell the urease enzyme might be exported to the supernatant or be membrane-associated. To test this idea, a construct where the C-terminus of the *ure1* coding

region was fused to the Green Fluorescent Protein (GFP) was transformed into the wt background. Three independent tranformants that had integrated the *ure1_GFP* construct by homologous recombination at the *ure1* locus were identified by PCR (data not shown). To test the functionality of the fusion protein, medium alkanization on urea was tested. All three tranformants failed to produce medium alkanization when growing on solid or liquid urea medium and no ammonia sectretion was deteced (data not shown). This phenotype resembled that of the Δ*ure1* mutants, suggesting that the Ure1_GFP fusion protein is enzymatically inactive.

In an alternative approach, we tested whether urease enzymatic activity could be detected in the culture supernatant of the wt strain. To this aim, urease activity was measured by determining ammonia production from urea by crude protein extracts of fungal mycelium and of the culture supernatant. In the presence of urea, the protein extracts of the wt and the Δ*ureG+ureG* strains released 71,3 mM and 55,7 mM ammonia, respectively, after 60 minutes suggesting the presence of urease enzymatic activity (Figure 19). However, no urease activity was detected in the Δ*ureG* mutant or in the 10x concentrated supernatants of any of the strains. Even though we cannot exclude that extracellular urease might be membrane-associated, these results strongly suggest that the urease protein of *F. oxysporum* is exclusively intracellular and not secreted into the culture supernatant.

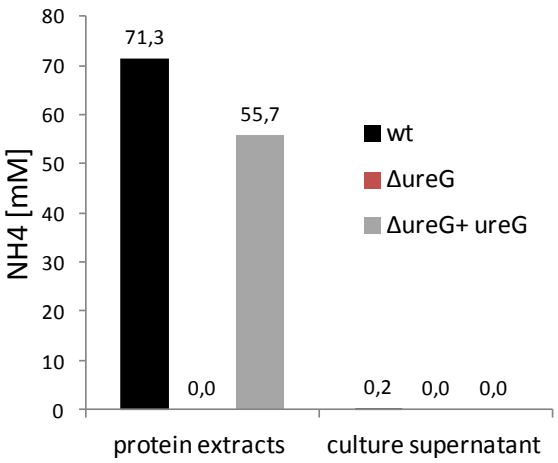

Figure 19. Urease is not secreted in *F. oxysporum*. 2 x 10^8 microconidia of the indicated strains were germinated for 14 h in 100 ml PDB and transferred to 50 ml liquid MM media containing either 50 mM urea. Mycelia and culture supernatants were harvested after 7 h incubation and total protein was extracted from mycelia. Intracellular protein extracts were diluted to the same volume of the dialyzed culture supernatants or to the supernatants concentrated 10 x by lyophilisation. Urease enzymatic activity was determined by measuring the concentration of ammonia released from urea after 60 min.

2.12. UreG contributes to invasive growth of *F. oxysporum* on living apple tissue

The apple slice infection assay assesses the ability of invasive growth on living fruit tissue. Previous work showed that Δ*fmk1* mutants are impaired in invasion and colonization of living fruit tissue (Di Pietro et al., 2001; Rispail and Di Pietro, 2009), while the Δ*msb2* mutants had a reduced capacity (Perez-Nadales and Di Pietro, 2011). Three independent Δ*ureG* mutants (Δ*ureG*#5, Δ*ureG*#6, and ΔureG#7) tested for invasive growth on apple slices showed a slight reduction in the diameter of the infected tissue area compared to the wt (Figure 20A,B).

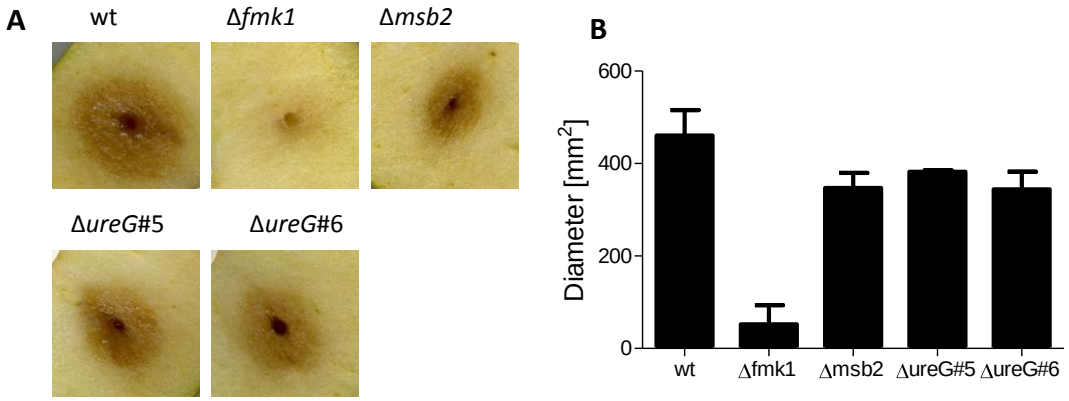

Figure 20. UreG contributes to invasive growth on living fruit tissue. (A) Apple fruits were point-inoculated with 5 x 10^4 microconidia of the indicated strains and incubated in a humid chamber at 28°C for 3 days. Experiments were performed three times, each with two technical repeats. Data shown are from one representative experiment. **(B)** Ten apple slice infections per indicated strain were performed and diameters of the affected tissue area were measure on day 3 after inoculation. Bars represent standard errors calculated from ten technical replicates. Diameter values of the three Δ*ureG* mutants are not significantly different to the wild type according to Mann-Whitney test ($p<0.05$).

2.13. UreG and Ure1 contribute to virulence of *F. oxysporum* on tomato plants

The role of urease in fungal pathogenicity on plants has not been investigated. To determine the importance of UreG and Ure1 in virulence of *F. oxysporum* on tomato plants, roots were inoculated with the different mutants, using the wt and the Δ*fmk1* mutant as positive and negative control, respectively. Plants inoculated with the wt strain showed a continuous increase in wilt disease symptoms and all the plants were dead 34 days after inoculation (Figure 21). As decribed previously plants inoculated with the Δ*fmk1* mutant failed to display

any disease symptoms (Di Pietro et al., 2001). Moreover, we confirmed the reduced mortality caused by the Δ*msb2* mutants as described previously (Perez-Nadales and Di Pietro, 2011). Two independent Δ*ureG* (Figure 21A) and three independent Δ*ure1* mutants (Figure 21B) showed a significantly reduced ability to kill tomato plants. Whereas the wt caused 100 % mortality after 34 days, the Δ*ureG* mutants only caused mortalities between 30 and 40% and the Δ*ure1* mutants caused mortalities between 30 and 50%.

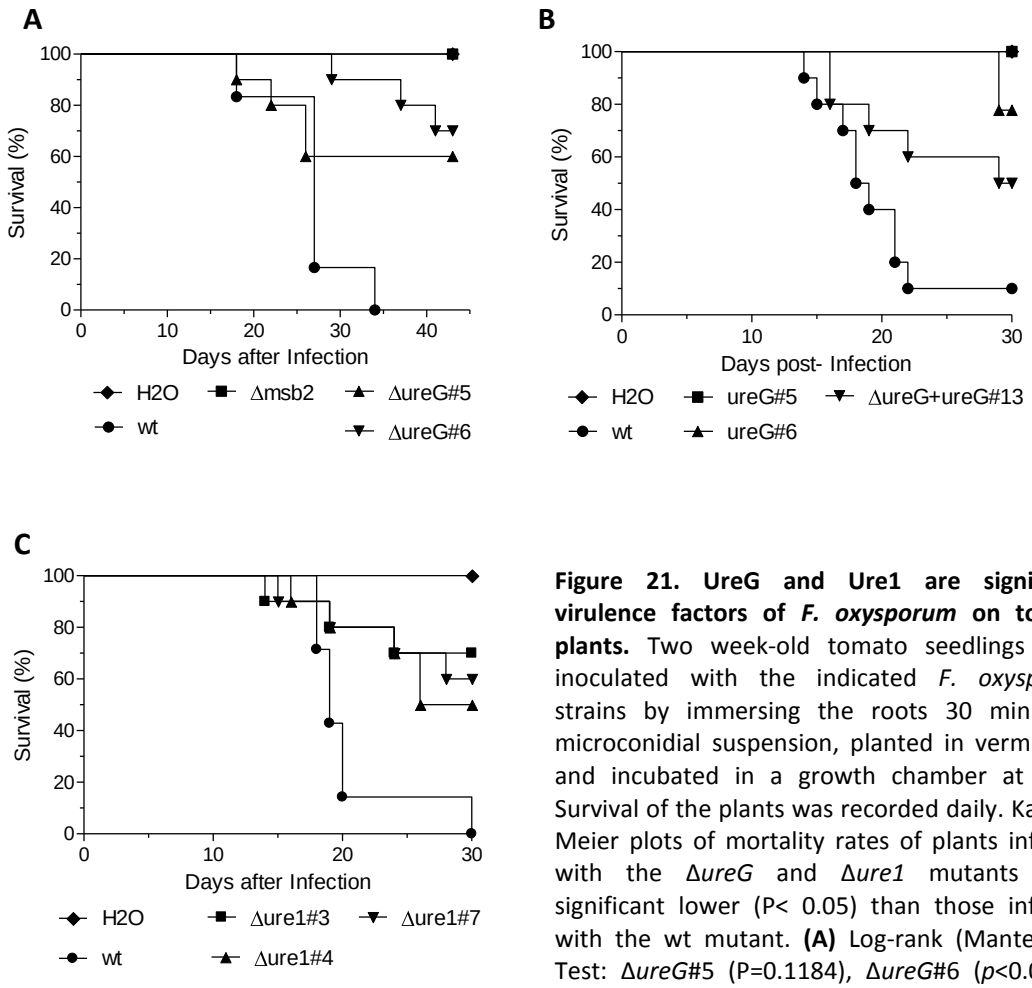

Figure 21. UreG and Ure1 are significant virulence factors of *F. oxysporum* on tomato plants. Two week-old tomato seedlings were inoculated with the indicated *F. oxysporum* strains by immersing the roots 30 min in a microconidial suspension, planted in vermiculite and incubated in a growth chamber at 28°C. Survival of the plants was recorded daily. Kaplan–Meier plots of mortality rates of plants infected with the Δ*ureG* and Δ*ure1* mutants were significant lower (P< 0.05) than those infected with the wt mutant. **(A)** Log-rank (Mantel-Cox) Test: Δ*ureG*#5 (P=0.1184), Δ*ureG*#6 (*p*<0.0001). **(B)** Log-rank (Mantel-Cox) Test: Δ*ure1*#3 (*p*=0.0045), Δ*ure1*#4 (*p*=0.0131), Δ*ure1*#7 (*p*=0.0081). Ten plants were used per treatment. The experiment was performed three times with similar results.

2.14. UreG, but not Ure1 contributes to virulence of *F. oxysporum* on *Galleria*

Urease has been reported as a virulence factor in two important human fungal pathogens, *C. neoformans* (Cox et al., 2000) and *C. immitis* (Cole, 1997). As described previously, *F. oxysporum* is able to infect, colonize and kill *G. mellonella* larvae (Navarro-Velasco et al., 2011). After injection of wt microconidia we observed progressive melanization of the larvae, a typical symptome in infected animals, and a mortality rate of 100% after five days (Figure 22A). The Δ*msb2* mutant caused the same mortality rate as the wt, whereas two independent Δ*ureG* mutants caused significantly reduced mortality, a phenotype that was completely restored in the complemented strain. Interestingly, three indepentent Δ*ure1* mutans showed no significant reduction in virulence and caused mortality rates similar to those of the wt (Figure 22B).

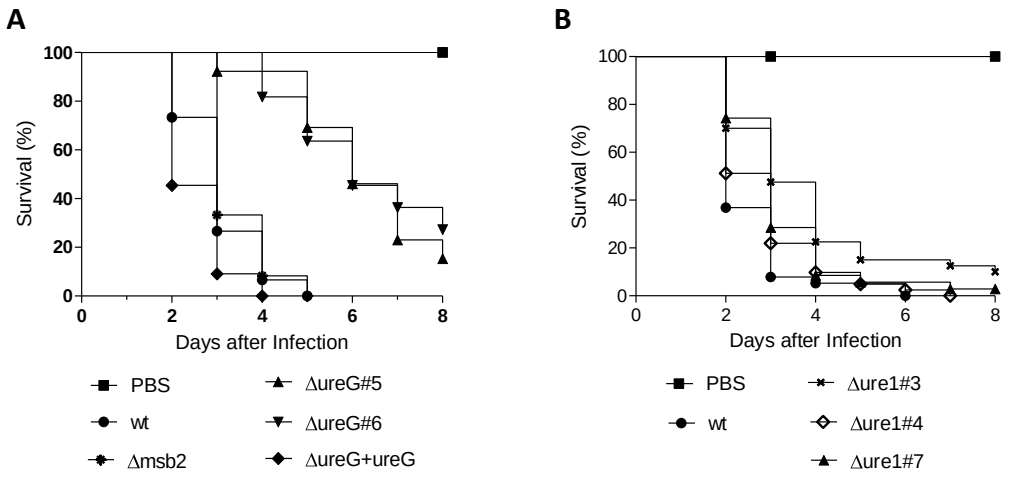

Figure 22. UreG but not Ure1 is required for virulence *F. oxysporum* in the *Galleria* infection model. Kaplan–Meier plots of *G. mellonella* survival after injection of 1.6 x 10^5 microconidia of the indicated *F. oxysporum* strains in PBS into the hemocoel of the larvae and incubation at 30°C. **(A)** Δ*ureG#5* and Δ*ureG#6* but not Δ*msb2* mutants caused significantly reduced mortality on *G. mellonella* (p< 0,0001) **(B)** Mortality caused by three independent Δ*ure1* mutants was not significantly different from the wt. Experiments was performed three times with similar results. Graphs show mortality rates of one representative experiment with 15 larvae per treatment.

2.14.1. Urea biosynthesis genes are highly expressed in *F. oxysporum* during *Galleria* infection

The reduced virulence of the Δ*ureG* mutants in the invertebrate model *G. mellonella* prompted us to investigate expression of genes involved nitrogen source assimilation during *F. oxysporum* infection. Real time qPCR was performed on cDNA obtained from infected larvae inoculated either with microconidia of the wt or the Δ*ureG* and Δ*ure1* mutant strains. We analyzed fungal genes encoding key enzymes involved in nitrogen uptake and assimilation (Lopez-Berges et al. 2014), including the nitrate/nitrite transporter (*nt*), the nitrate reductase (*nit1*), the glutamine synthetase 1 (*gs1*) or the ammonia permease (mepB), as well as enzymes involved in arginine biosynthesis such as arginosuccinate lyase (*al*) or arginine catabolism such as arginase (*car1*), urease (*ure1* and *ure2*), urease accessory protein G (*ureG*), ornithine aminotransferase (*oat*), ornithine decarboxylase (*odc*).

Interestingly, genes encoding enzymes involved in the arginine and urea biosynthesis pathway were highly expressed during infection of *Galleria,* including glutamine synthetase and argininosuccinate lyase (Figure 23 A, B). The glutamine synthetase gene showed higher transcript levels in the wt than in the Δ*ureG* and Δ*ure1* mutants. The highest expression was obtained for the gene encoding arginase which converts arginine to urea (Kinne-Saffran and Kinne, 1999; Mendz and Hazell, 1996; Mendz et al., 1998). The *car1* gene was expressed at higher level in the wt and the Δ*ure1* strain than in the Δ*ureG* mutant. Interestingly, none of the two urease genes (*ure1* and *ure2*) were expressed during *Galleria* infection, but *ureG* expression was detected in the wt and in the Δ*ure1* mutant. No transcripts were detected for the nitrite, ammonia or urea transporter or the nitrate reductase genes.

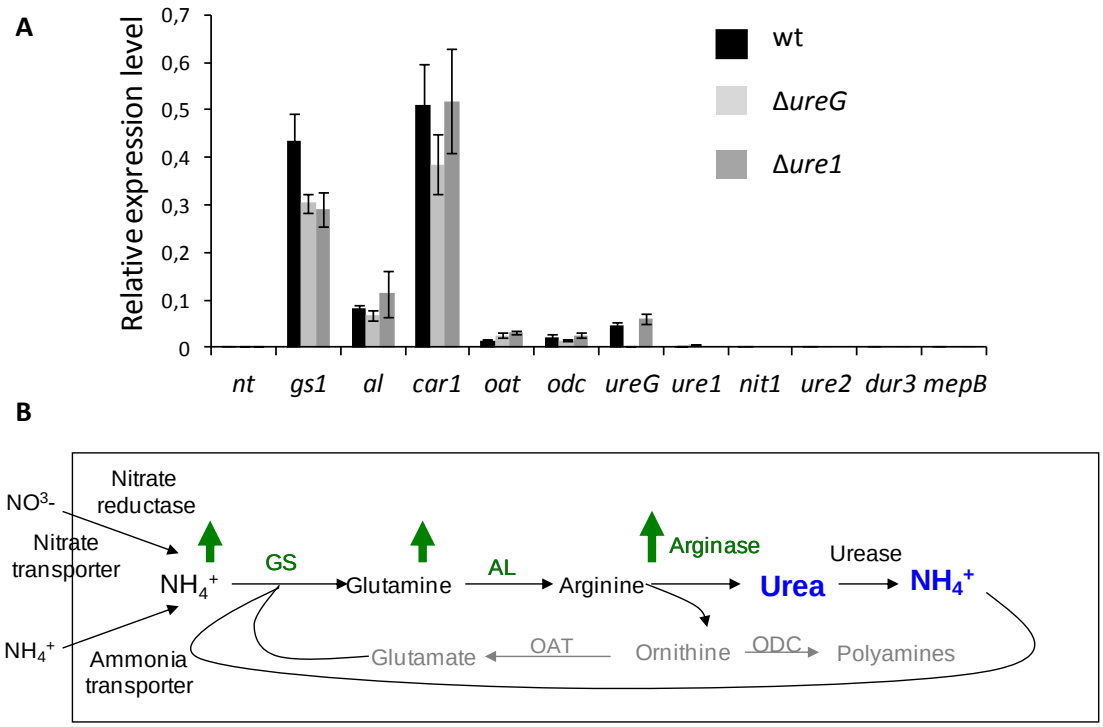

Figure 23. Urea biosynthesis genes in *F. oxysporum* are highly expressed during *Galleria* infection. **(A)** *G. mellonella* larvae were inoculated by injection of 1.6 x 10^5 microconidia of the indicated *F. oxysporum* strains into the hemocoel and incubated humid chamber at 30°C. Two days after inoculation, three larvae of each treatment were randomly chosen for RNA extraction. Real time qPCR representing mean values of the relative transcript levels normalized to the *actin* gene of *F. oxysporum*. Mean values and standard errors were calculated from 3 independent *G. mellonella* larvae. As a negative control qPCR was performed with all gene-specific primers using cDNA obtained from non-inoculated *G. mellonella* larvae, and no amplification was detected (data not shown). Abbreviations for genes: *nt*: nitrate/nitrite transporter (FOXG_ FOXG_00635); *gs1*: glutamine synthetase 1 (FOXG_05182); *al*: argininosuccinate lyase (FOXG_01957); *car1*: arginase (FOXG_12915); *oat1*: ornithine aminotransferase (FOXG_09346); *odc*: ornithine decarboxylase (FOXG_07603); *ureG*: urease asseccory protein G (FOXG_13832); *ure1*: urease1 (FOXG_01071); *nit1*: nitrate reductase (FOXG_04181); *ure2*: urease2 (FOXG_17146); *dur3*: urea transporter (FOXG_12291); *mepB*: ammonia permease (FOXG_00462). **(B)** Simplified model representing key proteins in nitrogen source assimilation tested by the qPCR analysis in (A). Enzymes involved in nitrogen source uptake and assimilation include the nitrate/nitrite transporter (NT), nitrate reductase (NIT1), the ammonia permease (mepB) and glutamine synthetase 1 (GS1); enzymes involved in arginine biosynthesis and catabolism, respectively, arginosuccinate lyase (AL) and arginase (CAR1); urease (URE1), ornithine aminotransferase (OAT) and ornithine decarboxylase (ODC).

2.15. UreG is a virulence factor of *F. oxysporum* on immunodepressed mice

Previous work showed that genes important for infection in *Galleria* often also play a significant role in virulence in the mouse infection model (Navarro-Velasco et al., 2011; Ortoneda et al., 2004). Inoculation of immunodepressed mice with wt conidia caused a mortality of 70 % of the infected mice after ten days (Figure 24). By contrast, the Δ*ureG* mutant caused significantly attenuated mortality, with only two of the ten infected mice succumbing to infection (p=0.019). Mortality was restored in the Δ*ureG+ureG* complemented strain. Moreover, the Δ*ure1* mutant also caused high mortality. Collectively, these results are very similar to those obtained in the *Galleria* infection model.

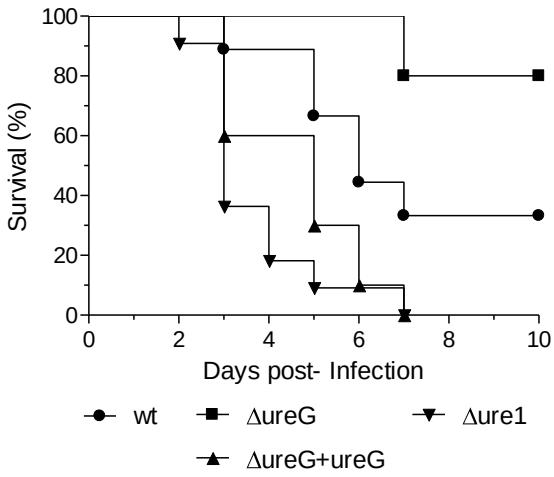

Figure 24. UreG is required for full virulence of *F. oxysporum* on immunodepressed mice. Oncins France 1 male mice (n=10) were inoculated by tail vein injection with $2x10^6$ microconidia of the indicated strains. Immunosuppressive treatment (a single intraperitonal dose of 150 mg cyclophosphamide per kg body weight and a single intravenous dose of 150 mg 5-fluorouracil) was applied one day prior to infection. Survival was recorded for 10 days. The Δ*ureG* mutant caused significantly less mortality (p=0.019) than the wt and the complemented strains.

2.16. *F. oxysporum* arginase is required for utilization of arginine as a nitrogen source

Arginase is the only enzyme known so far to convert arginine into urea (Witte, 2011). The high expression of the *F. oxysporum* arginase gene *car1* during *G. mellonella* infection (Figure 23) led us to further investigate the biological role of arginase. Three independent Δ*car1* mutants showed normal growth on complete medium (YPDA, Figure 25) and on MM containing urea as the sole nitrogen and carbon source (data not shown), but dramatically impaired growth on MM containing 5mM arginine as the sole nitrogen source in comparison to the wt, Δ*ure1*, Δ*ureG* and the complemented Δ*car1+car1* strain (Figure 25). This result

shows that *F. oxysporum* arginase is important for the utilization of arginine as a nitrogen source.

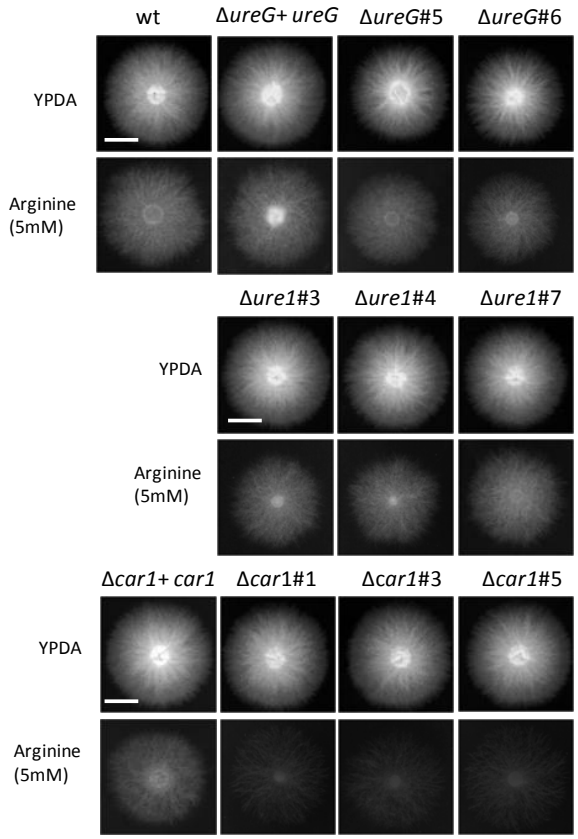

Figure 25. *F. oxysporum* arginase Car1 is required for growth on arginine as a sole nitrogen source. 2 x 10^4 microconidia of the indicated strains were spot-inoculated on complete medium (YPDA) or on MM containing 5 mM arginine as the sole nitrogen source. Plates were incubated for three days at 28°C. Scale bar, 1 cm.

To determine the importance of Car1 in mobilization of intracellular arginine, we measured urease activity by performing the ammonia assay in liquid culture (Section 2.7.) using the Δ*car1* mutant. This strain allows us to determine urease ammonia which is produced only by utilizing enviromental urea; by comparing (substating) it from the ammonia concentration produced by the wt, which can convert enviromental urea and urea derived from arginine degradation. Comparing the Δ*car1* mutant with the wt strain, the concentration of ammonia in urea medium after 72h resulted in difference of almost 20 mM (wt: 52.5 mM; Δ*car1*: 34.2 mM). Therefore the Δ*car1* mutant produces only 65.14% of the ammonia (by using extracellular urea) than measured with the wt strain.

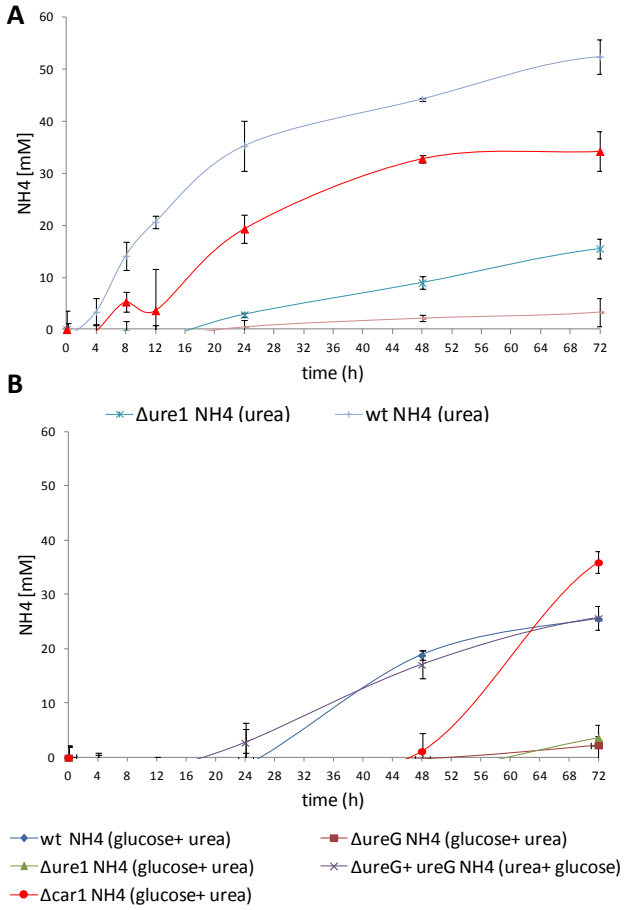

Figure 26. 2x 10^8 microconidia of the indicated strains were germinated for 14 h in 100 ml PDB. The germlings were transferred to 50 ml liquid MM media containing **(A)** 50 mM urea or **(B)** 50 mM urea with 3% glucose. Supernatants were taken to) determine the release of ammonia during the indicated time period of 72 hours. Mean values and standard errors were calculated from 3 biological repeats.

2.17. Arginase is not required for invasive growth on living plant tissue

Invasive growth of three independent Δ*car1* mutans on apple slices was similar to that of the wt strain, suggesting that Car1 has no role in this process.

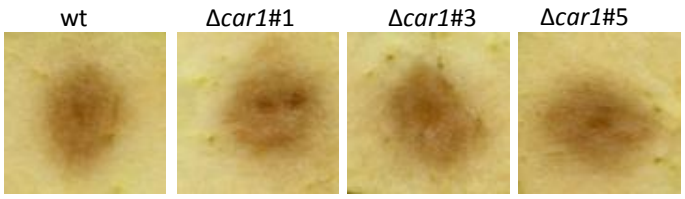

Figure 27. Car1 does not contribute to invasive growth on living fruit tissue. Apple slices were point-inoculated with 5x 10^4 microconidia of the indicated strains and incubated in a humid chamber at 28°C for 3 days. Experiments were performed three times, each with two technical repeats. Data shown are from one representative experiment.

2.18. Arginase contributes to virulence of *F. oxysporum* on tomato plants, *Galleria* and immunodepressed mice

In previous studies, arginase produced by the fungal pathogens *C. albicans* and *C. posadasii* was suggested to play a role in modulation of the innate immunite response by murine macrophages (Das et al., 2010; Ghosh et al., 2009; Mirbod-Donovan et al., 2006). Based on our finding that the *F. oxysporum car1* gene is highly expressed during *G. mellonella* infection (Figure 23), we set out to test the role of arginase during plant and animal infection. Arginase knockout mutants displayed significant reduced virulence on tomato plants (p = 0.0129; Figure 28A) and on *G. mellonella* (Δ*car1#1* (p = 0.0043), Δ*car1#3* (p = 0.0031), Δ*car1#5* (p = 0.0026); Figure 28B). Infection of immunodepressed mice showed a reduced virulence of the arginase mutant, however the drop in mortality was not statistical significant (p=0.3390; Figure 29).

It is important to note, however *G. mellonella* showed significant degrees of correlation with the mouse model (Navarro-Velasco et al., 2011), cases of discrepancy imply also major differences including body temperature or the lack of an adaptive immune system (Kavanagh and Reeves, 2004), which might contribute to the severity of the outcome.

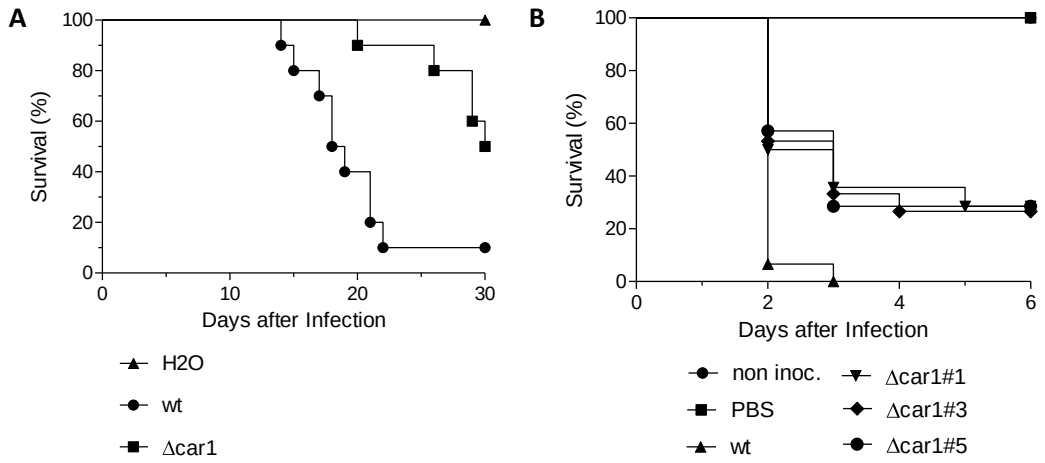

Figure 28. Δ*car1* mutants show attenuated virulence on tomato plants and in the *Galleria* infection model. (A) Two week-old tomato seedlings were inoculated with the indicated *F. oxysporum* strains by immersing the roots in a microconidial suspension, planted in vermiculite and incubated in a growth chamber at 28°C. Survival of plants was recorded daily. Mortality rate of plants infected with the Δ*car1*#3 mutant was significant lower (p = 0.0129) than those of plants infected with the wt. **(B)** *G. mellonella* larvae were inoculated by injection of 1.6 x 10^6 microconidia of the indicated *F. oxysporum* strains into the hemocoel and incubated at 30°C. Three independent arginase mutants Δ*car1#1* (p = 0.0043), Δ*car1#3* (p = 0.0031), Δ*car1#5* (p = 0.0026), caused significantly reduced mortality compared to the wt. Data shown are from one representative experiment with 15 larvae per treatment. Experiments were performed three times with similar results.

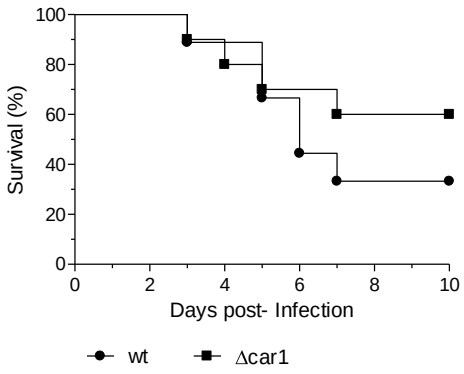

Figure 29. Car1 is required for full virulence on immunodepressed mice. Oncins France 1 male mice (n=10) were inoculated by tail vein injection with 2x10^6 microconidia of the indicated strains. Immunosuppressive treatment (a single intraperitonal dose of 150 mg cyclophosphamide per kg body weight and a single intravenous dose of 150 mg 5-fluorouracil) was applied one day prior to infection. Survival was recorded for 10 days. The Δ*car1* mutant caused a drop in mortality, however this value (p=0.3390) is not significantly different from the wt strain.

3. Discussion

3.1. *F. oxysporum FOXG_13832* encodes a conserved urease accessory protein G (UreG) essential for urease function

The process of urease activation by incorporation of nickel into the active site is a prime example of chaperone-mediated metal transfer to an enzyme. The maturation of Ni-urease includes metallocenter biosynthesis which requires the suite of accessory proteins for the proper incorporation of the nickel cofactor into the catalytic site. Urease accessory protein UreG belongs to the G3E family of P-loop GTPases (G3E family) (Leipe et al., 2002). Members of the G3E family perform two major functions in metallocenter assembly: the insertase role, i.e. energy-dependent incorporation of the cofactor into the catalytic site of the target protein, and the metallochaperone role, i.e. delivery of a metal cofactor to a target metalloprotein (Haas et al., 2009). As in other fungi *F. oxysporum* lacks a structural homologue of the bacterial nickel divalent cation chaperone UreE. However, UreG contains an additional histidine stretch at the C-terminus that allows it to combine the functions of bacterial UreE and UreG proteins, similar to UreG proteins in plant systems. Likewise, the structural urease protein of *F. oxysporum* contains the α-, β-, and γ-subunits of the bacterial urease fused into a single protein, as described before for other eukaryotic ureases (Follmer, 2008; Jabri et al., 1995).

A similar double role has also been proposed for HypB accessory proteins of the (Ni,Fe)-hydrogenase maturation system (Casalot and Rousset, 2001). Bacterial HypB proteins are important for activation of Ni-containing hydrogenases and are characterized by a conserved P-loop and the ability to bind nickel. In addition, some HypB proteins such as that from *Rhizobium lehuminosarum* also contain a His-rich stretch at the N-terminus (Rey et al., 1994). Both accessory proteins (UreG for urease and HypB for hydrogenase) belong to the G3E family of P-loop GTPases and are involved in the incorporation of the Ni cofactor to their enzyme (Leipe et al., 2002).

The deduced amino acid sequence of the *F. oxysporum FOXG_13832* gene shows a high degree of identity with bacterial, fungal and plant UreG proteins. *F. oxysporum* UreG contains a predicted P-loop motif (PROSITE accession number PDOC00017) characteristic proteins that bind ATP or GTP (Saraste et al., 1990). This glycine-rich region, which typically forms a flexible loop between a β-strand and a α-helix, consists of the consensus amino acid sequence GPVGSGKT, and interacts with one of the phosphate groups of the nucleotide (Freyermuth et al., 2000). The presence of the P-loop suggests an energy requirement for urease activation by *F. oxysporum* UreG.

The second role for UreG present as a poly-histidine stretch in its N-terminal was described to be involved in Ni^{2+} trafficking (Freyermuth et al., 2000; Witte, 2011).
In the fungal pathogen *C. neoformans* the nickel chaperone function of the urease depends on the orthologue of UreG (Singh et al., 2013). A mutant lacking *ureG* lacks urease activity due to a failure of nickel incorporation into the enzyme. The nickel binding activity of UreG was localized to the conserved histidine-rich domain, as shown by the complete absence of urease activity in a strain carrying an UreG version lacking the histidine-rich residues (Singh et al., 2013).
We found that the number of histidine residues at the N-terminal of UreG proteins varies in different organisms. In *F. oxysporum* UreG, 8 of the first 25 residues are histidines as in *F. verticillioides* and *A. nidulans*, compared to 7 in *F. graminearum* and none in the bacterium *K. aerogans*. By contrast, more histidine residues were found at the N-termini of UreG proteins of *N. crassa* (14), *M. oryzae* (9), *A. fumigatus* (9), *C. neoformans* (15), *S. pombe* (17) and *A. thaliana* (13). In *G. max* a very long His stretch (23 of the first 58 residues) has been reported (Real-Guerra et al., 2012), and UreG from *Anabaena variabilis* contains 29 histidines (Haas et al., 2009). A similar variation in the number of histinine residues involved in Ni^{2+} binding has been reported for COG0523 proteins, another member of the G3E family of P-loop GTPases (Haas et al., 2009). A comparison of the amino acid sequence of 887 COG0523 proteins from different kingdoms revealed that like UreG and HypB, COG0523 proteins can be present with

or without His-stretches, suggesting a patched distribution of insertase and metallochaperone activity among various members. Approximately 40% of the sequences analyzed contained a histidine-rich region, while the rest contained the minimal HxHxHxH motif, where x represents 0 - 4 residues (Haas et al., 2009).

In conclusion, structural analysis of *F. oxysporum* UreG suggests that the protein 1) contains all the conserved amino acid residues and domain architecture found in UreG orthologues from other fungi and plants; 2) may be responsible for providing energy for the urease reaction based on the presence of the conserved P-loop motif described for ATP-or GTP-binding proteins; 3) may be involved in Ni^{2+} trafficking essential for urease function by virtue of possessing a His-enriched C-terminus. These characteristics indicate that UreG might be an essential factor for a functional urease system. The results obtained from analysis from Δ*ureG* and Δ*ure1* mutants further corroborate this idea and will be discussed in the following section.

3.2. UreG and urease contribute to medium alkalinization via ammonia secretion

Urease catalyzes the hydrolysis of urea to yield ammonia and carbamate. The latter then spontaneously hydrolyzes to form carbonic acid and a second molecule of ammonia. At physiological pH, the carbonic acid proton dissociates and the ammonia molecules equilibrate with water to become protonated, resulting in increase in pH (Mobley et al., 1995). In our study we used several pH-dependent methods to measure urease activity, including a pH electrode (Bibby and Hukins, 1992) or colormetric assays using the pH indicator Bromocresol Purple. To detect urease activity, we adjust the ingredients of Christensen`s urea agar (Christensen, 1946) to the common MM used for *F. oxysporum.* A similar approach was described for *C. neoformans*, where Christensen`s urea agar was adjusted to the common minimal medium used for this fungus (Choi et al., 2012). Using this method, we detected medium alkalinization with the *F. oxysporum* wt strain but not with the

Δ*ureG* and Δ*ure1* mutant strains, indicative for a lack of urease activity. We further noted that, during growth on urea, the wt strain released ammonia into the medium. Ammonia secretion occurred concomitantly with the pH increase, suggesting that ammonia ions are responsible for medium alkalinization. Indeed, mutations in the *ure1* and *ureG* genes abolished both ammonium secretion and medium alkalinization. We therefore conclude that the extracellular alkalinization produced by *F. oxysporum* during growth in urea medium results from ammonia secretion and depends on a functional urease system.

An important finding was provided by the upregulation of *ureG* accessory protein expression upon glucose depletion, coinciding with the onset of ammonia secretion. In stark contrast, the *ure1* urease gene displayed a constantly low expression. This indicates that urease activity in *F. oxysporum* is not regulated at the level of urease gene expression, but might be controlled through expression and abundance of the accessory protein G. Similarly, in *A. thaliana* no transcriptional regulation by urea was observed for urease, arginase, ornithine carbamyl transferase, arginosuccinate synthetase, or arginosuccinate lyase. Interestingly, only the urease accessory protein UreG was upregulated in roots of urea-grown plants (Merigout et al., 2008).

Although *F. oxysporum* Δ*ure1* mutants are still able to grow on urea as the sole nitrogen source, they fail to alkalinize the medium indicative of a lack of urease activity. The same phenotype was observed when the accessory protein *ureG* was deleted, demonstrating that UreG is essential for a functional urease in *F. oxysporum*. In *C. neoformans* it has been shown that all accessory proteins are essential for urease activity, but in contrast to *F. oxysporum* the corresponding mutants failed to grow on medium containing urea as a sole nitrogen source (Singh et al., 2013). This implies there must be additional mechanisms in *F. oxysporum* for assimilation of urea via an urease-independent pathway (see discussion section 3.3.).

When the human pathogen *Coccoides immitis* was grown in sugar-free, nitrogen-containing medium, it released ammonia during the saprobic phase resulting in a significant increase in

pH (Bumb, 1925). Similarly, *C. posadasii* grown in an acidic, sugar free medium released ammonium ions and ammonia which increased the pH of its extracellular environment. Parasitic phase cultures of this pathogen also respond to acidification of their external environment by secretion of NH_4^+ and NH_3 (Cole, 1997).

The urease complex has been studied extensively in bacteria (Mobley et al., 1995) and plants (Torisky and Polacco, 1990; Witte et al., 2001; Witte and Medina-Escobar, 2001). Comparatively little is known about the role of urease in fungi. *Schizosaccharomyces pombe* was the first unicellular eukaryote for which the urease gene was reported as part of a complex involved in pH increase on urea medium (Tange and Niwa, 1997). The first urease gene cloned from a pathogenic fungus was that of *C. immitis* (Yu et al., 1997).

One striking observation was the formation of crystalline structures during growth of *F. oxysporum* in urea medium. These crystals were detected in the wt but not in Δ*ureG* and Δ*ure1* mutant, were strictly correlated with medium alkalinization and appeared initially after 48 h with abundance increasing over time. In humans, microbial urease activity has been linked to urolithiasis (stone formation), and an estimated 15-20% of urinary stones are thought to be a consequence of a bacterial infection of the urinary tract leading to an increase in the pH of urine. The most common bacteria responsible for these infections are *Proteus mirabilis* or *Ureaplasma urealyticum*, but other genera such as *Pseudomonas*, *Klebsiella* or *Staphylococcus* are also implicated (Burne and Chen, 2000; Rosenstein and Hamilton-Miller, 1984). High concentrations (0.5M) of ammonia in urine as a result of urease-mediated urea hydrolysis results in a pH increase and in precipitation of the normally soluble polyvalent ions present in urine, the two primary compounds formed being struvite ($MgNH_4PO4 \times 6H_2O$) and apatite [$Ca_{10}(PO_4)_6 \times CO_3$] (Mobley et al., 1995). Interestingly, mice infected with *P. mirabilis* tended to develop urolithiasis. While struvite stones were observed frequently in mice infected with the wt strain, but were never found in those infected with an urease mutant (Johnson et al., 1993; Jones et al., 1990).

Based on these previous results, we suggest that the crystal structures detected in the *F. oxysporum* cultures resulted from the precipitation of normally soluble polyvalent ions, as described for urolithiasis. Precipitation of the excess ammonium as struvite crystals could explain the constant ammonia concentration and stable pH detected in urea cultures after 72h. To our knowledge this is the first evidence showing that a fungus can cause ammonia precipitation and the development of struvite structures in culture.

We never observed the crystal structures in cultures of Δ*ureG* or Δ*ure1* mutants, which were unable to increase the medium pH on urea above 7. Strikingly, these two mutants developed high amounts of chlamydospores, thick-walled survival structures arising from hyphal or conidial cells. Chlamydospores in *F. oxysporum* are generally induced during aging or under unfavorable environmental conditions such as low temperatures or carbon starvation, and represent the main structures for long-time survival during long time periods in the soil (Couteaudier and Alabouvette, 1990; Kono et al., 1995; Nelson, 1981b; Schippers, 1981b; Stevenson and Becker, 1972).

Taken together, these results demonstrate that: 1) *F. oxysporum* produces urease activity which leads to alkalinization of the extracellular medium in the presence of urea; 2) environmental alkalinization correlates with and is caused by ammonia secretion, 3) urea medium alkalinization by the fungus leads to precipitation of normally soluble polyvalent ions and formation of struvite crystals; and 4) lack of a functional urease causes symptoms of nutrient starvation *in F. oxysporum* as detected by the development of chlamydospores.

3.3. *F. oxysporum* can use urease-independent pathways for urea utilization and environmental alkalinization

Somewhat unexpectedly, *F. oxysporum* Δ*ure1* and Δ*ureG* mutants displayed only partially impaired growth on urea as the sole nitrogen and carbon source: Thus, while these genes are important in urea utilization, there must be additional mechanisms in *F. oxysporum* for

assimilation of urea via an urease-independent pathway. It is known that the *Hemiascomycetes* (yeasts and yeast-like fungi, the majority belonging to the class *Saccharomycetes*) use an alternative urease-independent pathway to convert urea, ATP and bicarbonate into ammonia and carbon dioxide (Navarathna et al., 2010). In *S. cerevisiae* and *C. albicans*, for example, urea is metabolised by the enzyme urea amidolyase (Dur1, 2; Degradation of URea), a cytoplasmic, biotin-dependent enzyme (Roon et al., 1972) with two enzymatic functions: urea is first carboxylated to allophanate in an ATP-dependent reaction by urea carboxylase, and allophanate is then hydrolysed to ammonia and carbon dioxide by allophanate hydrolase (Altschul et al., 1997; Carter et al., 2009; Labadorf et al., 2010). Indeed, analysis of the genome sequence revealed that *F. oxysporum* contains both the urease and the urea amidolyase system, as reported for most *Sordariomycetes* except *N. crassa* (Strope et al., 2011). We thus speculate that the urea amidolyase allows *F. oxysporum* to utilize urea as a nitrogen source in the absence of urease, as in the case of the Δ*ure1* and Δ*ureG* mutants. A possible explanation of the strong delay of ammonia by the mutants in urea medium is that urease-mediated one-step urea breakdown is simpler and therefore faster than the energy-consuming, biotin-dependent urea amidolyase system which requires a two-step mechanism. A second possible cause for the low amount of ammonia secreted by the urease mutants could be the lack of sufficient biotin in the medium. *C. albicans* strains, for example, are biotin auxotrophis (Odds, 1988). Moreover, high amounts biotin are required for optimum growth of *S. cerevisiae* on urea, allantonic acid or allantoin as the sole nitrogen sources (Di Carlo et al., 1953).

Interestingly two other plant pathogens, *F. graminearum* and *M. oryzae* also have both the urease and the urea amidolyase systems. This raises the question why plant pathogens possess two distinct enzymes to convert urea, if plants recycle virtually all of their amino groups and thus do not excrete urea, and suggests a possible role of urease in virulence.

Another member of the G3E family of P-loop GTPases, the COG0523 proteins, have been implicated in the virulence of several fungal pathogens whose hosts are known to induce Zn-limitation (Haas et al., 2009). This concept is based on nutritional immunity as a defense strategy against invading pathogens (Kochan, 1973), where the host organism actively

deprives metals from the invaders inducing both hypoferremia and hypozincemia (deficiency of iron and zinc, respectively, in the blood) as part of the acute inflammatory response (Liuzzi et al., 2005; Motley et al., 2004; Weinberg, 1975). Therefore, the mechanisms that enable a pathogen to overcome this host-induced Zn-starvation are considered essential to a pathogen's ability to cause infection (Kim et al., 2004; Panina et al., 2003; Pasquali et al., 2008).

In a putative scenario of nickel deprivation within the host, it might be a selective advantage for the pathogen to retain two pathways of urea degradation and ammonia secretion. The use of urea amidolyase Dur1,2 would allow *F. oxysporum* to overcome the nickel-dependent function of the urease Ure1. It has been suggested that the use of urea amidolyase allows hemiascomyces such as *C. albicans* to achieve urea degradation and kidney colonization in the nickel—deficient host environment (Navarathna et al., 2010).

In *C. neoformans* which lacks urea amidolyase, mutation of components of the urease, its accessory proteins or the nickel transporter Nic1 leads to absence of urease activity and the lack of ammonia (Singh et al., 2013). By contrast, urease deletion mutants of *C. posadasii* which also lacks the urea amidolyase system (Strope et al., 2011), cause only a partial reduction in ammonia secretion (Wise et al., 2013). Interestingly, an additional pathway for production of ammonia was recently described in this fungal human pathogen, namely the allantoin degradation pathway which is conserved in filamentous fungi, yeast, bacteria and higher plants but absent in mammals. The allantoin degradation pathway converts allantoin to ammonia and carbon dioxide, allowing the use of allantoin as the sole nitrogen source. Conversion of allantoin to ammonia in *S. cerevisiae* is carried out by the *DAL1*, *DAL2*, and *DAL3* gene products, which work sequentially to generate urea (Yoo et al., 1985). Urea is then degraded to ammonia in a two-step process by the *DUR1,2* protein. Alternatively, the ureidoglycolate hydrolase (Ugh; EC 3.5.3.19) performs the terminal step of allantoin catabolism by catalyzing the hydrolysis of ureidoglycolate to glyoxylate, releasing CO_2 and ammonia. In *C. posadasii* the the Δ*ugh*/Δ*ure* double mutant shows a significant reduction of extracellular ammonia in the culture medium compared with the wt and the Δ*ure* strains, correlating with reduced virulence (Wise et al., 2013). Since the *F. oxysporum* genome

contains a predicted protein (GenBank accession number EGU87042) with 56% identity to Ugh of *C. posadasii*, further investigation of the role of this enzyme should provide interesting information about the function of ammonia secretion during virulence of *F. oxysporum*.

In summary, we conclude that 1) *F. oxysporum* has urease-independent mechanisms for the utilization of urea, probably provided by urea amidolyase; and 2) *F. oxysporum* encodes a putative a putative ureidoglycolate hydrolase which represents a potential mechanism contributing to ammonia secretion independently of urease.

3.4. Extracellular alkalinization by ammonia secretion is triggered by carbon deprivation and regulated through carbon-catabolite/glucose repression

When *F. oxysporum* was grown in urea in the presence of glucose, ammonium secretion and medium alkalinization was strongly delayed compared to urea alone, and was only initiated when glucose was depleted from the medium. This effect was not detected with the non-fermentable carbon sources galactose and glycerol, suggesting that repression of ammonia secretion and medium alkalinization is specific for glucose. These results suggest that urease-dependent ammonia secretion and medium alkalinization is controlled by a glucose repression mechanism. Glucose or carbon catabolite repression is a known mechanism in fungi, whereby the presence of a preferred carbon source, often glucose, triggers a signalling cascade that prevents the utilization of non-preferred carbon sources as well as the function of different catabolic routes and other cellular processes (Johnston, 1999; Rolland et al., 2002; Zaman et al., 2008). Among pathways that control the cellular response to glucose levels in *S. cerevisiae* are the Ras2-cAMP protein kinase A (PKA) pathway (Thevelein and Voordeckers, 2009); the glucose induction pathway which involves the membrane receptors and glucose sensors Snf3 and Rgt2 (Ozcan and Johnston, 1999) and the transcription factor Rgt1; and the glucose repression pathway mediated by the nutrient-sensing AMP-dependent

kinase (AMPK) Snf1 (sucrose non-fermenting 1) and the transcription factor Mig1 (for review see (Carlson, 1999; Forsberg and Ljungdahl, 2001; Rolland et al., 2002; Santangelo, 2006).

To further examine the hypothesis that urease-mediated environmental alkalinization is glucose repressed, we tested the available *F. oxysporum* Δ*snf1* and Δ*hxk1* (hexokinase 1) mutants, two genes with a possible role in glucose metabolism. The roles of these two proteins have been studied in detail in *S. cerevisiae*. The hexokinase Hxk2 phosphorylates glucose to glucose 6-phosphate allowing it to enter glycolysis and carbon metabolism. Hxk2 also plays a role in carbon catabolite repression mediated by the transcriptional repressor Mig1 (Zimmermann and Scheel, 1977). Hxk2 interacts with Mig1 to generate a repressor complex located in the nucleus of *S. cerevisiae* (Moreno et al., 2005) and interacts with Snf1 (Ahuatzi et al., 2007) causing its inhibition in high glucose growth condition (Tomas-Cobos and Sanz, 2002).

High glucose levels in the cell lead to inactivation of the Snf1 complex, thereby inhibiting Snf1-mediated phosphorylation and nuclear export of the Mig1. Thus, Mig1 remains in the nucleus, preventing expression of carbon catabolite repressed genes. At low intracellular glucose concentrations Snf1 becomes activated and phosphorylates Mig1, which is translocated to the cytosol thereby releasing glucose repression (Christensen et al., 2009). Besides activation of glucose-repressed genes, the Snf1 pathway in *S. cerevisiae* also regulates the response to environmental stresses such as alkaline pH, where Snf1 is phosphorylated and required for growth under these conditions (Hong and Carlson, 2007). It has been shown previously that a *F. oxysporum* Δ*snf1* mutant displayed reduced expression of several genes encoding cell wall-degrading enzymes, poor growth on non-preferred carbon sources and a delay in wilt symptoms on plants (Ospina-Giraldo et al., 2003).

If hexokinase acted as the only key enzyme in *F. oxysporum* to channel glucose into glycolysis, the Δ*hxk1* mutant should be affected in glucose utilization as well as in glucose repression of ammonia release and medium alkalinization. However, we found that Δ*hxk1* was still able to deplete glucose from the medium and showed a similar delay in ammonia secretion and alkalinization of urea medium as the wild type strain. This result suggest the presence of additional hexokinases or glucokinases in *F. oxysporum* which are able to phosphorylate

glucose and are in line with previous findings in our group revealing normal growth of the Δ*hxk1* mutant on glucose and other fermentable hexoses, even though the mutant displayed significantly reduced virulence on tomato plants (Gonzalez-Garcia et al., unpublished).

In our experiments we only detected ammonia secretion in absence of glucose. If glucose repression of ammonia secretion and alkalinization in *F. oxysporum* was controlled through the Snf1 complex, the Δ*snf1* mutant should have a defect in activation of these processes after glucose depletion. However, we found the opposite outcome, namely a reduced glucose repression in the Δ*snf1* mutant, as detected by an onset of ammonia secretion before complete glucose depletion. Moreover, the Δ*snf1* mutant secreted significantly more ammonia than the wt, reaching a concentration which was double that secreted by the wt strain. This result argues against a key role of Snf1 in promoting ammonia secretion after glucose depletion in *F. oxysporum*. However we cannot yet exclude a role of glucose sensing and carbon catabolite repression in this process. In *S*. *cerevisiae* Mig2, a functional homolog of Mig1 (Lutfiyya and Johnston, 1996), represses the transcription of genes involved in metabolism of poor carbon sources under high glucose conditions, but is not regulated by Snf1 (Lutfiyya et al., 1998; Treitel and Carlson, 1995). Moreover, it has been suggested that the mechanisms mediating carbon catabolite by the Mig1 orthologue in filamentous ascomycetes, CreA, are somewhat distinct from those reported in *S. cerevisiae* (Vautard et al., 1999).

The observed initial medium acidification by *F. oxysporum* in the presence of glucose could be related to the breakdown of glucose, a well known effect of the glycolysis. In *C. albicans*, for example, alkalinization of acidic medium, associated with the release of ammonia has been described as a glucose-reversible phenomenon (Vylkova et al., 2011). The mechanism of this effect was explained by a model based on the utilization of amino acids as the primary source of carbon (Figure 1). Under carbon-rich conditions, nitrogen is generally stored in the form of glutamate or glutamine. However, under carbon-starved conditions the amino acids are used as a carbon source. Amino acids are catabolized through several routes and converted into tricarboxylic acid (TCA) cycle intermediates, resulting in acetyl-CoA, succinyl-CoA, α-ketogluterate or oxyloacetate forming glutamate. Each product includes de-

amination steps to remove the amino group (s). This process involves transaminases. In many vertebrates, the amino group is then feet into the urea cycle and the excess nitrogen is excreted in the form of urea. Fungi are able to convert urea into ammonia and CO_2 by urease or urea amidolyase (Dur1,2). Since high concentrations of cytosolic ammonia are toxic (Hess et al., 2006), the excretion of the excess ammonia would detoxify the cytosol and raise extracellular pH.

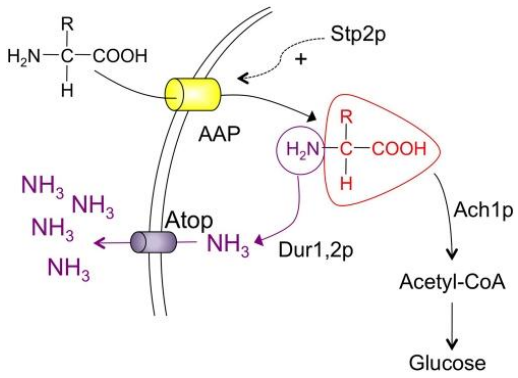

Figure 1. Model of environmental alkalinization by *C. albicans*. Under conditions in which amino acids are metabolized as carbon sources, the cell upregulates transmembrane transporters for various amino acids (facilitated by the Stp2p transcription factor). Amino acids are converted into tricarboxylic acid (TCA) cycle intermediates via several routes. Many of these require acetyl-CoA production and intracellular transport mediated by acetyl-CoA hydrolase (Ach1p). Degradation of amino acids often involves deamination of the amino group to alpha-ketoglutarate, forming glutamate. This amino group is then removed through the urea cycle and is excreted in the form of urea. In mammals, excess nitrogen is secreted as urea, whereas in *C. albicans,* urea is converted by urea amidolyase (Dur1,2) into CO_2 and ammonia. The latter is exported from the cell in a process involving the Ato proteins (Figure taken from (Vylkova et al., 2011)).

In *C. albicans,* extracellular alkalinization requires carbon deprivation and exogenous amino acids (Vylkova et al., 2011), a condition encountered inside phagocytic cells. It has been suggested that extracellular pH provides a morphogenetic signal which stimulates the filamentous hyphal form essential for virulence in this fungus (Biswas et al., 2007). The transcription factors Rim101/PacC and Mnl1 are required for the alkaline pH response (Davis, 2003). Interestingly, however, the alkalinization observed in *C. albicans* in the absence of carbon is independent of the Rim101/PacC pH response pathway. This suggests that this phenomenon is independent of this pH adaptation machinery (Vylkova et al., 2011).

It is possible that the mechanism controlling extracellular alkalinization in *F. oxysporum* is linked with carbon metabolism and amino acid catabolism as described for *C. albicans* (Vylkova et al., 2011). This would imply that environmental alkalinization by the fungus is a

side effect of ammonia secretion to avoid cell toxicity through the high cytosolic ammonia concentration associated with low glucose levels. This idea is further supported by our results showing that high concentrations of ammonia are secreted during growth on casaminoacids in the absence, but not in the presence of glucose, suggesting that under glucose starvation the amino acids are used as a carbon source, leading to a secretion of the excess ammonia.

Further supporting this hypothesis are studies in the bacterium *H. pylori* where ammonium generated from urea was shown to be incorporated into amino acids (Williams et al., 1996). Interestingly, the UreA subunit of the urease complex in this species was found to interact with glutamine synthetase (GlnA) (Stingl et al., 2008), the enzyme that catalyzes the synthesis of glutamine from glutamate and NH_4^+ in the presence of ATP. Glutamine is necessary for several essential metabolic pathways, such as synthesis of purine, pyrimidine, peptidoglycan and amino acids (Reitzer, 1996). It has been suggested that the direct physical interaction of glutamine synthetase with UreA may allow the urease product ammonium to be directly incorporated into glutamine through the action of GlnA (Stingl et al., 2008).

Research in plant metabolism showed that the concentration of many amino acids were significantly lower when rice plants were supplied with urea, possibly due to the limited availability of carbon skeletons for amino acid biosynthesis (Cao et al., 2010). This is supported by an increase in the concentration of asparagine in the presence of urea, since the expression of asparagine synthetase has been associated with carbon starvation in plants (Lea, 2007).

In conclusion, we note that 1) urease activity in *F. oxysporum* under the conditions studied is controlled in a rate-limiting fashion by the abundance of the accessory protein UreG; 2) urease-derived ammonia secretion is specifically repressed in the presence of glucose; 3) the protein kinase Snf1 is not required for activation of ammonia secretion upon relief from glucose repression; 4) amino acids are used as a primary carbon source during glucose starvation, and therefore environmental alkalinization may be part of a detoxification mechanism for the excess ammonia resulting from the utilization of amino acids as a source of carbon

3.5. Glucose repression of urease-dependent medium alkalizing is linked to nitrogen metabolite repression

The mutant strains Δ*meab* (FOXG_02277), Δ*mep*B (FOXG_00462) and Δ*areA* (FOXG_03165) failed to show glucose repression of the increase in pH and ammonia secretion. The decrease of glucose concentration in these mutants was similar to the wt strain, excluding the hypothesis that they cannot uptake or use glucose. Interestingly, on casaminoacids the mutants showed the same glucose repression as the wt, suggesting that this phenotype is specific for urea.

The genes affected in the three mutants are involved in different aspects of nitrogen metabolite repression (NMR). In fungi, NMR ensures that genes required for the utilization of alternative nitrogen sources are only transcribed in the absence of preferred sources such as ammonium or glutamine (Arst and Cove, 1973; Marzluf, 1997). This process requires the GATA factor AreA/Nit-2. Loss of *areA* in *A. nidulans* or *nit-2* in *N. crassa* renders these species incapable of utilizing nitrogen sources other than ammonium or glutamine (Arst and Cove, 1973; Fu and Marzluf, 1987; Kudla et al., 1990; Marzluf, 1997; Stewart and Vollmer, 1986). In *F. oxysporum* the GATA factor AreA is strictly required for de-repression of NMR genes (Lopez-Berges et al., 2010). One example is the ammonium permease gene *mepB*, which is strongly downregulated on ammonium by nitrogen catabolite repression, dependent on the bZIP protein MeaB. Thus, a Δ*meaB* mutant displays nitrogen source-independent activation of NMR genes and of certain virulence functions (Lopez-Berges et al., 2010). In non-alkalinizing *C. albicans* cells growing in the presence of high glucose condition the genes for two ammonia permeases (*Mep1* and *Mep2*), were significantly induced compared to glucose starvation conditions, suggesting a possible role of ammonium uptake during these conditions- However, the corresponding gene deletion mutants were not impaired in environmental medium alkalinization (Vylkova et al., 2011).

One possible explanation for our results is that urease activity might be controlled by a nitrogen metabolite repression mechanism, based on a model where MeaB acts upstream of AreA, mediating its negative regulation through the uptake of ammonia. In the presence of

the preferred nitrogen source ammonia, and AreA represses NMR genes including *mepB* itself (Lopez-Berges et al., 2010). Recently it was been confirmed in *F. oxysporum* that a Δ*areA* mutant shows reduced growth on non-preferred nitrogen sources (Lopez-Berges et al., 2010), including urea (Lopez-Berges et al., 2014).

Since urea acts as a non-preferred nitrogen source, in our assays AreA is releasing NMR. The *ureG* gene encoding the urease accessory protein might be under the control of NMR, with a direct effect on urease activation. This idea is supported by quantitative real-time PCR revealing an increase in expression of *ureG* under glucose depletion conditions as well as by the fact that Δ*areA* displayed reduced ammonia secretion in urea medium whereas Δ*mepB* behaved as the wt. A link between urease and NMR has been described in *A. nidulans,* who can use urea as a nitrogen source (Darlington et al., 1965; Scazzocchio and Darlington, 1968). The transcription of a specific urea transporter (UreA) was not inducible by urea, strongly repressed by ammonium and required AreA (Abreu et al., 2010). Further expression studies in the presence of absence of ammonium are needed to corroborate the hypothesis that *F. oxysporum ureG* is controlled by NMR.

Interestingly, in the tomato pathogen *Colletotrichum coccodes* nitrogen metabolism associated with AreA is linked to alkalinization (Alkan et al., 2008). Δ*areA* mutants showed severely ammonia secretion and reduced decay development likely due to impaired utilization of external nonreduced nitrogen sources (Marzluf, 1997). In this fungal pathogen both the environmental pH and nitrogen availability are major regulators of ammonification (Alkan et al., 2008).

It has been reported that AreA is not only controlled by nitrogen source, but also by carbon starvation. In *A. nidulans* AreA is rapidly inactivated in response to carbon starvation and genes dependent on AreA, such as those involved in nitrogen source utilization, are not induced under nitrogen starvation in the absence of a carbon source (Fraser et al., 2001). This event was described for the enzyme formamidase (formamide amidohydrolase, EC 2.5.1.49), which mediates the highly specific hydrolysis of formamide to produce formate and ammonia (Hynes, 1975a). Like urea, formate is a single carbon molecule, and hence

formamide can only serve only as a nitrogen source and not as a carbon source for *Aspergillus* spp.

Therefore we propose the following scenario in our assays. Urea is sensed as a poor nitrogen source leading to the expression of AreA-repressed NMR genes. On the other hand, lack of a carbon source would lead to AreA inactivation and lack of de-repression of NMR genes. Reduced expression in response to carbon starvation described for formamidase (Fraser et al., 2001; Hynes, 1972) has also been observed for other NMR enzymes such as nitrate reductase (Hynes, 1973). This has been suggested a specific effect on NMR genes, rather than a general effect of carbon starvation on gene expression, since carbon starvation leads to increased levels of acetamidase activity even in AreA mutants and relieves ammonia repression (Hynes, 1972; Hynes, 1975b).

AreA is essential for transcriptional activation of NMR genes involved in the utilization of nitrogen sources, irrespective of the carbon source present. By contrast, in the case of compounds that can serve as both nitrogen and carbon sources, AreA is only required for gene expression under conditions of carbon catabolite repression (Arst, 1985; Arst and Cove, 1973; Davis et al., 1993; Gonzalez et al., 1997). This control allows the organism to utilize a given compound as a nitrogen source in the presence of a preferred carbon source, but as a carbon source in the presence of a preferred nitrogen source. For example, the set of genes involved in proline utilization in *A. nidulans* is repressed only when both ammonium and glucose are present, but not in the presence of either glucose or ammonium alone (Arst, 1980; Arst and Cove, 1973; Gonzalez et al., 1997). Thus, in the wt repression of the proline transporter PrnB requires the presence of both glucose and ammonia, whereas in the Δ*areA* mutant the presence of glucose is sufficient for repression. But it has been suggested that in this mutant ammonia has an additional repressive activity, likely due to a direct effect of ammonium on the transporter which is not mediated by AreA (Valdez-Taubas et al., 2004).

Because urea has a single carbon molecule, we assume that it can be used by *F. oxysporum* only as a nitrogen source. According to the above, AreA would be required for transcriptional activation of the urease system irrespective of the carbon source present. Therefore we have less activity in the Δ*areA* mutant in glucose lacking urea media. However this conclusion is in

contradiction with the subsequent ammonia secretion of Δ*areA* in glucose rich urea medium suggestive for a different regulation mechanism in *F. oxysporum.*

Here we found a higher expression of *ureG* than of *ure1* when *F. oxysporum* was grown on urea medium, suggesting that urease activity may be controlled by transcriptional levels of the accessory protein UreG. However, urease might be regulated differently in other organisms. In certain plant systems total urease activity is not influenced by urea or other external nitrogen sources, including rice (Cao et al., 2010), potato (Witte et al., 2002) and several other plants (Gerendas J., 1999a). In the bacterium *K. aerogenes* urease activity is expressed under conditions of low nitrogen availability and subject to regulation by the global nitrogen regulatory system (Magasanik, 1988). In *S. pombe* urease expression is neither subject to nitrogen repression nor to urea induction (Lubbers et al., 1996). In *C. neoformans,* however, urease activity is regulated by transcriptional activation of the structural urease gene in urea medium (Singh et al., 2013). *C. neoformans* presents an anomaly from the archetypical NMR mechanism because the AreA orthologue is also required for utilization of the preferred nitrogen source ammonium. The biological relevance of this mechanism in nitrogen metabolism in *C. neoformans* may be linked to the primary ecological niche of this fungus, nutrient-rich pigeon guano, where 70% of the nitrogen is present in form of uric acid (Staib et al., 1978; Staib et al., 1976), and nitrogen availability becomes scarce upon infection of humans. Beyond the differences in nitrogen availability encountered by *C. neoformans* during its infection cycle, there is additional evidence supporting a role of nitrogen metabolism in virulence. For example, the virulence factor urease is implicated in nitrogen-scavenging and invasion of the central nervous system (Cox et al., 2000; Olszewski et al., 2004; Shi et al., 2010).

Our results support the following scenario:

During growth on urea + glucose, the ammonia produced from the urease is secreted, but is taken up at a similar rate by the permease MepB (therefore no increase of the ammonia in the medium is detected). MepB is expressed, because urea is a non-preferred nitrogen source. It was previously shown that *mepB* expression on non-preferred nitrogen sources requires the bZIP factor MeaB and the GATA factor AreA (Lopez-Berges et al. 2010). Thus a

common phenotype of the Δ*meab*, Δ*mep*B and Δ*areA* mutants is the lack of MeaB protein during growth on non-preferred nitrogen sources including urea. Therefore, ammonia is produced and secreted, but not taken up by these mutants, and it accumulates rapidly in the medium increasing the pH.

As soon as glucose becomes depleted in the wt no more ammonium is taken up by MepB, and therefore it accumulates extracellularly, increasing the pH. The mechanism for this could be either that a) MepB is inactivated or recycled from the plasma membrane in the absence of glucose by an unknown mechanism, and/or b) the inactivation of AreA in the absence of glucose prevents expression of the *mepB* gene, and therefore MepB becomes depleted from the membrane.

3.6. Urease is not secreted in *F. oxysporum*

Urease activity in *F. oxysporum* was determined using a pH-dependent indicator on solid medium or ammonia measurements in culture supernatants. Both methods measure extracellular conditions and therefore fail to indicate whether urease activity functions intra- or extracellularly. The absence of detectable transcripts of the putative urea transporter gene *dur3* led us to hypothesize that urease activity could be extracellular, thereby transforming urea in ammonia outside of the cell.

Although urease protein lacks a detectable signal peptide, different mechanisms have been described how urease can become located extracellularly. In *H. pylori*, urease enzymatic activity was detected on the cell surface (Dunn et al., 1997; Phadnis et al., 1996). The postulated mechanism of urease release is that cells undergo spontaneous autolysis, followed by adsorption of the enzymatically active enzyme to the surface of intact viable bacteria (Dunn and Phadnis, 1998). A similar mechanism has been suggested for the fungal pathogen *C. posadasii*. During the parasitic cycle the cells rupture and release their contents, including active urease which subsequently associates with the surface of intact endospores and the membranous outer wall fraction (Hung et al., 2000; Hung et al., 2002). In *C.*

neoformans, urease activity was identified in polysaccharide-containing vesicles (Rodrigues et al., 2008). These vesicles appeared to be associated with the Golgi apparatus-derived secretory pathway (Yoneda and Doering, 2006), and expected to fuse with the plasma membrane to release their contents to the extracellular space (Ponnambalam and Baldwin, 2003). Interestingly, vesicle production was observed during macrophage infection, suggesting that *C. neoformans* uses vesicular secretion as a mechanism to deliver virulence factors such as urease to the extracellular space (Rodrigues et al., 2007).

To test whether urease in *F. oxysporum* functions intra- and/or extracellularly, we compared urease activity in the culture supernatants to that in cell protein extracts. Ammonia production from urea was detected exclusively in the cell extract. We were unable to detect any urease activity in the culture supernatans. This result strongly suggests that urease is not secreted by *F. oxysporum* under the tested conditions. However, we cannot exclude that under certain conditions urease might function extracellularly or membrane associated as prevoiusly reported for *H. pylori* (Dunn et al., 1997; Phadnis et al., 1996) and *C. posadasii* (Hung et al., 2000; Hung et al., 2002).

One explanation for the lack of expression of the putative urea transporter Dur3 might be that *F. oxysporum* contains additional proteins that transport urea. Alternatively, urea uptake might not need an active transporter. *A. thaliana,* for example, has the high affinity secondary urea transporter Dur3 but also uses passive urea transport mediated by aquaporins, which conduct selected low molecular solutes through a channel along a concentration gradient (Witte, 2011).

In conclusion we propose that 1) the urease enzyme in *F. oxysporum* is not secreted, although it cannot be excluded that urease might become membrane-associated or extracellular under certain conditions; 2) urea uptake and intracellular transport does not require transcriptional activation of the predicted urea transporter Dur3; 3) additional urea transporters or passive transport mechanisms may play a role in urea uptake of *F. oxysporum*.

3.7. UreG and urease contribute to virulence on tomato plants

Functional studies on the role of urease in fungal virulence are largely restricted to the human pathogens *C. neoformans* (Cox et al., 2000) and *C. immitis* (Cole, 1997). Although genome annotation revealed the presence of urease in plant pathogenic fungi (Strope et al., 2011) little is known about their activation and regulation, and to our knowledge the role of fungal urease during plant infection has not been studied before.

Here we demonstrate that *F. oxysporum* mutants lacking *ureG* or *ure1* display loss of urease activity and reduced virulence on tomato plants. Neither of the mutants was affected in cellophane penetration under standard assay conditions (Lopez-Berges et al., 2010; Prados Rosales and Di Pietro, 2008), suggesting that the role of urease may be associated to infection inside the host rather than to impaired ability of root penetration.

Since urease activity is required for secretion of ammonia and medium alkalinization on urea we speculate that this process might be of relevance during plant infection. A role of ammonia secretion and pH modulation in virulence has been demonstrated for *Colletotrichum* spp. (Prusky et al., 2001). This phytopathogen uses local secretion of ammonia into the host tissue to increase the pH of the host tissue. This ammonification is regulated by the ambient acidic pH and nitrogen availability (Alkan et al., 2008). The resulting alkalinization modulates expression of pathogenicity genes and the activity of secreted cell wall-degrading enzymes like pectate lyase that contributes to virulence (Kramer-Haimovich et al., 2006; Yakoby et al., 2001). Thus, local alkalinization as a result of ammonia increase contributes to virulence by initiating virulence gene expression and at the same time provides the milieu necessary for optimal fungal growth (Prusky et al., 2001).

Previous results in our group demonstrated that the ability of *F. oxysporum* to infect tomato plants is influenced by pH. Infected tomato plants watered at pH 5 developed significantly less mortality than plants watered at pH 7. Moreover, *F. oxysporum* can cause alkalinization in the presence of tomato roots (Segorbe et al., unpublished).

pH is an important rhizosphere property. Plant roots can acidify the rhizosphere by up to two pH units compared to the surrounding soil through the release of protons, bicarbonate,

organic acids and CO_2 (Atwell, 1999). The distinct rhizosphere pH has a major impact on the thin layer of intense biological activity in close proximity to the roots. In addition to proton fluxes, release of CO_2 by respiring roots and microbes is likely to cause strong acidification of the rhizosphere, especially near root apices where respiration is most rapid (Atwell, 1999). Since *F. oxysporum* is a soil-borne pathogen initiating infection through the plant roots, it is important to note that urea is the most widely used nitrogen fertilizer in agriculture on a global scale (http://faostat.fao.org). It is therefore likely that in agricultural settings the presence of high concentrations of urea in the soil could provide the substrate for this urease-producing fungus to secrete ammonia and produce extracellular alkalinization.

While the urea substrate is likely present at high concentrations in the soil, once the fungus invades the plant tissue it is confronted with a totally different nutritional environment. To examine the role of urease during plant infection of *F. oxysporum*, knowledge on the availability of the substrate urea in plants is essential. It is generally assumed that plants mainly take up ammonium and nitrate as nitrogen sources, which are generated by microbial conversion of urea in the soil. However, plants also possess an urea transporter and are able to hydrolyze urea and use it as a nitrogen source (Witte, 2011). In addition, plant cells can recycle nitrogen from urea that originates from arginase-catalyzed breakdown of arginine (Zonia et al., 1995). Inside the mitochondria, arginine is degraded by arginase into the ornithine and urea (Polacco, 1993b). Urea is then exported to the cytoplasm and hydrolyzed by urease. Additionally urea accumulates in source leaves of older plants and in germinating seeds (Zonia et al., 1995). Currently, arginine catabolism is the only confirmed source of urea in plants (Witte, 2011).

Although in *A. thaliana* urea is principally metabolized in the roots, around 20% is translocated to the aerial parts before hydrolysis by cytoplasmic ureases (Merigout et al., 2008). Large amounts of urea were found in shoots of rice plants grown on urea (Gerendas J., 1998), suggesting a transport of urea molecules from the roots to the aerial parts of the plant. Thus, although the concentration of urea in plants is generally low (0.2- 0.9mM in Arabidopsis and rice (Cao et al., 2010; Merigout et al., 2008)) it could be used as a substrate by the fungal urease to generate ammonium that could be either used for metabolism or, in

the absence of a fermentable carbon source, secreted to cause alkalinization of the extracellular medium.

In plants, assimilation of carbon and nitrogen sources and their subsequent distribution are closely linked. The plant can be viewed as a coordinated network of assimilatory regions (sources) and regions of resource utilization (sinks), and the vascular system provides a path for transport of assimilates from source to sink (Atwell, 1999). In vascular plants, it is the phloem that carries the transport sap, a water-based solution rich in sugars particularly sucrose and glucose, which is produced mainly in the leaves where the majority of photosynthesis takes place, to the non-photosynthetic parts of the plant such as the roots, or to storage structures such as tubers or bulbs (Lalonde et al., 2004).

Polacco and Holland suggested that wounding or infection of the immature plant embryo can lead to release of arginase from affected mitochondria, resulting in massive arginine degradation and formation of large amounts of urea. Subsequently urea hydrolysis by urease and production of ammonia could have a toxic effect upon herbivores and pathogens, contributing to plant defense (Polacco, 1993b). It is conceivable that pathogens like *F. oxysporum* can avoid the toxic effect of urea via hydrolysis by urease, and use the produced ammonia to support infection through an increase of the environmental pH. A similar strategy was suggested for *C. neoformans* brain invasion (Shi et al., 2010) and *C. posadasii* infection in mammals (Mirbod-Donovan et al., 2006) (see following section 3.8.).

Our results support the scenario where urease and the accessory protein UreG play a role in pH modulation by ammonia secretion and the resulting ammonification contributes to virulence of *F. oxysporum* on tomato plants.

3.8. Δ*ureG* but not Δ*ure1* contributes to virulence in animal infection models

F. oxysporum mutants lacking the accessory protein UreG displayed significantly reduced virulence in two animal infection models, *Galleria* and immunodepressed mice. Urease was previously shown to act as a virulence factor in two human fungal pathogens, *C. neoformans*

(Cox et al., 2000) and *C. immitis* (Cole, 1997), as well as the two bacterial pathogens *H. pylori* (Eaton et al., 1991) and *P. mirabilis* (Jones et al., 1990).

Urease in fungal pathogens may play a role in ensuring utilization of host urea as a nitrogen source. In humans, urea is present at millimolar concentration in the subcutaneous adipose tissue, central nervous system (CNS), epithelial lining fluid and blood serum (Ronne-Engstrom et al., 2001; Tyvold et al., 2007; Waring et al., 2008; Zielinski et al., 1999). *C. neoformans* urease null mutants enter the mouse brain less effeciently and are less virulent than the wild type strain (Olszewski et al., 2004; Shi et al., 2010). It has been suggested that the ammonia resulting from the ezymatic degradation of urea causes damage to the endothelium, increases permeability and favours transmigration of fungal cells (Shi et al., 2010).

In this work we showed that urease function, measured as ammonia secretion, strongly depends on the availability of glucose. Reported concentrations of glucose in human tissue are estimated to be below 0.05 mM (e.g in the lung), compared to relatively high glucose levels in blood (6–8 mM) (de Prost and Saumon, 2007). It is feasible that the glucose-limited conditions in certain organs of infected mice lead to high urease activities and ammonia secretion, facilitating invasive fungal growth in the tissue. Considering that the availability of glucose varies in the different mouse organs, our hypothesis would be in line with the observation that *F. oxysporum* develops chlamydospores in some organs such as the lungs (Schafer et al., 2014). Chlamydospores are known to be produced in unfavorable conditions such as carbon starvation (Couteaudier and Alabouvette, 1990; Kono et al., 1995; Nelson, 1981b; Schippers, 1981b; Stevenson and Becker, 1972).

Besides glucose being limited *in vivo*, additional environmental factors may accentuate the need to metabolize sugars. Most fungi are obligate or facultative aerobes and generate most of their ATP via the respiratory pathway. However, oxygen levels within the host tissue are considerably lower than atmospheric levels (21%) and may thus not be sufficient to support a respiratory mode of growth. For example within the parenchyma of healthy lungs the oxygen level is around 14%, but can drop to 2–4% (Grahl and Cramer, 2010). Thus, fungal

pathogens in the host may experience severe hypoxic stress and require the use of a fermentative metabolism for sustained energy production (Fuller and Rhodes, 2012).

In *C. neoformans* deletion of the urease (Δ*ure1*) or of any accessory protein, including the UreG orthologue or the nickel transporter, lead to a significant decrease in virulence. By contrast, in *F. oxysporum* only the Δ*ureG* mutants displayed reduced virulence in the two animal infection models, while the Δ*ure1* mutants displayed wt virulence levels. These differences could be explained by two hypotheses. First, *F. oxysporum* has two putative urease genes, *ure1* and *ure2* in its genome, but only a single *ureG* gene. Even though we were unable to detect *ure2* transcripts under the conditions studied, *ure1* expression was also very low in contrast to *ureG* which was signifcantly upregulated in conditions of glucose depletion and during *Galleria* infection. Low levels of Ure2 present in the fungus could account for the very low enzymatic activity detected by our urease assay in the Δ*ure1* mutant, and might be sufficient for maintaining virulence on animal hosts. The single UreG protein is likely to be required for the activation of both ureases. Likewise, in the plant *G. max* which also has two structural ureases (Meyer-Bothling and Polacco, 1987; Torisky et al., 1994), mutation of the single gene encoding the UreG accessory protein eliminated both urease activities (Freyermuth et al., 2000) as well as background activity thought to be of bacterial origin (Meyer-Bothling et al., 1987).

Unexpectedly we observed a faster mortality in mice infected with the Δ*ure1* mutant than in those infected with the wt strain. This phenotype is reminiscent of reports from *H. pylori*, where the virulence factor urease stimulates the production by macrophages of nitrite oxide, a potent inhibitor of *H. pylori* growth (Gobert et al., 2002b). It is possible that the absence of urease in *F. oxysporum* leads to a reduced production of nitrite oxide (NO) by mouse macrophages, thus causing an increase of fungal growth and higher mortality in the animals.

An alternative hypothesis to explain the difference in virulence between the Δ*ureG* and the Δ*ure1* mutants is that the urease accessory protein UreG has additional functions besides urease activation which contributes to virulence on animal hosts. This might explain the high expression levels of *ureG* during *Galleria* infection. Although no urease-independent function of UreG has been reported so far, we briefly speculate on the possibility of such a function in

F. oxysporum UreG. The presence of a fully conserved P-loop motif in *F. oxysporum* UreG suggests a possible GTPase activity for this protein. Although studies in *K. aerogenes* and *H. pylori* suggested that UreG does not, by itself, hydrolyze GTP or ATP (Mehta et al., 2003; Moncrief and Hausinger, 1997), UreG from *Bacillus pasteurii* displayed a clear GTPase activity (Zambelli et al., 2005). If a similar GTPase activity should exist in the UreG protein in *F. oxysporum*, it might account for the urease-independent role of UreG in virulence.

Another possibility is that *F. oxysporum* UreG might be involved in metal (Zn^{2+} and Ni^{2+}) delivery to additional metal enzymes other than urease. In plants, Zn^{2+} acts as a functional, structural or regulatory cofactor for a large number of enzymes with diverse properties (Brown, 1993). Importantly, in *G. max* incubation of UreG with Zn^{2+} results in a change in tertiary structure of the protein backbone, suggesting that the metal ion assumes an important structural role in stabilizing protein conformation beyond its role in catalytic activity (Real-Guerra et al., 2012). UreG proteins belong to the class of intrinsically unstructured proteins that require the interaction with cofactors or other protein partners to perform their function (Zambelli et al., 2005), and are able to perform catalysis (Zambelli et al., 2012). UreG has been described as the only known natural member of the class of intrinsically disordered proteins lacking a rigid tertiary structure (Zambelli et al., 2012; Zambelli et al., 2007; Zambelli et al., 2005; Zambelli et al., 2009). Therfore It is possible that UreG acts as a scaffold protein or a hub for protein-cofactor interactions or protein-protein interaction networks, binding several different partners in regulatory processes (Zambelli et al., 2012).

If *F. oxysporum* UreG can undergo different conformational changes, it might also have the ability to engage in distinct protein interactions to catalyze distinct reactions. In this context it is important to note that UreG belongs to a growing family of G-proteins regulated by homodimerization (Gasper et al., 2009). Two other well-characterized nickel-delivering NTPases, HypB and CooC1, share strikingly similar properties with UreG. HypB is a close relative of UreG, responsible for delivering nickel to hydrogenases. Similar to UreG, it exhibits a varying degree of dimerization in the presence of guanine nucleotides, but achieves complete dimerization in the presence of both GTP and nickel (Chan et al., 2012).

Important to mention is that in *H. pylori* the urease accessory protein UreG physically interacts with HypB (Stingl et al., 2008), a GTPase and accessory protein essential for Ni^{2+} incorporation into hydrogenase (Maier et al., 1993). Similar to *H. pylori* where the maturation events of these two nickel-containing proteins are interconnected (Olson et al., 2001), in *F. oxysporum* UreG might interact with HypB. Interestingly, [NiFe] hydrogenase in *H. pylori* not only allows this organism to utilize hydrogen as an energy source, but is also required for bacterial colonization in a mouse model (Olson and Maier, 2002).

We conclude that 1) UreG plays an important role during animal infection; 2) glucose limitation during infection might be important for urease function and contribute to virulence on animal hosts; 3) Ure2 might be responsible for low amounts of ammonia secretion and virulence on animal infection models of the Δ*ure1* mutant; 4) the urease accessory protein UreG might have an additional role in virulence beyond the activation of the ureases Ure1 and Ure2, related to different cellular processes.

3.9. UreG interact with the mucin transmembrane protein Msb2 in a YTH assay

In this work the urease accessory protein UreG was identified as an protein interactor of the cytoplasmic tail of Msb2 in an YTH screen against a cDNA library of *F. oxysporum* (see previous chapter). The transmembrane protein Msb2 was previously shown to promote invasive growth and plant infection via surface-induced phosporylation of Fmk1 (Perez-Nadales and Di Pietro, 2011). Although Δ*ureG* mutants displayed slightly impaired invasive growth on apple fruits and reduced virulence on tomato plants, none of the other key Δ*msb2* phenotypes were detected in the Δ*ureG* mutants. For example, we failed to detect impaired ability to penetrate cellophane membranes, reduced phosphorylation of the MAPK Fmk1 or reduced expression of the downstream pathway effector *fpr1* in the Δ*ureG* strains. This suggests that UreG does not function in activation of the Fmk1 pathway as Msb2 does. Moreover, the Δ*ureG* strains also lacked another Fmk1-independent Δ*msb2* phenotype namely increased sensitivity to CFW.

To our knowledge, a putative link between the mucin protein Msb2 and UreG or any component of the urease complex has not been reported before, raises questions on the significance of the putative physical interaction. In the following section it will be discussed how UreG and the urease complex might be connected to Msb2 or the Fmk1 MAPK signaling pathway.

In *S. cerevisiae*, filamentous growth occurs in response to limiting nitrogen (Gimeno et al., 1992) or glucose (Cullen and Sprague, 2000) and is regulated by multiple signaling pathways including the nutrient responsive TOR pathway (Rohde and Cardenas, 2004),Ras-cAMP-PKA (Gimeno et al., 1992), Snf1 (Cullen and Sprague, 2000) and the Kss1 MAPK pathway commonly referred to as the filamentous growth pathway (Liu et al., 1993; Roberts and Fink, 1994), which is orthologous to the Fmk1 cascade in *F. oxysporum* (Rispail et al., 2009). Although the filamentous growth MAPK pathway is stimulated by nutrient limitation (Pitoniak et al., 2009), the plasma-membrane regulators Msb2 and Sho1 (Cullen et al., 2004; Cullen and Sprague, 2000; O'Rourke and Herskowitz, 1998) are not thought to sense nutrients directly. Rather, the MAPK pathway is sensitized to nutrient levels by regulatory inputs from Ras2-cAMP-PKA (Chavel et al., 2010; Mosch et al., 1996) and has been suggested to regulate proteolytic processing of Msb2 (Cullen et al., 2004) by starvation-dependent induction of genes that encode its cognate proteases (Vadaie et al., 2008).

A recent study revealed a connection between the major glucose-sensing (AMPK) pathway and the filamentous growth MAPK cascade, whereby Mig1, Mig2 and the AMPK Snf1 are required for induction of the filamentous growth pathway in response to glucose limitation (Karunanithi and Cullen, 2012). This provides a direct link between glucose sensing (via AMPK) and cell differentiation (via MAPK), where Mig1 and Mig2 are direct associated with the cytosolic domain of Msb2 (Karunanithi and Cullen, 2012). In earlier studies, only the small GTPase Cdc42 was shown to associate in a Y2H analysis with the cytosolic domain of Msb2 (Cullen et al., 2004).

In glucose starvation, Mig1 is exported from the nucleus in an Snf1-dependent manner (De Vit et al., 1997; DeVit and Johnston, 1999). Snf1 is required for filamentous growth (Cullen and Sprague, 2000) and it has been suggested that a Δ*snf1* mutant is defective for induction

of filamentous growth in response to glucose depletion, because Mig1 does not exit the nucleus and is unable to regulate Msb2 at the cytosol–plasma membrane interface (Karunanithi and Cullen, 2012).

The cAMP/PKA pathway in *S. cerevisiae* is involved in glucose sensing (Rolland et al., 2000; Santangelo, 2006). In glucose-starved cells of *C. neoformans,* this pathway is rapidly activated by addition of glucose via the G protein α subunit Gpa1 (Xue et al., 2006). Interestingly, it has been shown in this pathogen that PKA negatively regulates the level of extracellular urease (Choi et al., 2012).

Similar to the MAPK Kss1 in *S. cerevisiae*, Fmk1 in *F. oxysporum* regulates multiple functions including virulence on plants, invasive growth and cellophane invasion in response to nutrient limitation (Di Pietro et al., 2001; Qi and Elion, 2005; Truckses et al., 2004). Recent results in our group have shown that Fmk1 phosphorylation is increased by alkaline pH (Segorbe et al. unpublished). Based on this information and on that from other fungal systems, we propose the following regulatory link between glucose sensing (via AMPK) and cell differentiation (via MAPK) in *F. oxysporum*: glucose starvation and regulatory inputs from Ras-cAMP-PKA may regulate activation of Msb2 by starvation-dependent mechanisms. Under glucose limitation, Snf1 phosphorylates and mediates export of the Mig1 orthologue CreA from the nucleus, leading to transcriptional derepression of glucose-repressed genes. If CreA directly associates with the cytosolic domain of Msb2, as described for *S. cerevisiae* Mig1, this association might lead to the release of UreG which could activate the urease complex, causing an increase in extracellular pH and triggering Fmk1 pathway activation. This model would be in line with reports showing that PKA activation caused by glucose addition negatively regulates urease activity (Choi et al., 2012).

In an Δ*msb2* mutant, UreG could not be sequestered and would be able to activate urease even in glucose limiting conditions. Under glucose limiting conditions the fungus could be able to overcome the need of carbon by a catabolism process of amino acids and/protein degradation. This amino acid recycling process would need in parallel the activation of urease and following detoxification of the cytoplasma from the excess ammonia would rise the environmental pH which is produced by this reaction.

Interestingly, when MM plates containing urea as a sole nitrogen and carbon source were buffered to low pH (4 or 5), only the Δ*fmk1* mutant, but not the wt, was able to produce a pH increase. Moreover, in liquid MM the Δ*fmk1* mutant secreted almost double the amount of ammonia than the wt strain. These findings suggest that the MAPK Fmk1 might be required for inhibition of urease function at low pH, shown by the lack of alkalinization in the wt at pH 4 and 5. This putative negative control would be lacking in the Δ*fmk1* mutant, leading to a high secretion of ammonia even at low pH and causing medium alkalinization..

We propose that, 1) Msb2 contributes to *ureG* expression; 2) glucose negatively regulates urease activity, putatively via Fmk1; 3) acidic conditions could lead to an Fmk1-dependent inhibition of urease function.

3.10. F. oxysporum arginase contributes to arginine catabolism and ammonia secretion

In the urea cycle, the enzyme arginase (Car1) hydrolyzes L-arginine to L-ornithine and urea (Kinne-Saffran and Kinne, 1999; Mendz and Hazell, 1996; Mendz et al., 1998). Car1 would be the only enzyme in *F. oxysporum* that generates urea *in vivo,* as described for plants (Witte, 2011). Because urease production from arginine hydrolysis is blocked in the Δ*car1* mutant, the only source of urea would be extracellular. Thus, an urease assay with the Δ*car1* mutant would provide important information on the metabolic source of ammonia in urea-grown culture supernatants. We compared the concentration of ammonia secreted in urea medium by the Δ*car1* mutant with that of the wt strain and found that it was reduced approximately 35% (wt: 52.5 mM, Δ*car1*: 34.2 mM). This suggests that the ammonia secreted by the wt originates in about 65% from extracellular urea and in 35% from intracellular arginine recycling.

This suggests the following scenario. As mentioned above, *F. oxysporum* secretes less ammonia in the presence of glucose. It would make biological sense to channel all available

ammonia into production of amino acids while sufficient carbon (glucose) is available. However, once glucose is depleted carbon is obtained from amino acid recycling via arginase, among others, thereby generating an excess of ammonia that needs to be secreted for detoxification, triggering an increase in extracellular pH.

3.11. *F. oxysporum* arginase contributes to virulence on tomato plants and animals

Previous reports showed that a mutation of the arginine biosynthesis gene argininosuccinate lyase (*arg1*) causes reduced pathogenicity in *F. oxysporum* f.sp. *melonis* (Namiki et al., 2001). Here we show that *F. oxysporum* mutants lacking the arginine-degrading enzyme Car1 have attenuated virulence on tomato plants. One possible explanation for this result is that *F. oxysporum* uses plant arginine as an important source of nutrients. Arginine is the most important single metabolite for nitrogen storage in many plant seeds (Vanetten C.H, 1967) and high arginine concentrations are found in underground storage organs of several plants (Reviewed in (Witte, 2011). Indeed, the impaired growth of the Δ*car1* mutant on arginine suggests that the use of plant arginine by this mutant is completely blocked during infection.
Interestingly, we also found a significant reduction in virulence of Δ*car1* mutants on *G. mellonella* and on immunodepressed mice. Additionally, the *F. oxysporum car1* gene was highly expressed during *G. mellonella* infection and slightly reduced in the Δ*ureG* mutant. This could be explained by a feedback mechanism, whereby the accumulation of urea which cannot be converted in the Δ*ureG* mutant results in a down-regulation of the urea-producing enzyme arginase. This idea is in line with the reduced expression of the glutamine synthetase in the Δ*ureG* mutant which could be caused by the lack of ammonia needed for amino acid synthesis.
The finding that Car1 is essential for the use of extracellular arginine by *F. oxysporum in vitro* implies that this fungus is also able to metabolize arginine from the host. In the pathogen *H. pylori* it has been reported that arginase competes for host arginine with nitrite oxide

synthase (iNOS) produced by macrophages, and that this competition increases the outcome of infection (Chaturvedi et al., 2007; Gobert et al., 2001). The iNOS product nitric oxide (NO) is an important component of innate immunity in murine macrophages and acts as an effective antimicrobial agent against intracellular pathogens (Chakravortty and Hensel, 2003). By channeling host arginine towards the arginase pathway, the fungus might thus limit the substrate for iNOS from macrophages, thereby reducing the amount of NO produced (Das et al., 2010). In addition, diverting host arginine into its own arginase pathway would support fungal growth and production of polyamines known to downregulate pro-inflammatory cytokine release (Munder et al., 1999). In this regard, a study on *C. albicans* pathogenesis should be taken in account. In order to escape from macrophages after being ingested, *Candida* induces it own intracellular arginase and urea amidolyase to achive hyphal switching. In addition two exogenous arginase are secreted out, provide survival benefit by reducing nitrosative stress via quenching the iNOS substrate arginine (Ghosh et al., 2009).

Different mechanisms are described how pathogenic arginases that are intracellular and not secreted can get access to the host arginine pool. *Helicobacter* possess its own arginine transport protein to uptake arginine present in the extracellular milieu (Yoshiyama and Nakazawa, 2000). Beside to their own endogenous arginine uptake systems *Leishmania* employs the unique ability to recruit host arginine transporters to their vacuoles (Shaked-Mishan et al., 2006; Wanasen and Soong, 2008). Whereas Mycobacteria infection also upregulates host arginine transport it utilizes this host-derived amino acid for its own benefit instead of synthesizing its own (Talaue et al., 2006). Taken together pathogen-encoded arginases can modulate iNOS activity irrespective of their spatial localization by modulating the cellular distribution of arginine.

Loss of arginase in *F. oxysporum* might thus leave more arginine available for host iNOS to produce NO radicals, resulting in more efficient defense (Lahiri et al., 2010). Different pathogens have been suggested to use this strategy to survive in the host, including *Salmonella typhimurium* (Lahiri et al., 2008), *Mycobacterium tuberculosis* (El Kasmi et al., 2008), *Leishmania mexicana* (Gaur et al., 2007) or *Schistosoma mansoni* (Thompson et al., 2008) .

We conclude that 1) *F. oxysporum* arginase functions in utilization of extracellular arginine and in intracellular arginine breakdown; 2) under the conditions studied, around 35% of the secreted ammonia might ultimately derive from intracellular amino acid catabolism; 3) reduced virulence of Δ*car1* mutants in plant and animal models might be due to different causes, including inability to use host arginine as a nutrient source or to prevent production of NO radicals produced by host macrophages.

Conclusions

Chapter 1

1. The invasive fusariosis murine model of *F. oxysporum* leads to symptoms similar to those reported in humans
2. *F. oxysporum* displays distinct invasion strategies in different organs of the host
3. Persistence of *F. oxysporum* in the immunocompetent host can lead to subsequent systemic infection upon immunosuppressive treatment

Chapter 2

1. *F. oxysporum* germlings undergo rapid recognition and uptake by murine macrophages
2. *F. oxysporum* germlings continue hyphal growth after phagocytosis, leading to escape and associated macrophage lysis
3. The rate of macrophage killing increases with the number of internalized *F. oxysporum* cells
4. Phagocytosed *F. oxysporum* inhibits completion of macrophage mitosis, resulting in large multinucleated daughter cells

Chapter 3

1. The Y2H sceen identified FOXG_13832, a putative urease accessory protein G as an interactor of the cytoplasmic tail of Msb2

Chapter 4

1. *F. oxysporum* urease accessory protein G is essential for urease function
2. UreG and Ure1 contribute to medium alkalinization via ammonia secretion
3. Extracellular alkalinization by ammonia secretion is triggered by glucose deprivation and regulated by carboncatabolite repression
4. Glucose repression of urease-dependent medium alkalinization is linked to nitrogen metabolism

5. UreG and Ure1 contribute to virulence on tomato plants
6. UreG, but not Ure1 contributes to virulence in animal infection models
7. *F. oxysporum* arginase is required for arginine catabolism and contributes to ammonia secretion
8. *F. oxysporum* Car1 contributes to virulence on tomato plants and in animal infection models

References

Abreu, C., et al., 2010. UreA, the major urea/H+ symporter in Aspergillus nidulans. Fungal Genet Biol. 47**,** 1023-33.

Agrios, G. N. (Ed.) 1997. Plant Pathology. Academic Press Inc., San Diego, CA, EEUU.

Agrios, G. N., 2005a. Plant pathology Academic Press Inc, New York, USA.

Agrios, G. N., 2005b. Plant Pathology. New York, USA, Academic Press Inc. 5edn.

Aguetoni Cambui, C., et al., 2009. Detection of urease in the cell wall and membranes from leaf tissues of bromeliad species. Physiol Plant. 136**,** 86-93.

Ahuatzi, D., et al., 2007. Hxk2 regulates the phosphorylation state of Mig1 and therefore its nucleocytoplasmic distribution. J Biol Chem. 282**,** 4485-93.

Alkan, N., et al., 2008. Role of ammonia secretion and pH modulation on pathogenicity of Colletotrichum coccodes on tomato fruit. Mol Plant Microbe Interact. 21**,** 1058-66.

Altschul, S. F., et al., 1997. Gapped BLAST and PSI-BLAST: a new generation of protein database search programs. Nucleic Acids Res. 25**,** 3389-402.

Anaissie, E., et al., 1991. Comparison of the in vitro antifungal activity of free and liposome-encapsulated amphotericin B. Eur J Clin Microbiol Infect Dis. 10**,** 665-8.

Andersen, J. A., 1975. Benurestat, a urease inhibitor for the therapy of infected ureolysis. Invest Urol. 12**,** 381-6.

Armstrong, G. M., and Armstrong, J. K., 1981. Formae speciales and races of Fusarium oxysporum causing wilt diseases. Philadelphia, PA, Pennsylvania State University Press.

Arst, H. N., Jr, and Scazzocchio, C. (Ed.) 1985. Formal genetics and molecular biology of the control of gene expression in Aspergillus nidulans

. . Orlando: Academic Press, Orlando.

Arst, H. N., Jr, MacDonald, D.W., and Jones, S.A. (198, 1980. Regulation of proline transport in Aspergillus nidulans Gen Microbiol. 116**,** 285-294.

Arst, H. N., Jr., Cove, D. J., 1973. Nitrogen metabolite repression in Aspergillus nidulans. Mol Gen Genet. 126**,** 111-41.

Atwell, B. J., Kriedemann,P.E.,Turnbull, C.G.N., Plants in Action In: R. L. B. Derek Eamus, (Ed.), Adaptation in Nature, Performance in Cultivation. Australian Society of Plant Scientists, New Zealand Society of Plant Biologists, and New Zealand Institute of Agricultural and Horticultural Science 1999.

Bach, S. J., Killip, J. D., 1961. Studies on the purification and the kinetic properties of arginase from beef, sheep and horse liver. Biochim Biophys Acta. 47**,** 336-43.

Baker, B., et al., 1997. Signaling in plant-microbe interactions. Science. 276**,** 726-33.

Balasubramanian, A., Ponnuraj, K., 2010. Crystal structure of the first plant urease from jack bean: 83 years of journey from its first crystal to molecular structure. J Mol Biol. 400**,** 274-83.

Bayram, O., Braus, G. H., 2012. Coordination of secondary metabolism and development in fungi: the velvet family of regulatory proteins. FEMS Microbiol Rev. 36**,** 1-24.

Bayram, O., et al., 2008. VelB/VeA/LaeA complex coordinates light signal with fungal development and secondary metabolism. Science. 320**,** 1504-6.

Becker-Ritt, A. B., et al., 2007. Antifungal activity of plant and bacterial ureases. Toxicon. 50**,** 971-83.

Beckman (Ed.) 1987a. The nature of wilt diseases of plants. APS Press, St Paul, MN (EEUU).

Beckman, C. H., 1987b. The nature of wilt disease of plants. American Phytopathological Society, St. Paul, Minn.

Beckman, C. H. (Ed.) 1987c. The nature of wilt disease of plants.

Bell, G. D., et al., 1987. 14C-urea breath analysis, a non-invasive test for Campylobacter pylori in the stomach. Lancet. 1, 1367-8.
Benini, S., et al., 1999. A new proposal for urease mechanism based on the crystal structures of the native and inhibited enzyme from Bacillus pasteurii: why urea hydrolysis costs two nickels. Structure. 7, 205-16.
Bharathi, M. J., et al., 2003. Epidemiological characteristics and laboratory diagnosis of fungal keratitis. A three-year study. Indian J Ophthalmol. 51, 315-21.
Bibby, J. M., Hukins, D. W., 1992. Measurement of pH to quantify urease activity. J Biochem Biophys Methods. 25, 231-6.
Biswas, S., et al., 2007. Environmental sensing and signal transduction pathways regulating morphopathogenic determinants of Candida albicans. Microbiol Mol Biol Rev. 71, 348-76.
Blakeley, R. L., et al., 1969a. Jack bean urease (EC 3.5.1.5). Demonstration of a carbamoyl-transfer reaction and inhibition by hydroxamic acids. Biochemistry. 8, 1991-2000.
Blakeley, R. L., et al., 1969b. Jack bean urease (EC 3.5.1.5). A new purification and reliable rate assay. Biochemistry. 8, 1984-90.
Blanchard, A., et al., 1988. Characteristics of Ureaplasma urealyticum urease. J Bacteriol. 170, 2692-7.
Blattler, D. P., et al., 1967. Dissociation of urease by glycol and glycerol. Nature. 216, 274-5.
Bodey, G. P., et al., 2002. Skin lesions associated with Fusarium infection. J Am Acad Dermatol. 47, 659-66.
Bogdan, C., 2001. Nitric oxide and the regulation of gene expression. Trends Cell Biol. 11, 66-75.
Boisnard, S., et al., 2008. Role of Sho1p adaptor in the pseudohyphal development, drugs sensitivity, osmotolerance and oxidant stress adaptation in the opportunistic yeast Candida lusitaniae. Yeast. 25, 849-59.
Bok, J. W., Keller, N. P., 2004. LaeA, a regulator of secondary metabolism in Aspergillus spp. Eukaryot Cell. 3, 527-35.
Bok, J. W., et al., 2006. Secondary metabolic gene cluster silencing in Aspergillus nidulans. Mol Microbiol. 61, 1636-45.
Booth, C., 1971. The Genus Fusarium. The Eastern Press limited London and Reading.
Bouarab, K., et al., 2002. A saponin-detoxifying enzyme mediates suppression of plant defences. Nature. 418, 889-92.
Boutati, E. I., Anaissie, E. J., 1997. Fusarium, a significant emerging pathogen in patients with hematologic malignancy: ten years' experience at a cancer center and implications for management. Blood. 90, 999-1008.
Braedel, S., et al., 2004. Aspergillus fumigatus antigens activate innate immune cells via toll-like receptors 2 and 4. Br J Haematol. 125, 392-9.
Brakhage, A. A., 2005. Systemic fungal infections caused by Aspergillus species: epidemiology, infection process and virulence determinants. Curr Drug Targets. 6, 875-86.
Brown, G. D., 2011. Innate antifungal immunity: the key role of phagocytes. Annu Rev Immunol. 29, 1-21.
Brown, G. W., Jr., 1966. Studies in comparative biochemistry and evolution. I. Avian liver arginase. Arch Biochem Biophys. 114, 184-94.
Brown, P. H., Cakmak, I., Zhang, Q., Form and function of zinc plants. In: A. D. Roberts, (Ed.), Zinc in solis and plants: proceedings of the international symposium on "zinc in soils and plants". Kluwer Academic Publishers, The Netherlands, 1993, pp. 93-106.
Brownfield, D. L., et al., 2008. Analysis of Arabidopsis arginase gene transcription patterns indicates specific biological functions for recently diverged paralogs. Plant Mol Biol. 67, 429-40.
Buga, G. M., et al., 1996. Arginase activity in endothelial cells: inhibition by NG-hydroxy-L-arginine during high-output NO production. Am J Physiol. 271, H1988-98.

Burgess, L. W., General ecology of the Fusaria. In. Fusarium: Diseases, Biology and Taxonomy. The Pennsylvania State University Press, Pennsylvania PA, 1981, pp. 225-235.
Burne, R. A., Chen, Y. Y., 2000. Bacterial ureases in infectious diseases. Microbes Infect. 2, 533-42.
Bury-Mone, S., et al., 2004. Responsiveness to acidity via metal ion regulators mediates virulence in the gastric pathogen Helicobacter pylori. Mol Microbiol. 53, 623-38.
Callow, J. A., Models for host-pathogen interactions. The applied mycology of Fusarium Ed. Cambridge University Press, 1987, pp. 39-69.
Canteros, C. E., et al., 1996. A rapid urease test for presumptive identification of Cryptococcus neoformans. Mycopathologia. 136, 21-3.
Cao, F. Q., et al., 2010. Identification and characterization of proteins involved in rice urea and arginine catabolism. Plant Physiol. 154, 98-108.
Caracuel, Z., et al., 2005. Fusarium oxysporum gas1 encodes a putative beta-1,3-glucanosyltransferase required for virulence on tomato plants. Mol Plant Microbe Interact. 18, 1140-7.
Caracuel, Z., et al., 2003. The pH signalling transcription factor PacC controls virulence in the plant pathogen Fusarium oxysporum. Mol Microbiol. 48, 765-79.
Carlini, C. R., Polacco, J.C., 2008. Toxic properties of urease. Crop Sci. 48, 1665-1672.
Carlson, M., 1999. Glucose repression in yeast. Curr Opin Microbiol. 2, 202-7.
Carter, E. L., et al., 2009. Interplay of metal ions and urease. Metallomics. 1, 207-21.
Carter, E. L., et al., 2011. Iron-containing urease in a pathogenic bacterium. Proc Natl Acad Sci U S A. 108, 13095-9.
Casalot, L., Rousset, M., 2001. Maturation of the [NiFe] hydrogenases. Trends Microbiol. 9, 228-37.
Cederbaum, S. D., et al., 2004. Arginases I and II: do their functions overlap? Mol Genet Metab. 81 Suppl 1, S38-44.
Chakravortty, D., Hensel, M., 2003. Inducible nitric oxide synthase and control of intracellular bacterial pathogens. Microbes Infect. 5, 621-7.
Chan, K. H., et al., 2012. Interaction between hydrogenase maturation factors HypA and HypB is required for [NiFe]-hydrogenase maturation. PLoS One. 7, e32592.
Chang, C. I., et al., 2001. Macrophage arginase promotes tumor cell growth and suppresses nitric oxide-mediated tumor cytotoxicity. Cancer Res. 61, 1100-6.
Chaturvedi, R., et al., 2007. L-arginine availability regulates inducible nitric oxide synthase-dependent host defense against Helicobacter pylori. Infect Immun. 75, 4305-15.
Chavel, C. A., et al., 2010. Multiple signals converge on a differentiation MAPK pathway. PLoS Genet. 6, e1000883.
Chen, R. E., Thorner, J., 2007. Function and regulation in MAPK signaling pathways: lessons learned from the yeast Saccharomyces cerevisiae. Biochim Biophys Acta. 1773, 1311-40.
Choi, J., et al., 2012. Regulated expression of cyclic AMP-dependent protein kinase A reveals an influence on cell size and the secretion of virulence factors in Cryptococcus neoformans. Mol Microbiol. 85, 700-15.
Christensen, T. S., et al., 2009. Reconstruction and logical modeling of glucose repression signaling pathways in Saccharomyces cerevisiae. BMC Syst Biol. 3, 7.
Christensen, W. B., 1946. Urea decomposition as a means of differentiating Proteus and paracolon cultures from each other and from Salmonella and Shigella types. J. Bacteriol. 52, 461–466.
Clayton, C. L., et al., 1990. Nucleotide sequence of two genes from Helicobacter pylori encoding for urease subunits. Nucleic Acids Res. 18, 362.
Cole, G. T., 1997. Ammonia production by *Coccidiodes immitis* and its possible significance to the host fungus interplay. Host-Fungus Interplay (Stevens D & Odds F, eds). 247-263.
Collins, C. M., D'Orazio, S. E., 1993. Bacterial ureases: structure, regulation of expression and role in pathogenesis. Mol Microbiol. 9, 907-13.

Cooper, T. G., et al., 1980. Structural analysis of the dur loci in S. cerevisiae: two domains of a single multifunctional gene. Genetics. 94**,** 555-80.
Cooper, T. G., Sumrada, R., 1975. Urea transport in Saccharomyces cerevisiae. J Bacteriol. 121**,** 571-6.
Correll, J. C., 1991. The relationship between formae speciales, races and vegetative compatibility groups in Fusarium oxysporum. Phytopathology. 81**,** 1061-1064.
Couteaudier, Y., Alabouvette, C., 1990. Survival and inoculum potential of conidia and chlamydospores of Fusarium oxysporum f.sp. lini in soil. Can J Microbiol. 36**,** 551-6.
Cox, G. M., et al., 2000. Urease as a virulence factor in experimental cryptococcosis. Infect Immun. 68**,** 443-8.
Craig, P. M., et al., 1992. Helicobacter pylori secretes a chemotactic factor for monocytes and neutrophils. Gut. 33**,** 1020-3.
Creaser, E. H., Porter, R. L., 1985. The purification of urease from Aspergillus nidulans. Int J Biochem. 17**,** 1339-41.
Csank, C., et al., 1998. Roles of the Candida albicans mitogen-activated protein kinase homolog, Cek1p, in hyphal development and systemic candidiasis. Infect Immun. 66**,** 2713-21.
Cullen, P. J., 2007. Signaling mucins: the new kids on the MAPK block. Crit Rev Eukaryot Gene Expr. 17**,** 241-57.
Cullen, P. J., et al., 2004. A signaling mucin at the head of the Cdc42- and MAPK-dependent filamentous growth pathway in yeast. Genes Dev. 18**,** 1695-708.
Cullen, P. J., Sprague, G. F., Jr., 2000. Glucose depletion causes haploid invasive growth in yeast. Proc Natl Acad Sci U S A. 97**,** 13619-24.
Darlington, A. J., et al., 1965. Biochemical and genetical studies of purine breakdown in Aspergillus. Nature. 206**,** 599-600.
Das, P., et al., 2010. Modulation of the arginase pathway in the context of microbial pathogenesis: a metabolic enzyme moonlighting as an immune modulator. PLoS Pathog. 6**,** e1000899.
Davidson, R. C., et al., 2003. A MAP kinase cascade composed of cell type specific and non-specific elements controls mating and differentiation of the fungal pathogen Cryptococcus neoformans. Mol Microbiol. 49**,** 469-85.
Davis, D., 2003. Adaptation to environmental pH in Candida albicans and its relation to pathogenesis. Curr Genet. 44**,** 1-7.
Davis, D., et al., 2000. Candida albicans RIM101 pH response pathway is required for host-pathogen interactions. Infect Immun. 68**,** 5953-9.
Davis, M. A., et al., 1993. Fungal catabolic gene regulation: molecular genetic analysis of the amdS gene of Aspergillus nidulans. Genetica. 90**,** 133-45.
de Groot, M. J., et al., 1998. Agrobacterium tumefaciens-mediated transformation of filamentous fungi. Nat Biotechnol. 16**,** 839-42.
de Pauw, B. E., Meunier, F., 1999. The challenge of invasive fungal infection. Chemotherapy. 45 Suppl 1**,** 1-14.
de Prost, N., Saumon, G., 2007. Glucose transport in the lung and its role in liquid movement. Respir Physiol Neurobiol. 159**,** 331-7.
De Vit, M. J., et al., 1997. Regulated nuclear translocation of the Mig1 glucose repressor. Mol Biol Cell. 8**,** 1603-18.
Dean, R., et al., 2012. The Top 10 fungal pathogens in molecular plant pathology. Mol Plant Pathol. 13**,** 414-30.
Delgado-Jarana, J., et al., 2005. Fusarium oxysporum G-protein beta subunit Fgb1 regulates hyphal growth, development, and virulence through multiple signalling pathways. Fungal Genet Biol. 42**,** 61-72.

Denkhaus, E., Salnikow, K., 2002. Nickel essentiality, toxicity, and carcinogenicity. Crit Rev Oncol Hematol. 42, 35-56.
DeVit, M. J., Johnston, M., 1999. The nuclear exportin Msn5 is required for nuclear export of the Mig1 glucose repressor of Saccharomyces cerevisiae. Curr Biol. 9, 1231-41.
Di Carlo, F. J., et al., 1953. The mechanism of allantoin catabolism by yeast. Arch Biochem Biophys. 44, 468-74.
Di Pietro, A., et al., 2001. A MAP kinase of the vascular wilt fungus Fusarium oxysporum is essential for root penetration and pathogenesis. Mol Microbiol. 39, 1140-52.
Di Pietro, A., Gonzalez Roncero, M.I., Ruiz Roldán, C., and Claus, H., 2009. From tools of survival to weapons of destruction: role of cell wall-degrading enzymes in plant infection. In The Mycota. 181-200.
Di Pietro, A., Roncero, M. I., 1998. Cloning, expression, and role in pathogenicity of pg1 encoding the major extracellular endopolygalacturonase of the vascular wilt pathogen Fusarium oxysporum. Mol Plant Microbe Interact. 11, 91-8.
Dignani, M. C., Anaissie, E., 2004. Human fusariosis. Clin Microbiol Infect. 10 Suppl 1, 67-75.
Dixon, N. E., et al., 1980a. Jack bean urease (EC 3.5.1.5). III. The involvement of active-site nickel ion in inhibition by beta-mercaptoethanol, phosphoramidate, and fluoride. Can J Biochem. 58, 481-8.
Dixon, N. E., et al., 1975. Letter: Jack bean urease (EC 3.5.1.5). A metalloenzyme. A simple biological role for nickel? J Am Chem Soc. 97, 4131-3.
Dixon, N. E., et al., 1980b. Jack bean urease (EC 3.5.1.5). IV. The molecular size and the mechanism of inhibition by hydroxamic acids. Spectrophotometric titration of enzymes with reversible inhibitors. Can J Biochem. 58, 1323-34.
Dunker, A. K., et al., 2005. Flexible nets. The roles of intrinsic disorder in protein interaction networks. FEBS J. 272, 5129-48.
Dunn, B. E., et al., 1990. Purification and characterization of urease from Helicobacter pylori. J Biol Chem. 265, 9464-9.
Dunn, B. E., Phadnis, S. H., 1998. Structure, function and localization of Helicobacter pylori urease. Yale J Biol Med. 71, 63-73.
Dunn, B. E., et al., 1997. Localization of Helicobacter pylori urease and heat shock protein in human gastric biopsies. Infect Immun. 65, 1181-8.
Eaton, K. A., et al., 1991. Essential role of urease in pathogenesis of gastritis induced by Helicobacter pylori in gnotobiotic piglets. Infect Immun. 59, 2470-5.
Eaton, K. A., Krakowka, S., 1994. Effect of gastric pH on urease-dependent colonization of gnotobiotic piglets by Helicobacter pylori. Infect Immun. 62, 3604-7.
El Kasmi, K. C., et al., 2008. Toll-like receptor-induced arginase 1 in macrophages thwarts effective immunity against intracellular pathogens. Nat Immunol. 9, 1399-406.
Evans, D. J., Jr., et al., 1991. Characterization of the Helicobacter pylori urease and purification of its subunits. Microb Pathog. 10, 15-26.
Fan, Y., et al., 2010. Skin Microvascular Thrombosis in Fusarium Infection in Two Early Biopsied Cases. Case Rep Dermatol. 2, 76-81.
Farman, M. L., et al., 2002. Analysis of the structure of the AVR1-CO39 avirulence locus in virulent rice-infecting isolates of Magnaporthe grisea. Mol Plant Microbe Interact. 15, 6-16.
Fields, S., Song, O., 1989. A novel genetic system to detect protein-protein interactions. Nature. 340, 245-6.
Fishbein, W. N. (Ed.) 1969. A sensitive and non-inhibitory catalytic stain for urease. Ann Arbor-Humphrey Science press, Ann Arbor, Mich.

Fisher, M. C., et al., 2002. Molecular and phenotypic description of Coccidioides posadasii sp. nov., previously recognized as the non-California population of Coccidioides immitis. Mycologia. 94, 73-84.
Flor, H. H., 1947. Inheritance of pathogenicity in Melampsora lini. Phytopathology. 32, 653-669.
Flor, H. H., 1971. Current status of the gene for gene concept. Annu Rev Phytopathol. 9, 275-296.
Flores, T., et al., 2008. Arginase-negative mutants of Arabidopsis exhibit increased nitric oxide signaling in root development. Plant Physiol. 147, 1936-46.
Follmer, C., 2008. Insights into the role and structure of plant ureases. Phytochemistry. 69, 18-28.
Follmer, C., et al., 2004. Jackbean, soybean and Bacillus pasteurii ureases: biological effects unrelated to ureolytic activity. Eur J Biochem. 271, 1357-63.
Forsberg, H., Ljungdahl, P. O., 2001. Sensors of extracellular nutrients in Saccharomyces cerevisiae. Curr Genet. 40, 91-109.
Foster, C. S., 1992. Fungal keratitis. Infect Dis Clin North Am. 6, 851-7.
Fraser, J. A., et al., 2001. The formamidase gene of Aspergillus nidulans: regulation by nitrogen metabolite repression and transcriptional interference by an overlapping upstream gene. Genetics. 157, 119-31.
Fravel , D., Olivain, C., and Alabouvette, C., 2003. Fusarium oxysporum and its biocontrol. New Phytologist. 157, 493-502.
Freyermuth, S. K., et al., 2000. The soybean Eu3 gene encodes an Ni-binding protein necessary for urease activity. Plant J. 21, 53-60.
Friedrich, B., Magasanik, B., 1977. Urease of Klebsiella aerogenes: control of its synthesis by glutamine synthetase. J Bacteriol. 131, 446-52.
Fritig, B., et al., 1998. Antimicrobial proteins in induced plant defense. Curr Opin Immunol. 10, 16-22.
Fu, Y. H., Marzluf, G. A., 1987. Characterization of nit-2, the major nitrogen regulatory gene of Neurospora crassa. Mol Cell Biol. 7, 1691-6.
Fuller, K. K., Rhodes, J. C., 2012. Protein kinase A and fungal virulence: a sinister side to a conserved nutrient sensing pathway. Virulence. 3, 109-21.
Funck, D., et al., 2008. Ornithine-delta-aminotransferase is essential for arginine catabolism but not for proline biosynthesis. BMC Plant Biol. 8, 40.
Garcia-Rodas, R., et al., 2011. The interaction between Candida krusei and murine macrophages results in multiple outcomes, including intracellular survival and escape from killing. Infect Immun. 79, 2136-44.
Gasper, R., et al., 2009. It takes two to tango: regulation of G proteins by dimerization. Nat Rev Mol Cell Biol. 10, 423-9.
Gaur, U., et al., 2007. An effect of parasite-encoded arginase on the outcome of murine cutaneous leishmaniasis. J Immunol. 179, 8446-53.
Ge, X., Cain K., Hirschberg R. , 1990. Urea metabolism and urease regulation in the cyanobacterium Anabaena variabilis. Can. J. Microbiol. 36, 218-222.
Gerendas J., P. J. C., Freyermuth S.K, Sattelmacher B., 1999a. Significance of nickel for plant growth and metabolism. J Plant Nutr Soil Sci. 162, 241-256.
Gerendas J., S. B., 1997. Significance of N souce (urea cs. NH4NO3) and Ni supply for growth, urease activity and nitrogen metabolism of zucchini (Curcubita pepo convar. giromontiina). Plant Soil. 196, 217-222.
Gerendas J., S. B., 1999b. Influence of Ni supply on growth and nitrogen metabolism of Brassica napus L. grown with NH4NO3 or urea as N source. Ann.Bot.London. 83, 65-71.
Gerendas J., Z. Z., Sattelmacher B., 1998. Influence of N and Ni supply on nitrogen metabolism and urease activity in rice (Oryza sativa L.). J. Exp. Bot. . 49, 1545-1554.

Gersuk, G. M., et al., 2006. Dectin-1 and TLRs permit macrophages to distinguish between different Aspergillus fumigatus cellular states. J Immunol. 176, 3717-24.
Ghosh, S., et al., 2009. Arginine-induced germ tube formation in Candida albicans is essential for escape from murine macrophage line RAW 264.7. Infect Immun. 77, 1596-605.
Gimeno, C. J., et al., 1992. Unipolar cell divisions in the yeast S. cerevisiae lead to filamentous growth: regulation by starvation and RAS. Cell. 68, 1077-90.
Glibert, P. M., Harrison, J., Heil, C., Seitzinger, S., 2006. Escalating worldwide use of urea- a global change contributing to coastral eutrophication. Biogeochemistry. 77, 441-463.
Gobert, A. P., et al., 2002a. Helicobacter pylori induces macrophage apoptosis by activation of arginase II. J Immunol. 168, 4692-700.
Gobert, A. P., et al., 2000. L-Arginine availability modulates local nitric oxide production and parasite killing in experimental trypanosomiasis. Infect Immun. 68, 4653-7.
Gobert, A. P., et al., 2001. Helicobacter pylori arginase inhibits nitric oxide production by eukaryotic cells: a strategy for bacterial survival. Proc Natl Acad Sci U S A. 98, 13844-9.
Gobert, A. P., et al., 2002b. Cutting edge: urease release by Helicobacter pylori stimulates macrophage inducible nitric oxide synthase. J Immunol. 168, 6002-6.
Goldraij, A., Polacco, J. C., 1999. Arginase is inoperative in developing soybean embryos. Plant Physiol. 119, 297-304.
Goldraij, A., Polacco, J. C., 2000. Arginine degradation by arginase in mitochondria of soybean seedling cotyledons. Planta. 210, 652-8.
Gonzalez, G. M., et al., 2013. Murine model of disseminated fusariosis: evaluation of the fungal burden by traditional CFU and quantitative PCR. Mycopathologia. 176, 219-24.
Gonzalez, R., et al., 1997. The integration of nitrogen and carbon catabolite repression in Aspergillus nidulans requires the GATA factor AreA and an additional positive-acting element, ADA. EMBO J. 16, 2937-44.
Gow, N. A. R., van de Veerdonk, F.L., Brown,A.J.P., Netea, M.G., , 2012. Candida albicans morphogenesis and host defence: discriminating invasion from colonization. Nat. Rev. Microbiol. http://dx.doi.org/10.1038/nrmicro2711.
Graham, D. Y., et al., 1987. Campylobacter pylori detected noninvasively by the 13C-urea breath test. Lancet. 1, 1174-7.
Grahl, N., Cramer, R. A., Jr., 2010. Regulation of hypoxia adaptation: an overlooked virulence attribute of pathogenic fungi? Med Mycol. 48, 1-15.
Granstorm M., L. P., Bengtsson C., Megraud F. (Ed.) 2008. Helicobacter 13.
Griffith, D. P., et al., 1978. Acetohydroxamic acid: clinical studies of a urease inhibitor in patients with staghorn renal calculi. J Urol. 119, 9-15.
Guarro, J., Gene, J., 1995. Opportunistic fusarial infections in humans. Eur J Clin Microbiol Infect Dis. 14, 741-54.
Gugnani, H. C., et al., 1976. Mycotic keratitis in Nigeria. A study of 21 cases. Br J Ophthalmol. 60, 607-13.
Ha, N. C., et al., 2001. Supramolecular assembly and acid resistance of Helicobacter pylori urease. Nat Struct Biol. 8, 505-9.
Haas, C. E., et al., 2009. A subset of the diverse COG0523 family of putative metal chaperones is linked to zinc homeostasis in all kingdoms of life. BMC Genomics. 10, 470.
Hahn, M. G., 1996. Microbial elicitors and their receptors in plants. Annu Rev Phytopathol. 34, 387-412.
Hamilton-Miller, J. M., Gargan, R. A., 1979. Rapid screening for urease inhibitors. Invest Urol. 16, 327-8.
Hammond-Kosack, K. E., Jones, J. D., 1996. Resistance gene-dependent plant defense responses. Plant Cell. 8, 1773-91.

Hazel, S. L., Lee A. (Ed.) 1985. The adaptation of motile strains of Campylobacter pyloridis to gastric mucus and their association with gastric epithelial intercellular spaces. Public Health Laboratory Service, London, Ottawa.
Hess, D. C., et al., 2006. Ammonium toxicity and potassium limitation in yeast. PLoS Biol. 4, e351.
Hibbs, J. B., Jr., et al., 1987. Macrophage cytotoxicity: role for L-arginine deiminase and imino nitrogen oxidation to nitrite. Science. 235, 473-6.
Hibbs, J. B., Jr., et al., 1988. Nitric oxide: a cytotoxic activated macrophage effector molecule. Biochem Biophys Res Commun. 157, 87-94.
Hirsch-Kolb, H., et al., 1970. Comparative physical-chemical studies of mammalian arginases. Comp Biochem Physiol. 37, 345-59.
Hohl, T. M., et al., 2005. Aspergillus fumigatus triggers inflammatory responses by stage-specific beta-glucan display. PLoS Pathog. 1, e30.
Hohmann, S., et al., 2007. Yeast osmoregulation. Methods Enzymol. 428, 29-45.
Holland, M. A., Polacco, J. C., 1992. Urease-null and hydrogenase-null phenotypes of a phylloplane bacterium reveal altered nickel metabolism in two soybean mutants. Plant Physiol. 98, 942-8.
Holm, L., Sander, C., 1997. An evolutionary treasure: unification of a broad set of amidohydrolases related to urease. Proteins. 28, 72-82.
Hong, S. P., Carlson, M., 2007. Regulation of snf1 protein kinase in response to environmental stress. J Biol Chem. 282, 16838-45.
Houterman, P. M., et al., 2008. Suppression of plant resistance gene-based immunity by a fungal effector. PLoS Pathog. 4, e1000061.
Hsu, P. C., et al., 2011. Candida albicans Hap43 is a repressor induced under low-iron conditions and is essential for iron-responsive transcriptional regulation and virulence. Eukaryot Cell. 10, 207-25.
Hu, L. T., Mobley, H. L., 1990. Purification and N-terminal analysis of urease from Helicobacter pylori. Infect Immun. 58, 992-8.
Hube, B., 2004. From commensal to pathogen: stage- and tissue-specific gene expression of Candida albicans. Curr Opin Microbiol. 7, 336-41.
Hung, C. Y., et al., 2000. A major cell surface antigen of Coccidioides immitis which elicits both humoral and cellular immune responses. Infect Immun. 68, 584-93.
Hung, C. Y., et al., 2002. A parasitic phase-specific adhesin of Coccidioides immitis contributes to the virulence of this respiratory Fungal pathogen. Infect Immun. 70, 3443-56.
Hynes, M. J., 1972. Mutants with altered glucose repression of amidase enzymes in Aspergillus nidulans. J Bacteriol. 111, 717-22.
Hynes, M. J., 1973. The effect of lack of a carbon source on nitrate-reductase activity in Aspergillus nidulans. J Gen Microbiol. 79, 155-7.
Hynes, M. J., 1975a. Amide utilization in Aspergillus nidulans: evidence for a third amidase enzyme. J Gen Microbiol. 91, 99-109.
Hynes, M. J., 1975b. Studies on the role of the areA gene in the regulation of nitrogen catabolism in Aspergillus nidulans. Aust J Biol Sci. 28, 301-13.
Ignarro, L. J., et al., 1987. Endothelium-derived relaxing factor produced and released from artery and vein is nitric oxide. Proc Natl Acad Sci U S A. 84, 9265-9.
Ikematsu, M., et al., 2007. Electrochemical treatment of human urine for its storage and reuse as flush water. Sci Total Environ. 382, 159-64.
Imazaki, I., et al., 2007. Fow2, a Zn(II)2Cys6-type transcription regulator, controls plant infection of the vascular wilt fungus Fusarium oxysporum. Mol Microbiol. 63, 737-53.
Iniesta, V., et al., 2002. Arginase I induction in macrophages, triggered by Th2-type cytokines, supports the growth of intracellular Leishmania parasites. Parasite Immunol. 24, 113-8.

Isaacson, R. E., 2002. Genomics and the prospects for the discovery of new targets for antibacterial and antifungal agents. Curr Pharm Des. 8, 1091-8.
Ishibashi, Y., 1982. [Keratomycosis in Japan reported from 1976 to 1980]. Nihon Ganka Gakkai Zasshi. 86, 651-6.
Jabri, E., et al., 1995. The crystal structure of urease from Klebsiella aerogenes. Science. 268, 998-1004.
Jahn, B., et al., 2002. PKSP-dependent reduction of phagolysosome fusion and intracellular kill of Aspergillus fumigatus conidia by human monocyte-derived macrophages. Cell Microbiol. 4, 793-803.
Jenkinson, C. P., et al., 1996. Comparative properties of arginases. Comp Biochem Physiol B Biochem Mol Biol. 114, 107-32.
Johnson, D. E., et al., 1993. Contribution of Proteus mirabilis urease to persistence, urolithiasis, and acute pyelonephritis in a mouse model of ascending urinary tract infection. Infect Immun. 61, 2748-54.
Johnston, M., 1999. Feasting, fasting and fermenting. Glucose sensing in yeast and other cells. Trends Genet. 15, 29-33.
Jones, B. D., et al., 1990. Construction of a urease-negative mutant of Proteus mirabilis: analysis of virulence in a mouse model of ascending urinary tract infection. Infect Immun. 58, 1120-3.
Jones, D. B., et al., 1970. Mycotic keratitis in South Florida: a review of thirty-nine cases. Trans Ophthalmol Soc U K. 89, 781-97.
Jones, J. D., Dangl, J. L., 2006. The plant immune system. Nature. 444, 323-9.
Joobeur, T., et al., 2004. The Fusarium wilt resistance locus Fom-2 of melon contains a single resistance gene with complex features. Plant J. 39, 283-97.
Jung, W. H., et al., 2010. HapX positively and negatively regulates the transcriptional response to iron deprivation in Cryptococcus neoformans. PLoS Pathog. 6, e1001209.
Kaltwasser, H., et al., 1972. Control of urease formation in certain aerobic bacteria. Arch Mikrobiol. 81, 178-96.
Kaltwasser, H., Schlegel, H. G., 1966. NADH-Dependent coupled enzyme assay for urease and other ammonia-producing systems. Anal Biochem. 16, 132-8.
Karunanithi, S., Cullen, P. J., 2012. The filamentous growth MAPK Pathway Responds to Glucose Starvation Through the Mig1/2 transcriptional repressors in Saccharomyces cerevisiae. Genetics. 192, 869-87.
Katz, S. A., 1964. Direct potentiometric determination of urease activity. Anal. Chem. 36, 2500-2501.
Kavanagh, K., Reeves, E. P., 2004. Exploiting the potential of insects for in vivo pathogenicity testing of microbial pathogens. FEMS Microbiol Rev. 28, 101-12.
Kenny, G. E., 1983. Inhibition of the growth of Ureaplasma urealyticum by a new urease inhibitor, flurofamide. Yale J Biol Med. 56, 717-22.
Keppler-Ross, S., et al., 2010. Recognition of yeast by murine macrophages requires mannan but not glucan. Eukaryot Cell. 9, 1776-87.
Khan, M. R., et al., 2006. Biological control of fusarium seedling blight disease of wheat and barley. Phytopathology. 96, 386-94.
Khil, P. P., et al., 2004. Crystal structure of the Escherichia coli YjiA protein suggests a GTP-dependent regulatory function. Proteins. 54, 371-4.
Kim, H., et al., 1990. The gastric juice urea and ammonia levels in patients with Campylobacter pylori. Am J Clin Pathol. 94, 187-91.
Kim, S., et al., 2004. Zinc uptake system (znuA locus) of Brucella abortus is essential for intracellular survival and virulence in mice. J Vet Med Sci. 66, 1059-63.
Kim, S. H., et al., 2011. Helicobacter pylori arginase mutant colonizes arginase II knockout mice. World J Gastroenterol. 17, 3300-9.

Kinne-Saffran, E., Kinne, R. K., 1999. Vitalism and synthesis of urea. From Friedrich Wohler to Hans A. Krebs. Am J Nephrol. 19, 290-4.
Kobashi, K., et al., 1971. Effect of acyl residues of hydroxamic acids on urease inhibition. Biochim Biophys Acta. 227, 429-41.
Kochan, I., 1973. The role of iron in bacterial infections, with special consideration of host-tubercle bacillus interaction. Curr Top Microbiol Immunol. 60, 1-30.
Kojima, S., et al., 2007. AtDUR3 represents the major transporter for high-affinity urea transport across the plasma membrane of nitrogen-deficient Arabidopsis roots. Plant J. 52, 30-40.
Kojima, S., et al., 2006. Molecular mechanisms of urea transport in plants. J Membr Biol. 212, 83-91.
Kono, Y., et al., 1995. Alterations in superoxide dismutase and catalase in Fusarium oxysporum during starvation-induced differentiation. Biochim Biophys Acta. 1268, 35-40.
Kossel A., D. H. D., 1904. Über die Arginase. Z Physiol Chem. 41, 321-331.
Krajewska, B., 2009. Ureases I. Functional, catalytic and kinetic properties: A review. J Mol Catal B Enzym. 59, 9-21.
Kramer-Haimovich, H., et al., 2006. Effect of ammonia production by Colletotrichum gloeosporioides on pelB activation, pectate lyase secretion, and fruit pathogenicity. Appl Environ Microbiol. 72, 1034-9.
Krantz, M., et al., 2006. Comparative genomics of the HOG-signalling system in fungi. Curr Genet. 49, 137-51.
Krishnamurthy, P., et al., 1998. Helicobacter pylori containing only cytoplasmic urease is susceptible to acid. Infect Immun. 66, 5060-6.
Krogmeier, M. J., et al., 1989. Phytotoxicity of foliar-applied urea. Proc Natl Acad Sci U S A. 86, 8189-91.
Kudla, B., et al., 1990. The regulatory gene areA mediating nitrogen metabolite repression in Aspergillus nidulans. Mutations affecting specificity of gene activation alter a loop residue of a putative zinc finger. EMBO J. 9, 1355-64.
Kuhn, N. J., et al., 1995. Purification of human hepatic arginase and its manganese (II)-dependent and pH-dependent interconversion between active and inactive forms: a possible pH-sensing function of the enzyme on the ornithine cycle. Arch Biochem Biophys. 320, 24-34.
Kullberg, B. J., et al., 1999. Modulation of neutrophil function in host defense against disseminated Candida albicans infection in mice. FEMS Immunol Med Microbiol. 26, 299-307.
Kumamoto, C. A., Vinces, M. D., 2005. Contributions of hyphae and hypha-co-regulated genes to Candida albicans virulence. Cell Microbiol. 7, 1546-54.
Kuswandi, B., 2003. Simple optical fibre biosensor based on immobilised enzyme for monitoring of trace heavy metal ions. Anal Bioanal Chem. 376, 1104-10.
Labadorf, A., et al., 2010. Genome-wide analysis of alternative splicing in Chlamydomonas reinhardtii. BMC Genomics. 11, 114.
Labigne, A., et al., 1991. Shuttle cloning and nucleotide sequences of Helicobacter pylori genes responsible for urease activity. J Bacteriol. 173, 1920-31.
Lahiri, A., et al., 2008. Arginase modulates Salmonella induced nitric oxide production in RAW264.7 macrophages and is required for Salmonella pathogenesis in mice model of infection. Microbes Infect. 10, 1166-74.
Lahiri, A., et al., 2010. New tricks new ways: exploitation of a multifunctional enzyme arginase by pathogens. Virulence. 1, 563-5.
Lalonde, S., et al., 2004. Transport mechanisms for organic forms of carbon and nitrogen between source and sink. Annu Rev Plant Biol. 55, 341-72.
Lanver, D., et al., 2010. Sho1 and Msb2-related proteins regulate appressorium development in the smut fungus Ustilago maydis. Plant Cell. 22, 2085-101.

Larena, I., et al., 2002. Production, Survival, and Evaluation of Solid-Substrate Inocula of Penicillium oxalicum, a Biocontrol Agent Against Fusarium Wilt of Tomato. Phytopathology. 92, 863-9.
Larkin, R. P., Fravel, D. R., 2002. Effects of Varying Environmental Conditions on Biological Control of Fusarium Wilt of Tomato by Nonpathogenic Fusarium spp. Phytopathology. 92, 1160-6.
Latge, J. P., 1999. Aspergillus fumigatus and aspergillosis. Clin Microbiol Rev. 12, 310-50.
Latge, J. P., 2001. The pathobiology of Aspergillus fumigatus. Trends Microbiol. 9, 382-9.
Lea, P. J., Sodek, L., Parry, M.A.J., Shewry, R., Halford, N.G., 2007. Asparagine in plants. Ann Appl. Biol. 150, 1-26.
Lee, M. H., et al., 1992. Klebsiella aerogenes urease gene cluster: sequence of ureD and demonstration that four accessory genes (ureD, ureE, ureF, and ureG) are involved in nickel metallocenter biosynthesis. J Bacteriol. 174, 4324-30.
Lee, S. G., Calhoun, D. H., 1997. Urease from a potentially pathogenic coccoid isolate: purification, characterization, and comparison to other microbial ureases. Infect Immun. 65, 3991-6.
Leipe, D. D., et al., 2002. Classification and evolution of P-loop GTPases and related ATPases. J Mol Biol. 317, 41-72.
Levin, D. E., 2005. Cell wall integrity signaling in Saccharomyces cerevisiae. Microbiol Mol Biol Rev. 69, 262-91.
Lewis, L. E., et al., 2012a. Stage specific assessment of Candida albicans phagocytosis by macrophages identifies cell wall composition and morphogenesis as key determinants. PLoS Pathog. 8, e1002578.
Lewis, L. E., et al., 2012b. Candida albicans infection inhibits macrophage cell division and proliferation. Fungal Genet Biol. 49, 679-80.
Li Destri Nicosia, M. G., et al., 2001. Heterologous transposition in Aspergillus nidulans. Mol Microbiol. 39, 1330-44.
Li, K., et al., 2001. Recombinant urease and urease DNA of Coccidioides immitis elicit an immunoprotective response against coccidioidomycosis in mice. Infect Immun. 69, 2878-87.
Liesegang, T. J., Forster, R. K., 1980. Spectrum of microbial keratitis in South Florida. Am J Ophthalmol. 90, 38-47.
Liu, H., et al., 1993. Elements of the yeast pheromone response pathway required for filamentous growth of diploids. Science. 262, 1741-4.
Liu, L. H., et al., 2003. AtDUR3 encodes a new type of high-affinity urea/H+ symporter in Arabidopsis. Plant Cell. 15, 790-800.
Liuzzi, J. P., et al., 2005. Interleukin-6 regulates the zinc transporter Zip14 in liver and contributes to the hypozincemia of the acute-phase response. Proc Natl Acad Sci U S A. 102, 6843-8.
Lopez-Berges, M. S., et al., 2009. Identification of virulence genes in Fusarium oxysporum f. sp. lycopersici by large-scale transposon tagging. Mol Plant Pathol. 10, 95-107.
Lopez-Berges, M. S., et al., 2012. HapX-mediated iron homeostasis is essential for rhizosphere competence and virulence of the soilborne pathogen Fusarium oxysporum. Plant Cell. 24, 3805-22.
Lopez-Berges, M. S., et al., 2013. The velvet complex governs mycotoxin production and virulence of Fusarium oxysporum on plant and mammalian hosts. Mol Microbiol. 87, 49-65.
Lopez-Berges, M. S., et al., 2010. A nitrogen response pathway regulates virulence functions in Fusarium oxysporum via the protein kinase TOR and the bZIP protein MeaB. Plant Cell. 22, 2459-75.
Lopez-Berges, M. S., et al., 2014. Combinatorial function of velvet and AreA in transcriptional regulation of nitrate utilization and secondary metabolism. Fungal Genet Biol. 62, 78-84.
Lorenz, M. C., et al., 2004. Transcriptional response of Candida albicans upon internalization by macrophages. Eukaryot Cell. 3, 1076-87.

Low, C. Y., Rotstein, C., 2011. Emerging fungal infections in immunocompromised patients. F1000 Med Rep. 3**,** 14.

Lubbers, M. W., et al., 1996. Purification and characterization of urease from schizosaccharomyces pombe. Can J Microbiol. 42**,** 132-40.

Luo, Y., et al., 2008. The outcome of phagocytic cell division with infectious cargo depends on single phagosome formation. PLoS One. 3**,** e3219.

Lutfiyya, L. L., et al., 1998. Characterization of three related glucose repressors and genes they regulate in Saccharomyces cerevisiae. Genetics. 150**,** 1377-91.

Lutfiyya, L. L., Johnston, M., 1996. Two zinc-finger-containing repressors are responsible for glucose repression of SUC2 expression. Mol Cell Biol. 16**,** 4790-7.

Luther, K., et al., 2007. Phagocytosis of Aspergillus fumigatus conidia by murine macrophages involves recognition by the dectin-1 beta-glucan receptor and Toll-like receptor 2. Cell Microbiol. 9**,** 368-81.

Ma, L. J., et al., 2010. Comparative genomics reveals mobile pathogenicity chromosomes in Fusarium. Nature. 464**,** 367-73.

Ma, Y., et al., 2008. The sho1 sensor regulates growth, morphology, and oxidant adaptation in Aspergillus fumigatus but is not essential for development of invasive pulmonary aspergillosis. Infect Immun. 76**,** 1695-701.

Madrid, M. P., et al., 2003. Class V chitin synthase determines pathogenesis in the vascular wilt fungus Fusarium oxysporum and mediates resistance to plant defence compounds. Mol Microbiol. 47**,** 257-66.

Magasanik, B., 1988. Reversible phosphorylation of an enhancer binding protein regulates the transcription of bacterial nitrogen utilization genes. Trends Biochem Sci. 13**,** 475-9.

Mai, U. E., et al., 1992. Surface proteins from Helicobacter pylori exhibit chemotactic activity for human leukocytes and are present in gastric mucosa. J Exp Med. 175**,** 517-25.

Mai, U. E., et al., 1991. Soluble surface proteins from Helicobacter pylori activate monocytes/macrophages by lipopolysaccharide-independent mechanism. J Clin Invest. 87**,** 894-900.

Maier, T., et al., 1993. The product of the hypB gene, which is required for nickel incorporation into hydrogenases, is a novel guanine nucleotide-binding protein. J Bacteriol. 175**,** 630-5.

Maiti, I. B., Kolattukudy, P. E., 1979. Prevention of fungal infection of plants by specific inhibition of cutinase. Science. 205**,** 507-8.

Makristathis, A., et al., 1998. Highly significant role of Helicobacter pylori urease in phagocytosis and production of oxygen metabolites by human granulocytes. J Infect Dis. 177**,** 803-6.

Marletta, M. A., et al., 1988. Macrophage oxidation of L-arginine to nitrite and nitrate: nitric oxide is an intermediate. Biochemistry. 27**,** 8706-11.

Marr, K. A., et al., 2004. Detection of galactomannan antigenemia by enzyme immunoassay for the diagnosis of invasive aspergillosis: variables that affect performance. J Infect Dis. 190**,** 641-9.

Marshall, B. J., Barrett, L.J., Prakesh, C., McCallum, R.W., Guerrant, R.L. (Ed.) 1988. Protection of Campylobacter pyloridis nut not Campylobacter jejuni against acid susceptibility by urea. University of Göteborg, Göteborg, Sweden.

Martin de Llano, J. J., et al., 1989. Selective silver staining of urease activity in polyacrylamide gels. Anal Biochem. 177**,** 37-40.

Martinez-Rocha, A. L., et al., 2008. Rho1 has distinct functions in morphogenesis, cell wall biosynthesis and virulence of Fusarium oxysporum. Cell Microbiol. 10**,** 1339-51.

Marzluf, G. A., 1997. Genetic regulation of nitrogen metabolism in the fungi. Microbiol Mol Biol Rev. 61**,** 17-32.

Maurer, M., et al., 2006. Treatment processes for source-separated urine. Water Res. 40**,** 3151-66.

Mayayo, E., et al., 1999. Experimental pathogenicity of four opportunist Fusarium species in a murine model. J Med Microbiol. 48, 363-6.
McDonald, J. A., et al., 1972. Urease: a sensitive and specific radiometric assay. Enzymologia. 42, 1-9.
McGee, D. J., Mobley, H. L., 2000. Pathogenesis of Helicobacter pylori infection. Curr Opin Gastroenterol. 16, 24-31.
McGee, D. J., et al., 1999. Helicobacter pylori rocF is required for arginase activity and acid protection in vitro but is not essential for colonization of mice or for urease activity. J Bacteriol. 181, 7314-22.
McKenzie, C. G., et al., 2010. Contribution of Candida albicans cell wall components to recognition by and escape from murine macrophages. Infect Immun. 78, 1650-8.
Mech, F., et al., 2011. Automated image analysis of the host-pathogen interaction between phagocytes and Aspergillus fumigatus. PLoS One. 6, e19591.
Mehta, N., et al., 2003. Roles of conserved nucleotide-binding domains in accessory proteins, HypB and UreG, in the maturation of nickel-enzymes required for efficient Helicobacter pylori colonization. Microb Pathog. 35, 229-34.
Mendoza-Mendoza, A., et al., 2009. Hap2 regulates the pheromone response transcription factor prf1 in Ustilago maydis. Mol Microbiol. 72, 683-98.
Mendz, G. L., Hazell, S. L., 1996. The urea cycle of Helicobacter pylori. Microbiology. 142 (Pt 10), 2959-67.
Mendz, G. L., et al., 1998. In situ characterization of Helicobacter pylori arginase. Biochim Biophys Acta. 1388, 465-77.
Menegassi, A., et al., 2008. Urease from cotton (Gossypium hirsutum) seeds: isolation, physicochemical characterization, and antifungal properties of the protein. J Agric Food Chem. 56, 4399-405.
Merigout, P., et al., 2008. Physiological and transcriptomic aspects of urea uptake and assimilation in Arabidopsis plants. Plant Physiol. 147, 1225-38.
Meyer-Bothling, L. E., Polacco, J. C., 1987. Mutational analysis of the embryo-specific urease locus of soybean. Mol Gen Genet. 209, 439-44.
Meyer-Bothling, L. E., et al., 1987. Pleiotropic soybean mutants defective in both urease isozymes. Mol Gen Genet. 209, 432-8.
Michielse, C. B., Rep, M., 2009a. Pathogen profile update: Fusarium oxysporum. Molecular Plant Pathology. 10, 311-324
Michielse, C. B., Rep, M., 2009b. Pathogen profile update: Fusarium oxysporum. Mol Plant Pathol. 10, 311-24.
Michielse, C. B., et al., 2009. Insight into the molecular requirements for pathogenicity of Fusarium oxysporum f. sp. lycopersici through large-scale insertional mutagenesis. Genome Biol. 10, R4.
Mirbod-Donovan, F., et al., 2006. Urease produced by Coccidioides posadasii contributes to the virulence of this respiratory pathogen. Infect Immun. 74, 504-15.
Mirbod, F., et al., 2002. Purification and characterization of urease isolated from the pathogenic fungus Coccidioides immitis. Med Mycol. 40, 35-44.
Mobley, H. L., et al., 1988. Characterization of urease from Campylobacter pylori. J Clin Microbiol. 26, 831-6.
Mobley, H. L., Hausinger, R. P., 1989. Microbial ureases: significance, regulation, and molecular characterization. Microbiol Rev. 53, 85-108.
Mobley, H. L., et al., 1995. Molecular biology of microbial ureases. Microbiol Rev. 59, 451-80.
Mohamed, M. S., Greenberg, D. M., 1945. Liver arginase; preparation of extracts of high potency, chemical properties, activation-inhibitation, and pH-activity. Arch Biochem. 8, 349-64.

Moncrief, M. B., Hausinger, R. P., 1997. Characterization of UreG, identification of a UreD-UreF-UreG complex, and evidence suggesting that a nucleotide-binding site in UreG is required for in vivo metallocenter assembly of Klebsiella aerogenes urease. J Bacteriol. 179**,** 4081-6.

Montalvo, J. G., Jr., 1970. An improved urease electrode. Anal Biochem. 38**,** 357-63.

Mora, J., et al., 1965. Characteristics of arginases from ureotelic and non-ureotelic animals. Biochem J. 96**,** 588-94.

Moreno, F., et al., 2005. Glucose sensing through the Hxk2-dependent signalling pathway. Biochem Soc Trans. 33**,** 265-8.

Mori, M., 2007. Regulation of nitric oxide synthesis and apoptosis by arginase and arginine recycling. J Nutr. 137**,** 1616S-1620S.

Morsdorf, G., Kaltwasser, H., 1989. Ammonium assimilation in Proteus vulgaris, Bacillus pasteurii, and Sporosarcina ureae. Arch Microbiol. 152**,** 125-31.

Mosch, H. U., et al., 1996. Ras2 signals via the Cdc42/Ste20/mitogen-activated protein kinase module to induce filamentous growth in Saccharomyces cerevisiae. Proc Natl Acad Sci U S A. 93**,** 5352-6.

Motley, S. T., et al., 2004. Simultaneous analysis of host and pathogen interactions during an in vivo infection reveals local induction of host acute phase response proteins, a novel bacterial stress response, and evidence of a host-imposed metal ion limited environment. Cell Microbiol. 6**,** 849-65.

Mulrooney, S. B., Hausinger, R. P., 1990. Sequence of the Klebsiella aerogenes urease genes and evidence for accessory proteins facilitating nickel incorporation. J Bacteriol. 172**,** 5837-43.

Mulrooney, S. B., Hausinger, R. P., 2003. Nickel uptake and utilization by microorganisms. FEMS Microbiol Rev. 27**,** 239-61.

Mulrooney, S. B., et al., 1989. Regulation of gene expression and cellular localization of cloned Klebsiella aerogenes (K. pneumoniae) urease. J Gen Microbiol. 135**,** 1769-76.

Mulvaney, R. L., Bremner, J.M., 1981. Soil Biochem. 5**,** 153- 196.

Munder, M., et al., 1999. Th1/Th2-regulated expression of arginase isoforms in murine macrophages and dendritic cells. J Immunol. 163**,** 3771-7.

Musher, B., et al., 2004. Aspergillus galactomannan enzyme immunoassay and quantitative PCR for diagnosis of invasive aspergillosis with bronchoalveolar lavage fluid. J Clin Microbiol. 42**,** 5517-22.

Naggie, S., Perfect, J. R., 2009. Molds: hyalohyphomycosis, phaeohyphomycosis, and zygomycosis. Clin Chest Med. 30**,** 337-53, vii-viii.

Namiki, F., et al., 2001. Mutation of an arginine biosynthesis gene causes reduced pathogenicity in Fusarium oxysporum f. sp. melonis. Mol Plant Microbe Interact. 14**,** 580-4.

Nathan, C., Shiloh, M. U., 2000. Reactive oxygen and nitrogen intermediates in the relationship between mammalian hosts and microbial pathogens. Proc Natl Acad Sci U S A. 97**,** 8841-8.

Navarathna, D. H., et al., 2010. Evolutionary aspects of urea utilization by fungi. FEMS Yeast Res. 10**,** 209-13.

Navarro-Velasco, G. Y., et al., 2011. Galleria mellonella as model host for the trans-kingdom pathogen Fusarium oxysporum. Fungal Genet Biol. 48**,** 1124-9.

Nelson, P. E. (Ed.) 1981a. Fungal Wilt Diseases of Plants: Life cycle and epidemiology of Fusarium oxysporum. Academic Press, Inc., New York, N.Y.

Nelson, P. E., 1981b. Fungal Wilt Diseases of Plants: Life cycle and epidemiology of Fusarium oxysporum:. Academic Press, Inc., New York,. 51–80.

Nelson, P. E., et al., 1994. Taxonomy, biology, and clinical aspects of Fusarium species. Clin Microbiol Rev. 7**,** 479-504.

Netea, M. G., et al., 1999. Increased susceptibility of TNF-alpha lymphotoxin-alpha double knockout mice to systemic candidiasis through impaired recruitment of neutrophils and phagocytosis of Candida albicans. J Immunol. 163, 1498-505.
Newman, S. L., et al., 2005. Enhanced killing of Candida albicans by human macrophages adherent to type 1 collagen matrices via induction of phagolysosomal fusion. Infect Immun. 73, 770-7.
Neyroz, P., et al., 2006. Intrinsically disordered structure of Bacillus pasteurii UreG as revealed by steady-state and time-resolved fluorescence spectroscopy. Biochemistry. 45, 8918-30.
Norice, C. T., et al., 2007. Requirement for Candida albicans Sun41 in biofilm formation and virulence. Eukaryot Cell. 6, 2046-55.
Nucci, M., Anaissie, E., 2002. Cutaneous infection by Fusarium species in healthy and immunocompromised hosts: implications for diagnosis and management. Clin Infect Dis. 35, 909-20.
Nucci, M., Anaissie, E., 2006. Emerging fungi. Infect Dis Clin North Am. 20, 563-79.
Nucci, M., Anaissie, E., 2007. Fusarium infections in immunocompromised patients. Clin Microbiol Rev. 20, 695-704.
O'Donnell, K., et al., 1998. Multiple evolutionary origins of the fungus causing Panama disease of banana: concordant evidence from nuclear and mitochondrial gene genealogies. Proc Natl Acad Sci U S A. 95, 2044-9.
O'Rourke, S. M., Herskowitz, I., 1998. The Hog1 MAPK prevents cross talk between the HOG and pheromone response MAPK pathways in Saccharomyces cerevisiae. Genes Dev. 12, 2874-86.
Odake, S., et al., 1994. Inhibition of Helicobacter pylori urease activity by hydroxamic acid derivatives. Biol Pharm Bull. 17, 1329-32.
Odake, S., et al., 1992. Inhibition of urease activity by dipeptidyl hydroxamic acids. Chem Pharm Bull (Tokyo). 40, 2764-8.
Odds, F. C., 1988. Candida and candidiasis. Bailliere: Tindall.
Odds, F. C., et al., 1998. Evaluation of possible correlations between antifungal susceptibilities of filamentous fungi in vitro and antifungal treatment outcomes in animal infection models. Antimicrob Agents Chemother. 42, 282-8.
Olson, J. W., Maier, R. J., 2002. Molecular hydrogen as an energy source for Helicobacter pylori. Science. 298, 1788-90.
Olson, J. W., et al., 2001. Requirement of nickel metabolism proteins HypA and HypB for full activity of both hydrogenase and urease in Helicobacter pylori. Mol Microbiol. 39, 176-82.
Olszewski, M. A., et al., 2004. Urease expression by Cryptococcus neoformans promotes microvascular sequestration, thereby enhancing central nervous system invasion. Am J Pathol. 164, 1761-71.
Ori, N., et al., 1997. The I2C family from the wilt disease resistance locus I2 belongs to the nucleotide binding, leucine-rich repeat superfamily of plant resistance genes. Plant Cell. 9, 521-32.
Ortoneda, M., et al., 2004. Fusarium oxysporum as a multihost model for the genetic dissection of fungal virulence in plants and mammals. Infect Immun. 72, 1760-6.
Ospina-Giraldo, M. D., et al., 2003. Loss of function of the Fusarium oxysporum SNF1 gene reduces virulence on cabbage and Arabidopsis. Curr Genet. 44, 49-57.
Osterholzer, J. J., et al., 2009. Cryptococcal urease promotes the accumulation of immature dendritic cells and a non-protective T2 immune response within the lung. Am J Pathol. 174, 932-43.
Ozcan, S., Johnston, M., 1999. Function and regulation of yeast hexose transporters. Microbiol Mol Biol Rev. 63, 554-69.
Palmer, R. M., et al., 1988. Vascular endothelial cells synthesize nitric oxide from L-arginine. Nature. 333, 664-6.
Palmer, R. M., et al., 1987. Nitric oxide release accounts for the biological activity of endothelium-derived relaxing factor. Nature. 327, 524-6.

Panina, E. M., et al., 2003. Comparative genomics of bacterial zinc regulons: enhanced ion transport, pathogenesis, and rearrangement of ribosomal proteins. Proc Natl Acad Sci U S A. 100, 9912-7.
Pareja-Jaime, Y., et al., 2010. Chitin synthase-deficient mutant of Fusarium oxysporum elicits tomato plant defence response and protects against wild-type infection. Mol Plant Pathol. 11, 479-93.
Pareja-Jaime, Y., et al., 2008. Tomatinase from Fusarium oxysporum f. sp. lycopersici is required for full virulence on tomato plants. Mol Plant Microbe Interact. 21, 728-36.
Park, B. J., et al., 2009. Estimation of the current global burden of cryptococcal meningitis among persons living with HIV/AIDS. AIDS. 23, 525-30.
Park, I. S., Hausinger, R. P., 1995. Requirement of carbon dioxide for in vitro assembly of the urease nickel metallocenter. Science. 267, 1156-8.
Pasquali, P., et al., 2008. Attenuated Salmonella enterica serovar Typhimurium lacking the ZnuABC transporter confers immune-based protection against challenge infections in mice. Vaccine. 26, 3421-6.
Patterson, T. F., et al., 2009. Case records of the Massachusetts General Hospital. Case 22-2009. A 59-year-old man with skin and pulmonary lesions after chemotherapy for leukemia [corrected]. N Engl J Med. 361, 287-96.
Paul, E. N. M., Cecilia, D. E., J.A., 1994. Taxonomy, biology, and clinical aspect of *Fusarium* species. Clin. Microbiol. Rev., . 7, 479- 504.
Perez-Nadales, E., Di Pietro, A., 2011. The membrane mucin Msb2 regulates invasive growth and plant infection in Fusarium oxysporum. Plant Cell. 23, 1171-85.
Phadnis, S. H., et al., 1996. Surface localization of Helicobacter pylori urease and a heat shock protein homolog requires bacterial autolysis. Infect Immun. 64, 905-12.
Pietro, A. D., et al., 2003. Fusarium oxysporum: exploring the molecular arsenal of a vascular wilt fungus. Mol Plant Pathol. 4, 315-25.
Pitoniak, A., et al., 2009. The signaling mucins Msb2 and Hkr1 differentially regulate the filamentation mitogen-activated protein kinase pathway and contribute to a multimodal response. Mol Biol Cell. 20, 3101-14.
Polacco, J. C., Havir, E. A., 1979. Comparisons of soybean urease isolated from seed and tissue culture. J Biol Chem. 254, 1707-15.
Polacco, J. C., Holland, M.A., 1993a. Roles of urease in plant cells. International Review of Cytology-A Survey of Cell Biology. 145, 65-103.
Polacco, J. C., Holland, M.A., 1993b. Roles of urease in plant cells. Int Rev Cytol. 145, 65–103.
Polack, F. M., et al., 1971. Keratomycosis. Medical and surgical treatment. Arch Ophthalmol. 85, 410-6.
Ponnambalam, S., Baldwin, S. A., 2003. Constitutive protein secretion from the trans-Golgi network to the plasma membrane. Mol Membr Biol. 20, 129-39.
Pope, A. J., et al., 1998. Effect of potent urease inhibitor, fluorofamide, on Helicobacter sp. in vivo and in vitro. Dig Dis Sci. 43, 109-19.
Prados-Rosales, R. C., et al., 2012. A PR-1-like protein of Fusarium oxysporum functions in virulence on mammalian hosts. J Biol Chem. 287, 21970-9.
Prados Rosales, R. C., Di Pietro, A., 2008. Vegetative hyphal fusion is not essential for plant infection by Fusarium oxysporum. Eukaryot Cell. 7, 162-71.
Prusky, D., et al., 2001. Local modulation of host pH by Colletotrichum species as a mechanism to increase virulence. Mol Plant Microbe Interact. 14, 1105-13.
Qi, M., Elion, E. A., 2005. MAP kinase pathways. J Cell Sci. 118, 3569-72.
Qui-Xiang, L., Freney, J.R., Keerthisinghe, D.G., Peoples, M.B., 1994. Soil Biol. Biochem. 26, 1059-1065.
Ragsdale, S. W., 2009. Nickel-based Enzyme Systems. J Biol Chem. 284, 18571-5.

Real-Guerra, R., et al., 2012. Biochemical and structural studies on native and recombinant Glycine max UreG: a detailed characterization of a plant urease accessory protein. Plant Mol Biol. 78, 461-75.

Reczkowski, R. S., Ash, D. E., 1994. Rat liver arginase: kinetic mechanism, alternate substrates, and inhibitors. Arch Biochem Biophys. 312, 31-7.

Reitzer, L. J. (Ed.) 1996. Ammonia assimilation and the biosythesis of glutamine, glutamate, aspartate, asparagine, L-alanine and D-alanine. American Society for Microbiology (ASM) Press, Washington, DC.

Rep, M., et al., 2004. A small, cysteine-rich protein secreted by Fusarium oxysporum during colonization of xylem vessels is required for I-3-mediated resistance in tomato. Mol Microbiol. 53, 1373-83.

Reuben, A., et al., 1989. Antifungal susceptibility of 44 clinical isolates of Fusarium species determined by using a broth microdilution method. Antimicrob Agents Chemother. 33, 1647-9.

Rey, L., et al., 1994. Purification of Rhizobium leguminosarum HypB, a nickel-binding protein required for hydrogenase synthesis. J Bacteriol. 176, 6066-73.

Reyes-Dominguez, Y., et al., 2010. Heterochromatic marks are associated with the repression of secondary metabolism clusters in Aspergillus nidulans. Mol Microbiol. 76, 1376-86.

Rispail, N., Di Pietro, A., 2009. Fusarium oxysporum Ste12 controls invasive growth and virulence downstream of the Fmk1 MAPK cascade. Mol Plant Microbe Interact. 22, 830-9.

Rispail, N., et al., 2009. Comparative genomics of MAP kinase and calcium-calcineurin signalling components in plant and human pathogenic fungi. Fungal Genet Biol. 46, 287-98.

Roberts, R. L., Fink, G. R., 1994. Elements of a single MAP kinase cascade in Saccharomyces cerevisiae mediate two developmental programs in the same cell type: mating and invasive growth. Genes Dev. 8, 2974-85.

Rodman, J. S., 1999. Struvite stones. Nephron. 81 Suppl 1, 50-9.

Rodrigues, M. L., et al., 2008. Extracellular vesicles produced by Cryptococcus neoformans contain protein components associated with virulence. Eukaryot Cell. 7, 58-67.

Rodrigues, M. L., et al., 2007. Vesicular polysaccharide export in Cryptococcus neoformans is a eukaryotic solution to the problem of fungal trans-cell wall transport. Eukaryot Cell. 6, 48-59.

Rohde, J. R., Cardenas, M. E., 2004. Nutrient signaling through TOR kinases controls gene expression and cellular differentiation in fungi. Curr Top Microbiol Immunol. 279, 53-72.

Roldan-Arjona, T., et al., 1999. Tomatinase from Fusarium oxysporum f. sp. lycopersici defines a new class of saponinases. Mol Plant Microbe Interact. 12, 852-61.

Rolland, F., et al., 2000. Glucose-induced cAMP signalling in yeast requires both a G-protein coupled receptor system for extracellular glucose detection and a separable hexose kinase-dependent sensing process. Mol Microbiol. 38, 348-58.

Rolland, F., et al., 2002. Glucose-sensing and -signalling mechanisms in yeast. FEMS Yeast Res. 2, 183-201.

Roman, E., et al., 2009. Msb2 signaling mucin controls activation of Cek1 mitogen-activated protein kinase in Candida albicans. Eukaryot Cell. 8, 1235-49.

Roman, E., et al., 2005. The Sho1 adaptor protein links oxidative stress to morphogenesis and cell wall biosynthesis in the fungal pathogen Candida albicans. Mol Cell Biol. 25, 10611-27.

Roncero, C., Duran, A., 1985. Effect of Calcofluor white and Congo red on fungal cell wall morphogenesis: in vivo activation of chitin polymerization. J Bacteriol. 163, 1180-5.

Ronne-Engstrom, E., et al., 2001. Intracerebral microdialysis in neurointensive care: the use of urea as an endogenous reference compound. J Neurosurg. 94, 397-402.

Roon, R. J., et al., 1972. Urea amidolyase. The involvement of biotin in urea cleavage. J Biol Chem. 247, 7539-45.

Roon, R. J., Levenberg, B., 1972. Urea amidolyase. I. Properties of the enzyme from Candida utilis. J Biol Chem. 247**,** 4107-13.
Rose, W. C., et al., 1954. The amino acid requirements of man. V. The role of lysine, arginine, and tryptophan. J Biol Chem. 206**,** 421-30.
Rosenstein, I., et al., 1980. The effect of acetohydroxamic acid on the induction of bacterial ureases. Invest Urol. 18**,** 112-4.
Rosenstein, I. J., Hamilton-Miller, J. M., 1984. Inhibitors of urease as chemotherapeutic agents. Crit Rev Microbiol. 11**,** 1-12.
Rosenstein, I. J., et al., 1981. Role of urease in the formation of infection stones: comparison of ureases from different sources. Infect Immun. 32**,** 32-7.
Rotowa, N. A., et al., 1990. In vitro activities of polyene and imidazole antifungal agents against unusual opportunistic fungal pathogens. Mycoses. 33**,** 203-11.
Rudkin, F. M., et al., 2013. Altered dynamics of Candida albicans phagocytosis by macrophages and PMNs when both phagocyte subsets are present. MBio. 4**,** e00810-13.
Ruiz-Herrera, J., Gonzalez, J., 1969. A continuous method for the measurement of urease activity. Anal Biochem. 31**,** 366-74.
Ruiz-Roldan, M. C., et al., 2008. Role of the white collar 1 photoreceptor in carotenogenesis, UV resistance, hydrophobicity, and virulence of Fusarium oxysporum. Eukaryot Cell. 7**,** 1227-30.
Ryals, J. A., et al., 1996. Systemic Acquired Resistance. Plant Cell. 8**,** 1809-1819.
Salomone-Stagni, M., et al., 2007. A model-based proposal for the role of UreF as a GTPase-activating protein in the urease active site biosynthesis. Proteins. 68**,** 749-61.
Santangelo, G. M., 2006. Glucose signaling in Saccharomyces cerevisiae. Microbiol Mol Biol Rev. 70**,** 253-82.
Saraste, M., et al., 1990. The P-loop--a common motif in ATP- and GTP-binding proteins. Trends Biochem Sci. 15**,** 430-4.
Sarikaya Bayram, O., et al., 2010. LaeA control of velvet family regulatory proteins for light-dependent development and fungal cell-type specificity. PLoS Genet. 6**,** e1001226.
Scazzocchio, C., 2000. The fungal GATA factors. Curr Opin Microbiol. 3**,** 126-31.
Scazzocchio, C., Darlington, A. J., 1968. The induction and repression of the enzymes of purine breakdown in Aspergillus nidulans. Biochim Biophys Acta. 166**,** 557-68.
Schafer, K., et al., 2014. Murine Model for Fusarium oxysporum Invasive Fusariosis Reveals Organ-Specific Structures for Dissemination and Long-Term Persistence. PLoS One. 9**,** e89920.
Schäfer, K., et al., 2014. Murine Model for Fusarium oxysporum Invasive Fusariosis Reveals Organ-Specific Structures for Dissemination and Long-Term Persistence. PLoS One. 9**,** e89920.
Schippers, B., and W. H. van Eck (Ed.) 1981a. Formation and survival of chlamydospores in Fusarium. In P. E. Nelson, T. A. Toussoun, and R. J. Cook (ed.).
Schippers, B. a. V. E., W.H (Ed.) 1981b. Formation and survival of chlamydospores in Fusarium. Universitiy Park and London., The Pennsylvania State University Press.
Schreiber, S., et al., 2004. The spatial orientation of Helicobacter pylori in the gastric mucus. Proc Natl Acad Sci U S A. 101**,** 5024-9.
Schrettl, M., et al., 2010. HapX-mediated adaption to iron starvation is crucial for virulence of Aspergillus fumigatus. PLoS Pathog. 6**,** e1001124.
Seet, B. T., Pawson, T., 2004. MAPK signaling: Sho business. Curr Biol. 14**,** R708-10.
Shaik, M. M., et al., 1980. An improved method for the detection and preservation of urease activity in polyacrylamide gels. Anal Biochem. 103**,** 140-3.
Shaked-Mishan, P., et al., 2006. A novel high-affinity arginine transporter from the human parasitic protozoan Leishmania donovani. Mol Microbiol. 60**,** 30-8.

Sheppard, D. C., et al., 2006. Comparison of three methodologies for the determination of pulmonary fungal burden in experimental murine aspergillosis. Clin Microbiol Infect. 12, 376-80.
Shi, M., et al., 2010. Real-time imaging of trapping and urease-dependent transmigration of Cryptococcus neoformans in mouse brain. J Clin Invest. 120, 1683-93.
Silveira, F. P., Husain, S., 2007. Fungal infections in solid organ transplantation. Med Mycol. 45, 305-20.
Singh, A., et al., 2013. Factors required for activation of urease as a virulence determinant in Cryptococcus neoformans. MBio. 4, e00220-13.
Sissons, C. H., et al., 1992. Processes involved in the regulation of urease levels in Streptococcus salivarius by pH. Oral Microbiol Immunol. 7, 159-64.
Sissons, C. H., et al., 1990. pH regulation of urease levels in Streptococcus salivarius. J Dent Res. 69, 1131-7.
Slocum, R. D., 2005. Genes, enzymes and regulation of arginine biosynthesis in plants. Plant Physiol Biochem. 43, 729-45.
Smith, C. P., 2009. Mammalian urea transporters. Exp Physiol. 94, 180-5.
Snyder, W. C., Hansen, H. N., 1940. The species concept in Fusarium. Am. J. Bot. . 27, 64-67.
Snyder, W. C., Hansen, H.N, 1940. The species concept in Fusarium. Am J Bot. 27, 64-67.
Sole, A., et al., 2005. Aspergillus infections in lung transplant recipients: risk factors and outcome. Clin Microbiol Infect. 11, 359-65.
Somssich, I. E. a. H., K., 1998. Pathogen defense in plants - a paradigm of biological complexity. Trends Plant Sci. 3, 86-90.
Sonoki, T., et al., 1997. Coinduction of nitric-oxide synthase and arginase I in cultured rat peritoneal macrophages and rat tissues in vivo by lipopolysaccharide. J Biol Chem. 272, 3689-93.
Soriano, A., et al., 2000. UreE stimulation of GTP-dependent urease activation in the UreD-UreF-UreG-urease apoprotein complex. Biochemistry. 39, 12435-40.
Soriano, A., Hausinger, R. P., 1999. GTP-dependent activation of urease apoprotein in complex with the UreD, UreF, and UreG accessory proteins. Proc Natl Acad Sci U S A. 96, 11140-4.
Soto, G., et al., 2010. TIP5;1 is an aquaporin specifically targeted to pollen mitochondria and is probably involved in nitrogen remobilization in Arabidopsis thaliana. Plant J. 64, 1038-47.
Staib, F., et al., 1978. Epidemiology of Cryptococcus neoformans. Mycopathologia. 65, 73-6.
Staib, F., et al., 1976. Growth of Cryptococcus neoformans on uric acid agar. Zentralbl Bakteriol Orig A. 236, 374-85.
Stebbins, N. E., Polacco, J. C., 1995. Urease Is Not Essential for Ureide Degradation in Soybean. Plant Physiol. 109, 169-175.
Stevenson, I. L., Becker, S. A., 1972. The fine structure and development of chlamydospores of Fusarium oxysporum. Can J Microbiol. 18, 997-1002.
Stewart, V., Vollmer, S. J., 1986. Molecular cloning of nit-2, a regulatory gene required for nitrogen metabolite repression in Neurospora crassa. Gene. 46, 291-5.
Sticher, L., et al., 1997. Systemic acquired resistance. Annu Rev Phytopathol. 35, 235-70.
Stingl, K., et al., 2008. In vivo interactome of Helicobacter pylori urease revealed by tandem affinity purification. Mol Cell Proteomics. 7, 2429-41.
Strope, P. K., et al., 2011. Molecular evolution of urea amidolyase and urea carboxylase in fungi. BMC Evol Biol. 11, 80.
Sumner, J. B., Kirk, J. S., 1931. Antiurease. Science. 74, 102.
Sumrada, R., et al., 1976. Urea transport-defective strains of Saccharomyces cerevisiae. J Bacteriol. 125, 1048-56.
Szewczyk, E., et al., 2006. Fusion PCR and gene targeting in Aspergillus nidulans. Nat Protoc. 1, 3111-20.

Takken, F., Rep, M., 2010. The arms race between tomato and Fusarium oxysporum. Mol Plant Pathol. 11, 309-14.
Talaue, M. T., et al., 2006. Arginine homeostasis in J774.1 macrophages in the context of Mycobacterium bovis BCG infection. J Bacteriol. 188, 4830-40.
Tange, Y., Niwa, O., 1997. Identification of the ure1+ gene encoding urease in fission yeast. Curr Genet. 32, 244-6.
Tatebayashi, K., et al., 2007. Transmembrane mucins Hkr1 and Msb2 are putative osmosensors in the SHO1 branch of yeast HOG pathway. EMBO J. 26, 3521-33.
Taylor, P. R., et al., 2002. The beta-glucan receptor, dectin-1, is predominantly expressed on the surface of cells of the monocyte/macrophage and neutrophil lineages. J Immunol. 169, 3876-82.
Thevelein, J. M., Voordeckers, K., 2009. Functioning and evolutionary significance of nutrient transceptors. Mol Biol Evol. 26, 2407-14.
Thompson, R. W., et al., 2008. Cationic amino acid transporter-2 regulates immunity by modulating arginase activity. PLoS Pathog. 4, e1000023.
Todd, C. D., et al., 2006. Update on ureide degradation in legumes. J Exp Bot. 57, 5-12.
Todd, M. J., Hausinger, R. P., 1989. Competitive inhibitors of Klebsiella aerogenes urease. Mechanisms of interaction with the nickel active site. J Biol Chem. 264, 15835-42.
Tomas-Cobos, L., Sanz, P., 2002. Active Snf1 protein kinase inhibits expression of the Saccharomyces cerevisiae HXT1 glucose transporter gene. Biochem J. 368, 657-63.
Toren, E. C., Jr., Burger, F. J., 1968. Trace determination of metal ion inhibitors of the urea-urease system by a pH-stat kinetic method. Mikrochim Acta. 1049-58.
Torisky, R. S., et al., 1994. A single gene (Eu4) encodes the tissue-ubiquitous urease of soybean. Mol Gen Genet. 242, 404-14.
Torisky, R. S., Polacco, J. C., 1990. Soybean Roots Retain the Seed Urease Isozyme Synthesized during Embryo Development. Plant Physiol. 94, 681-9.
Treitel, M. A., Carlson, M., 1995. Repression by SSN6-TUP1 is directed by MIG1, a repressor/activator protein. Proc Natl Acad Sci U S A. 92, 3132-6.
Truckses, D. M., et al., 2004. Jekyll and Hyde in the microbial world. Science. 306, 1509-11.
Tyvold, S. S., et al., 2007. Continuous monitoring of the bronchial epithelial lining fluid by microdialysis. Respir Res. 8, 78.
Uversky, V. N., Dunker, A. K., 2010. Understanding protein non-folding. Biochim Biophys Acta. 1804, 1231-64.
Vadaie, N., et al., 2008. Cleavage of the signaling mucin Msb2 by the aspartyl protease Yps1 is required for MAPK activation in yeast. J Cell Biol. 181, 1073-81.
Valdez-Taubas, J., et al., 2004. Ammonium-induced internalisation of UapC, the general purine permease from Aspergillus nidulans. Fungal Genet Biol. 41, 42-51.
Van Loon, L. C., 1997. Induced resistance in plants and role of pathogenesis-related proteins. Eur J Plant Pathol. 103, 753-765.
Vanetten C.H, K. W. F., Peters J.E., et al., , 1967. Plant seeds as protein sources for food and feed. Evaluation based on amino acid composition of 379 species. J.Agric.Food Chem. 15, 1077-1089.
Vautard, G., et al., 1999. The glucose repressor CRE1 from Sclerotinia sclerotiorum is functionally related to CREA from Aspergillus nidulans but not to the Mig proteins from Saccharomyces cerevisiae. FEBS Lett. 453, 54-8.
Vivas, M., et al., 2010. The cell recognition model in chlorolichens involving a fungal lectin binding to an algal ligand can be extended to cyanolichens. Plant Biol (Stuttg). 12, 615-21.

Vylkova, S., et al., 2011. The fungal pathogen Candida albicans autoinduces hyphal morphogenesis by raising extracellular pH. MBio. 2, e00055-11.
Wald, A., et al., 1997. Epidemiology of Aspergillus infections in a large cohort of patients undergoing bone marrow transplantation. J Infect Dis. 175, 1459-66.
Walsh, T. J., et al., 1996. Recent progress and current problems in treatment of invasive fungal infections in neutropenic patients. Infect Dis Clin North Am. 10, 365-400.
Wanasen, N., Soong, L., 2008. L-arginine metabolism and its impact on host immunity against Leishmania infection. Immunol Res. 41, 15-25.
Waring, W. S., et al., 2008. Serum urea concentration and the risk of hepatotoxicity after paracetamol overdose. QJM. 101, 359-63.
Weatherburn, M. W., 1967. Phenol-hypochloride reaction for determination of ammonia. Anal. Chem. 39, 971-974.
Weinberg, E., 1975. Metal starvation of pathogens by hosts. Bioscience. 25, 314-318.
Williams, C. L., et al., 1996. Helicobacter pylori utilises urea for amino acid synthesis. FEMS Immunol Med Microbiol. 13, 87-94.
Wilsenach, J. A., et al., 2007. Phosphate and potassium recovery from source separated urine through struvite precipitation. Water Res. 41, 458-66.
Wilson, K. T., et al., 1996. Helicobacter pylori stimulates inducible nitric oxide synthase expression and activity in a murine macrophage cell line. Gastroenterology. 111, 1524-33.
Winkler, R. G., et al., 1988. Ureide catabolism in nitrogen-fixing legumes. Trends Biochem Sci. 13, 97-100.
Wise, H. Z., et al., 2013. Extracellular ammonia at sites of pulmonary infection with Coccidioides posadasii contributes to severity of the respiratory disease. Microb Pathog. 59-60, 19-28.
Witte, C. P., 2011. Urea metabolism in plants. Plant Sci. 180, 431-8.
Witte, C. P., et al., 2001. Functional characterisation of urease accessory protein G (ureG) from potato. Plant Mol Biol. 45, 169-79.
Witte, C. P., Medina-Escobar, N., 2001. In-gel detection of urease with nitroblue tetrazolium and quantification of the enzyme from different crop plants using the indophenol reaction. Anal Biochem. 290, 102-7.
Witte, C. P., et al., 2005. Analysis of two alleles of the urease gene from potato: polymorphisms, expression, and extensive alternative splicing of the corresponding mRNA. J Exp Bot. 56, 91-9.
Witte, C. P., et al., 2002. Leaf urea metabolism in potato. Urease activity profile and patterns of recovery and distribution of (15)N after foliar urea application in wild-type and urease-antisense transgenics. Plant Physiol. 128, 1129-36.
Wu, G., Morris, S. M., Jr., 1998. Arginine metabolism: nitric oxide and beyond. Biochem J. 336 (Pt 1), 1-17.
Xue, C., et al., 2006. G protein-coupled receptor Gpr4 senses amino acids and activates the cAMP-PKA pathway in Cryptococcus neoformans. Mol Biol Cell. 17, 667-79.
Yakoby, N., et al., 2001. Colletotrichum gloeosporioides pelB is an important virulence factor in avocado fruit-fungus interaction. Mol Plant Microbe Interact. 14, 988-95.
Yoneda, A., Doering, T. L., 2006. A eukaryotic capsular polysaccharide is synthesized intracellularly and secreted via exocytosis. Mol Biol Cell. 17, 5131-40.
Yoo, H. S., et al., 1985. Identification of the ureidoglycolate hydrolase gene in the DAL gene cluster of Saccharomyces cerevisiae. Mol Cell Biol. 5, 2279-88.
Yoshiyama, H., Nakazawa, T., 2000. Unique mechanism of Helicobacter pylori for colonizing the gastric mucus. Microbes Infect. 2, 55-60.
Yu, J. J., et al., 1997. Isolation and characterization of the urease gene (URE) from the pathogenic fungus Coccidioides immitis. Gene. 198, 387-91.

Yu, Z., et al., 2004. Pairwise interactions of the six human MCM protein subunits. J Mol Biol. 340, 1197-206.
Zaborska, W., et al., 2004. Heavy metal ions inhibition of jack bean urease: potential for rapid contaminant probing. J Enzyme Inhib Med Chem. 19, 65-9.
Zaman, S., et al., 2008. How Saccharomyces responds to nutrients. Annu Rev Genet. 42, 27-81.
Zambelli, B., et al., 2012. Insights in the (un)structural organization of Bacillus pasteurii UreG, an intrinsically disordered GTPase enzyme. Mol Biosyst. 8, 220-8.
Zambelli, B., et al., 2011. Chemistry of Ni2+ in urease: sensing, trafficking, and catalysis. Acc Chem Res. 44, 520-30.
Zambelli, B., et al., 2007. Biochemical studies on Mycobacterium tuberculosis UreG and comparative modeling reveal structural and functional conservation among the bacterial UreG family. Biochemistry. 46, 3171-82.
Zambelli, B., et al., 2005. UreG, a chaperone in the urease assembly process, is an intrinsically unstructured GTPase that specifically binds Zn2+. J Biol Chem. 280, 4684-95.
Zambelli, B., et al., 2009. Zn2+-linked dimerization of UreG from Helicobacter pylori, a chaperone involved in nickel trafficking and urease activation. Proteins. 74, 222-39.
Zhao, Y., et al., 2010. Detection of Aspergillus fumigatus in a rat model of invasive pulmonary aspergillosis by real-time nucleic acid sequence-based amplification. J Clin Microbiol. 48, 1378-83.
Zielinski, H., et al., 1999. Modeling the interactions of particulates with epithelial lining fluid antioxidants. Am J Physiol. 277, L719-26.
Zimmer, B. L., Roberts, G. D., 1979. Rapid selective urease test for presumptive identification of Cryptococcus neoformans. J Clin Microbiol. 10, 380-1.
Zimmermann, F. K., Scheel, I., 1977. Mutants of Saccharomyces cerevisiae resistant to carbon catabolite repression. Mol Gen Genet. 154, 75-82.
Zonia, L. E., et al., 1995. Essential role of urease in germination of nitrogen-limited Arabidopsis thaliana seeds. Plant Physiol. 107, 1097-103.

Supplementary figures

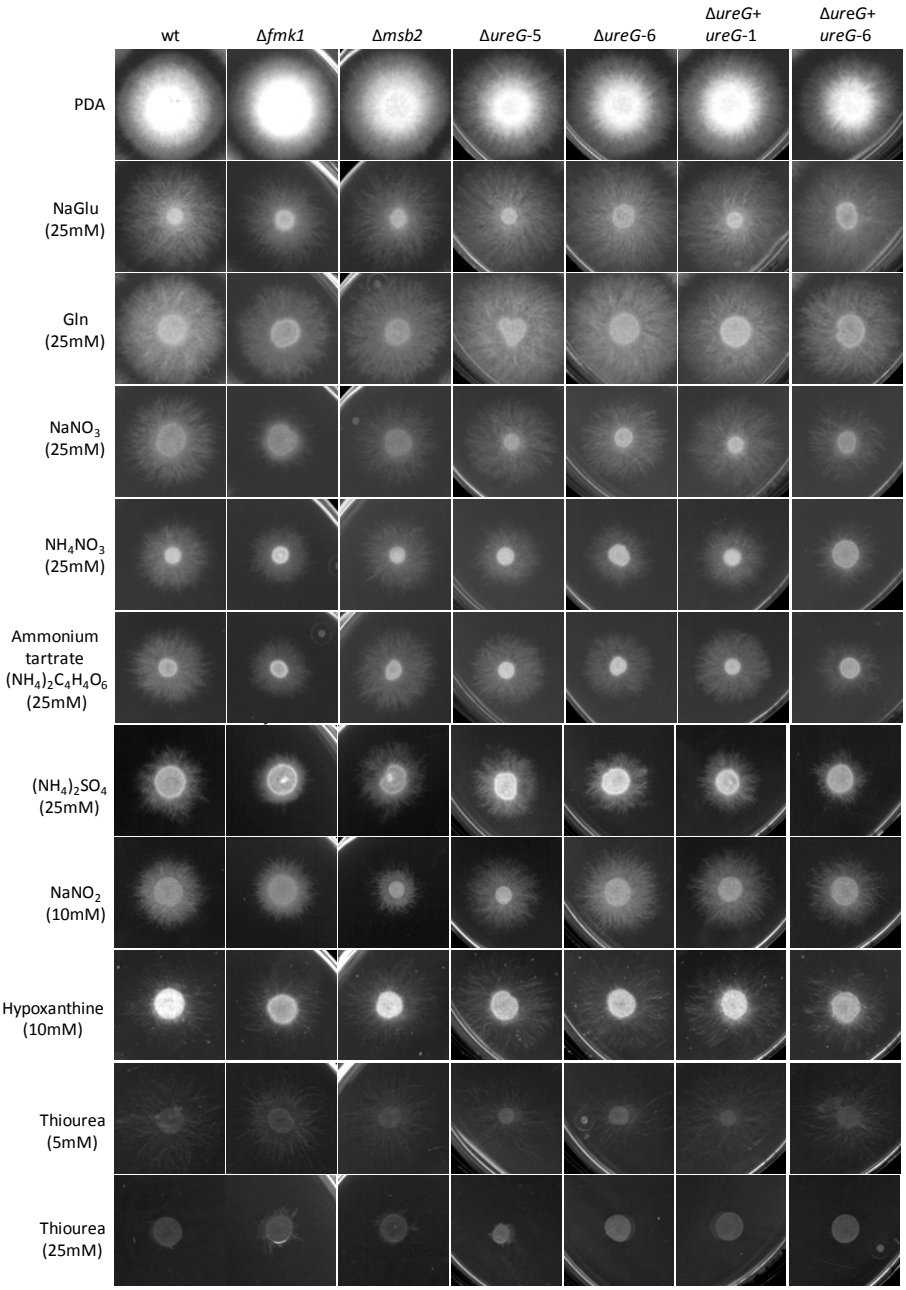

Figure S1. Δ*ureG* shows no aberrant growth on different nitrogen source. 2 x 10^4 microconidia of the indicated strains were spot-inoculated on complete medium (PDA) or on MM containing the indicated nitrogen source. Plates were incubated for three days at 28°C.

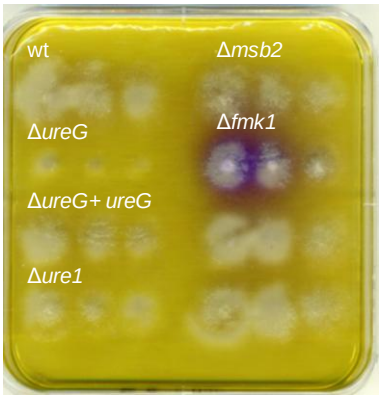

Figure S2. Δ*fmk1* alkalizes acidic urea medium (buffered at pH5). Microconidia of the indicated strains were inoculated on minimal medium (MM) containing 50 mM urea as the sole nitrogen and carbon source and the pH indicator Bromocresol purple. Urease activity was determined indirectly through the alkalinization of the medium represented by a colour change of the pH indicator (yellow <5.2; purple >6.8). Plates were incubated for 3 days at 28°C. Data shown are from one representative experiment. Experiments were performed three times with three technical repeats each, providing similar results.

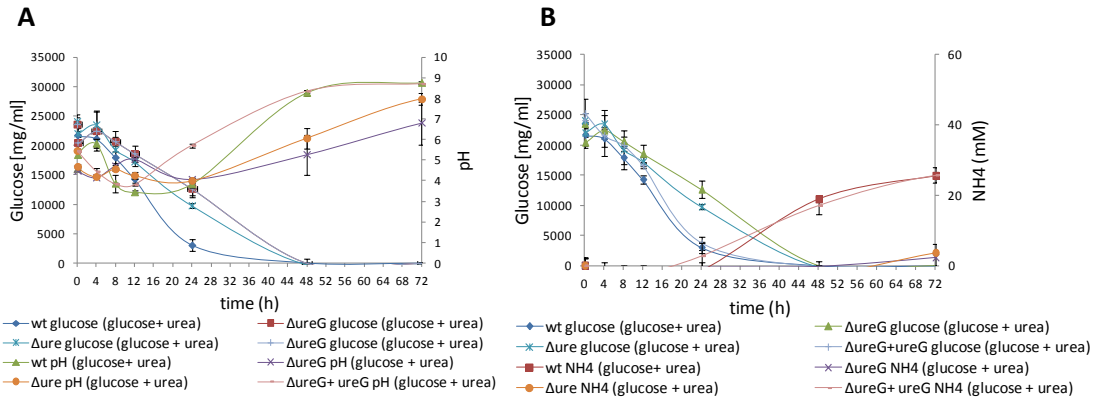

Figure S3. Gene complementation strains of ΔureG restores the ammonia secretion and medium alkalinization. 2 x 10^8 microconidia of the indicated strains were germinated for 14 h in 100 ml PDB and transferred to 50 ml liquid MM media containing 50 mM urea plus 3% glucose. Samples of the culture supernatant were taken at the indicated time points to measure pH **(A)**, concentration of ammonia **(B)** or of glucose **(A,B)**. Mean values and standard errors were calculated from 3 biological repeats

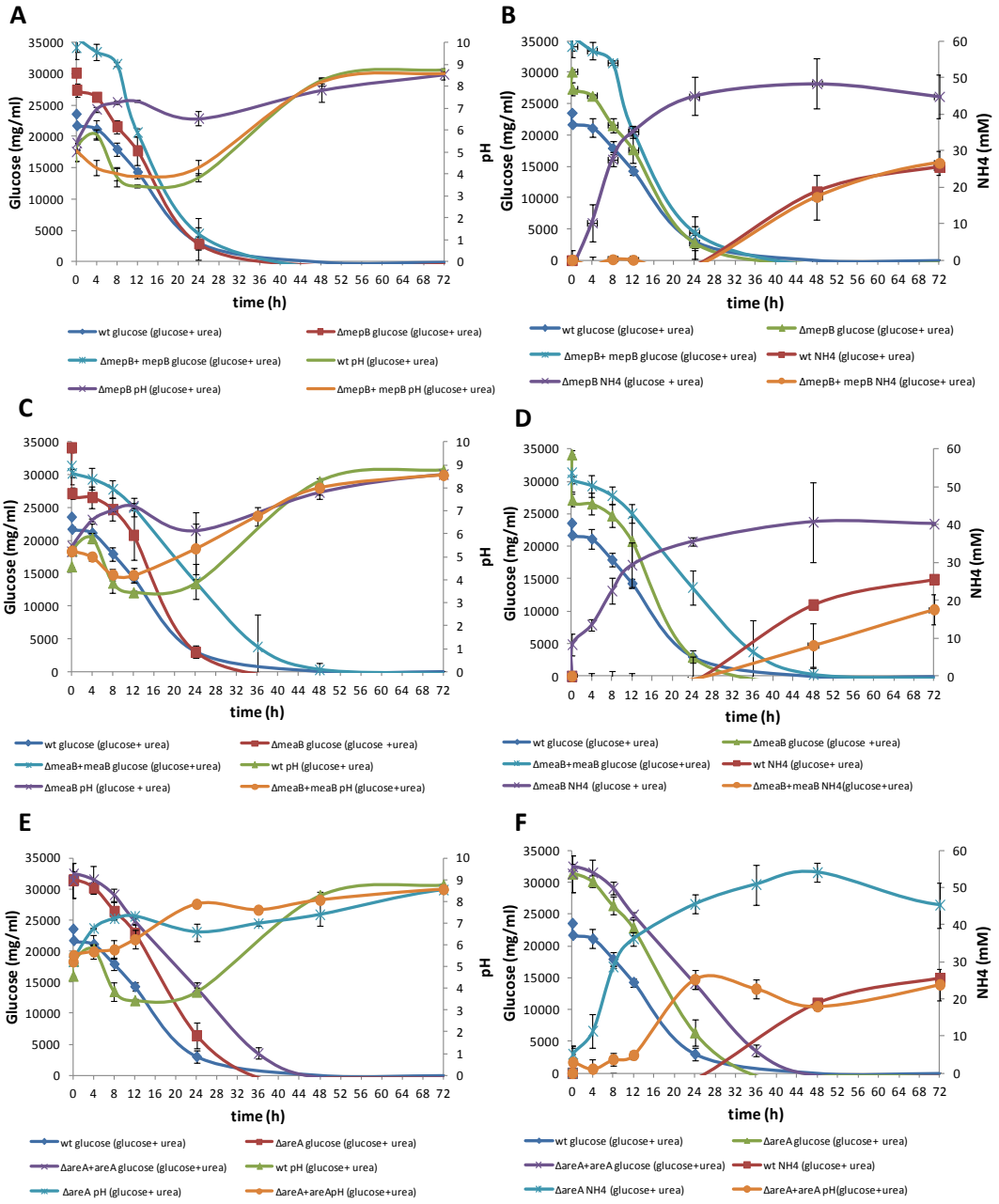

Figure S4 . Gene complementation strains of Δ*mepB*, Δ*meaB* and Δ*areA* restore the wt phenotype showing carbon catabolite repression of ammonium secretion. 2 x 10^8 microconidia of the indicated strains were germinated for 14 h in 100 ml PDB and transferred to 50 ml liquid MM media containing either 50 mM urea, urea plus 3% glucose, 1% casaminoacids, or casamoinoacids plus 3% glucose. Samples of the culture supernatant were taken at the indicated time points to measure pH **(A,C,E)**, or concentration of ammonia **(B,D,F)** or glucose **(A-F)**. Mean values and standard errors were calculated from 3 biological repeats.